

Stefan Reichert

An approach to investigate surface roughness influence on the running-in behaviour of mixed-lubricated sliding contacts using the finite element method

Ein Ansatz zur Untersuchung des Einflusses der Oberflächenrauheit auf das Einlaufverhalten von mischreibungsbefahenen Gleitkontakten unter Verwendung der Finite Elemente Methode

Band 124

Systeme ■ Methoden ■ Prozesse

Univ.-Prof. Dr.-Ing. Dr. h.c. A. Albers
Univ.-Prof. Dr.-Ing. S. Matthiesen
(Hrsg.)

Copyright: IPEK ▪ Institut für Produktentwicklung, 2019
Karlsruher Institut für Technologie (KIT)
Die Forschungsuniversität in der Helmholtz-Gemeinschaft

Alle Rechte vorbehalten

Druck: Stolzenberger Druck und Werbung GmbH & Co. KG, Leimen
06224-7697915

ISSN 1615-8113

An approach to investigate surface roughness influence on the running-in behaviour of mixed- lubricated sliding contacts using the finite element method

Zur Erlangung des akademischen Grades eines
DOKTORS DER INGENIEURWISSENSCHAFTEN (Dr.-Ing.)
von der KIT-Fakultät für Maschinenbau des
Karlsruher Instituts für Technologie (KIT)

angenommene
DISSERTATION

von

Dipl.-Ing. Stefan Reichert

Tag der mündlichen Prüfung: 16. August 2019
Hauptreferent: Univ.-Prof. Dr.-Ing. Dr. h.c. A. Albers
Korreferent: Prof. Dr.-Ing. Gerhard Poll

Vorwort der Herausgeber

Wissen ist einer der entscheidenden Faktoren in den Volkswirtschaften unserer Zeit. Der Unternehmenserfolg wird mehr denn je davon abhängen, wie schnell ein Unternehmen neues Wissen aufnehmen, zugänglich machen und verwerten kann. Die Aufgabe eines Universitätsinstitutes ist es, hier einen wesentlichen Beitrag zu leisten. In den Forschungsarbeiten wird ständig Wissen generiert. Dieses kann aber nur wirksam und für die Gemeinschaft nutzbar werden, wenn es in geeigneter Form kommuniziert wird. Diese Schriftenreihe dient seit mehr als 20 Jahren als eine Plattform zum Transfer und macht damit das Wissenspotenzial aus aktuellen Forschungsarbeiten am IPEK - Institut für Produktentwicklung Karlsruhe* am Karlsruher Institut für Technologie (KIT) verfügbar. Die Forschung des IPEK ist dabei strukturiert in die Kategorien Systeme, Methoden und Prozesse, um so der Komplexität heutiger Produktentwicklung ganzheitlich gerecht zu werden. Erst die Verknüpfung dieser drei Kategorien ermöglicht die Synthese innovativer Systeme durch Nutzung neuester Methoden und Prozesse. Gleichzeitig werden durch die Systemsynthese die erforschten neuen Methoden und Prozesse validiert und deren Mehrwert für die Praxis abgesichert. Dieses Forschungskonzept prägt nicht nur das IPEK-Leitbild sondern auch den Charakter dieser Schriftenreihe, da immer alle drei Kategorien und deren Wechselwirkungen berücksichtigt werden. Jeder Band setzt hier individuelle Schwerpunkte und adressiert dabei folgende Forschungsgebiete des IPEK:

- das Entwicklungs- und Innovationsmanagement,
- die Entwicklungs- und Konstruktionsmethodik,
- der Leichtbau von der Ebene des ganzen Systems bis hinunter zur Optimierung des Bauteils,
- die Validierung technischer Systeme auch unter Berücksichtigung der NVH Aspekte (Noise, Vibration, Harshness) mit dem Fokus auf Schwingungen und Akustik an Komponenten und in den Gesamtsystemen sowie deren subjektiver Beurteilung durch den Menschen,
- die Antriebssystemtechnik mit den Schwerpunkten komplette Antriebslösungen für Fahrzeuge und Maschinen,
- das Design, die Tribologie und Erprobung von Kupplungen und Bremsen sowie
- die Gerätetechnik mit dem Schwerpunkt auf Power-Tools.

Die Forschungsberichte stellen Ergebnisse unserer Forschung sowohl anderen Wissenschaftlern als auch den Unternehmen zu Verfügung um damit die Produktentwicklung in allen ihren Facetten mit innovativen Impulsen zu optimieren.

Albert Albers und Sven Matthiesen

* Eh.: Institut für Maschinenkonstruktionslehre und Kraftfahrzeugbau, Universität Karlsruhe (TH)

Vorwort zu Band 124

In vielen Maschinen ist eine der größten Herausforderungen die Übertragung von Kräften zwischen relativ bewegten Elementen und Teilsystemen. Hierzu werden im Allgemeinen Lagersysteme eingesetzt. Diese Lagersysteme können durch unterschiedliche Konzepte umgesetzt werden. Bei sogenannten Gleitkontakten bewegen sich die Wirkflächen direkt aufeinander oder werden je nach Konzept durch einen Schmierstoff als zusätzliches Element unter Nutzung des Aufbaus von hydrodynamischen Schmierfilmen getrennt, um so die Reibung zu senken. Als weiteres Konzept haben die sogenannten Wälzkontakte eine hohe Bedeutung. Eine Ausprägung sind die verschiedenen Bauarten von Wälzlagern. Hier wird durch Einbringen von zusätzlichen Wirkkörpern zwischen den, sich relativ bewegenden Wirkflächen der beiden kontaktierenden Teilsysteme, die Abwälzbewegung dieser Zwischenelemente – im Allgemeinen Kugeln oder Rollen – zur Reduzierung der Reibung genutzt. Dabei entstehen bei relativ hohen Flächenpressungen in den Wirkflächenpaaren zwischen Wirkkörper und den Laufbahnen lokale elastische Verformungen. Bei Anwesenheit von Schmierstoff bilden diese Wälzlager sogenannte elasto-hydrodynamische Schmierfilme aus. Beiden Konzepten gemein ist, dass die Schmierfilmhöhe von verschiedenen Parametern abhängig ist und Betriebszustände auftreten, bei denen es nicht zu einer vollständigen Trennung der Wirkflächen kommt. Man spricht in diesem Zusammenhang vom Mischreibung. Auf der mikroskopischen Größenskala betrachtet, treten beim Mischreibungskontakt sowohl fest-fest Wirkflächenpaare wie auch fest-flüssig Wirkflächenpaare auf, das heißt ein Teil der Kräfte wird über einen Festkörperkontakt übertragen, während der andere Teil der Kräfte weiterhin über einen Flüssigkeitsfilm übertragen wird. Diese sogenannten Mischreibungskontakte sind in der Praxis höchst relevant. Bis heute werden diese im Wesentlichen auf der Basis von experimentellen Grunddaten untersucht, dimensioniert und ausgelegt. Um das Verständnis von tribologischen Phänomenen zu steigern, ist es notwendig, durch geeignete Simulationsansätze auf der Basis numerischer Methoden eine genaue Abbildung der Verhältnisse zu erreichen. Damit ist es möglich, den Mischreibungszustand gezielt bei der Auslegung zu berücksichtigen. Die Mischreibungszustände sind im Allgemeinen bei Gleitkontakten nahe am Reibungsminimum. Somit ist dieser Zustand durchaus für eine Optimierung der Verluste in Maschinensystemen relevant und interessant. Gleichzeitig gilt es aber, den auftretenden Verschleiß zu berücksichtigen und zu kontrollieren. Hierzu neue Konzepte zu finden, hat sich Herr Dr.-Ing. Stefan Reichert in seiner wissenschaftlichen Arbeit zum Ziel gesetzt. Er hat durch eine Modellbildung auf Basis der Finiten Elemente für Mischreibungskontakte unter Berücksichtigung der Oberflächenrauigkeiten Lösungsansätze gefunden, um ein tieferes Verständnis des Betriebsverhaltens zu erlangen und gleichzeitig bei der Dimensionierung und Gestaltung von Lagersystemen zu unterstützen. Durch die Aufbereitung hin zu einem Konstruktionswerkzeug macht er seine

Forschung auch für die Praxis nutzbar. Die Arbeit bietet wertvolle Impulse für die weitere Forschung auf dem Gebiet der Tribologie und gleichzeitig erhebliches Potential für die praktische Konstruktion in den Unternehmen.

August 2019

Albert Albers

Preface to volume 124

One of the biggest challenges in many technical applications is the transmission of forces between relatively moving elements and subsystems. Bearing systems are generally used for this purpose. These bearing systems can be realized by different concepts. In so-called sliding contacts, the contacting surfaces move directly towards each other or, depending on the concept, are separated by a lubricant as an additional element using the hydrodynamic effect to reduce friction. As a further concept, the rolling contacts are of great importance. One characteristic is the different types of rolling bearings. By introducing additional rolling elements between the relatively moving surfaces of the two contacting subsystems, the rolling motion of these intermediate elements - generally balls or rollers - is used to reduce friction. This results in local elastic deformations at relatively high surface pressures in the working surface pairs between the rolling elements and the inner and outer ring. In the presence of lubricant, these rolling bearings form so-called elasto-hydrodynamic lubricating films. What both concepts have in common is the fact that the lubricant film height depends on various parameters and that operating conditions can occur, in which the asperities of the contacting surfaces are not completely separated. This regime is called mixed lubrication. On the microscopic scale, both solid-solid working surface pairs and solid-fluid working surface pairs occur during mixed-lubrication. This means that some of the forces are transmitted via solid contact, while the other part of the forces is transmitted via a fluid film. These so-called mixed friction contacts are highly relevant in practice. Up to now, these are essentially investigated, dimensioned and designed on the basis of experimental data. In order to extend the understanding of tribological phenomena, it is necessary to achieve a detailed representation of the conditions by suitable simulations on the basis of numerical methods. Thus, it is possible to take into account mixed friction phenomena into the design phase of machine elements. The mixed friction regime is generally close to the friction minimum for sliding contacts. Thus, this state is relevant and important for the optimization of friction losses in machine systems. At the same time, the occurring wear phenomena had to be taken into account and controlled. Dr.-Ing. Stefan Reichert has set himself the goal of finding new concepts for this in his scientific work. On the basis of a numerical approach based on the finite element method and taking into account surface roughness influence, he has found solutions for gaining a deeper understanding of mixed lubrication and at the same time to support the dimensioning and design of bearing systems. By transforming his research into a design tool, he also makes this numerical approach usable in practice. The work offers valuable impulses for further research in the field of tribology and at the same time considerable potential for practical design in companies.

Kurzfassung

Um den Einfluss der Oberflächenrauheit auf das Reibungs- und Verschleißverhalten zu untersuchen, stehen nur begrenzte experimentelle Möglichkeiten zur Verfügung. Bedingt durch die spanende Endbearbeitung von Lagerschalen und Wellen bewirkt eine Veränderung der Werkstücktopographie, resultierend aus der Variation der Schnittparameter im Herstellprozess, immer auch eine Veränderung der Welligkeit und der Grenzschicht einer Oberfläche. Daher ist es mit experimentellen Methoden aktuell nicht möglich, die Rauheit isoliert zu betrachten. Hierzu wird in der vorliegenden Forschungsarbeit eine Methode zur Untersuchung des Einflusses der Oberflächentopographie auf das Reibungs- und Verschleißverhalten von geschmierten Kontakten vorgestellt, die Entwickler bei der ressourcenschonenden Auslegung von technischen Oberflächen unterstützt. Die Methode basiert auf numerischen Modellen auf der Mikroskala, die sowohl für trockenlaufende als auch für geschmierte Systeme einen genaueren Einblick in den tribologischen Kontakt ermöglicht.

Die Untersuchungen wurden mit der Finite-Elemente-Software ABAQUS auf der Mikroskala durchgeführt. Ein bestehendes Mischreibungsmodell wurde hierzu um eine Verschleißroutine erweitert, die die Berechnung von lokalen Verschleißtiefen an beiden tribologischen Partnern erlaubt. Die numerischen Modelle von trockenlaufenden Kontakten wurden experimentell anhand von Nanoindenterversuchen validiert. Die Modelle von geschmierten Kontakten wurden mit numerischen Methoden verifiziert.

Um das initiale Zielsystem für die Berechnungsmethode zu entwickeln, wurde mit Hilfe des Contact, Channel and Connector Approach (C&C²-A) ein tribologisches System methodisch analysiert und unter Verwendung der PGE-Produktgenerationsentwicklung eine Validierungsumgebung für die Untersuchung des Einflusses der Oberflächenrauheit auf Reibung und Verschleiß geschaffen. Auf dieser Grundlage wird ein Untersuchungsansatz mit dem Schwerpunkt auf der Modellbildung des mikroskopischen Mischreibungskontaktes und den zutreffenden Annahmen und verwendeten Randbedingungen entwickelt. Das trockenlaufende Kontaktmodell wurde anschließend anhand von experimentellen Nanoindenterversuchen validiert, wobei nur sehr geringe Abweichungen in der gemessenen und berechneten Reibkraft auftraten. Das geschmierte Kontaktmodell wurde anhand von Konvergenzuntersuchungen und Vergleichen mit anerkannten Berechnungsverfahren in der Strömungsmechanik verifiziert.

Anschließend wurde eine Parameterstudie durchgeführt, wobei Einflüsse von Materialeigenschaften der Festkörper und des Fluides und Randbedingungen wie Fluiddruck im Schmierpalt und Anpresskraft auf das Reibungs- und

Verschleißverhalten untersucht wurden. Es konnte dabei gezeigt werden, dass besonders die Anpresskraft in der Einlaufphase einen großen Einfluss auf die Verschleißtiefe in der stationären Phase des tribologischen Systems hat. Weiterhin wurden unterschiedlich gefertigte Oberflächen untersucht und auch hier konnten große Unterschiede in Reibung und Verschleiß aufgezeigt werden. Abschließend wurde die zeitliche Entwicklung der Oberflächentopographie betrachtet und mit experimentell ermittelten Werten verglichen. Auch hier konnten identische Veränderungen ausgewählter statistischer Rauheitsparameter beobachtet werden.

Abstract

Only limited experimental possibilities are available to investigate the influence of surface roughness on friction and wear behaviour. Due to the cutting finish of bearings and shafts, a change in the workpiece topography, resulting from the variation of the cutting parameters in the manufacturing process, always results in a change in waviness and the boundary layer of a surface. Therefore, it is currently not possible to view roughness in isolation using experimental methods. The present research paper presents a method for investigating the influence of surface topography on the friction and wear behaviour of lubricated contacts, which supports developers in the resource-saving design of technical surfaces. The method is based on numerical models on the microscale, which allows a more precise insight into the tribological contact for both dry-running and lubricated systems.

The investigations were carried out with the finite element software ABAQUS on the microscale. An existing mixed friction model was extended by a wear routine which allows the calculation of local wear depths at both tribological partners. The numerical models of dry-running contacts were validated experimentally using nanoindenter tests. The models of lubricated contacts were verified with numerical methods.

In order to develop the initial target system for the calculation method, a tribological system is methodically analyzed using the Contact, Channel and Connector Approach (C&C²-A) and a validation environment for the investigation of the influence of surface roughness on friction and wear was created using the PGE - Product Generation Engineering. On this basis, an investigative approach was developed focusing on the modelling of the microscopic mixed friction contact and the assumptions to be made and boundary conditions used. The dry running contact model was validated by experimental nanoindenter tests, whereby only very small deviations in the measured and calculated friction force occurred. The lubricated contact model was verified by means of convergence investigations and comparisons with recognized calculation methods in fluid mechanics.

Subsequently, a parameter study was carried out in which influences of material properties of the solids and the fluid and boundary conditions such as fluid pressure in the lubrication gap and contact force on the friction and wear behaviour were investigated. It could be shown that especially the contact force in the running-in phase has a large influence on the wear depth in the stationary phase of the tribological system. Furthermore, differently manufactured surfaces were investigated and also here large differences in friction and wear could be shown. Finally, the temporal development of the surface topography was examined and compared with experimentally determined values. Here, too, identical changes of selected statistical roughness parameters could be observed.

Danksagung

Die vorliegende Arbeit entstand während meiner Tätigkeit als wissenschaftlicher Mitarbeiter am IPEK – Institut für Produktentwicklung am Karlsruher Institut für Technologie (KIT).

Besonderer Dank gilt meinem Doktorvater Herrn Univ.-Prof. Dr.-Ing. Dr. h.c. A. Albers, Leiter des IPEK – Institut für Produktentwicklung am KIT, für die wissenschaftliche Betreuung dieser Arbeit und für das in mich gesetzte Vertrauen und die mir gewährten Freiräume. Während der engen Zusammenarbeit hatte ich dank der übertragenen Verantwortung und seinem Vertrauen die Gelegenheit mich fachlich und persönlich weiterzuentwickeln.

Herrn Prof. Dr.-Ing. Gerhard Poll, Leiter des Instituts für Maschinenkonstruktion und Tribologie an der Gottfried Wilhelm Leibniz Universität Hannover, danke ich für die Übernahme des Korreferats und die damit verbundenen Mühen.

Mein Dank gilt außerdem allen Mitarbeitern des Instituts, sowohl im wissenschaftlichen als auch im administrativen Bereich und in der Industriewerkstatt. Ebenso gilt mein Dank den wissenschaftlichen Hilfskräften und studentischen Abschlussarbeitern. Sie alle haben wesentlich zum Gelingen der vorliegenden Arbeit beigetragen, speziell Herr Steffen Heldmaier und Herr Jusuf Sümer.

Mein größter Dank gilt allen, die in meinem privaten Umfeld zum Gelingen dieser Arbeit beigetragen haben, besonders meinen Eltern Marianne und Bruno und meinem Bruder Uwe, die mich stets nach Kräften unterstützt haben.

Karlsruhe, den 16. August 2019

Stefan Reichert

Acknowledgement

The present work was written during my time as a scientific assistant at the IPEK - Institute of Product Engineering at Karlsruhe Institute of Technology (KIT).

Special thanks go to my doctoral supervisor Univ.-Prof. Dr.-Ing. Dr. h.c. A. Albers, head of the IPEK - Institute for Product Engineering at KIT, for the scientific supervision of this work and for the confidence and open spaces granted to me. During the close cooperation, I had the opportunity to develop professionally and personally because of the responsibility and trust placed in me.

I would like to thank Prof. Dr.-Ing. Gerhard Poll, Head of the Institute of Machine Design and Tribology at the Gottfried Wilhelm Leibniz University of Hanover, for the assumption of the co-lecture and the efforts involved.

I would also like to thank all the staff of the Institute, both in the scientific and administrative areas and in the industrial workshop. I would also like to thank the scientific assistants and student research assistants. All of them have contributed significantly to the success of the present work, especially Mr. Steffen Heldmaier and Mr. Jusuf Sümer.

My greatest thanks go to everyone who has contributed to the success of this work in my private environment, especially my parents Marianne and Bruno and my brother Uwe, who have always supported me to the best of their ability.

Karlsruhe, 16. August 2019

Stefan Reichert

Content

1	INTRODUCTION	1
2	FUNDAMENTALS AND STATE OF THE ART.....	4
2.1	Basics of product development process.....	4
2.1.1	Process Model of " KaSPro - Karlsruher Schule für Produktentwicklung"	5
2.1.2	Product Model – Contact, Channel and Connector Approach (C&C ² -A)	9
2.1.3	PGE-Product Generation Engineering.....	10
2.2	Technical surfaces	13
2.2.1	Surface topography.....	13
2.2.2	Characterization of surface topography by statistical parameters.....	15
2.2.3	Surface metrology	18
2.2.4	Generation of rough surface profiles	20
2.3	Friction.....	20
2.3.1	Tribological systems.....	21
2.3.2	Friction measurements.....	22
2.3.3	Microstructural friction mechanism	23
2.3.4	Types of friction.....	29
2.4	Wear	30
2.4.1	Wear measurements.....	32
2.4.2	Microstructural wear mechanism.....	33
2.4.3	Types of wear	37
2.5	Fluid mechanics theory	38
2.5.1	Mathematical description of flow	38
2.5.2	Fluid properties and thermal effects	40
2.5.3	Influence of surface roughness on fluid mechanics	41
2.5.4	Elastohydrodynamic lubrication.....	44
2.6	Numerical methods in lubrication and tribology	45
2.6.1	Discretization method.....	46
2.6.2	Multibody simulation.....	49
2.6.3	Contact modelling	49
2.7	Fluid structure interaction in simulations	51
2.7.1	FSI in conventional Computational Fluid Dynamics.....	51
2.7.2	FSI modelled with the Coupled Eulerian Lagrangian Method (CEL)	53
2.8	State of the Art: Experimental investigations in tribology	55
2.8.1	Experimental investigations of sliding systems.....	56
2.8.2	Experimental investigations of friction systems	57

2.9	State of the Art: Numerical investigations in tribology.....	57
2.9.1	Non-lubricated friction simulation	58
2.9.2	Mixed-lubricated friction simulation	58
2.9.3	Wear simulation	60
2.10	Summary	61
3	RESEARCH OBJECTIVES	62
3.1	Research potential.....	62
3.2	Research hypothesis	63
3.3	Research questions	64
4	SYSTEM ANALYSIS AND MODEL DESIGN.....	65
4.1	Demonstrator definition	65
4.2	Classification in the product development process.....	69
4.3	System analysis with the Contact, Channel and Connector Approach (C&C ² -A)...	73
4.4	Benefit by coupling of various simulation methods	77
4.5	Establishment of the initial target system	79
5	NUMERICAL MODEL AT THE MICROSCOPIC SCALE	81
5.1	Establishment of operating conditions in journal bearings	81
5.2	Numerical model for mixed-lubrication	84
5.2.1	Discretization of technical surfaces and importation into FEM.....	84
5.2.2	Applied boundary conditions	87
5.2.3	Fluid structure interaction and contact definitions	89
5.2.4	Material model for solid and fluid parts	91
5.2.5	Implementation of residual stresses	93
5.3	Implementation of wear	93
5.4	Numerical model of dry friction.....	96
5.5	User interface to couple the various simulation methods.....	97
6	VERIFICATION AND VALIDATION OF THE MICROSACLE MODEL	101
6.1	Validation of rough surface generation.....	101
6.2	Convergence of the mixed lubrication model.....	103
6.2.1	Convergence of the solid mesh.....	103
6.2.2	Convergence of the fluid mesh.....	106
6.3	Convergence of the wear model	107
6.4	Comparison between the CEL- and CFD method in a hydrodynamic regime	108
6.5	Investigation of permitted scaling factors for wear simulation	112
6.6	Validation of the dry running wear model with nanoindenter device	113
6.6.1	Demonstrator of dry running model	113
6.6.2	Comparison between experimental and numerical results.....	116
6.7	Summary	120

7	RESULTS ON FRICTION AND WEAR UNDER MIXED-LUBRICATED CONDITIONS	122
7.1	Influence of the fluid viscosity on friction and wear	122
7.2	Impact of solid properties on friction and wear	124
7.3	Influence of fluid pressure on friction and wear	127
7.4	Influence of normal load on friction and wear	130
7.5	Influence of running in procedure on friction and wear	133
7.6	Influence of the surface machining on friction and wear	137
7.6.1	Impact of the machining type	137
7.6.2	Impact of the machining direction	140
7.7	Influence of residual stresses from metal cutting on friction and wear	142
7.8	Evolution of roughness parameter	144
8	CONCLUSION AND OUTLOOK	149
9	REFERENCES	152

Symbols

α	$\frac{w}{m^2 \cdot K}$	Heat transfer coefficient
γ	J	Surface energy
$\dot{\gamma}$	s^{-1}	Shear rate
δ	%	Single share of product generation engineering
δ_1, δ_2	μm	Randomly distributed roughness amplitudes
η	$Pa \cdot s$	Dynamic viscosity
η_0	$Pa \cdot s$	Viscosity at atmospheric pressure
ϑ	$^\circ$	Angle of the asperities
θ	$^\circ$	Tilt angle of the asperities
λ	$\frac{w}{m \cdot K}$	Thermal conductivity
λ_c	mm	Cut-off wavelength for roughness filter
λ_{def}	-	Contact ratio due to plastic deformation
λ_f	mm	Cut-off wavelength of the high pass filter
λ_s	mm	Cut-off wavelength of the low pass filter
μ	-	Coefficient of friction
μ_D	-	Component of deformation in friction
ρ	$\frac{kg}{m^3}$	Density
σ	-	Normalized Variance
σ_{crit}	$\frac{N}{mm^3}$	Critical yield strength
$\vec{\tau}$	$\frac{N}{mm^3}$	Normal and shear stresses
τ_{crit}	$\frac{N}{mm^3}$	Critical shear stress limit
τ_{max}	$\frac{N}{mm^3}$	Maximum shear stress
τ_s	$\frac{N}{mm^3}$	Mean boundary layer shear stress
ϕ_s		Shear flow factor
ϕ_x, ϕ_y		Pressure flow factors
a_{adh}	-	Coefficient of adhesion
α_p	GPa^{-1}	Barus pressure coefficient
A_r	mm^2	Real contact area
A_V	mm^2	Wear surface
$A_{1,2}$	mm^2	Deformation area due to abrasion
c	μm	Cutting level
d	mm	Wall thickness
d_{part}	μm	Penetration depth of wear particles

d_H	mm	Hydraulic diameter
\vec{f}	N	Force vector
f_{ab}	-	Abrasion factor
$f_{scaling}$	-	Scaling factor of the wear routine
F_A	N	Adhesion force
F_N	N	Normal force
F_R	N	Friction force
F_{Rd}	N	Dynamic friction force
F_{RS}	N	Static friction force
h	mm	Nominal film thickness
h_T	mm	Local film thickness
$h_{V,i,n}$	mm	Wear depth of previous time increment
$h_{V,i+1,n}$	mm	Summed wear depth on a single surface node
H	-	Hardness
i_x	μs	Calculation step of the wear routine
k	$\frac{mm^3}{N \cdot m}$	Wear coefficient
k_1, k_2	-	Constants
ku	-	Kurtosis
ln	mm	Measuring distance of profile
L_{xz}	mm	Length of the lubrication gap
L_y	mm	Height of the lubrication gap
m	μm	Mean roughness profile
M_R	Nm	Friction torque
p	$\frac{N}{mm^3}$	Fluid pressure
$p_{i,n}$	$\frac{N}{mm^3}$	Local contact pressure of a single node
P	$\frac{N}{mm^3}$	Surface pressure
\dot{q}	$\frac{W}{m^2}$	Heat flux density
R_a	μm	Arithmetical mean height
R_e	-	Reynolds number
R_k	μm	Core roughness
$R_{mr}(c)$	%	Material ratio
R_p	μm	Maximum peak height
R_{pk}	μm	Reduced peak height
R_q	μm	Root mean square height
R_v	μm	Maximum pit height
R_{vk}	μm	Reduced valley depth
R_z	μm	Average surface roughness

r	μm	Radius of wear particles
r_{tip}	μm	Radius of the probe tip for profile measurement
s	m	Sliding distance
sR_a	μm	3D Arithmetical mean height
sk	-	Skewness
S_{ku}	μm	3D Kurtosis
sR_{pk}	μm	3D reduced peak height
sR_q	μm	3D Root mean square height
s_R	m	Sliding distance
S_{sk}	μm	3D Skewness
sR_{vk}	μm	3D reduced valley depth
sR_z	μm	3D average surface roughness
t	s	Duration of stresses
T	K	Temperature
U_1, U_2	$\frac{m}{s}$	Sliding velocity
v	$\frac{m}{s}$	Sliding velocity
\vec{v}	$\frac{m}{s}$	Velocity vector
V	m^3	Volume
V_V	m^3	Wear volume
W	J	Specific surface energy
$\Delta s_{i,n}$	μm	Incremental sliding distance of a single node

Abbreviation

ACF	Auto-Correlation function
AFM	Atomic Force Microscopy
CEL	Coupled Eulerian Lagrangian
CFD	Computational Fluid Dynamics
CGM	Conjugate Gradient Method
CV	Carryover variation
CVT	Continuously Variable Transmission
C&C ² -A	Contact & Chanel Approach
DIN	Deutsches Institut für Normung (German Institute of Normalization)
EHD	Elastohydrodynamics
EHL	Elastohydrodynamic Lubrication
EV	Embodiment variation
FEM	Finite Element Method
FFT	Fast Fourier Transformation
FIB	Focused Ion Beam
FSI	Fluid Structure Interaction
FVM	Finite Volume Method
GPS	Geometrical Product Specifications
GUI	Graphical user interface
iPeM	Integrated product engineering model
ISO	International Organization for Standardization
IP	Integration Point
MBS	Multi Body Simulation
NSE	Navier-Stokes-Equation
PGE	Product Generation Engineering
PIV	Particle Image Velocimetry
PV	Principle Variation
RNT	Radio Nuclide Technique
SEM	Scanning electron microscopy
TEM	Transmission Electron Microscopy
WSP	Working Surface Pair

1 Introduction

In order to reduce the fuel consumption and CO₂ emissions of vehicles, operating strategies such as start-stop systems have been introduced in the automotive industry. Due to this strategy, it is generally possible to achieve fuel consumption advantages of around 6 to 8 % in urban driving (Sander, Allmaier, Witt & Skiadas, 2017), which has led to a rapid spread of the automatic start-stop system. One problem of this new operating strategies is the oil that is at rest in the stop phase. Due to the frequent and pronounced stop phases, lubrication in the tribological contacts cannot be maintained. With every change from stop to start, the oil must be transported again into the lubrication gap, which results in increased mixed friction in the machine elements. The additional solid contact component causes increased wear of the machine elements, which leads to premature failure. Due to the changed operating conditions, journal bearings, piston rings, timing chains and further components in drive train must be adapted and further developed (Sander, Allmaier & Priebisch, 2016). In previous work, surface roughness was identified as a decisive factor influencing the friction behavior (Lorentz & Albers, 2013), which must consequently be specifically designed for the further development of resource efficient tribological systems.

To be able to design the surface roughness in a targeted manner, a fundamental understanding of the influence of surface roughness on friction and wear must first be created. To date, however, it has not been possible to evaluate the influence of surface roughness in an isolated, experimental way, since further material properties such as boundary layer, form and waviness profile are also changed due to manufacturing processes (finishing processes) to define the surface topography of the workpiece. Since the influence of surface topography of the machine elements with regard to friction and wear under mixed-lubricated conditions can only be validated experimentally after the completion of the machine element, there is the need for a method that allows an early validation. According to Albers, Behrendt, Klingler and Matros (2016), in addition to physical approaches, the validation can be carried out using virtual approaches. Due to the limited experimental investigation methods described above, a numerical approach on the microscopic level will be developed in the present work to investigate the influence of surface roughness on friction and wear in a clearly earlier stage of the product generation process. Numerical models offer the possibility to keep a certain parameter field constant and only vary the target variable to be examined and thus to determine its influence.

The knowledge gained in these investigations will help to extend the understanding of the influence of surface roughness on friction and wear. Furthermore, this developed method is intended to support product developers in the targeted conditioning of tribological friction partners in order to design machine elements in a resource-efficient manner and thus to increase their lifetime. The main objective of the present work is consequently to create a methodology to predict friction and wear in the running-in phase on the microscopic scale and to support the product developer in the specific design of technical surfaces. The challenges are to merge different modelling approaches from the areas of product development, continuum mechanics, fluid mechanics and coupling of various simulation methods.

The present work is structured into 8 chapters, which are shown in Figure 1-1.

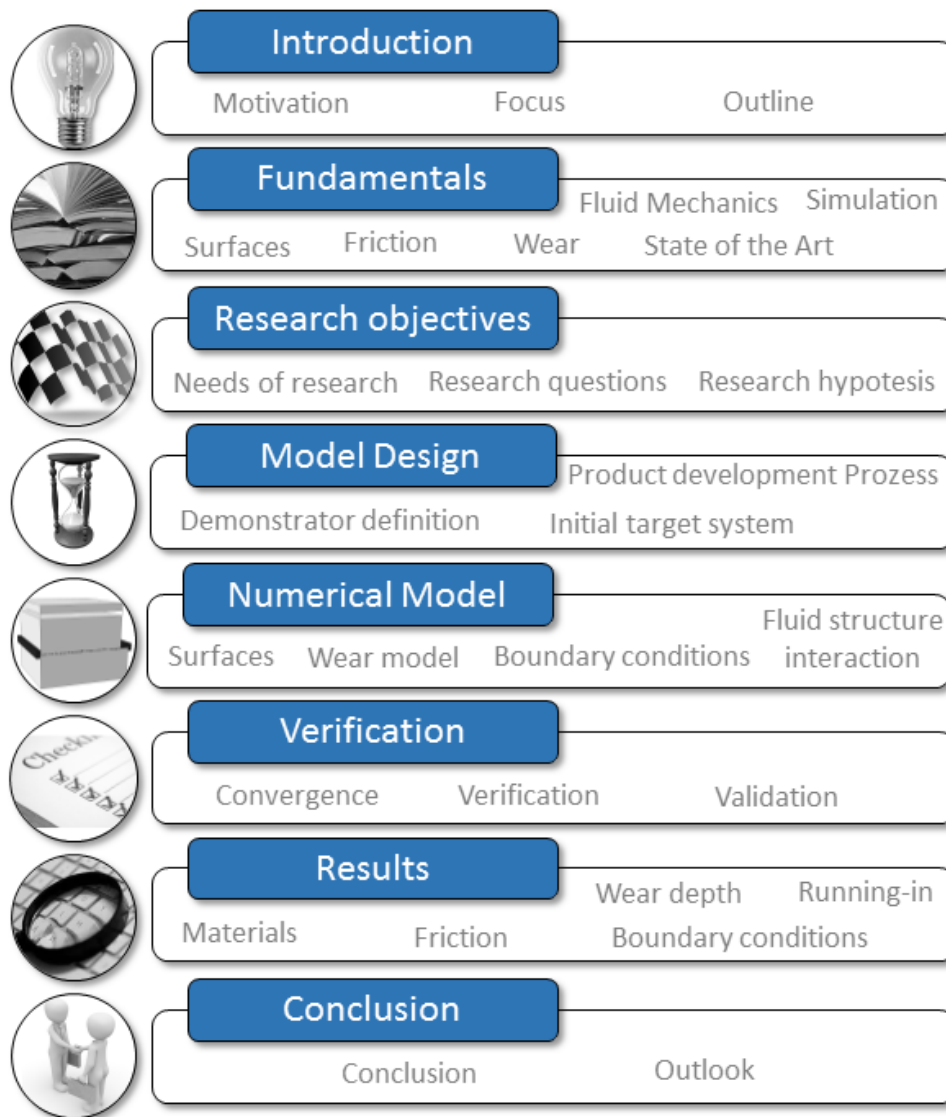


Figure 1-1: Structure of the present work

In order to achieve the aims of the present work, the necessary understanding of the various disciplines is first of all created in the fundamentals and relevant research is shown in the state of the art (chapter 2). The focus is on the methods of product development, technical surfaces, friction and wear and the numerical modelling of mixed-lubrication. Based on the current state of the art, the work is motivated and the objective is pointed out (chapter 3). To serve the operationalization of the objective, research questions are derived. In chapter 4, the initial target systems for methods and models are derived, which allow the investigation of the influence of surface topography on the friction and wear behavior in sliding systems. The final model setup of the finite element model is presented in chapter 5, including the corresponding boundary conditions and the graphical user interface to support the product developer. The numerical verification of the mixed-lubricated wear model and an experimental validation of the dry running model is presented in chapter 6. The experimental validation was carried out with a microscopic nanoindenter. In chapter 7, the influence of different parameters on friction and wear is examined. Furthermore, the temporal development of surface topography is investigated more closely in order to identify the locations of wear. In the last chapter 8, the results are summarized and an outline is provided about pursuing needs of research in the field of numerical tribosimulation.

2 Fundamentals and state of the art

In this chapter, the most important fundamentals are described in order to understand the tribological phenomena occurring in lubricated sliding systems on the microscale level and to handle these phenomena with numerical methods. At the beginning, the methodology is provided, to identify first the relevant components of a tribological system and to assign the correct functions to them and second, to develop a validation system, based on a reference system.

Next, each component to set up a numerical model to investigate mixed-lubricated contacts is provided. First, the occurring phenomena in sliding systems due to solid contact are presented, including the characterization of rough technical surfaces and their influence on the friction behavior and the relevant microstructural friction and wear mechanism present in this type of contact. For the investigation of lubricated contacts, fluid mechanics theory is introduced to describe the fluid flow in a lubrication gap. Further the influence of rough surfaces on hydrodynamic regimes is described, because of the big relevance to the focus of this work.

According to the present work, which is based on numerical investigations, available numerical methods are presented in order to handle such tribological problems. A main issue is the modelling of fluid-structure-interactions (FSI) to describe the interaction between the lubricant and the solid bodies in coupled numerical models.

In the last two subsections, the research activities done in tribological systems are presented. These research activities are classified into experimental and numerical investigations. The experimental investigations include next to the sliding systems also friction systems. The numerical investigations are subdivided into friction and different types of wear.

2.1 Basics of product development process

„Product development is an endeavor comprised of the myriad, multi-functional activities done between defining a technology or market opportunity and starting production (Browning, Fricke & Negele, 2006). Following Albers (2011a), product engineering includes the development of the production system and the production process as well as all other activities throughout the product lifecycle such as sales or decommission that have a big impact on product development. There are several

process models known, to describe product engineering challenges (Albers & Braun, 2011a). The mentioned models are for example the German guideline 'VDI-Richtlinie 2221 (Verein Deutscher Ingenieure, 1993), the stage-gate-model by Cooper (1994), the V-model of the further German guideline 'VDI-Richtlinie 2206 (Verein Deutscher Ingenieure, 2004) and the process model by Gausemeier, Hahn, Kespohl and Seifert (2006).

These process models are often adapted to specific tasks in industry, but they have all certain disadvantages in common (Albers & Braun, 2011a). Their major limitation is the inadequate capability in handling complexity. In context of globalization, product engineering takes increasingly place in distributed locations and with an intensive exchange of information. The increasing cost and time pressure, as well as the trend towards individualized buyer markets, are also increasing complexity. Short-term changes in the product development process must also be responded more quickly. These factors are often not handled by the most process models.

Prescriptive models, which rigidly state sequential development steps, lead to the fact that the process iterations, which are customary in practice, cannot be considered. As a consequence, the innovative power of the developers is diminished in favor of increased risk thinking. On the other hand, (Albers & Braun, 2011a) emphasize that too open or too far-defined models offer less help for the product developer. These models deliberately leave a broad scope for interpretation in order to cover as many eventualities as possible.

Often the models support only the view of the operating product developer or the management. However, to ensure successful product development, both parties must be considered and further the establishment of a consistent knowledge management has to be guaranteed.

The process model according to Albers (2011a) is an approach to take into account the above aspects in a consistent model. Due to the great relevance of process models for the modelling of product development processes, the integrated product engineering model (iPeM) is presented in detail below. Based on this, the Contact & Chanel Approach (C&C²-A) is presented in this chapter, which is used for system analysis and modeling. Furthermore, the product Generation Engineering (PGE) is introduced to describe the procedure of further developments based on a reference system.

2.1.1 Process Model of "KaSPro - Karlsruher Schule für Produktentwicklung"

The integrated product engineering model (iPeM) is a framework to ensure a successful product development in the view of the operating product developer and

the management and is an integral part of the institute's research for more than 15 years (Albers, Reiss, Bursac & Breitschuh, 2016). The main issues of the iPeM are presented in more detail below.

System Triple of Product Engineering The basis of the iPeM is the so-called system triple of product engineering. The product engineering process is described by means of three mutually interacting systems: the system of objectives, the operating system and the system of objects. The interaction of the system triple is shown in Figure 2-1.

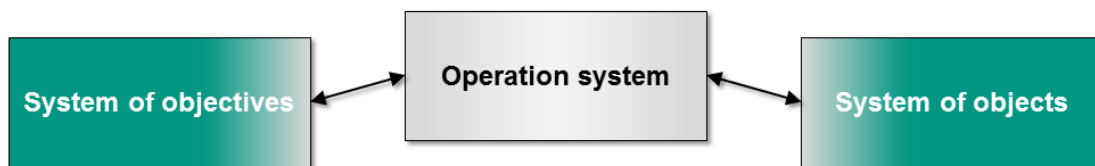


Figure 2-1: System triple of product engineering (Albers & Meboldt, 2007)

This system interaction can be traced back to Ropohl (2009), who understands product development as creation of technical systems (system of objectives) using appropriate measures (operating system) and under certain conditions (system of objects). In the view of this system understanding, Albers (2011b) give the following definitions for the interacting systems.

*“The **system of objectives** describes the mental anticipated and planned attributes of the system of objects and all information that is necessary for the process’ conduction. In addition to the relevant objectives for the product and the process, it also represents their interdependencies and boundary conditions.”*

*“The **operation system** is a socio-technical system that is composed of structured activities, methods and sub processes as well as resources for the realization (e.g. workforce, tools, workplaces, budget, knowledge etc.). The purpose of the operation system is to create both the system of objectives and the system of objects. For this, analysis as well as synthesis tasks apply alternately.”*

*“The **system of objects** contains all documents and items, representing solutions that correspond with the system of objectives. This includes marketable products but also any intermediate results of the engineering process, i.e. drawings, models, prototypes as well as project plans. These elements are linked to other elements within the system of objects or to respective objectives via the activities that produced them.”*

On the basis of these definitions, both the system of objectives and the system of objects are understood as dynamic systems, which are iteratively developed during product development (Albers & Braun, 2011b; Bursac, 2016). To develop the system

of objectives and the system of objects in a systematic way, different problem solving methods can be used. For this purpose, the problem solving method SPALTEN is presented below.

SPALTEN - Problem-Solving Process SPALTEN is a german acronym for a problem-solving process which means “to split” and further stands for a cycle of problem-solving activities in a specific structure and sequence (Albers, Reiss, Bursac & Richter, 2016):

- **S** - situation analysis
- **P** - problem containment
- **A** - alternative solutions
- **L** - selection of solution
- **T** - analysis of consequences
- **E** - deciding and implementation
- **N** - recapitulation and learning

The SPALTEN method is a universal approach and is not limited to special problems. Consequently, this method is suited equally for emergency situations and planning situations. SPALTEN is defined as a characteristic with fractal structure and is equivalent to the fact that every working step of the SPALTEN process can depict an own SPALTEN process. (Albers, Reiss, Bursac & Breitschuh, 2016)

Activities of Product Development In terms of system engineering, an overall problem can be separated into sub-problems which have to be solved during the engineering process and which represent a specific area of activity. These activities correspond with the life cycle of a product and within the certain activities, different information must be collected or generated for solving the overall problem. Although the alignment of the activities corresponds with the product lifecycle, the temporal execution of the problem-solving activities depends strongly on the specific situation in the individual design project. Due to the pronounced interactions of the activities, agile approaches are required to enable a parallel and iterative procedure in system engineering.

To assist product developer in agile processes, models are needed to take into account the described aspects of problem solving and system engineering. Such an approach, the integrated Product engineering Model (iPeM), is presented below.

iPeM – integrated Product engineering Model The temporal sequence of the activities in a product development process is depicted in a phase model. Once different activities are assigned to specific time intervals, they can be viewed as a phase with a certain duration. Phases are thus combined from several parallel activities, which is done dynamically and according to the requirements of the respective situation in project. In the phase model, three models are differentiated: reference, implementation and application model. The reference model describes generalized processes and time intervals. An implementation model is the specific planning of activities and resources. The application model is the actual course of a specific project. The comparison of the application and implementation model thus enables continuous monitoring of project progress (Albers, 2010; Albers & Meboldt, 2007; Braun, 2013).

The iPeM (c.f. Figure 2-2) is an approach that combines the above aspects system triple, problem solving process SPALTEN, activities of product development and phase model into a consistent model. It is a meta model, what means it has a generic character and contains all relevant elements for adapting to individual problems.

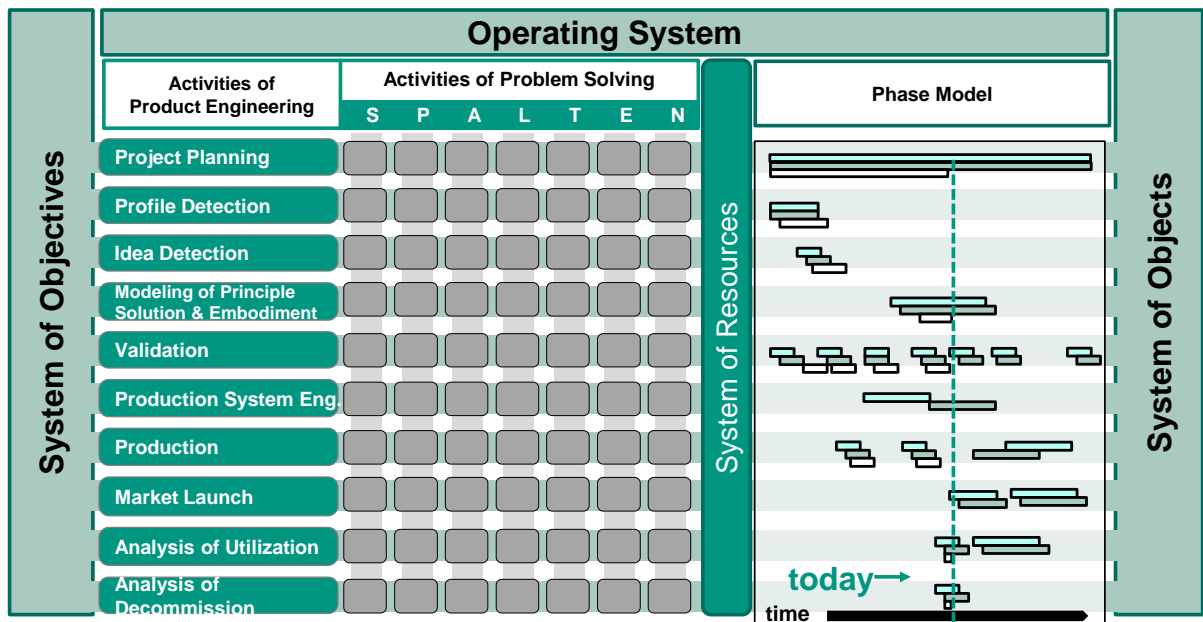


Figure 2-2: The integrated Product engineering Model (iPeM) (Albers, Reiss, Bursac & Richter, 2016)

Through the iPeM, the management can be supported in planning the product creation process in a dynamic phase model. On the other hand, the product developer can be supported at work, as the phase model is used to determine the further procedure and

the activity matrix is used to recommend the associated methods for successful product engineering (Albers, Reiss, Bursac, & Richter, 2016; Bursac, 2016).

2.1.2 Product Model – Contact, Channel and Connector Approach (C&C²-A)

Another type of models used in product engineering are product models. These serve as a communication basis and support the analysis of the object system to extend the knowledge base (Andreasen, 1994). Albers, Enkler & Ottnad (2011) presented that for the selection of adequate simulation methods and processes to fulfill the corresponding target system. The Contact, Channel and Connector Approach (C&C²-A) can support as a linking language between system of objectives, operating system and system of objects.

In the present work, C&C²-A is used, to identify relevant phenomena and interactions in the contact of a lubricated tribological system on the microscale level. With this product model, the shape can be linked with the corresponding functions and thus the modelling can be significant simplified. The main elements of the C&C²-A model are channel and support structures (CSS), which denote permanently or occasionally interacting physical structures of solid bodies, liquids, gases or fields, working surface pairs (WSP), which represent interfaces between these physical structures and connectors (C) modelling elements, which represent the “effect” and the state properties of the environment that is relevant for the function of a system. These elements are exemplary shown on the demonstrator of a multi-disc clutch in Figure 2-3.

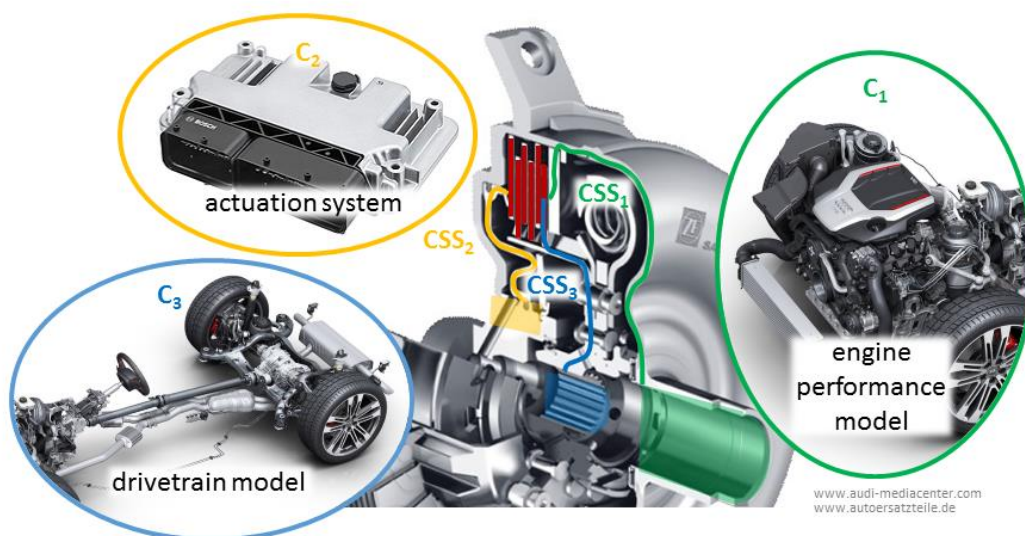


Figure 2-3: C&C²-A model, including an effect network and corresponding detailed physical structure of a multi-disc clutch (Albers & Wintergerst, 2014)

The initial modelling effort for model-based analysis methods and synthesis methods, which in contrast to purely function-based models integrates both function and shape aspects of technical system, is generally higher (Albers & Wintergerst, 2014). To justify this, these models and associated modeling methods must be both optimized and further developed for multiple reuse. The development of a WSP in the C&C²-A model, based on a reference system model is exemplarily shown in Figure 2-4.

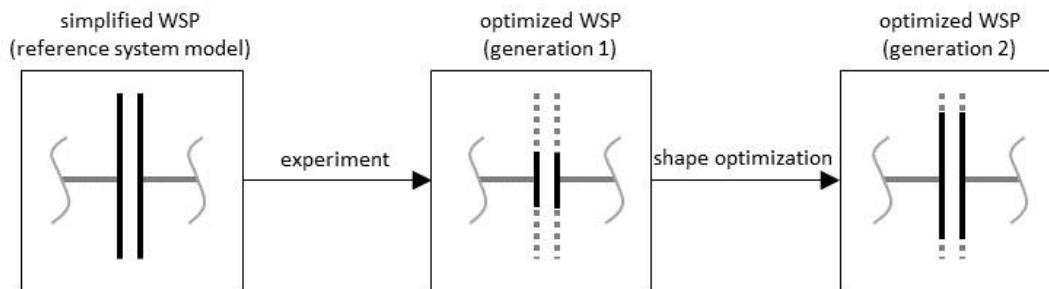


Figure 2-4: Development of a WSP (Albers, Gladysz, Kniel, Aschoff & Meyer, 2016)

The reuse of existing knowledge in form of reference system models and technologies (Albers, Matthiesen, Bursac, Moeser & Luedcke, 2015) from previous product generations for the development of subsequent product generations, is a core aspect of the PGE – Product generation Engineering according to Albers, Bursac & Wintergerst (2015). The PGE is described in detail in the next section.

2.1.3 PGE-Product Generation Engineering

The development of new products on the basis of a reference system results in an imbalance in the number of subsystems that have to be newly developed because of economic reasons and minimizing risk while at the same time developing a product as innovative as possible with good performance and fascination requirements (Albers, Bursac, Urbanec & Rachenkova, 2014). In order to resolve this target conflict, Albers, Matthiesen et al. (2015) introduced the approach of PGE – Product Generation Engineering and gives the following definition (Albers, Matthiesen et al., 2015):

“Product generation engineering is understood to be the development of a new generation of technical products by both a specific carryover variation (CV) and new development of partial systems. The shapes of new technical developments of individual functional units result from the activity of embodiment variation (EV) and the variation of solution principles, hereinafter referred to as the activity of principle variation (PV). New product generations are always based on a reference product that defines large parts of the basic structure.”

The reference system describes a starting point on which the development of the next product generation builds up and is defined as follows (Albers, Rapp et al., 2019):

*“The **reference system** for the development of a new product generation is a system whose elements originate from already existing or already planned socio-technical systems and the associated documentation and are the basis and starting point for the development of the new product generation.”*

By means of reference products, information and individual subsystems can be reused in the development of new product generations. It should be tried to incorporate basic attributes with as little variation as possible into new product generations and, at the same time, the available resources should be used to develop new performance and fascinating attributes as differentiating features. Several new development shares of partial systems of a product can be distinguished in a new product generation (Albers, Matthiesen et al., 2015).

- *“New development of a partial system of a product generation by **principle variation (PV)**, e.g. by adaptation from products having similar functions and properties in other contexts or by the systematic search for alternative solution principles using e.g. construction catalogs or creativity techniques.”*
- *“New development of a partial system by **embodiment variation (EV)**, with a known (and established) solution principle being carried over from a reference product or the general state of the art and the function-determining properties being varied to enhance the competitiveness, performance, and/or quality of fulfilling the function. Shape variation represents the most frequent activity of product development and a highly creative and complex process. An example is the enormous increase in the power density of gear drives by an optimization of flank geometry, material, state of the material, production process, and lubrication.”*
- *“**Carryover variation (CV)** of partial systems, i.e. existing solutions of reference products or component suppliers are transferred to new product generations. This activity shall hereinafter be referred to as CV and also has to be planned and controlled. Constructive adaptations are to be minimized, if possible.”*

The most important relationships of product generation engineering can also be represented by mathematical models. A new product generation (G_n) consists of a set of partial systems that are carried over (CS), a set of newly developed partial systems by embodiment variation (ES) and a set of newly developed partial systems by principle variation (PS) (Albers, Bursac et al., 2015):

$$G_n = CS_n \cup ES_n \cup PS_n \quad (2-1)$$

The single shares δ of a new generation are defined as:

$$\delta_{EVn} = \frac{|ES_n|}{|CS_n \cup ES_n \cup PS_n|} \tag{2-2}$$

$$\delta_{SVn} = \frac{|CS_n|}{|CS_n \cup ES_n \cup PS_n|} \tag{2-3}$$

$$\delta_{PVn} = \frac{|PS_n|}{|CS_n \cup ES_n \cup PS_n|} \tag{2-4}$$

In context of PGE, the integrated Product engineering Model (iPeM), introduced above in section 2.1.1, is also adapted to the modular design. Therefore, different layers like product generations, validation system, production system and strategy are added. The modular integrated Product engineering Model (iPeM) in the context of PGE is shown in Figure 2-5.

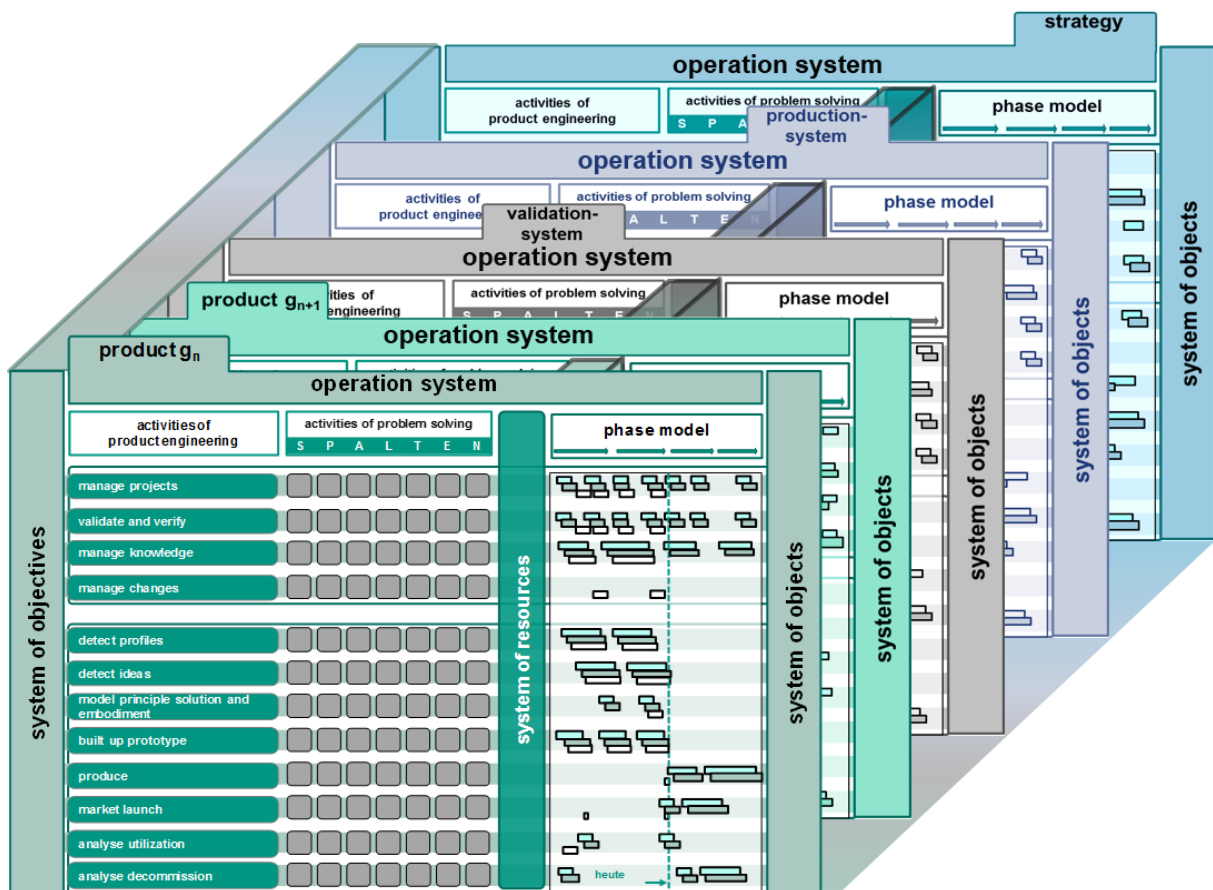


Figure 2-5: The integrated Product engineering Model (iPeM) in the context of PGE (Albers, Reiss, Bursac & Richter, 2016)

In this extended model, each layer consists of the same structure and the activities can be applied to each of these layers and modified with regard to the specific view. Following Albers, Behrendt, Klingler, Reiß & Bursac (2017), this structure enables a focused approach to the respective system in development with a simultaneous integration of the other layers. The interaction of the different layers can be shown in the connection of the layer “validation system” and the layer “product”. In the layer “validation system”, methods and models are developed to enable the validation of the developed product from the layer “product.” For example, to investigate journal bearings in a physical way, a test bench has to be planed, designed and validated as well. The layer “validation system” should not be distinguished from the basic activity “validation and verification” but provides the resources as a result.

The fact that products are developed in practice on the basis of reference products have already be shown in numerous practical examples. In the case of several generations of the dual mass flywheel, Albers, Bursac & Rapp (2017) explained the reasons for different variations in the transition between individual generations and the consequences and challenges of the development process.

2.2 Technical surfaces

Tribological technical surfaces are often perceived as ideally smooth in macroscopic applications. But on the microscopic scale, these surfaces show wide variations in form, waviness and roughness, resulting from different manufacturing processes. To evaluate these surface deviations, there are various measurements and test methods in surface metrology. Especially non-destructive optical measurements provide efficient results for the specification of technical surfaces.

2.2.1 Surface topography

Dependent on the wavelength of a technical surface, each measured profile, also called primary profile, can be classified in different surface deviations. In the primary profile, there are both short-wave (roughness) and long-wave (waviness) deviations combined. According to the international norm DIN EN ISO 4287 (Europäisches Komitee für Normung, 1998) the definitions and key parameter are specified, for describing the surface topography. Each rough surface can be separated into the following different classes:

- Form profile
- Waviness profile
- Roughness profile

- Atomistic roughness

As the smallest investigated scale is the microscopic scale in this work, deviations in microstructure and lattice structure are not mentioned any further. In the context of this work the different profile resolution are the macro-scale (form), the meso-scale (waviness) and the micro-scale (roughness).

Because there is no precise definition for the transition from roughness to waviness, the cut-off wavelength λ_c was introduced. The cut-off length of a profile filter is the wavelength at which the filter reduces the amplitude of a sine wave to 50 % (Volk, 2013).

In order to be able to determine the profile, roughness and waviness parameters, different filters must be applied to the measured primary profile. Low pass filter that provide low frequencies are applied to the form profile. In the case of a high pass filter, the high frequencies are filtered and the roughness can be determined accordingly. As an example, the transfer characteristic for the profiles is shown in Figure 2-6. The wavelength is plotted on the X-axis, the percentage transmission of the corresponding filter on the Y-axis.

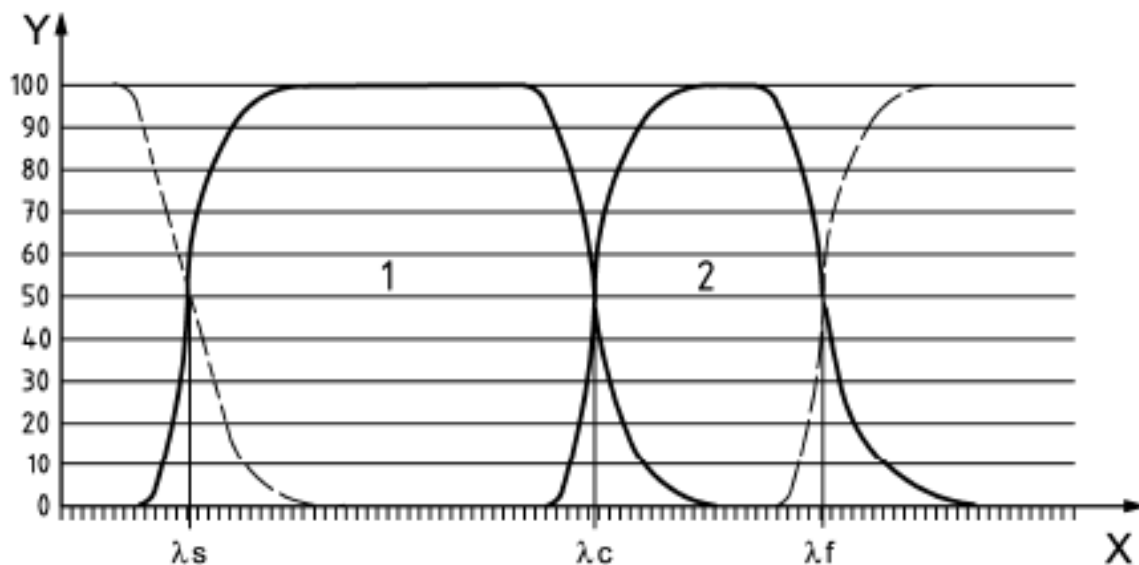


Figure 2-6: Transfer characteristic of the roughness and waviness profiles (Europäisches Komitee für Normung, 1998)

The high pass filter of the primary profile with the cut-off wavelength λ_c yields the roughness profile. In this filter, the long wave profile deviations are separated. The parameters of the roughness profile are evaluated over the measuring distance ln according to the Geometrical Product Specifications (GPS) (Europäisches Komitee für Normung, 1996b). The waviness profile is obtained by low pass filtering of the primary

profile with the cut-off wavelength λ_c and by high pass filtering with the cut-off wavelength λ_f . The relationship between the wavelengths λ_c and λ_f and the measuring distance ln is defined in DIN ISO 12085 (Europäisches Komitee für Normung, 1996a) and is shown in Table 2-1.

Table 2-1: Relationship between the wavelengths and the measuring distance (Europäisches Komitee für Normung, 1996a)

λ_c [mm]	λ_f [mm]	Measuring distance [mm]
0,02	0,1	0,64
0,1	0,5	3,2
0,5	2,5	16
2,5	12,5	80

After the low pass filtering of the measured values with the cut-off wavelength λ_s , the primary profile is obtained, the short wave components being separated off. Already during the measurement of the actual surface profile, the detected profile is filtered by the radius of the probes tip. The relationship between the wavelengths and the tip radius is shown in Table 2-2.

Table 2-2: Relationship between the wavelengths and the tip radius (Europäisches Komitee für Normung, 1996b)

λ_c [mm]	λ_s [μm]	λ_c/λ_s	r_{tip} [μm]
0,08	2,5	30	2
0,25	2,5	100	2
0,8	2,5	300	2
2,5	8	300	5
8	25	300	10

2.2.2 Characterization of surface topography by statistical parameters

According to Bhushan (2002), surfaces can be divided into different categories. Deterministic surface structures can be divided by simple analytical and empirical models. However, most of the technical surfaces are highly randomized due to manufacturing processes and can be characterized as isotropic and anisotropic or as

Gaussian distributed and non-Gaussian distributed. Manufacturing processes with a geometrically determined cutting edge (turning, bumping, planing) and a geometrically undefined cutting edge (grinding and planing) generally produce an anisotropic, non-Gaussian surface.

By calculating a single roughness parameter, a measured surface profile is significantly simplified. From a profile, the roughness parameter can always be clearly defined. However, the measured profile cannot be derived from a single characteristic. This operation is consequently not possible. For a holistic description of technical surfaces, it is thus always desirable to have several characteristic values which are determined from the measured points.

The surface characteristics to describe the profile, waviness and roughness can be derived into vertical and horizontal dimensions according to DIN EN ISO 4287 (Europäisches Komitee für Normung, 1998).

- Vertical parameters: maximum peak height (Index p), maximum pit height (v), profile amplitude (t), mean deviation of the profile (a), square mean value of the ordinate values (q), skewness (sk) and Kurtosis (ku)
- Horizontal parameters: mean groove width (Index Sm) and peak counting parameters (Pc)

The vertical parameters are often used to describe technical surface profiles. The roughness values can be calculated both for a profile and for a surface. Figure 2-7 shows an overview of the parameters.

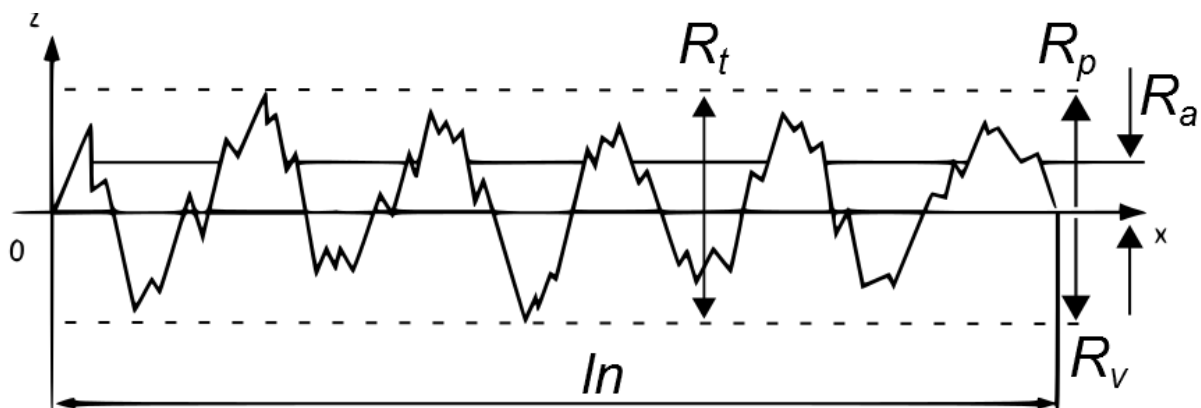


Figure 2-7: Vertical roughness parameters

- Mean roughness profile m :

$$m = \frac{1}{l_n} \int_0^{l_n} z(x) dx \quad (2-5)$$

- Arithmetical mean height R_a :

$$R_a = \frac{1}{\ln} \int_0^{\ln} |z(x) - m| dx \quad (2-6)$$

- Root mean square height R_q :

$$R_q = \sqrt{\frac{1}{\ln} \int_0^{\ln} z(x)^2 dx} \quad (2-7)$$

- Maximum peak height R_p :

$$R_p = \max(z(x)) - m \quad (2-8)$$

- Maximum pit height R_v :

$$R_v = |m - \min(z(x))| \quad (2-9)$$

- Skewness sk :

$$R_{sk} = \frac{1}{\sigma^3 \cdot \ln} \int_0^{\ln} (z(x) - m)^3 dx \quad (2-10)$$

- Kurtosis ku :

$$R_{ku} = \frac{1}{\sigma^4 \cdot \ln} \int_0^{\ln} (z(x) - m)^4 dx \quad (2-11)$$

- With the normalized variance σ :

$$\sigma^2 = \frac{1}{\ln} \int_0^{\ln} (z(x) - m)^2 dx \quad (2-12)$$

- Average surface roughness R_z :

$$R_z = \frac{1}{5} \int_1^5 z(x) dx \quad (2-13)$$

The above-described roughness characteristics allow a relative roughness evaluation based on the mean roughness line in the vertical direction. However, a statement about

the form, slope and size of the asperities is not possible. Since different roughness profiles can have the same roughness characteristics, Abbott and Firestone introduced a method for determining the material ratio $R_{mr}(c)$ in dependence to cutting level c . The material ratio is calculated from the sum of the single partial slices $MI_n(c)$, divided by the length of the entire measuring distance. Figure 2-8 shows the procedure for an arbitrary cutting depth c .

When the Abbott-Firestone-Curve is determined, the highest peaks (typically 5 %) are removed, since they cannot absorb contact forces during the loading.

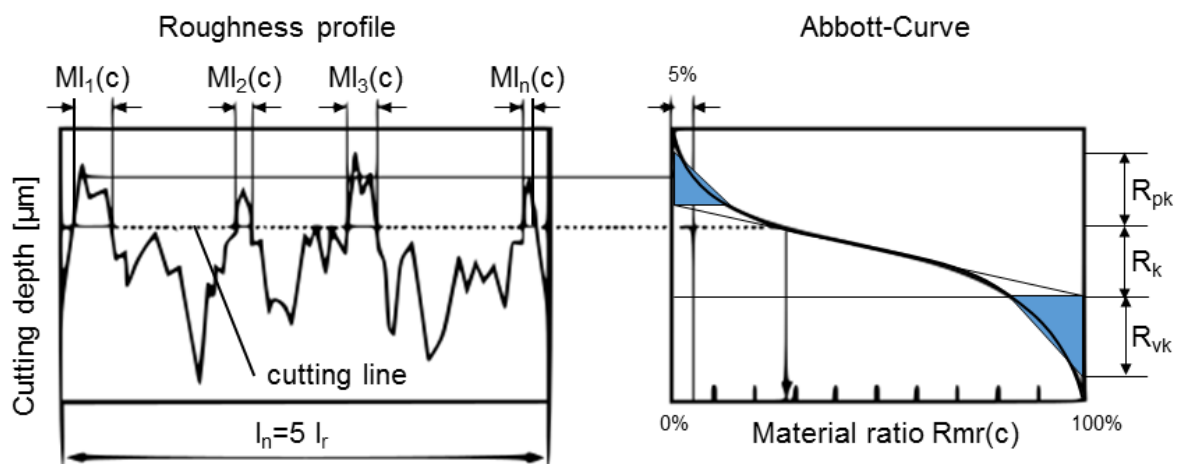


Figure 2-8: Abbott-Firestone-Curve (Volk, 2013)

Typical parameters that are used in combination with the Abbott-Firestone-Curve are the core roughness R_k , the reduced peak height R_{pk} and the reduced valley depth R_{vk} also shown in Figure 2-8. These parameters allow the separate assessment of core area, peak area and valley area, which have different significance for the functional behavior of the surfaces (Volk, 2013).

2.2.3 Surface metrology

There are different possibilities for measuring and evaluating the surface topography. The evaluation of the surfaces ranges from simple comparison patterns to touching and non-contact measurement devices. The most widely used measuring method in industry is the contacting profile method. A feed device moves a probe tip perpendicular to the groove direction over the surface of the work piece. The vertical stroke of the probe tip is converted into an electrical signal and evaluated by a control unit. A common method for non-contact measurement of surfaces is the white light sensor. Non-contact sensors are mainly used where surface contact is undesirable. Soft materials such as gold, copper or aluminum are, for example, materials which can be damaged by a probe tip. The measurement of softer materials, such as rubber,

silicone or textiles, where the surfaces can be flattened, is equally problematic. Such a device was also used for the measurement of the technical surfaces, implemented into the friction and wear models in this work. Therefore, this method is described in more detail below.

Instead of a probe tip, a white light spot is focused on the work piece during the measurement and guided over the surface at a small distance. The principle of the sensor is shown in Figure 2-9.

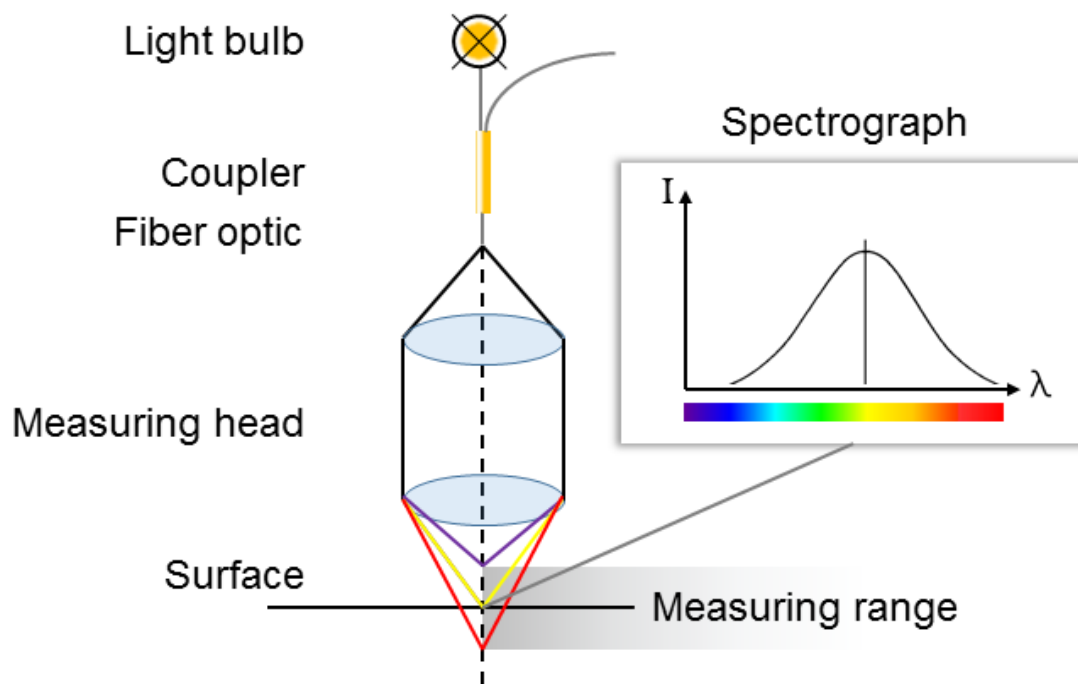


Figure 2-9: Principle of a white light sensor (Volk, 2013)

The lens used bundles the blue color portion more than the red one, which is why the focus of the blue light is closer to the lens than the focus of the red light. The vertical distance from the red to the blue focus determines the measuring range of the device. The light reflected on the surface is captured and imaged on a narrow aperture. Depending on the distance between the surface and the lens, it is possible for another color to pass through the aperture. The light fraction is determined by a spectrometer. This is a color measuring unit which determines the intensity for each color. With the known color property of the objective, it is possible to determine the distance of the emitted light from the objective.

2.2.4 Generation of rough surface profiles

To investigate the effects of surface roughness on the friction and wear behavior in lubricated tribological systems, digital surfaces are required which can be either measured from a rough surface or generated numerically. The digital surfaces can be implemented into computer aided engineering software.

Patir (1978) presented a method of generating three-dimensional random surface roughness with prescribed statistical properties by using correlation functions. This procedure is capable for generating Gaussian and non-Gaussian surfaces. Bakolas (2003) extended the method of the linear transformation of matrix, proposed by Patir (1978), by employing the non-linear Conjugate Gradient Method (CGM) and Fast Fourier Transformation (FFT). With this method, larger portions of the auto-correlation function (ACF) could be taken into account by minimizing the storage requirements and in order to achieve convergence. Wu (2000) developed also a numerical procedure for the simulation of three-dimensional surfaces based on FFT. With this method, surfaces with given ACF can be simulated. It could be shown that the average ACF of the profiles for the generated surfaces is correct.

Nowicki (2008) (Albers, Nowicki, & Enkler, 2006) generated virtual rough surfaces with desired properties by using evolutionary optimization methods. It could be shown, that the Abbott-Curve of the generated surface is nearly identical in comparison to the prescribed sample.

Savio (2010) created virtual surfaces based on measurements with a white-light interferometer. The measured data is exported as text-file containing the coordinates of each measured discretization point. The measured data was transferred into a solid body, because commercial CAE programs cannot import this type of data. The output file of the solid body is a neutral IGES format. This type of data-file can be implemented into various software. This method is also used in the present work, to create the solid bodies of the measured surfaces for the numerical investigations.

2.3 Friction

Friction is a motion resistance, expressing as a force between contacting surfaces against the initiation of a relative movement (static friction) or their maintenance (dynamic friction). In addition to this “outer friction”, there is the “internal friction” of substances (viscosity), which belongs to the rheology (Czichos & Habig, 2015).

The friction of a tribological system is described by different friction conditions, which are classified by the Stribeck-Curve, shown in Figure 2-10. These friction conditions are also used to classify wear and lubrication.

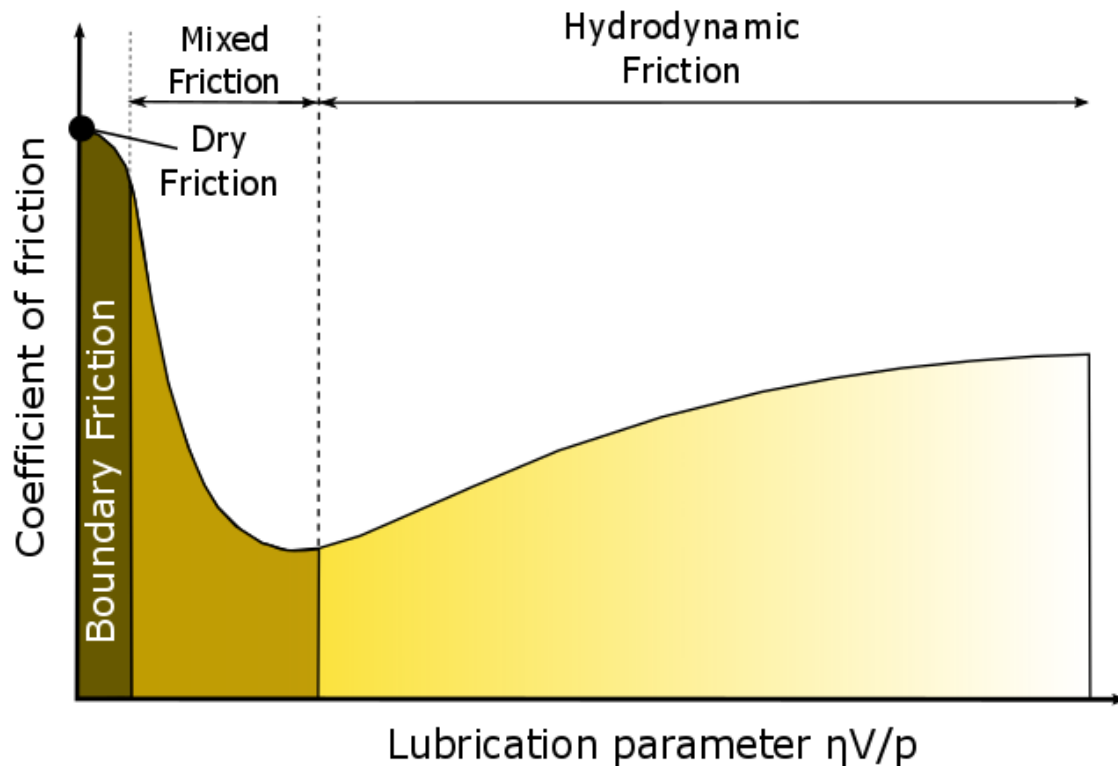


Figure 2-10: Friction conditions of a tribological system (Czichos & Habig, 2015)

Dry friction: Friction in direct contact of solid bodies. The lubrication gap trends to zero.

Boundary friction: Dry friction, in which the surfaces of the friction partners are covered with a molecular boundary layer film.

Mixed friction: Friction with coexistence of dry and hydrodynamic friction

Hydrodynamic friction: Friction in a tribological system, where the friction partners are completely separated by a lubrication film.

2.3.1 Tribological systems

Following the system theory, tribological systems can be subdivided into primary energy-, substance- and information-determined functional classes (Czichos & Habig, 2015). In the current work the focus is on energy-converting tribological systems. Such a system is present, for example, in journal and rolling bearings and joints and clutches.

Under the influence of tribological stresses, normal and tangential forces are present across the contact surfaces, causing irreversible processes in the boundary layer of the friction materials. These processes are influenced by numerous parameters that the tribological behavior can only be described as system-related behavior. Usually, there is no causal description possible due to the complex superimposed processes (Sommer, Heinz & Schöfer, 2014). Such a tribological system is schematically shown in Figure 2-11.

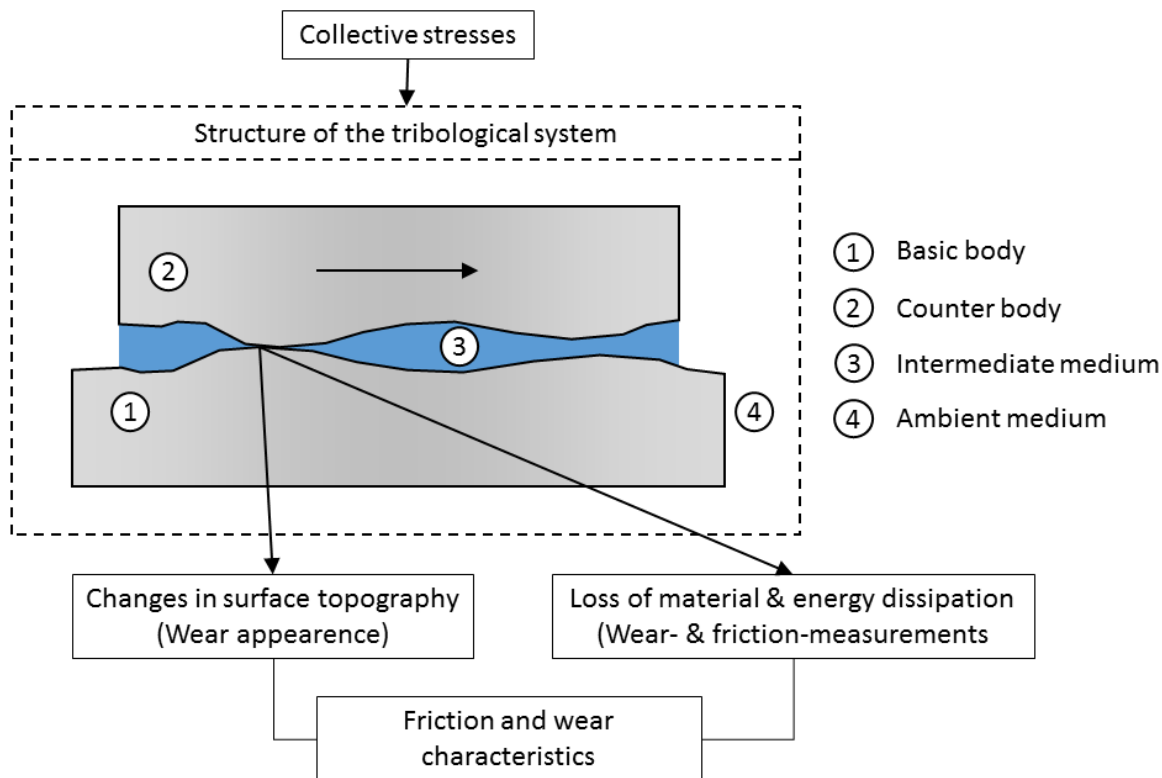


Figure 2-11: Schematic view of a tribological system (Deters, Fischer, Santer, & Stolz, 2002)

The material components of such a tribological system are referred as “system structure”. This consists of a basic and a counter body, which are moved relative to one another and an intermediate medium between the two bodies, which can be in the solid, liquid or gaseous aggregate state. Depending on the system boundary, the ambient medium can also be included in the consideration. External stresses, like the type of movement, the stresses and their course of time provide the collective stresses. Occurring wear, resulting from the load collective on the structure of the tribological system, is described by wear characteristics.

2.3.2 Friction measurements

Friction can be evaluated by force- or energy-based measured values. The measured values used in this work are described in detail below. The definitions are from the previous DIN 50281 (DIN German Institute for Standardization, 1977).

Friction Force F_R : Force which acts as a mechanical resistance to a (translational) movement as a result of friction and is opposed to the direction of movement. In this case, it is also possible to distinguish between the static friction force F_{RS} (without relative movement) and the dynamic friction force F_{Rd} (with relative movement).

Friction torque M_R : Torque which occurs as a resistance to a rotational relative movement as a result of friction.

Coefficient of friction $\mu = F_R/F_N$: Ratio of friction force F_R (parallel to the contact surface) and normal force F_N (perpendicular to the contact surface)

Friction work A_R for sliding: The (loss-) work to be carried out to maintain a movement process under friction:

$$A_R = \int_{s_R} F_R \cdot ds_R \quad (2-14)$$

with the sliding distance s_R .

Frictional energy P_R : The (loss) energy to be performed to maintain a motion process under friction, defined as instantaneous energy:

$$P_R = dA_R/dt \quad (2-15)$$

or mean energy:

$$P_R = \mu \cdot F_N \cdot v \quad (2-16)$$

with the sliding velocity v .

The friction is, by definition, an interaction of contacting bodies or substances. A friction measurement quantity therefore does not denote the property of a single body or a substance, but must always be based on the material pairing, which is generally the tribological system. In simplified symbolic form, the following applies for the friction measurement quantity (Czichos & Habig, 2015):

$$\text{friction measurement quantity} = f(\text{system structure, collective of stresses})$$

The system structure describes the bodies and substances, directly involved in the friction process as well as their relevant properties. The collective of stresses is defined by the kinematics, the normal force F_N , the sliding velocity v , the temperature T and the duration of the stresses t .

2.3.3 Microstructural friction mechanism

The representation of the friction measurement quantities has shown that each friction process has an energy expenditure. From the physical point of view, an energy balance can be considered through various individual processes of friction on the micro scale. Following Czichos (1971), the different phases of the energy balance can be illustrated in a simplified presentation. The overview about the energy balance of a friction process is shown in Figure 2-12.

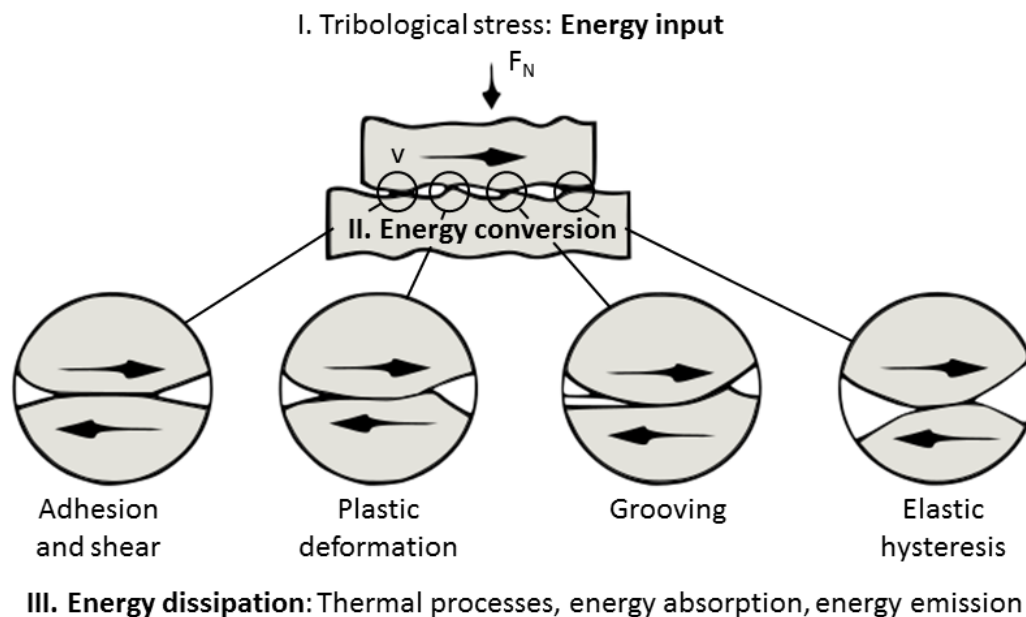


Figure 2-12: Energy balance of friction in a schematically simplified overview (Czichos & Habig, 2015)

In the case of a tribological system, the energy input (I) takes place by means of the respective tribological stresses. Single processes can be the interaction of technical surfaces, formation of the true contact surface, delamination of surface cover layers or interfacial bonding and energy.

The energy conversion (II) in tribological systems is caused by different friction mechanism. These occurring movement impeding and energy dissipating friction mechanism are called elementary processes of friction. As it can be seen in Figure 2-12, these processes are adhesion in relative motion, plastic deformations on the atomic- micro- and macro scale, grooving and elastic hysteresis. In this case, the micro contacts are distributed locally and temporally in a stochastic manner.

The energy dissipation (III) usually takes place by the generation of frictional heat in the contacting area, but can also be connected with energy emission processes.

The friction mechanism involved in energy conversion are described in more detail below.

Adhesion In general, adhesion is understood to mean all phenomena of molecular interactions in the contact surface of interacting materials (Bartel, 2010). If the friction partners move relatively, these bonds have to be separated and friction forces are initiated. The size of these bonding forces increases with the number of interacting atoms and with the reduction of the distance between the atoms. Adhesion is present in tribological systems with a relative movement between the intermediate medium and the solids and the boundary layer and the solids. In these interactions adhesion is

desirable, in contrast to the solid contact. Due to an intermediate medium in the solid contact of a tribological system, the adhesive forces can be reduced, but cannot be neglected.

The phenomena of adhesion can be defined following the principle of the Van der Waals forces, resulting from intermolecular attraction forces. The Van der Waals interaction forms the attractive interaction term in the Lennard-Jones potential, which indicates the interaction between uncharged, non-chemically bonded atoms. In Figure 2-13, the relation between the inter-atomic spacing and the potential energy is shown.

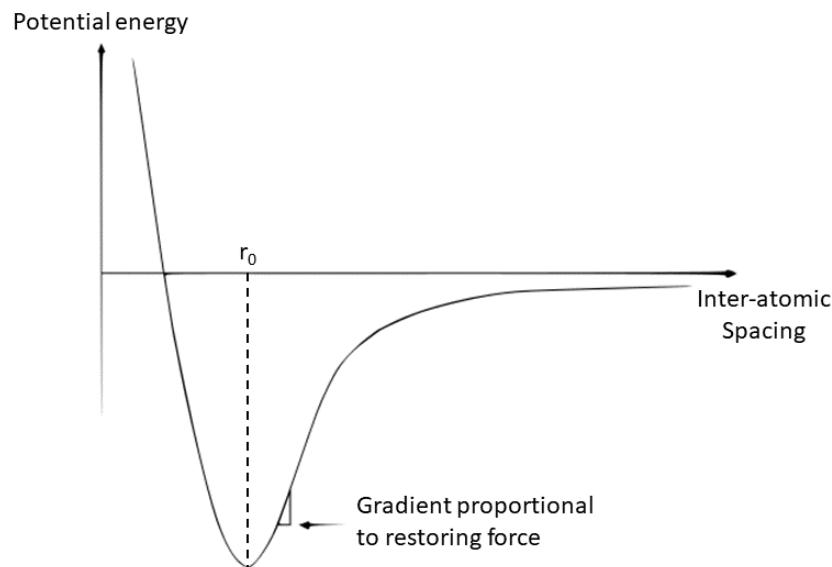


Figure 2-13: Lennard-Jones potential ("DoITPoMS - TLP Library The Stiffness of Rubber - Lennard-Jones potential")

At an average distance, the attracting forces dominate and the potential energy is clearly negative. With an increasing distance between the atoms, the attraction forces decrease.

A simple model for the adhesive components of solid friction of materials was provided by Bowden and Tabor (2001). The friction force F_R is calculated in dependence to the critical shear stress τ_{crit} and the real contact area A_r :

$$F_R = \tau_{crit} \cdot A_r \quad (2-17)$$

For a metallic friction partner under plastic contact deformations, the real contact area is defined as:

$$A_R = \frac{F_N}{P} \quad (2-18)$$

With the surface pressure P of the softer material. This formulation used in equation (2-17), the adhesive component of the coefficient of friction results in:

$$\mu = \frac{F_R}{F_N} = \frac{\tau_{crit}}{P} \quad (2-19)$$

The tangential component has the most important influence on friction resistance forces. A reasonable upper bond was also identified by Bowden and Tabor (2001). In this study, the critical shear stress limit τ_{crit} can be related to the smaller yield strength σ_{crit} of the interacting materials:

$$\tau_{crit} = \frac{\sigma_{crit}}{\sqrt{3}} \quad (2-20)$$

The assumption by Bowden and Tabor is that the critical yield stress is reached in the contact zone of the interacting bodies. Due to the neglect of tribochemical effects present in the boundary layer of the friction partners, the solids are treated as ideal at their contact zone.

To describe the normal component of the adhesion phenomena, the model by Bowden and Tabor was expanded by the interfacial energetic theory (Rabinowicz, 1995). The normal component rises the forces needed to initiate the relative sliding of the two bodies. For the description of the specific surface energy W , the surface energies $\gamma_{1,2}$ were introduced:

$$W = \gamma_1 + \gamma_2 - \gamma_{12} \quad (2-21)$$

γ_1 and γ_2 representing the surface energies of respective solids in contact and γ_{12} is the interfacial energy between the interacting surfaces. This description is only valid for ideal conditions like ideal smooth surface and atomic clean surfaces. The only experimental possibility for determining adhesion forces between two solid bodies under the loading with a normal force F_N is the measurement of the separation or adhesion force F_A required for their separation. The ratio of the adhesion force and the normal force is called coefficient of adhesion:

$$a_{adh} = \frac{F_A}{F_N} \quad (2-22)$$

Plastic Deformation If both materials of the friction partners have the same hardness, the deformation component will predominantly be characterized by a flattening of the roughness asperities. There are various theories to determine the proportion of the deformation component in the global coefficient of friction due to

plastic deformation at the asperity interactions. Green (1954) investigated the deformation of asperities under combined shear and pressure for ideal plastic metal junctions with the slip-line theory. Drescher (1959) developed a similar slip-line deformation model to determine the component of deformation of the coefficient of friction. In this model is assumed that in case of asperity contact, there are three different areas of plastic deformation. In Figure 2-14, the corresponding areas ABE, BED and BDC are shown.

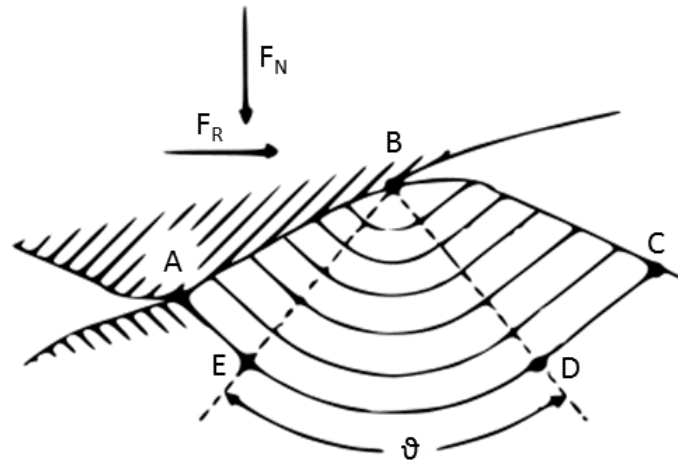


Figure 2-14: Model for the component of deformation in friction (Czichos & Habig, 2015)

The maximum shear stress in these areas is equal to the yield shear stress of the involved material. Following equation (2-23), a further important factor is λ_{def} which describes the amount of stresses, provoked by plastic deformation.

$$\mu_D = \lambda_{def} \cdot \tan \arcsin \left[\frac{\sqrt{2}}{4} \cdot \frac{(2 + \vartheta)}{(1 + \vartheta)} \right] \quad (2-23)$$

The factor λ_{def} is dependent on the ratio of the hardness and the young modulus of the contacting bodies. In relation to this model added Drescher (1959) that it is important to also to take into account the microstructure, hardening effects, thermal caused strain softening and the properties of the boundary layer.

Heilmann and Rigney (1981) developed a further approach to determine the component of deformation in friction. The friction losses are mainly attributed to plastic deformation. This approach is following formula (2-24):

$$\mu_D = \frac{A_r}{F_N} \cdot F \left(\frac{\tau_S}{\tau_{max}} \right) \quad (2-24)$$

With the maximum shear stress of the softer material τ_{max} and the mean shear stress τ_s in the sliding boundary layer. These shear stresses are depending on various experimental data like stress, sliding velocity and temperature and material properties like micro structure and hardening effects.

Grooving If the interacting materials have different hardness, the asperities of the harder material can penetrate the softer material. This phenomenon is resulting in a resistance of the material against grooving by the counter body in case of tangential displacement. There are two main types of grooving: due to the asperities of the counter body and due to wear particles in the contact area. In case of tangential movement of an ideal conical asperity, the coefficient of friction is dependent on the tilt angle θ of the asperity (Rabinowicz, 1995) as it can be seen in Figure 2-15.

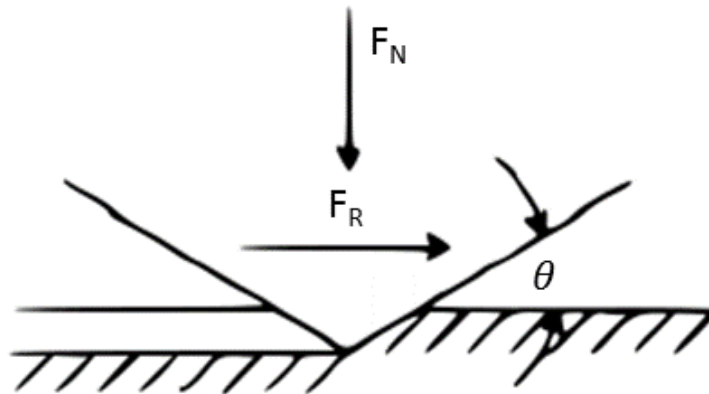


Figure 2-15: Component of grooving due to asperity interaction in friction (Czichos & Habig, 2015)

The resulting component of grooving is rather a limiting value due to the neglect of the pile-up effect, resulting in material accumulation in front of the grooving asperity. For brittle materials, Zum Gahr (1981) extended this approach by different material properties like fracture toughness, hardness and young modulus, to take into account micro-fracturing phenomena.

Sin, Saka and Suh (1979) investigated grooving due to wear particles in the contact area. It was pointed out that the component of grooving in friction is strongly dependent on the ratio of the radius of the particles r and the penetration depth d_{part} . This relation is shown in Figure 2-16.

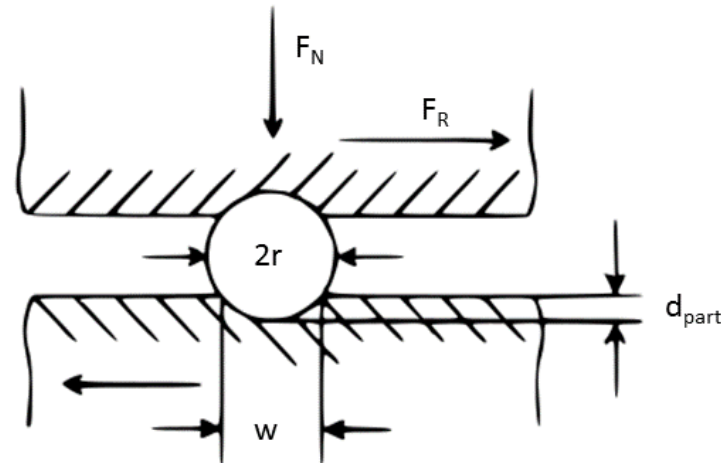


Figure 2-16: Component of grooving due to wear particles in friction (Czichos & Habig, 2015)

The application of this model has shown, that wear particles have an important influence on sliding friction. In the present work, wear particles are not taken into account since the calculation time is too high.

Elastic Hysteresis Due to the shearing of junctions as a result of adhesion effects at the surfaces, there is an energy dissipation in addition to deformation losses (Greenwood, Minshall & Tabor, 1961). The mechanical movement energy is transformed into a different energy form, which is mainly heat related. In addition to the frictional heat and associated mechanical vibrations in the friction partners, energy absorption and energy emission occur. During absorption, the friction mechanisms are related to the generation of lattice vibrations. In addition to the generation and transmission of electrical charges, sound emissions, photon emissions and ionic and electron emissions are also important in the energy emission.

2.3.4 Types of friction

In tribology, the friction is divided according to the kinematics of the application. Depending on the type of relative movement of the friction partners, the friction types are differentiated by sliding friction, rolling friction and drilling friction. The kinematics of the different types are shown in Figure 2-17 and are already investigated at the institute on the demonstrator of a CVT (Continuously Variable Transmission) chain – variator - contact by Albers, Behrendt & Ott (2006).

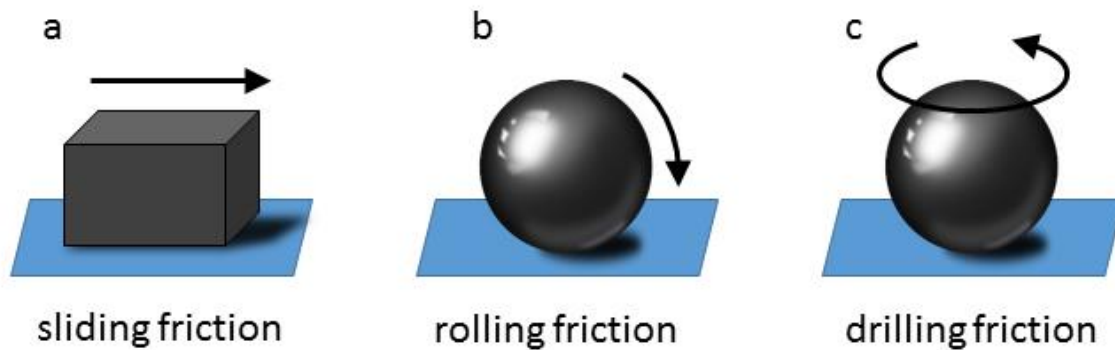


Figure 2-17: Types of motion between friction partners: **a** sliding friction, **b** rolling friction, **c** drilling friction

If two bodies experience a translator relative movement with different individual speeds or direction, a sliding movement is present, which is generally associated with sliding friction. A typical machine element, where sliding friction occurs is the journal bearing. This type of machine element is also the demonstrator in the present work.

If an axis of rotation is parallel to the contact surface and the movement direction is perpendicular to the axis of rotation, an ideal rolling movement occurs. Such a rolling movement is also associated with rolling friction. In the contact area of technical rolling movements, there is often micro-slip resulting from the superposition of normal and tangential forces. In the case of rolling movements, the friction resistance is significantly lower than the sliding resistance. The reason for this is the significantly lower shear stresses in the case of rolling friction.

In the case of a rotating body whose axis of rotation is perpendicular to the contact surface and in with only a rotation about this axis takes place, drilling movement and consequently drilling friction occurs. At the macroscopic scale, there is a steady state of the interacting surfaces. The drilling friction can be described phenomenologically as sliding friction with a velocity gradient of the contacting surfaces from the center of the axis of rotation in radial direction to the edge region of the contact. In technical application, the drilling friction occurs in jewel bearings (Czichos & Habig, 2015).

Next to this three main classifications of friction, there can be interferences in technical systems. For example, in rolling contact drives, a superposition of rolling and sliding friction is present. In cup bearings, there is a combination of sliding and drilling friction.

2.4 Wear

Following Czichos and Habig (2015), wear is the progressive loss of material from the surface of a solid body (basic body) caused by tribological stresses, i.e. contact and relative movement of a solid, liquid or gaseous counter body. A possible wear spectrum

of a basic body, characterized by the wear volume V_V divided by the Normal force F_N and the sliding distance s , is shown in Figure 2-18.

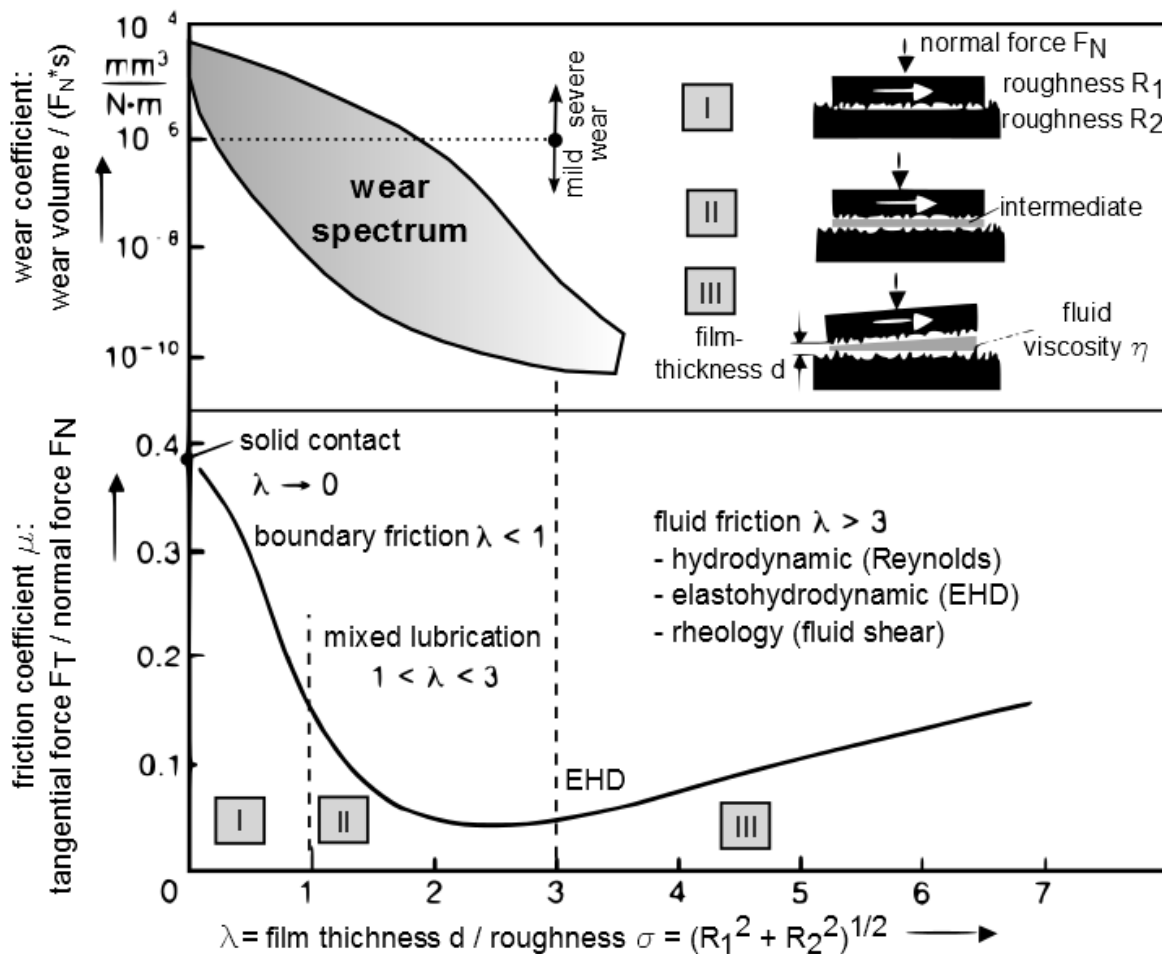


Figure 2-18: Wear spectrum by Czichos and Habig (2015 in Reichert, Lorentz, Heldmaier & Albers, 2016)

According to the wear spectrum, the wear coefficient k is used in friction conditions of dry-running and mixed lubrication, where solid interactions are present. The wear coefficient amounts to about 10^{-10} through $10^{-2} \text{ mm}^3/\text{Nm}$. The transition from mild wear to severe wear is defined for a wear coefficient of $10^{-6} \text{ mm}^3/\text{Nm}$. The wear coefficient depends on the whole tribological system and cannot be seen as a single material parameter. In general, the wear coefficient is obtained from experimental test, but there is some first research work (Albers & Reichert, 2017), to determine the wear coefficient by simulations.

Wear of materials leads to component damage and can cause a failure of the entire tribological or technical system. The temporal course of a wear process is often characterized by three phases. Such a typical wear depth curve is shown in Figure 2-19.

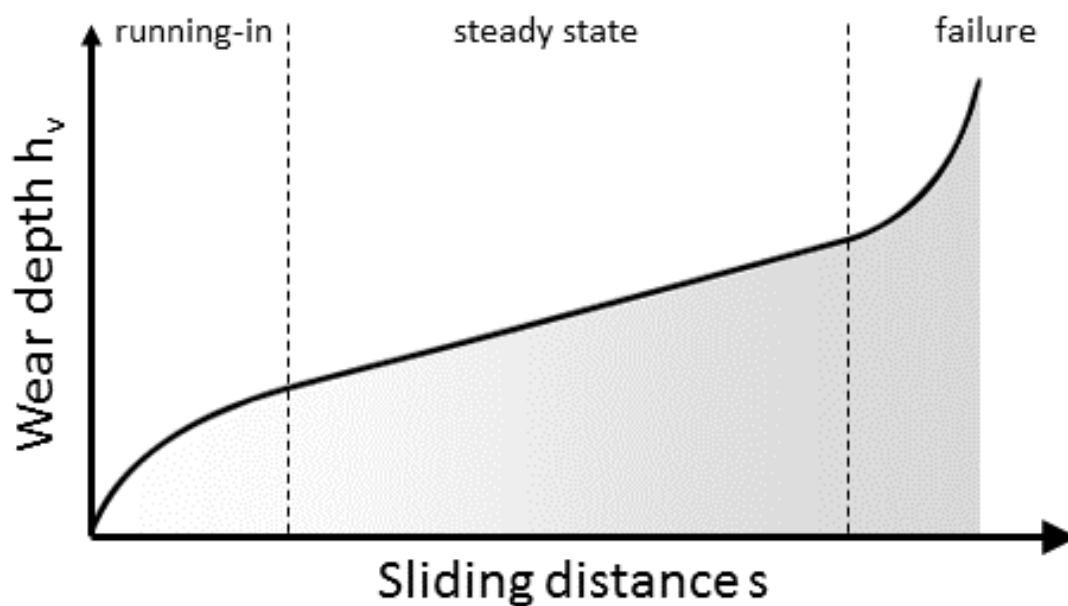


Figure 2-19: Three phases of a typical wear depth curve of a tribological system

While the running-in phase, a decreasing wear rate is identified. Next to the geometrical running-in process, which means the removal of the surface asperities, the material running-in process, which means a change in the monocrystalline boundary layer due to energy dissipation is present. An isolated investigation of these two phenomena is experimentally hardly possible. The decreasing wear rate can be explained with an increasing real contact area due to the removal of the surface asperities and consequently with a decreasing mean surface pressure. In the steady state phase, there is no significant change in the wear rate observed. In this case, there is no significant change of the surface topography because the ratio of normal load and real contact area remains constant. In the failure phase, the wear rate is clearly increasing, which in turn led to failure.

2.4.1 Wear measurements

When characterizing wear, a distinction between wear measurements and individual forms of wear is made. Wear measurements characterize the change in shape or mass of a body due to wear by measured values. Individual forms of wear describe the change of surface topography of tribologically stressed materials or components resulting from wear, as well as the type and shape of incidental wear particles.

Measured values of wear can be specified in different dimensions. The wear depth h_V is a one-dimensional change of the geometry and is usually recorded perpendicular to the contact surface. Wear surfaces A_V are two-dimensional changes of cross sections of tribologically stressed materials or components. Wear volume V_V is a three-dimensional change of geometrical areas or parts. The wear mass can also be

determined by the relation between the wear volume and the density of the worn material. Wear measurements can also be related to a reference value, which are called wear rates. For example, reference values can be the time or sliding distance.

As shown in Figure 2-18, the wear coefficient is often used in technical applications with different geometries, test times and stresses, to compare wear in a first approximation. The macroscopic wear coefficient k defines the the resulting wear volume V_V in relation to a constant normal load F_N and a certain sliding distance s :

$$k = \frac{V_V}{F_N \cdot s} \quad (2-25)$$

This coefficient does not include any statements on the wear mechanism. When using the wear coefficient to compare different measurements, care must be taken that the pressure, stress, temperature and friction regime are comparable. This wear measurement does not refer to the property of a single body or substance, but must be related to the whole tribological system:

$$\text{wear measurements} = f(\text{system structure, collective of stresses})$$

The wear coefficient can be determined in relation to the components of the tribological system (basic body and counter body) or in a system-dependent point of view, which means to sum of the wear measurements of the basic and counter body.

2.4.2 Microstructural wear mechanism

In this section, the wear mechanism on the microscale of a tribological contact are presented. These are physical and chemical interactions which lead to changes in material and shape. The mechanisms are both locally and temporally distributed on the surface asperities.

Following Czichos and Habig (2015), the fundamental mechanisms of contacting surfaces can be divided in force-, stress- and energy-driven interactions and in atomic and molecular interactions. The force-, stress- and energy-driven interactions lead to cracks and material separation and are characterized by fatigue and abrasive wear. The atomic and molecular interactions are attributed to the separation of chemical bonds in the contact area of surfaces. With participation of environmental medium and material separation processes, these mechanisms of wear are described by adhesion and corrosion. A survey of the different wear mechanisms and their manifestations is given in Figure 2-20.

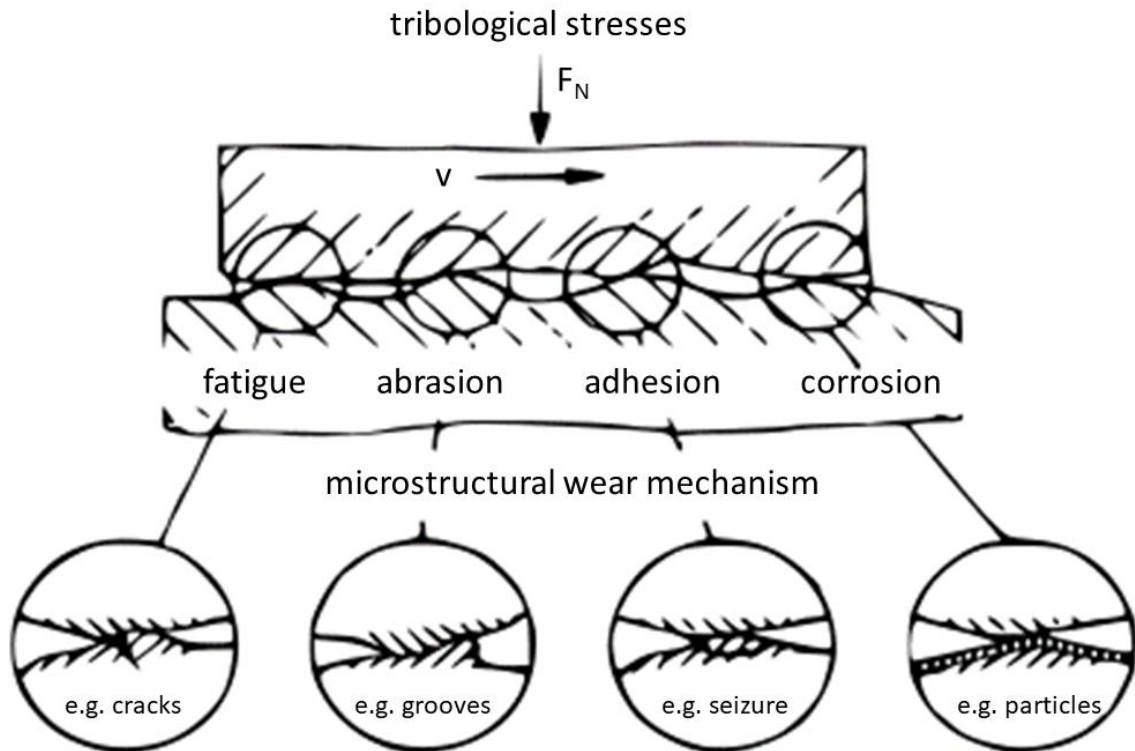


Figure 2-20: Wear mechanism on the microscale (Czichos & Habig, 2015)

The described mechanisms occur mostly superimposed. A single identification of a single wear mechanism is only possible with detailed analysis methods.

Fatigue wear At the contacting surfaces, there are contact forces, resulting from relative movement of the tribological partners. In regimes of boundary- and mixed-lubrication, these normal and tangential forces are transmitted by the surface asperities. In hydrodynamic lubrication, the forces are transferred via a separating lubrication gap. On account of periodic stresses of the micro contacts, there is an accumulation of damage, resulting in material fatigue. This type of wear is often observed in hertzian contacts such as rolling bearings or gears. With superimposed normal and tangential forces, stress maxima can occur below the surface, where cracks can be initiated. Modelling cracks with the FEM requires very small elements and a very high calculation time. Consequently, cracks are neglected in this work.

Abrasion If two contact partners differ in hardness and therefore the roughness peaks of the hard body, hard abrasive substances or separated hardened wear particles under load penetrate the softer solid and there is a relative movement, this is abrasion. Depending on ductile or brittle materials, micro-deformation and micro-cutting processes (for ductile materials) or micro-cracks (for brittle materials) occur. For brittle materials, the micro-deformation and micro-cutting processes are negligible. Rabinowicz (1995) developed the following model to determine the volume loss due to the isolated phenomena of metal cutting:

$$V_V = k_{ab} \cdot \frac{F_N \cdot s}{H} \quad (2-26)$$

The abrasive wear factor k_{ab} is dependent on the geometry of the abrasive particle, causing the cross section of the groove and the probability of a break off of the particle. A more accurate approach to take into account the deformation ratio next to the cutting ratio was established by Zum Gahr (1987):

$$f_{ab} = \frac{A_v - (A_1 + A_2)}{A_v} \quad (2-27)$$

The proportions of the different areas are shown in Figure 2-21 and are determined by microscopic analyses.

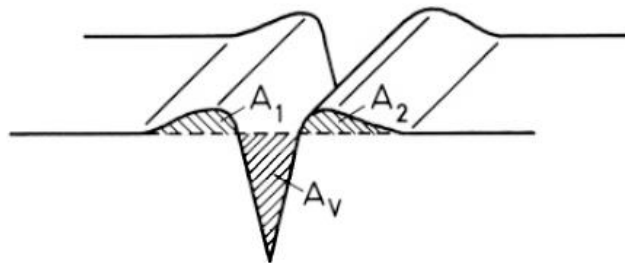


Figure 2-21: Area proportion for the abrasive processes deformation and cutting

For an abrasion factor $f_{ab} = 0$, there is only a deformation ratio and for $f_{ab} = 1$, there is only a cutting ratio due to abrasion. The volume loss for ductile materials can be calculated with the equation:

$$V_V = f_{ab} \cdot A_v \cdot s \quad (2-28)$$

The volume loss provoked by hard abrasive substances is dependent by the kinematic of the particle and it's sliding distance. If the particles are in a bounded or in loose form, is the main difference. Bounded particles ensure the longest sliding distance. In comparison if the particles are in a loose configuration, there are also rolling movements, resulting in a smaller sliding distance and less volume loss. Abrasion due to bounded particles is called two body abrasive wear in comparison to particles in a loose configuration, which is called three body abrasive wear. A further main characteristic for abrasive wear is the hardness ratio of the basic and counter body.

To describe abrasive wear with the FEM, very small elements are required. In a first study, (Reichert, Lorentz, Heldmaier et al., 2016) modelled the formation of wear particles under a sliding movement and non-lubricated conditions with the Johnson-Cook Damage model (Johnson & Cook, 1985). Particles arise, if the finite elements

around other elements are deleted and consequently lose the contact to the solid body. The elements are deleted in relation to strain, strain rate, temperature and pressure in course of a load. The main problem was that there is no interaction of the wear particles with the solid bodies and the calculation time is very high.

Adhesion In contrast to fatigue and abrasion, the wear mechanism adhesion is mainly based on material interactions between the contacting surfaces at the atomic and molecular level. At the roughness asperities, protective surface layers like an adsorption or reaction layer brake due to normal and shear stresses in the contact zone. The metal-bare areas assume local interface bonds which may have a higher strength than the initial material. For similar metallic materials of the tribological systems, the bonds can be more pronounced than for material-specific different friction partners. The strength of the interface bonds decides whether the separation takes place in the bonding level or in the material of one of the two solids (Sommer et al., 2014). If the separation takes place in the material, this leads to material transfer and consequently to adhesive wear. Adhesion is also composed of different individual processes, which in a simplified manner are characterized by Czichos & Habig (2015) as following:

- Deformation of surface asperities and normal and shear stresses
- Destruction of surface layers (especially oxide layers of metallic contact partners)
- Formation of adhesive surface bonds
- Destruction of adhesive surface bonds and material transfer
- Modification of transferring material fragments
- Separation of transferred or retransmitted material fragments in form of particles

A simplified modelling of adhesive wear is shown in Figure 2-22.

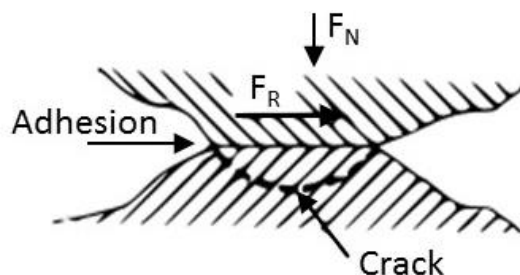


Figure 2-22: Simplified modelling of adhesive wear

For the description of adhesive wear, Archard (1953) determined the resulting volume loss V_V in dependence of the wear coefficient K , the normal load F_N , the sliding distance s and the hardness H of the softer material:

$$V_V = K \cdot \frac{F_N \cdot s}{H} \quad (2-29)$$

The wear coefficient K depends on the whole tribological system and is obtained in general from experimental investigations. Within the framework of the research contents of this work, a first approach of (Reichert, Lorentz, Heldmaier et al., 2016) was developed, to calculate the wear coefficient with the Johnson-Cook damage model (cf. abrasion) using the FEM.

Corrosion Tribochemical reactions result from chemical processes between solid bodies, lubricant and ambient medium, provoked by tribological stresses. Due to thermal and mechanical activation, there is a higher reactivity in the contact area and consequently new reaction products were build and removed. The chemical interactions in the boundary layer of a tribological systems cannot taken into account in a FEM analyses. The atomic and molecular interactions are on a nanoscale level and numerical investigations are carried out with molecular dynamic simulations.

2.4.3 Types of wear

Compared to the classification of friction (cf. 2.3.4) also different types of wear can be described in dependence to the kinematic relations of the basic and the counter body. In all types of wear, the described wear mechanism (cf. 2.4.2) can occur in different proportions. The main types of wear are:

- sliding wear
- rolling wear
- impact wear
- fretting wear

The main focus of the present work is wear simulation of sliding system. For this reason, in the following section, the mechanisms of sliding wear are described. The other types of wear are not discussed in detail, here.

Sliding wear is the result of different wear mechanisms under a relative sliding movement of the tribological partners. Sliding wear always occur in combination with sliding friction and the associated thermal processes. Further, all microstructural wear mechanism, described in section 2.4.2, can be present. The intensity of single wear mechanisms can only be determined from the appearance of the resulting wear track on the surface of a friction partner. In general, the wear processes in a sliding system can always be superimposed locally and temporal. A precise statement regarding the occurrence of a certain wear mechanism is thus not always clearly possible.

Sliding wear always provokes variations in the boundary layer of a friction partner. Due to thermal and mechanical stresses, there are microstructural changes in the material. Different layers of a friction material resulting from chemical and mechanical stresses are shown in Figure 2-23. The changes in the boundary layer are also called third body.

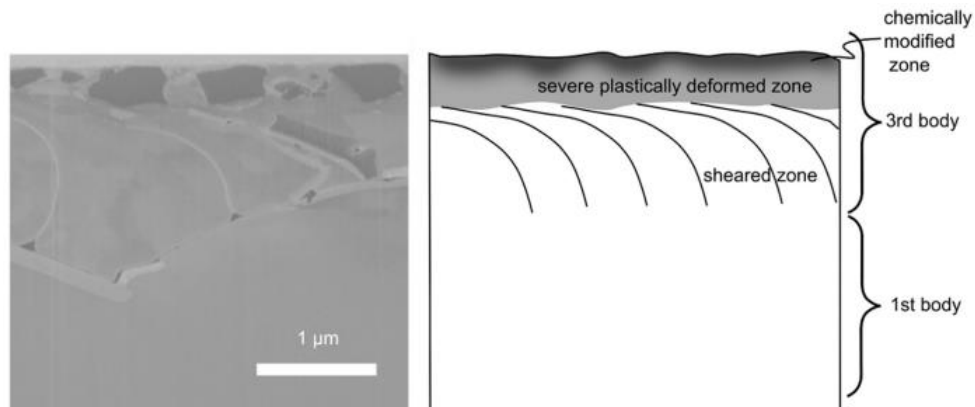


Figure 2-23: Schematic of the third body. Scanning electron microscope (SEM) image of a cross section in a worn surface on the left (Linsler, Schröckert, & Scherge, 2016).

The worn surface is resulting from investigations on a pin-on-disc device. Clear to see is the mechanical modification due to shear in the sheared zone and the microstructural changes due to chemical modifications in the severe plastically deformed zone.

2.5 Fluid mechanics theory

Next to the occurring phenomena in sliding systems due to solid contact, the fluid mechanics in tribological systems are described below. After the basics of the fluid mechanics theory, the influence of rough surfaces on hydrodynamic regimes is described. This is an important issue because of the big relevance to the focus of this work: the influence of rough surfaces in mixed-lubricated regimes.

If the solid bodies of a tribological system are completely divided by a fluid film, the fluid mechanics are very important to describe the phenomena occurring in the lubrication gap for laminar and turbulent flows. The conservation equations describe such flows completely and are presented below. Because of the better mathematical clarity, the equations are given in differential form.

2.5.1 Mathematical description of flow

Claude Navier and George Gabriel Stokes described fluid flow while preserving mass, momentum and energy. The first equation describes the conservation of mass. An infinitesimal volume element V in the Cartesian coordinate system is thereby recorded. The conservation of mass results in:

$$\frac{\partial \rho}{\partial t} + \vec{\nabla} \cdot (\rho \vec{v}) = 0 \quad (2-30)$$

With the fluid density ρ and the flow velocity vector \vec{v} . The conservation of mass states that within a volume element V the change over time in the density ρ and the change in the mass flow ($\rho \vec{v}$) in the respective spatial direction is equal to zero.

The momentum equation must be fulfilled for all spatial directions:

$$\frac{\partial(\rho \vec{v})}{\partial t} + \vec{\nabla} \cdot (\rho \vec{v} \otimes \vec{v}) = -\vec{\nabla} p + \vec{\nabla} \vec{\tau} + \rho \vec{f} \quad (2-31)$$

With the fluid pressure p , the normal and shear stresses $\vec{\tau}$ and the force vector \vec{f} , such as gravitation. Regarding at the energetic components, as well as the power and heat flows for a fluid volume element, the energy conservation is defined as:

$$\frac{\partial(\rho e)}{\partial t} + \vec{\nabla} \cdot [(\rho e + p) \vec{v}] = \vec{\nabla} \cdot (\vec{\tau} \vec{v}) + p \vec{f} \vec{v} - \vec{\nabla} \vec{q} + r \quad (2-32)$$

With the specific inner energy e .

In complex models, an analytic solution of the Navier-Stokes-Equation (NSE) is not possible. Assuming that in a first approximation the lubricant flow is iso-viscous and laminar, as well as the fluid flows between two ideally smooth, parallel bodies, the NSE can be simplified to the Reynolds equation (Reynolds, 1886). Furthermore, a thin gap geometry must be present. In order for a thin lubrication gap, the gap height L_y must be negligibly small in comparison to the gap length L_{xz} : $L_y \ll L_{xz}$ (cf. Figure 2-24).

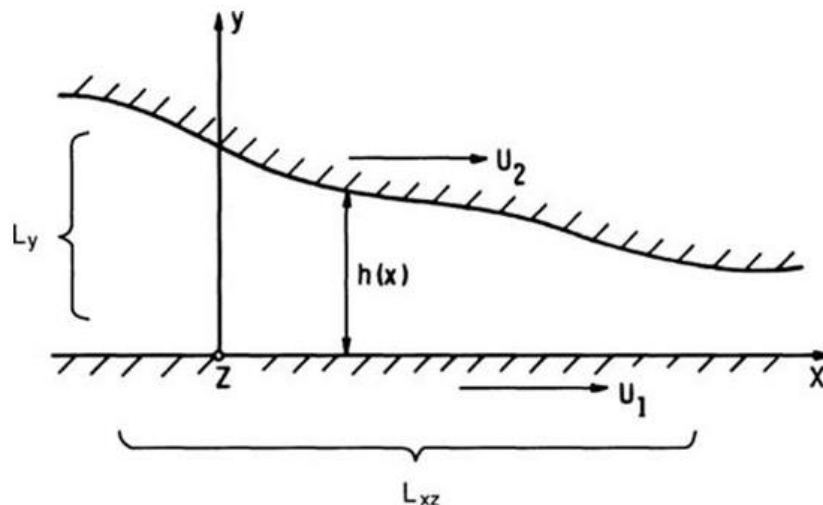


Figure 2-24: Lubrication gap of a hydrodynamic bearing (Szeri, 2011)

With his equation, Reynolds creates the basis for the analysis of hydrodynamic contacts. The Reynolds equation is defined as:

$$\frac{\partial}{\partial x} \left(\frac{\rho h^3}{12\eta} \frac{\partial p}{\partial x} \right) + \frac{\partial}{\partial z} \left(\frac{\rho h^3}{12\eta} \frac{\partial p}{\partial z} \right) = \frac{U_1 + U_2}{2} \frac{\partial \rho h}{\partial x} + \frac{\partial \rho h}{\partial t} \quad (2-33)$$

U_1 and U_2 are the velocities of the both surfaces in x-direction.

2.5.2 Fluid properties and thermal effects

There are two types of fluid flows, the laminar one and the turbulent one. To indicate the regime in the fluid flow, there is the so called Reynolds number Re , which is defined as:

$$Re = \frac{v \cdot d_H \cdot \rho}{\eta} \quad (2-34)$$

The Reynolds number is dependent on the velocity of the fluid is v , the hydraulic diameter d_H , the density ρ and the dynamic viscosity η . For values of $Re > 3000$ the lubricant flow is turbulent. For values of $Re < 2300$ the flow is laminar. If the Reynolds number is between the two limits, the flow is in a transition region. In this region, the flow can be assumed laminar (Szeri, 2011).

For Newtonian fluids, the dynamic viscosity η is the constant of proportionality between the relation of shear stress τ and the shear rate $\dot{\gamma}$, the velocity gradient of the height of the lubrication gap.

$$\tau = \eta \cdot \dot{\gamma} = \eta \frac{dv}{dz} \quad (2-35)$$

The dynamic viscosity η can be pressure and temperature dependent. A pressure dependency of the dynamic viscosity η can be determined by the Barus law:

$$\eta(p) = \eta_0 \cdot \exp(\alpha_p \cdot p) \quad (2-36)$$

In this equation, η_0 is the viscosity at atmospheric pressure, and α_p is the pressure coefficient of the fluid (Wisniewski, 2000).

To describe the temperature dependency of the dynamic viscosity η , the equation by Cameron can be used:

$$\eta(T) = k_1 \cdot \exp\left(\frac{k_2}{T + 95}\right) \quad (2-37)$$

In equation (2-37), k_1 and k_2 are constants and T is the temperature in °C.

A further important phenomenon in tribological contacts with a thin fluid film is heat transfer. Basically, three different heat transfer mechanisms can be distinguished: heat conduction, convection and heat radiation. In tribological contacts, convection phenomena have quite often the most important influence on the fluid temperature. In the present work, both conduction and convection effects have to be taken into account. The heat flux density \dot{q} through the contact is defined as:

$$\dot{q} = -\frac{\lambda}{d}(T_f - T_i) \quad (2-38)$$

T_f and T_i are the final and initial temperatures. λ is the material specific thermal conductivity and d is the wall thickness.

Convection is the energy transport in a fluid due to macroscopic movements of matter. The heat transfer between a moving fluid and a fixed wall is mainly due to convection. A new quantity is introduced, the heat transfer coefficient α , in order to calculate the heat flux density \dot{q} exchanged on the wall:

$$\dot{q} = \alpha(T_f - T_i) \quad (2-39)$$

2.5.3 Influence of surface roughness on fluid mechanics

To take into account the surface topography of the bodies in flow, Patir and Cheng (1978) extended the Reynolds equation, which are valid for flat and parallel surfaces. The developed "Average-Flow-Model" is based on pressure flow factors and shear flow factors, which are dependent on the surface topography, defining the local lubrication gap. These flow factors are calculated on the basis of statistical numerical simulation, based on random generated rough surfaces (Patir & Cheng, 1979). The generated two rough surfaces in contact under lubricated conditions are shown in Figure 2-25.

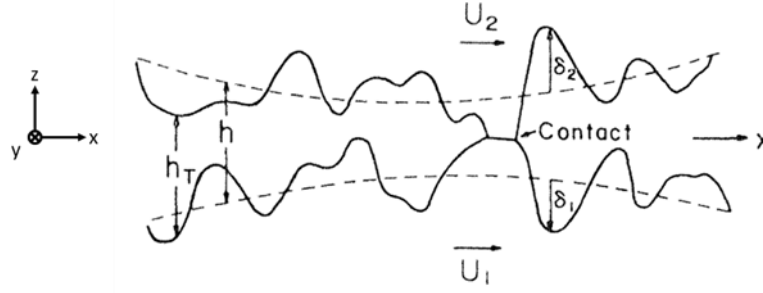


Figure 2-25: Rough surfaces under lubricated conditions (Patir & Cheng, 1978)

The ratio $h^* = \frac{h}{\sigma}$ can be used to determine whether it is necessary to use the corrected Reynolds equation for rough topographies. For a factor $h^* > 3$, a consideration according to the normalized Reynolds equation is sufficient. It is necessary to use the extended form according to Patir and Cheng for $h^* \leq 3$ (Effendi, 1987).

Consequently, the Reynolds equation by considering rough surface topography with the assumption of an incompressible fluid ($\rho = \text{constant}$) is extended to:

$$\begin{aligned} & \frac{\partial}{\partial x} \left(\phi_x \frac{h^3}{12\eta} \frac{\partial \bar{p}}{\partial x} \right) + \frac{\partial}{\partial y} \left(\phi_y \frac{h^3}{12\eta} \frac{\partial \bar{p}}{\partial y} \right) \\ & = \frac{U_1 + U_2}{2} \frac{\partial \bar{h}_T}{\partial x} + \frac{U_1 + U_2}{2} \sigma \frac{\partial \phi_s}{\partial t} + \frac{\partial \bar{h}_T}{\partial t} \end{aligned} \quad (2-40)$$

The nominal film thickness is h . The local film thickness is $h_T = h + \delta_1 + \delta_2$ with the randomly distributed roughness amplitudes δ_1 and δ_2 . The mean values across the lubrication gap are indicated by a line above the respective symbol. The standard deviation of the summed roughness amplitudes $\delta_{sum} = \delta_1 + \delta_2$ is $\sigma = \sqrt{\sigma_1^2 + \sigma_2^2}$. The pressure flow factors are ϕ_x and ϕ_y and the shear flow factor is ϕ_s . The flow factors contain the effects of shear and pressure on fluid between rough surfaces at different gap heights and are strongly dependent on the surface topography. The flow factors for three different surface topographies are shown in Figure 2-26. If the pressure flow factor reaches a value of 1.0 ($\phi_x, \phi_y = 1.0$), the flow is unrestricted. If the pressure flow factor trends against the value 0.0 ($\phi_x, \phi_y \rightarrow 0.0$), the flow is suppressed because of the small local lubrication gap. If the shear flow factor reaches the value 0.0 ($\phi_s = 0.0$), the flow is unaffected. In case of a shear flow factor above the value 0.0 ($\phi_s > 0.0$), an additional transport effect caused by the wall movement is present. Since the described approach is applied for generated rough surface profiles, the need to consider the influence of real measured surfaces on the phenomena occurring in a tribological contact in three-dimensional models becomes clear.

A further effect occurring in a hydrodynamic regime is cavitation. Cavitation describes the interruption of the fluid film due to gas or vapor phases in the fluid. The phase change of the fluid is caused by high pressure differences in the fluid.

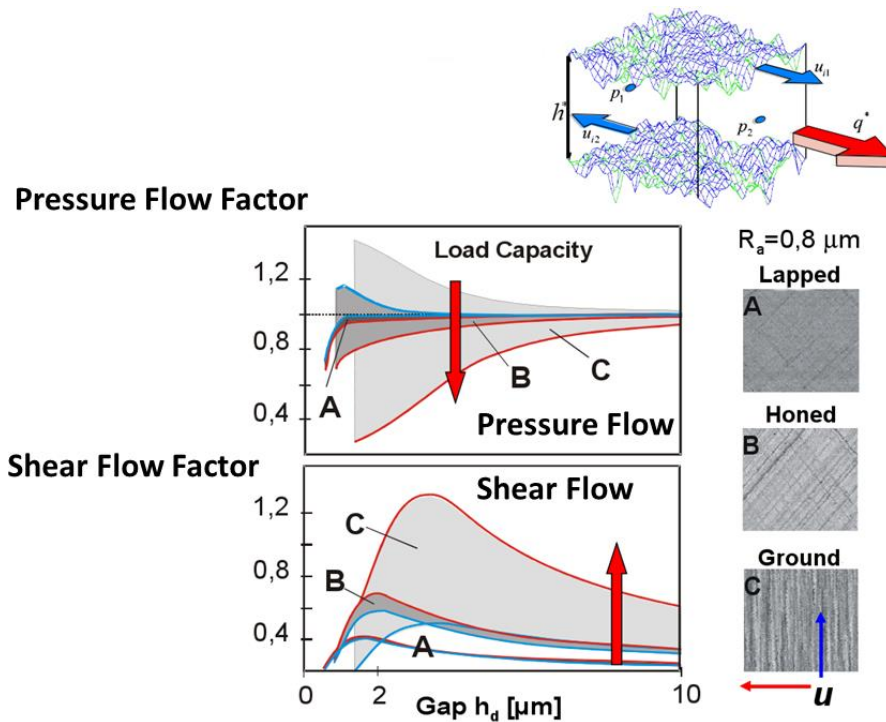


Figure 2-26: Influence of rough surfaces on hydrodynamic flow factors (Knoll, Boucke, Winijst, Stapelmann & Auerbach, 2016)

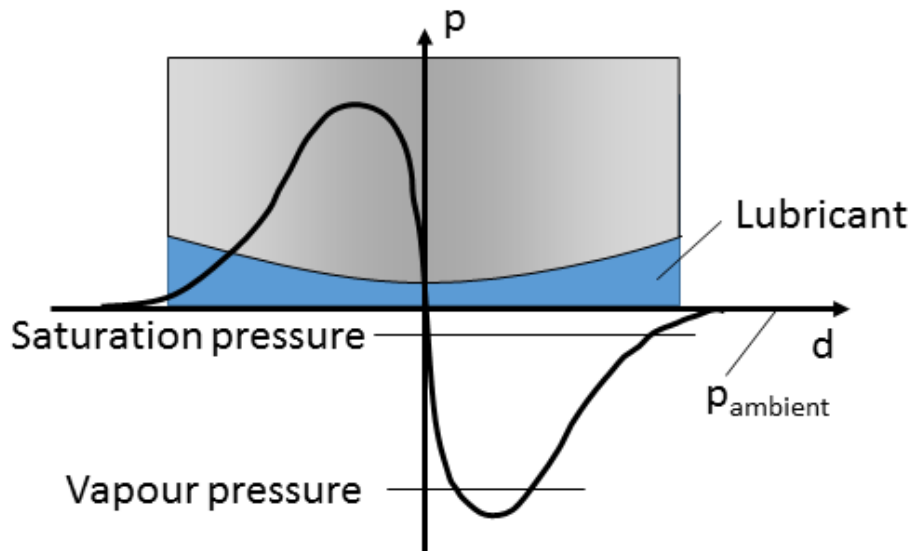


Figure 2-27: Pressure profile the converging-diverging lubrication gap (Dowson & Taylor, 1979)

Figure 2-27 shows a narrowing gap with subsequent expansion. The pressure distribution shows a sharp increase before the narrowest point of the lubrication gap

and an abrupt drop with negative pressure behind this point. The lines of the saturation pressure and the vapor pressure are shown. Below the vapor pressure, parts of the fluid change from the liquid to the gaseous phase. The sudden collapse of the steam bubbles under high pressure ensures a strong, local pressure increase, which can cause damage to the material. However, this is a special case and not present in every application. This cavitation damage in hydrodynamic bearings is also limited according to Dowson and Taylor (1979).

Even Tzeng and Saibel (1967) do not doubt the existence of cavitation in thin fluid films, but they do not see any need to consider them. Since the models greatly increase in complexity, but the multiplication is not justified by the low importance compared to other effects such as surface roughness.

2.5.4 Elastohydrodynamic lubrication

If, in addition to the hydrodynamic lubrication, the elastic deformation of the solid friction partners is taken into account, it is an elastohydrodynamic lubrication (EHL). This condition is obtained when the elastic deformation of the contact bodies is greater than or equal to the thickness of the lubrication film. EHL corresponds to the transition from the hydrodynamic to the mixed-lubricated regime as shown in Figure 2-28. This type of non-conformal contact usually occurs in roller bearings, gears, cam-follower-pairings and seals (Bartel, 2010). But also in journal bearings EHL can occur from the transition from mixed-lubrication to hydrodynamic lubrication and local elastic deformations have to be taken into account.

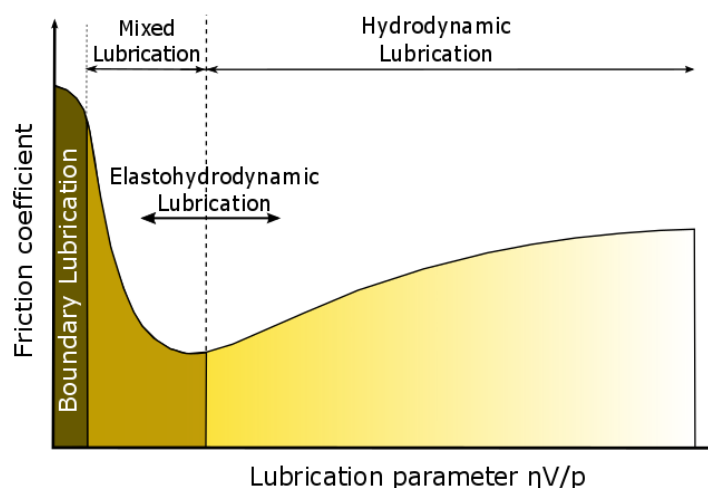


Figure 2-28: Stribeck diagram illustrating the lubrication regime

As the investigation of Krupka, Sperka & Hartl (2016) on the effect of surface roughness on lubricant film breakdown in EHL has shown, there is a big influence of the surface roughness on the present film thickness. In this work was pointed out, that the grooves with a length larger than the contact diameter can be considered as most

dangerous surface features on the effect of lubricant film breakdown. The effect of the breakdown is explained with a possible side leakage out of the groove. The corresponding experimental result in comparison with a smooth contact and consequently the influence on the film thickness is shown in Figure 2-29.

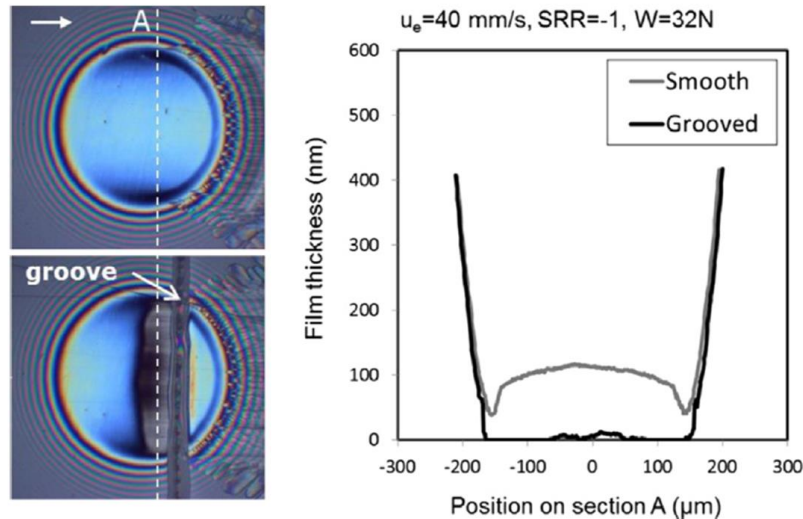


Figure 2-29: Comparison of smooth contact with the effect of a groove (Krupka et al., 2016)

It is clear to see, that the significant groove in contact leads to a breakdown of the lubricant film nearly over the whole contact width. The lubricant film for the smooth contact remains.

Numerical models for the investigation of such irregularities of the rough surfaces, especially if they cause lubricant film breakdown, are not able to take into account such complex phenomena.

2.6 Numerical methods in lubrication and tribology

In order to describe the phenomena in lubricated contacts, the flow theory must also be considered. The approaches presented in section 2.5 to describe the fluid flow, can only be calculated numerically. To solve the numerous complex nonlinear differential equations, the problem must be discretized in a corresponding calculation method. In this section, two discretization methods used in this work, the finite volume method (FVM) and the finite element method (FEM), are presented. In addition, the multi body simulation (MBS) is presented, which is often used in tribology to describe whole machine parts on the macroscale level. Since these methods are approximation solutions, each method must be verified experimentally and the convergence have to be checked.

2.6.1 Discretization method

There are three main methods to solve the numerous differential equations describing the fluid flow in lubricated contacts: The FEM, FVM and the finite difference method (FDM). Lecheler (2009) classified these discretization methods according to flexibility and accuracy. As shown in Figure 2-30, the FEM has the highest flexibility. The FVM, which is mainly used in CFD simulations, shows a good compromise between accuracy and flexibility. The FDM offers the highest accuracy.

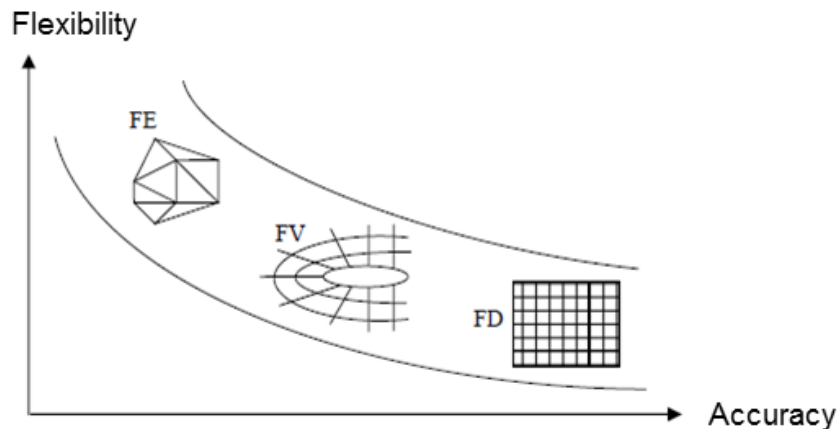


Figure 2-30: Classification of discretization methods (Laurien & Oertel, 2013)

Since the FEM and FVM have been used in this thesis, these two methods are described in more detail below.

Finite Volume Method The FVM is the standard tool in numerical flow mechanics, where it is used to solve flow problems, i.e. the Euler and Navier-Stokes equations. As the starting point, the FVM uses the integral form of the conservative equation. The solution area is subdivided into a finite number of subvolumes and the conservative equation is applied to each individual volume. The arrangement of the discrete small volumes is spatially-fixed and thus represents an eulerian discretization. The variable value is then calculated for the element node which is the center of gravity. The FVM can be used with many lattice types, why it is also suitable for the description of complex geometries (Ferziger & Perić, 2008).

According to Schäfer (2006), the FVM can be divided into the following categories:

- Discretization of the problem domain into control volumes.
- Formulation of integral balance equations for each control volume.
- Approximation of integrals by numerical integration.
- Approximation of function values and derivatives by interpolation with nodal values.
- Assembling and solution of discrete algebraic system.

In comparison to the FEM, the FVM is well suited for linear fluid simulations. In case of high non-linearities, this method is limited in stability and convergence. For this reason, the FEM is used for modelling structural mechanic problems where the geometry is more complex and deformable.

Finite Element Method The FEM is a widespread tool, to model complex problems in solid/structural mechanics and in other disciplines, such as heat conduction. In any way, this method can also be used to describe the interaction between a fluid and a flexible solid structure. For such problems, two element formulations are available: The lagrangian and the eulerian formulation. The lagrangian formulation consists of following the material particles of the continuum in their motion (Donea & Huerta, 2003). Consequently, the grid which follows the continuum in its motion, remain permanently connected to the material points and could lead to excessive distortion of the finite element mesh (Figure 2-31).

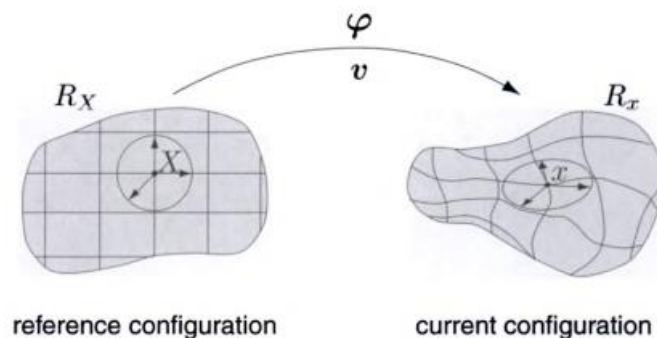


Figure 2-31: Lagrangian description of motion (Donea & Huerta, 2003)

This problem can be overcome with the Eulerian formulation. This formulation consists in discretizing a domain with an initial distribution of elements, which are initially defined as material and which not. With this approach, the finite element grid is spatially fixed and there are no excessive distortions of the mesh. Consequently, the Eulerian formulation is well suited for problems with high deformations like plastic deformations, fluid flow or hyper elastic materials.

The presented numerical methods distinguish between the explicit and implicit time discretization. The temporal discretization denotes the dissolution of the temporal derivatives in an equation system. For clarity, the following model equation is considered:

$$\frac{\partial u}{\partial t} = rhs(u) \quad (2-41)$$

Here, u is the sought quantity and in $rhs(u)$, all spatially discretized derivatives are combined. The time index n is to be used, which divides the time axis into equal intervals Δt . Thus the state variable u for the different time is obtained to:

$$u(t^{n-1}) = u^{n-1}, \quad u(t^n) = u^n, \quad u(t^{n+1}) = u^{n+1} \quad (2-42)$$

Here u is the sought distribution, which is calculated from the known solutions of the time steps $n, n - 1, n - 2, \dots$. The solution of equation (2-41) is shown in Figure 2-32, left as a trajectory field.

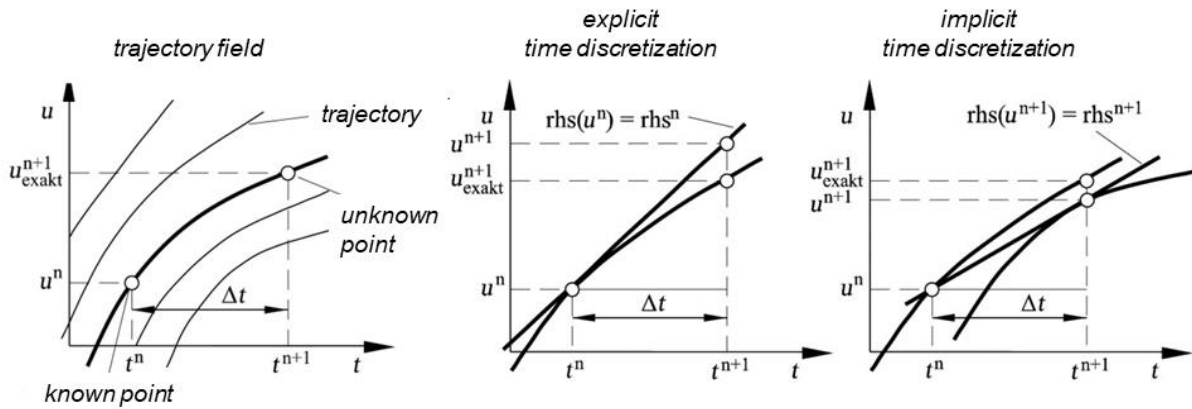


Figure 2-32: Time discretization (Laurien & Oertel, 2013)

The slope of the trajectories is given by the function $rhs(u)$. The unknown point $(t^{n+1}, u^{n+1}_{exact})$ is located on the trajectory through the known point (t^n, u^n) . Two methods can be used to approximate the desired function u^{n+1} : the explicit and the implicit euler discretization. The both methods are shown in Figure 2-32 in the middle (explicit) and on the right (implicit).

In the explicit method, the curved trajectory is replaced by a straight line whose slope is calculated from the old time steps. This follows the temporal discretization according to the explicit method:

$$\frac{u^{n+1} - u^n}{\Delta t} = rhs^n \Leftrightarrow u^{n+1} = u^n + \Delta t \cdot rhs^n \quad (2-43)$$

For the implicit method, the trajectory is approximated by a straight line of the slope of the still unknown quantity rhs^{n+1} . This results in the implicit time discretization:

$$\frac{u^{n+1} - u^n}{\Delta t} = rhs^{n+1} \quad (2-44)$$

Equation (2-44) cannot be resolved to u^{n+1} , since $rhs^{n+1} = rhs(u^{n+1})$.

The error of the approximation can be estimated by a Taylor series method (Barrio, Rodríguez, Abad & Blesa, 2011). The deviation is proportional to the time step Δt . With this method, an acceptable accuracy can be achieved for sufficient small time steps Δt . However, the computational time increases strongly. A possible remedy is the time discretization according to the Adams-Bashforth method (Durrant, 1991). Here, the accuracy is improved by increasing the further time step $n - 1$. A disadvantage is the increased memory due to the additional required values. As an alternative, the Crank-Nicolson method (Martínez-Ortiz, Molina & Laborda, 2011), the Leapfrog method (Durrant, 1991) or the use of correction methods can also lead to an increased order of convergence.

2.6.2 Multibody simulation

A multibody system is mostly defined by two or more rigid bodies with a relative movement between them on the macroscale level. Such systems can be divided in kinematic and dynamic problems (García de Jalón & Bayo, 1994). In kinematic problems the position or motion of the system is studied, without taking into account the forces and reactions that generate it. In dynamic problems, also the forces and the initial characteristics like mass, inertial tensor and the position of the gravity center, that influence the multibody system are involved. In general, dynamic problems are much more complex to solve than kinematic ones.

To investigate hydrodynamic problems with numerical simulations of multibody systems, the interaction of different computational disciplines is necessary. Knoll et al. (2016) used a coupled approach based on a non-linear multibody system in interaction with highly non-linear elasto-hydrodynamics and linear elastic structural dynamics for the numerical investigation of a journal bearing of a valve train shaft. In a first step, the Newtonian equations of movement are solved regarding the forces acting on the elastic bodies. With the determination of gap heights and their derivatives for the solution of the Reynolds equations, the hydrodynamics were modelled. The resulting forces from the hydrodynamic pressure distribution are applied in a last step on the structure. As described above, the limitation of this method is, that only linear elastic deformations can be handled.

2.6.3 Contact modelling

A precise contact definition for the interaction of solid and fluid parts is the most important technique for modelling the friction behavior of a tribological system in a numerical way. There are two different contact definitions in the used FE-software Abaqus/Explicit: the general contact method and the contact pairs method.

The general contact allows a very simple and intuitive implementation of the contact definitions with few restrictions regarding the usable surface types. By default, a

contact condition is generated between all free surfaces. Individual contact pairs can be excluded from the contact domain or their own contact properties can be assigned. The method is particularly suitable for models with the same contact properties between the single bodies. In addition, it is the only way to define contact between eulerian materials and lagrangian bodies ("Abaqus Analysis User's Guide 2016," 2015).

The contact pairs method has more restrictions with respect to the surface types that can be used. When defining the contacts, care must be taken to ensure that all contact definitions for the possible contact pairs are implemented individually. This method is particularly suitable for models with different contact properties, since the larger implementation effort is relativized here. In addition, various discretization methods are implemented, which are not available in a general contact domain.

There are two main discretization methods: the node-to-surface and the surface-to-surface formulation. The latter formulation is the most accurate one which leads to the lowest overlapping and penetration of the contacting surfaces. There are some other discretization methods but are not used in this work.

To define the normal contact behavior there are two classes available: the softened and the hard contact. The softened contact is only available for implicit solving and allows to increase the convergence, whereas the hard contact is very CPU-efficient and consequently requires less computing time. Further available softened formulations are the linear, tabular, exponential and the scale factor formulation. They are not used in the current work and therefore not treated in detail.

The tangential contact is also important and controls the friction behavior of the tribological system. To initiate sliding between two bodies, there are two possibilities available:

- Defining a coefficient of friction μ giving a relation between the normal and the tangential force
- Specifying a critical shear stress limit τ_{crit} , to define the sliding initiation

Both criterions lead to a constant limit for the sliding initiation. The advantage of the second criterion compared to the constant coefficient of friction is that regardless of the magnitude of the contact pressure stress, sliding will occur if the magnitude of the equivalent shear stress reaches this critical value τ_{crit} . This critical shear stress limit is typically used in cases when the contact pressure stresses may become very large, like it can occur in tribological contacts with real rough surfaces.

Phenomena like thermal exchange and heat generation are also encountered in contact definitions. There are no complex algorithms used. Heat generation is allowed due to the dissipation of energy created by the mechanical interaction of contacting

surfaces. The source of the heat is frictional sliding. The part of frictional energy converted into heat and the heat proportion between the surfaces has to be defined.

2.7 Fluid structure interaction in simulations

The fluid structure interaction (FSI) describes the interaction between fluids and solids (structure) in coupled numerical models. Following van Zuijlen (2006), there are two different approaches to model these interactions. The monolithic and the partitioned solver. In Figure 2-33 the two different coupling systems are shown.

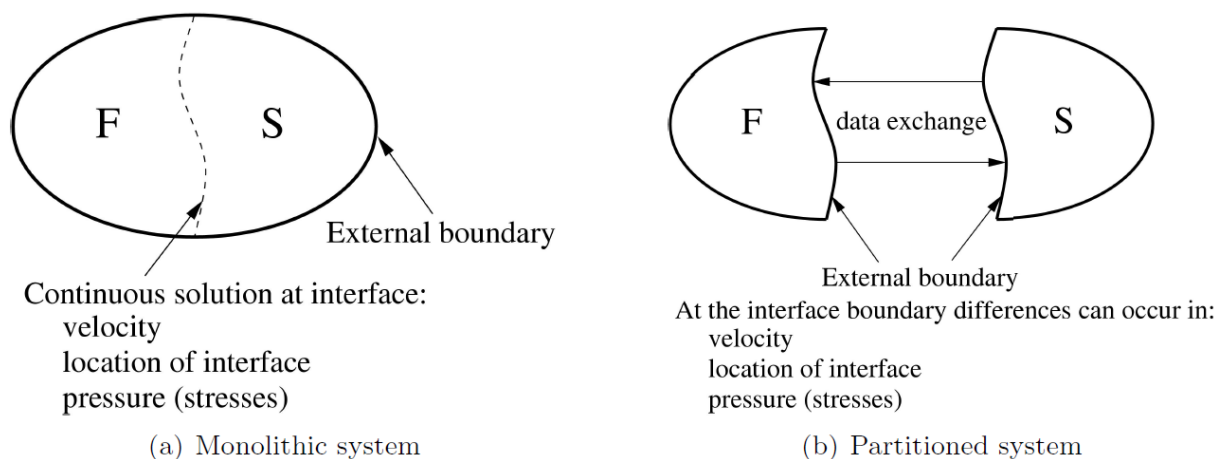


Figure 2-33: System coupling: **(a)** Monolithic coupling system, **(b)** partitioned coupling system for FSI (van Zuijlen, 2006)

In a monolithic FSI, all the necessary elements like physics modeling, discretization and solution algorithms are put together in a single computational model. The external boundary includes both, the fluid and the solid area (Figure 2-33, left). For a portioned solver, the physical areas must be considered separately. On a defined surface, the fluid solid interface, the data exchange takes place between the two areas (Figure 2-33, right).

The main challenge in FSI is to take into account the deformations of the solid bodies. This problem occurs due to the different discretization methods for the fluid and the solid entities. The fluid is following the euler discretization, whereas the solids are modelled with the lagrangian method. These two methods have to interact for a successful coupling of the physics of fluids and solids.

2.7.1 FSI in conventional Computational Fluid Dynamics

Conventional CFD methods are using a partitioned approach for modelling the FSI. Hereby, the interaction can either be uni- or bidirectional. In case of a lubricated tribological contact, the bidirectional coupling is necessary to model the interactions in a sufficient way. Here, not only one participant affects the other, both, fluid and solid,

affect each other. Specifically, in a hydrodynamic contact, the lubrication gap is defined by the distance of the two solid bodies, which influences the flow and pressure distribution in the fluid. On the other hand, the fluid pressure acts on the solid surfaces and is reflected there in form of stresses.

The working surface pair (WSP) Fluid/Solid forms the interface. This WSP is responsible for the data transfer from the fluid to the solid and from the solid to the fluid. The numerical solution is generated separately within two solution algorithms for the fluid and the structural mechanics. In a typical bidirectional FSI coupling, the results of the CFD analysis are the pressure and the temperature. At the interface they are transferred to the solid state as boundary conditions. For the solid bodies, quantities such as displacement or temperature are calculated separately and transferred to the fluid domain at the interface. Both analyzes are thus combined and repeated until an equilibrium of the mechanical and fluidic solution is achieved.

The transfer of the forces and displacements is applied to the nodes of the interface surface. Hereby, the mesh of the interactive surfaces need not to be conform. The interpolation (mapping), that is to say the setting on which nodes or elements the forces and displacements contained in the data transfer are applied, follows two distribution algorithms: The profile preserving data transfer and the conservative profile data transfer (Ansys, 2016).

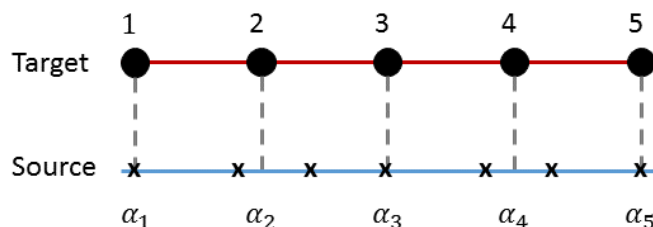


Figure 2-34: Profile preserving data transfer (Ansys, 2016)

Displacements are distributed on the target surface by means of profile preserving data transfer (Figure 2-34). For this purpose, the target is interpolated on the source surface. On the basis of this interpolation, on each target node a specific weight α_i is assigned from the source surface. With these weightings, the displacements of the source surface are transmitted proportionally to the target surface. Forces are distributed by the conservative profile data transfer from the sending to the receiving side (see Figure 2-35). The elements of both sides are subdivided into small sub faces and represented by so-called integration points (IP). In Figure 2-35, the integration points are marked by the symbol X. All sub faces of both sides are projected to a control surface. The weights of the sending side are calculated from the resulting surfaces. For example, a weight of $\alpha_1 = \frac{A_1}{A_1}$ and $\alpha_2 = \frac{A_2}{A_2+A_3}$ is to be assumed for the surfaces S_1 and S_2 .

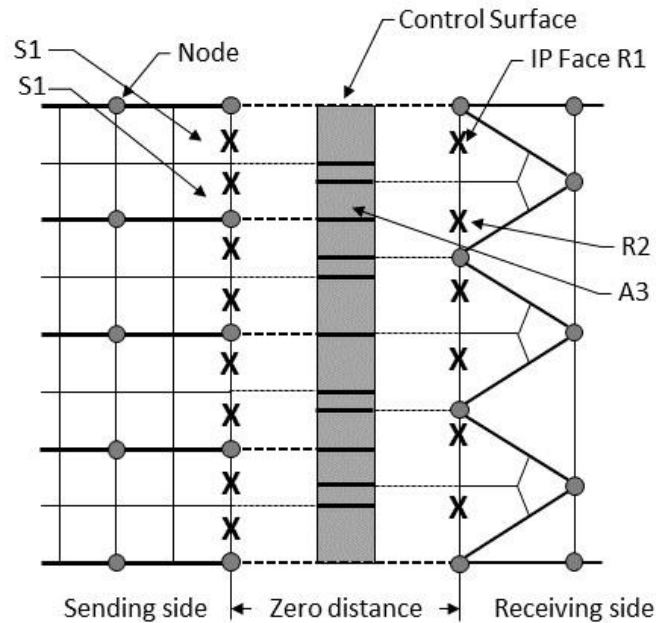


Figure 2-35: Conservative profile data transfer (Ansys, 2016)

2.7.2 FSI modelled with the Coupled Eulerian Lagrangian Method (CEL)

The Coupled Eulerian Lagrangian Method (CEL) describes the interaction of an eulerian mesh formulation with the langrangian mesh formulation within the same model. Consequently, the CEL method corresponds to a monolithic FSI. A direct coupling of the fluid and the solid mesh will lead to high mesh distortion of the fluid domain. Therefore, it is necessary to model the interaction between the fluid and the solid bodies with different meshing algorithm. On this account, the CEL method was implemented, where to solid bodies are following an lagrangian formulation and the fluid part an eulerian formulation. How mentioned in section 2.6.1, the Lagrangian formulation consists of following the material particles of the continuum in their motion, whereas the eulerian formulation consists of discretizing a domain with initial distributed elements, which are spatially fixed and where are no excessive mesh distortions. Within the eulerian formulation, no node displacement is calculated. The difference between the two element formulation is shown in and simplified example in Figure 2-36.

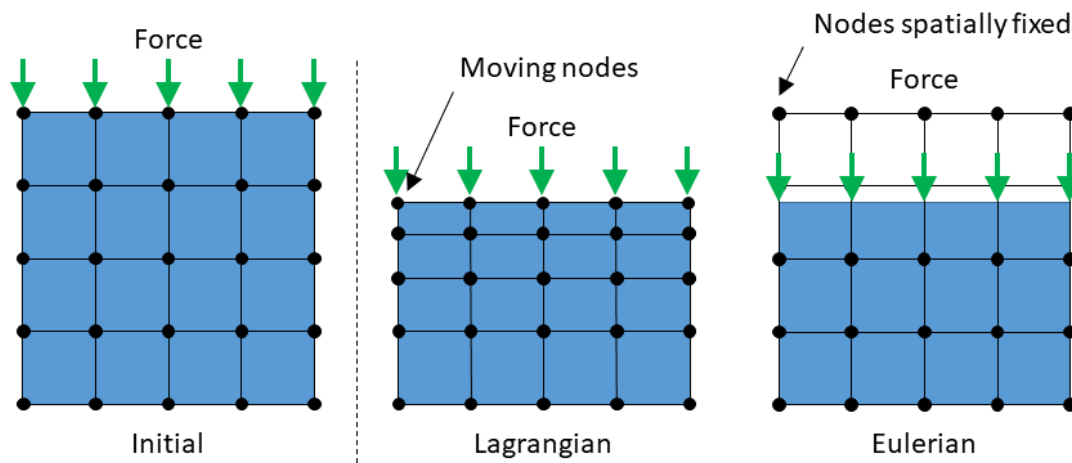


Figure 2-36: Difference between the lagrangian and the eulerian element formulation

The main difference of FSI of the CEL method in comparison to a conventional fluid mesh is that the eulerian mesh is not directly coupled to the solid bodies. The contact between the fluid and the solid is modelled with the eulerian lagrangian contact. This algorithm automatically calculates and tracks the contact between the fluid and the solid. It is not necessary to use compliant meshes for the interacting instances. The WFP Fluid/Solid transfers force, stress, pressure and temperature.

The contact definition of the CEL method is shown in Figure 2-37.

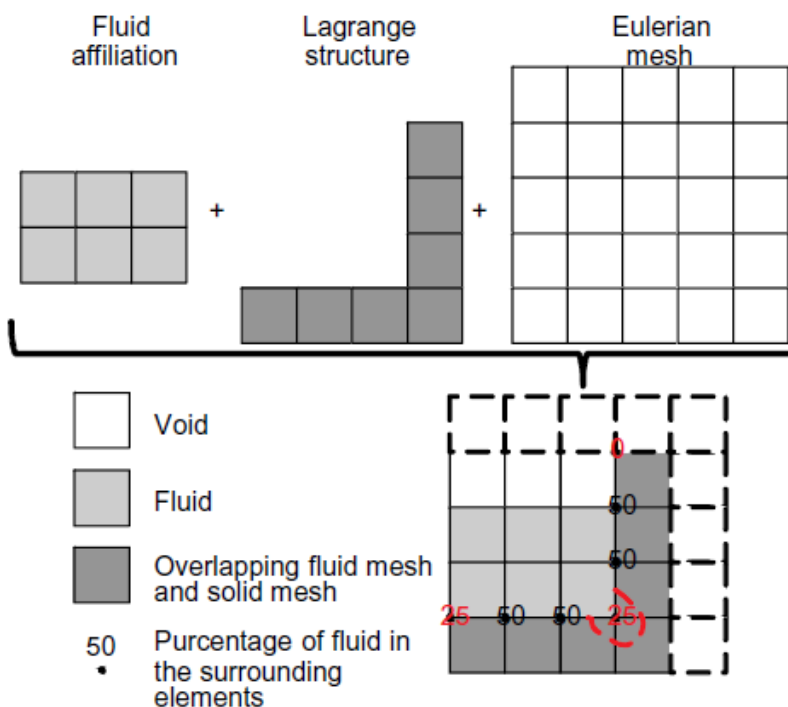


Figure 2-37: Contact definition of the CEL method (Albers & Lorentz, 2012a)

When a contact between the fluid and the solids occurs, depends on the surrounding elements of the solid nodes. If more than 50% of material is around a single node of the solid, a contact occurs between the parts. The last figure shows the problem of fluid penetration which occurs when only one full element surrounds a solid node, in case of angled edges (Albers & Lorentz, 2012a).

Donatellis, Gelosa, Sangalli, Spinelli & Vitali (2009) investigated the capability of the CEL technique on the example of a laminar benchmark problem. The good agreement of the results compared with the analytical solution is shown in Figure 2-38.

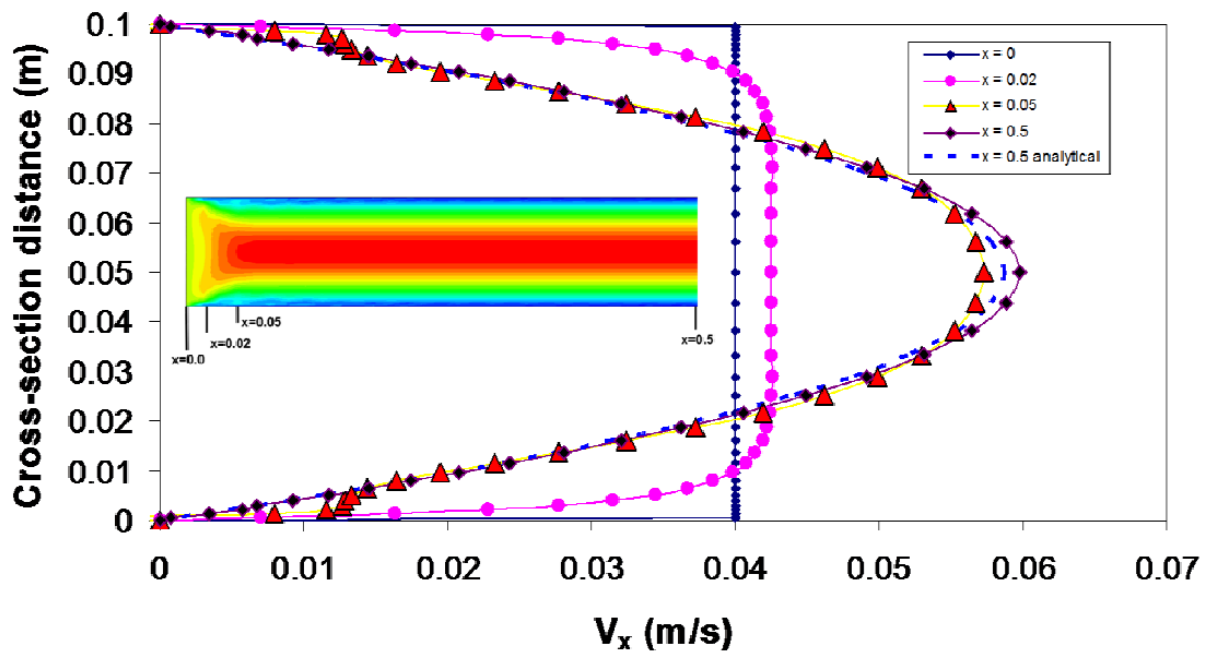


Figure 2-38: Velocity profile in channel flow (Donatellis et al., 2009)

The parabolic characteristic velocity profile is called Poiseuille flow. The channel flow was modelled in ABAQUS, using the CEL method. The velocity profile for $x = 0,5$ is almost identical to the analytical solution. The inflow effects for $x = \{0; 0,02; 0,05\}$ cannot be calculated analytically. For a satisfactory comparison, the flow must be fully developed. The evaluation of values at the inlet of the channel does not make a reasonable comparison due to inflow effects.

2.8 State of the Art: Experimental investigations in tribology

There are different experimental investigations to determine the influence of the surface topography on the friction and wear behavior. These works range from sliding systems like journal bearings to friction system like clutches. Different scales are used going from system tribometers on the macroscale to atomic force microscopy (AFM),

focused ion beam (FIB) and transmission electron microscopy (TEM) on the nanoscale.

2.8.1 Experimental investigations of sliding systems

A widespread approach for the investigation of sliding contacts is the pin-on-disc device. With this device, the contact (conform and non-conform) between a pin and a rotating planar disk can be examined under lubricated and non-lubricated conditions.

Kubiak and Mathia (2009) presented experimental results about the influence of different surface roughness (machining process) on the wear and friction process under dry and boundary lubrication in sliding conditions. The tribological conclusions could be made that the initial surface roughness has a strong influence on the coefficient of friction. The results have shown, that with an increasing 3D surface peak-to-valley average maximum height sR_z , the coefficient of friction is decreasing. There was also no strong influence of the initially imposed pressure on the sliding behavior. A non-conform contact was investigated by Le, Sutcliffe and Williams (2005) on a ball-on-flat microtribometer between an aluminum alloy strip and steel ball. It was also found that the coefficient of friction in lubricated conditions increases with the initial surface roughness owing to more severe solid-solid contact. Furthermore, it could be shown, that the coefficient of friction remains unchanged after eight cycles. Also Masouros found out that a high initial surface roughness gives high linear wear during running-in until a linear wear law controls the process (Masouros, Dimarogonas & Lefas, 1977). Sedlaček, Podgornik and Vižintin (2012) correlated the friction behavior with the standard roughness parameters. The conclusion was made that the standard parameters sR_a and sR_q are not sufficient to determine the tribological properties of contacting surfaces. The surface roughness parameters S_{ku} , S_{sk} and S_{vk} are in a good correlation with the friction behavior and can be used well for designing desired surface topographies. In this paper was outlined that there is a decreasing coefficient of friction with an increasing kurtosis S_{ku} . With the more negative skewness S_{sk} , the friction coefficient is decreasing. Linsler, Schlarb, Weingärtner and Scherge (2015) studied the contact of a lubricated AISi alloy disc in contact with a 100Cr6 pin with a radionuclide-assisted pin-on-disc device. It could be shown that the initial subsurface morphology clearly influences the running-in phase. Ultra-low wear rates are possible, when the internal flow is intense and dominates.

On system view the journal bearing is favorite demonstrator for the investigation of mixed-lubricated and hydrodynamic effects. Albers, Nguyen & Burger (2012) developed a journal bearing test bench, consisting of a shaft and two aerostatic bearing, to reduce the influence of the supporting bearings on the friction torque. With this device, a total power loss reduction of around 10 % has been experimentally verified as a result of reducing the lubricant flow rate. Dickerhof (2011) (Albers,

Dickerhof & Burger, 2008) used structure-borne sound emission analysis for the detection of mixed friction in journal bearings. This method was validated with the correlation of the Radio-Nuclide-Technique (RNT).

In the research field of mobile hydraulic components, Albers, Blust, Lorentz and Burger (2014) developed a test bench for the investigation of the contact between a cylinder and a control plate in an axial piston variable pump under sliding conditions. With this test bench, new tribological lightweight materials could be developed for this kind of application.

2.8.2 Experimental investigations of friction systems

In friction system like clutches, in which the friction serves to fill the function, also the influence of the surface roughness was investigated. Gao, Barber and Shillor (2002) investigated the influence of the surface roughness on the friction behavior in wet clutches. Mäki (2016) found out that the torque is primarily transmitted by asperity contacts rather than fluid films in mixed and boundary lubrication. The influence of the oil is rather significant. Furthermore, the temperature is shown to have a high impact on the friction coefficient, which decreases with increasing temperature. To get a better understanding about local friction phenomena in wet clutches, Marklund and Larsson (2008) investigated a small sample of a wet clutch friction disc on a pin on disc device and compared the results with the measurements from a test rig for the whole friction disc. A good correspondence between the results of the two different test applications could be achieved. There are the same trends in variation of the coefficient of friction throughout the whole range of speed and temperature. Also the investigations have shown that there is no greatly effect of the normal load on the coefficient of friction.

To improve the power density of wet clutch systems, Albers, Bernhardt and Ott (2010) investigated the fluid flow through the frictional contact with numerical and experimental methods. With the Particle-Image-Velocimetry (PIV) method could be shown that the oil distribution is strongly depending on the groove design. An increased groove area allows increased heat transfer has been proved in experimental tests. Therefore, advanced ceramics show potential to increase heat transfer and improve power density of lubricated clutch systems (Bernhardt, Albers, & Ott, 2013).

2.9 State of the Art: Numerical investigations in tribology

In this section a survey about numerical investigations of the friction and wear behavior is given. The different approaches are focused on the influence of real surface roughness on the tribological behavior and reach from the micro- to the macroscale.

2.9.1 Non-lubricated friction simulation

Many numerical investigations take part at the macroscopic scale and do not concern the surface roughness. Wriggers (1996) presents an overview with regard to the numerical simulation of non-lubricated frictional problems with an example on large deformations. By now, contact formulations used in these simulations are established for tribological investigations at the microscopic scale. This knowledge is used for the investigation of different research areas like brakes (Bakar, Li, James & Ouyang; Dmitriev, Österle & Kloß, 2008) and sealing technique (Bielsa, Canales, Martínez & Jiménez, 2010), rail-wheel contacts (Bucher et al., 2006), metal-forming (Leu, 2009) and machining techniques (Özel, Thepsonthi, Ulutan & Kaftanoğlu, 2011). Nevertheless, in these areas, the correlation between rough surfaces and the friction behavior in dry conditions was not evaluated. The most investigations focus on the contact stress and plasticization occurring in the contacts (Kogut & Etsion, 2004) and for determining the real contact areas between rough bodies (Yastrebov, Durand, Proudhon & Cailletaud, 2011).

First models done by Albers, Savio and Lorentz (2010) taking into account the surface roughness and adhesion effects, following Bowden and Tabor (2001), showed the impact of the machining direction and the surface orientation on the coefficient of friction. It cannot be stated that the smoother the surfaces are, the lower the friction coefficient is. It is also dependent on the real contact area. The same trend can be stated in lubricated contacts.

2.9.2 Mixed-lubricated friction simulation

Due to the huge calculation time for modelling mixed-lubricated contacts on the microscopic scale in regard to rough surfaces, Redlich (2002) investigated point contacts in a stationary regime with elastohydrodynamic contact models. In the same way, Chang (1995) investigated lubricated line contacts with sinusoidal generated profiles. Mihailidis, Retzepis, Salpistis and Panajiotidis (1999) introduced a model for the numerical prediction of the coefficient of friction and the temperature field of EHD contacts.

Because of the many required resources for the numerical investigation of tribological systems on the macroscopic scale, other approaches were used in parallel to the discretization methods like CFD and FEM. Andersson, Söderberg and Björklund (2007) developed analytical approaches for the investigation of sliding contacts running under different conditions in boundary and mixed-lubricated regime. Hu and Zhu (2000) used a multi-level integration method to calculate surface deformation in order to save computing time. The whole preceding approaches were not taking into account thermal exchange between the fluid and the solids. Larsson (2009)

investigated the influence of the surface roughness on the coefficient of friction with the FEM, but also did not take into account the thermal effects. Jackson and Green (2008) took into account the thermal exchange without modelling the surface roughness.

Wiersch (2004) integrated thermal effects in elastohydrodynamic contacts and coupled the fluid structure interaction with the thermal behavior also impacting the fluid. Knoll, Schlerege, Brandt, Busche and Longo (2007) and Bartel, Bobach, Illner and Deters (2011) developed similar approaches for the investigations of journal bearings, based on the flow factor theory (Almqvist, Fabricius, Spencer & Wall, 2011), the correction of the Reynolds equation.

If numerical investigations for mixed-lubricated regimes are carried out in transient conditions, there is a relative displacement of the two rough bodies. In elastohydrodynamic simulations, the displacement could cause distortions of the fluid mesh. To reduce these mesh distortions, remeshing methods (Schäfer, 2008) have been developed. Based on such approaches, Albers and Lorentz (2010) developed a finite element model for the investigation of mixed-lubricated contacts in a three dimensional configuration. The fluid structure interaction was modelled with the Coupled-Eulerian-Lagrangian method; whereby strong element distortions of the fluid mesh can be avoided. The model takes into account the surface topography, tangential adhesion effects following Bowden and Tabor (2001) and plastic deformations (Albers & Lorentz, 2012b). With this approach, the influence of different manufacturing process, surface orientations and boundary conditions could successfully be investigated (Lorentz, 2013a).

An important point of investigations on the microscopic scale is the transfer of the achieved results to the macroscopic scale, which is necessary to describe globally the tribological behavior. This is the reason; why multilevel modeling techniques are needed. Lorentz (2013a) used the numerical results on the microscale, to transfer them into a multi-body system. With the calculated coefficient of friction, the frictional behavior in dry running conditions of an intelligent lifting system could be investigated.

Jackson and Streater (2006) described a non-statistical multi-scale model of the normal contact between rough surfaces. Based on the Fast-Fourier-Transformation of real technical surfaces, he was able to reach the same results as Greenwood and Williamson (1966) in order to determine the plasticization of rough surfaces. This was achieved by taking into account different types of asperities, identified with their occurring frequency and applying to them a corresponding load. In this way, different scales from to micro to the macro could be covered.

2.9.3 Wear simulation

The empiric wear law by Archard (1953) is often used in numerical investigations for modelling different phenomena of wear with the finite element method. A macroscopic wear coefficient, in general determined in experiments, defines the volume loss per load of a tribological system at a constant load and sliding distance. This section is focus on modelling different forms of wear, like fretting, rolling and sliding wear.

2.9.3.1 Fretting wear

Fretting wear results from small relative movements between to contacting surfaces. There are two different types of fretting: partial slip and gross sliding. Under very high normal loads or small oscillating amplitudes, there are some local areas in contact in stick regime and some other are sliding. In this case, there is partial slip. If the normal load is reduced or the oscillating amplitude increased, the surface asperities are in a sliding regime and this is called gross sliding. McColl, Ding and Leen (2004) investigated the fretting wear in a cylinder-on-flat fretting configuration. The calculated and the measured wear profiles indicated a good agreement. Yue and Abdel Wahab (2017) modelled fretting wear with the wear law by Archard (1953) and implemented a varying coefficient of friction. With this approach, the accordance of experimental and numerical investigations could be improved.

2.9.3.2 Wear under sliding conditions

Bhattacharya (2011) modelled wear on an artificial cervical disc in a non-lubricated regime. Ali (2013) did the same investigations by the demonstrator of a hip implant device. Both of them neglected fluids in contact. Põdra and Andersson (1999) modelled a spherical pin-on-disc non-lubricated steel contact with the linear wear law by Archard (1953) and the Euler integration scheme. It could be shown, that the FE-software ANSYS is well suited for contact and wear simulations. Because of the variation of the experimental wear coefficients within the limits of 40 %, the numerical results could not be validated in a sufficient way. Argatov and Fadin (2011) indicated that the contact pressure is very important in determining the end of the running-in phase. This approach is a combination of the theory of elasticity in conjunction with Archard's wear law. Chmiel (2008) investigated dry sliding wear of a slipper on a rail. Also the wear law by Archard was used. Furthermore, Chmiel (2008) created a PYTHON script to rectify mesh distortions. With this code, wear could also be applied in an explicit calculation method in ABAQUS.

Wolf (2014) compared the wear law by Archard with the energetic wear approach by Fleischer. The calculated results regarding the wear depth, the contact pressure and the frictional dissipation for the demonstrator of a journal bearing are in a very good accordance.

2.9.3.3 Wear under rolling-sliding conditions

Khader, Kürten and Kailer (2012) used this approach for modelling wear in silicon nitride rolls in a rolling-sliding contact under dry conditions. The surfaces were ideally smooth and the experiments were carried out on a twin-disc tribometer. The results have shown that there was an acceptable accuracy. The simulations were carried out with ABAQUS and the user subroutine UMESHMOTION. With this routine, the surface nodes could be moved by using the adaptive mesh method in ABAQUS for applying local wear depths. With this subroutine, applicable with implicit analysis methods only, wear could be modelled on one surface.

Hegadekatte, Kurzenhäuser, Huber and Kraft (2008) developed a further method, predicting wear in rolling-sliding contacts. With the Global Incremental Wear Model, the pin wear on a pin-on-disc tribometer could be determined. For this approach, the wear law by Sarkar (1980) was used. Sarkar (1980) extended Archard's wear law by relating the coefficient of friction to the volume of material loss.

Ismail, Tauviqirrahman, Saputra, Jamari and Schipper (2013) investigated the running-in phase of a rolling contact of a rigid hemisphere on a rough surface. Above a certain load, a significant change in surface topology is observed. The observation was made that the running-in of rolling contacts takes place within the first few cycles. Telliskivi (2004) used the wear law by Archard (1953) for modelling wear of a disc-on-disc device. Next to the good agreement between experiments and numerical investigations, a good agreement in regard to the form change of the rollers was achieved.

2.10 Summary

As can be seen from the current state of research that tribosimulation of lubricated contacts is a complex and extensive topic. Suitable approaches exist for the tribological behavior of the solids as well as for the fluid (fluid mechanics), which however have to be combined in numerical calculation programs for the investigation of lubricated contacts. This fact is therefore a reason why there are no suitable models to investigate the influence of topography on friction and wear in lubricated contacts. The particular challenge in this work is therefore to create a modeling approach that supports product developers in the design of tribological systems.

3 Research objectives

Based on the explanations from the fundamentals and the state of the art in section 2, the following research objective is identified for this work. Firstly, the research needs are described, then concretized by research hypotheses and subsequently operationalized by research questions.

3.1 Research potential

As already shown in section 2.4, tribological systems are subjected to a running-in phase where increased friction and high wear rates occur. In context of resource-efficient machine elements, product developers are therefore endeavoring to keep the running-in phase as short as possible and thus to achieve a rapid formation of a stationary regime with lowest wear rates. In order to decrease these high wear rates during the running-in phase, a profound understanding of the influence of the surface topography must first be established.

In Figure 3-1, typical influences of a tribological system are shown. These factors are for example the materials of the base and counter body and the lubricant, the surface topography including roughness, waviness and form profiles of the friction partners, the boundary layer of the materials resulting from different manufacturing processes and the boundary conditions (speed, load, temperature).



Figure 3-1: Influences of a tribological system on the demonstrator of a bearing and a shaft

An isolated consideration of the surface topography in experimental investigations is not possible since a change in surface texture also leads to a change in the boundary layer due to the deviating energy dissipation during the manufacturing process. Furthermore, for microscopic investigations in machine elements, there are only few and very complex analysis methods, in order to display the contact properties under mixed-lubricated conditions. These experimental methods impact the contact itself so that no conclusion can be made on the tribological behavior.

For this reason, a numerical approach on the microscopic scale needs to be developed, to investigate the influence of surface roughness on friction and wear during the running-in phase. Numerical models offer the possibility to keep a certain parameter field constant and only to vary the target variable to be examined and thus to determine their influence.

The state of the art for numerical simulations regarding friction and wear shows (cf. section 2.9.3), that there are already some approaches to calculate wear of dry running tribological systems with the finite element method. However, an approach for lubricated contacts under sliding conditions is not yet available, which takes into account wear mechanism and the surface topography on the microscale. Such calculations are significant more complex and computer-intensive compared to dry running calculations due to the consideration of the solid/fluid interactions. Particular challenges are the small wear depths of a few nanometers, resulting for example from a single turn of a journal bearing. In order to be able to consider the running-in phase holistically, the approach has to be able to calculate long durations by means of the possibility of a time scale.

The aim of the present work is therefore defined as follows:

*The **main objective of the present work** is to create a methodology to predict wear in the running-in phase on the microscopic scale in order to support the product developer in the earlier specific design of technical surfaces of resource-efficient machine elements in the product development process.*

By using the developed numerical calculation method, the required experimental tests and consequently the development costs of tribological systems can be reduced.

3.2 Research hypothesis

The research hypotheses of the present work can be derived from the above mentioned research objective. These hypotheses represent the main assumptions on which the following investigations are based:

Research hypothesis 1

The finite element method is a suitable tool to predict the wear behavior during the running-in phase in an accurate way and to calculate small wear depths of a few nanometers.

Research hypothesis 2

For a successful implementation of the calculation method into the product development process, the product developer must be supported by a user-friendly environment. This environment must provide the modeling, calculation and evaluation.

3.3 Research questions

Based on the research needs and the underlying hypotheses, the following research questions can be derived. They are used to operationalize the objective. The research questions are classified into two main questions:

Research question 1

How to calculate a very small local material removal due to sliding wear on real rough surfaces, using the finite element method?

The main challenges are the calculation of small wear depths, the determination of the time window in which characteristic values are established to parameterize the selected wear laws. A further step is to investigate whether friction and wear can be correlated.

Research question 2

How can the achieved results regarding friction and wear made be useable to the product developer?

This question addresses the applicability of the whole calculation method in an intuitive, user-friendly environment.

The procedure for answering the research questions is presented in the following chapter.

4 System analysis and model design

In this chapter, the initial target system for the calculation method and the corresponding model is derived, which allows the investigation of the influence of surface topography on the friction and wear behavior in sliding systems. The establishment of the initial target system is based on the development objectives by using the introduced methods and processes of individual product development processes from chapter 2.1. Especially the product model C&C²-A is used for system analysis and with the PGE – Product Generation Engineering approach by Albers, the development of appropriate models is described effectively to achieve the objectives.

First the demonstrator (machine element to be investigated) is established and the development objectives are shown. Further, the multi-level description of the tribological system is derived, which is necessary to investigate the influence of the surface topography on friction and wear on the microscopic level. Subsequently, the investigation activities are integrated into the product development process and the derivation of the methods and models is developed. Afterwards, the tribological contact in a mixed-lubricated regime is analyzed with the product model C&C²-A and the relevant interactions, to be taken into account, are identified. As in this work the development of the present friction and wear approach is based on an existing reference model, the PGE – Product Generation Engineering by Albers (introduced in section 2.1.3) is used, to derive the different development generations of the friction and wear model systematically.

4.1 Demonstrator definition

At a first glance it seems obvious that the main practical objectives of tribological systems is to reduce friction and wear in case of solid interactions, which are declared as main disadvantages. However, this does not meet the requirements in every technical system. As shown in Figure 4-1, there are also applications where minimizing friction and maximizing wear or minimizing wear and maximizing friction or maximizing both friction and wear is desirable. For example, compared to journal bearings, where friction and wear are to be minimized as far as possible, clutches and brakes are other well-known tribological systems in the drive train where wear is to be reduced and

friction should be as high as possible for a secure transmission of the braking or clutch torque.

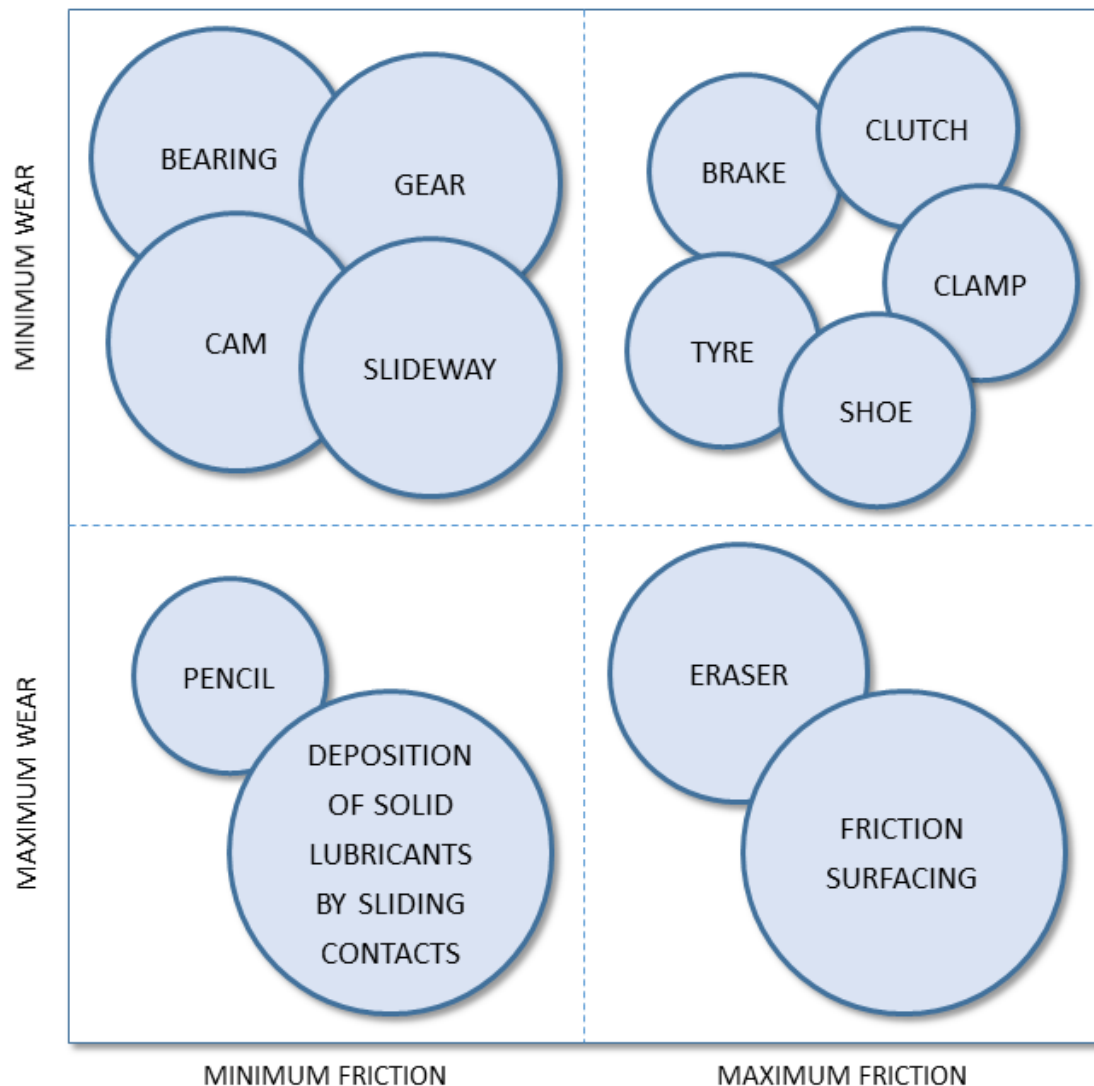


Figure 4-1: Portfolio of various applications in tribology with different friction and wear requirements (Stachowiak & Batchelor, 2005)

In the present work, journal bearings were chosen as demonstrator because these bearings are well researched with regard to sliding friction and there is the possibility to measure friction forces and wear rates on a journal bearing test bench within the investigation environment. The wear rates are measured continuously and in real-time with radionuclide-technique. As Scherge, Pöhlmann and Gervé (2003) mentioned, this method is especially suited to mechanical systems showing low wear rates due to its extremely high resolution.

Journal bearings can be classified into two types of friction regime. Non-lubricated journal bearings and lubricated journal bearings. If the boundary conditions permit the use of liquid lubricants, this is a suitable means for separating the friction partners and thus reducing friction and wear. In lubricated journal bearings (hydrodynamic

bearings), there are different lubrication regimes as introduced in section 2.3. In a hydrodynamic regime, the two friction partners are separated completely from each other by a disjunctive lubrication film and friction and wear occur in a very small level. If mixed lubrication is present, solid contact occurs between the roughness asperities of the interacting surfaces and friction and wear is increasing. To take into account surface topography, a single macroscopic approach is insufficient. To quantify the influence of surface topography on friction and wear in such a tribological system, multiscale investigations are necessary. On this account, an additional approach on the microscopic scale is necessary to establish friction and wear phenomena to be used at the macroscopic scale. The main development objectives are consequently:

- Extension of the understanding of the influence of surface roughness on the friction and wear behavior to minimize these two disadvantages in the context of journal bearings.
- Supporting the product developer in the specific design of resource efficient journal bearings and reduction of extensive experimental test

The isolated investigation of the influence of the topography has not been possible yet in experimental tests, since there are no suitable possibilities to look into the contact in mixed-lubricated systems. Due to variations in finishing and post-machining processes of the experimental sample, the boundary layer and the waviness will be changed as well. Therefore, a numerical approach is derived, which allows the variation of the surface roughness in isolation and their influence on friction and wear in the running-in phase. In the running-in phase, there are the highest wear rates, which are to be reduced in resource-efficient journal bearings. As described in section 2.4, in the steady state phase, the wear rates are significantly smaller.

Journal bearings are often used in combustion engines for example as main or connecting-rod bearings. In order to reduce fuel consumption and CO₂ emissions of vehicles, new operating strategies like start-stop systems have been implemented. As a result of these new strategies, new problems occur like the stationarity of the oil in powertrain components in the stop phase. Due to frequent and distinct static phases, the lubrication cannot all the time be kept in the tribological contacts of the machine elements. At every transition from stop to start, the liquid has to be transported back into the lubrication gap what consequently increases the occurrence of mixed-lubrication. In order to meet the new operating conditions, the bearings have to be adapted and evolved as mentioned in chapter 1. To take into account such operating conditions, a multilevel framework for the holistically investigation of journal bearings from the micro- to the macroscale is used. Such a multilevel description is shown in Figure 4-2 by using C&C²-A.

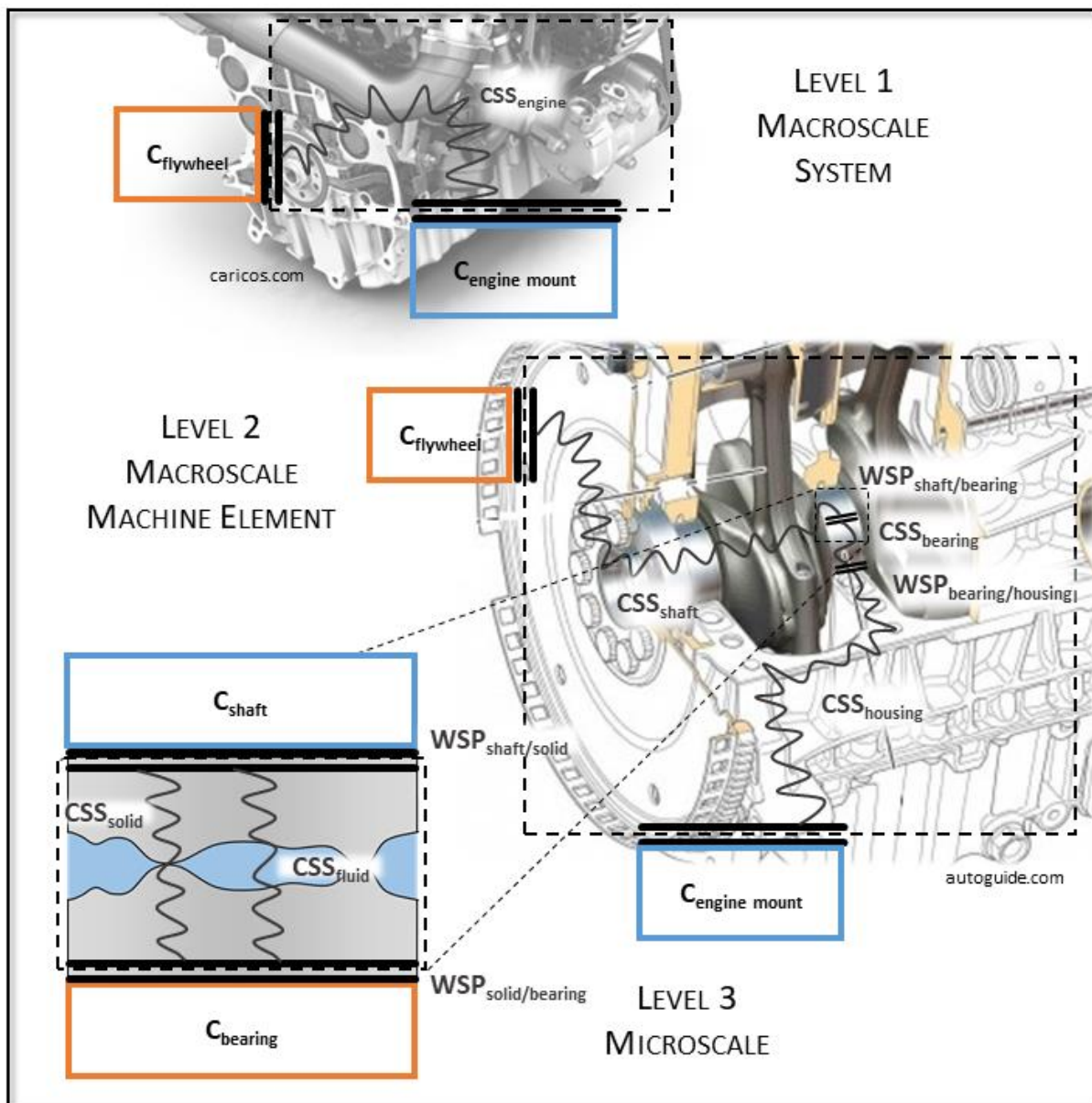


Figure 4-2: Multiscale description of a journal bearing in context of C&C²-A

Starting from a main bearing in a combustion engine, the entire system must first be considered in order to derive the relevant boundary conditions affecting the bearing. On the macroscale level 1, the whole system is shown in context of C&C²-A. The combustion engine corresponds to the channel and support structure CSS_{engine}, the connector C_{engine mount} contains information about the incoming boundary conditions and the connector C_{flywheel} contains information about the output at the flywheel. Both connectors need to be taken into account to determine the correct operating conditions. A further detailed view of the combustion engine is presented in macroscopic level 2. In this illustration, the combustion engine is divided into individual machine elements which are identified by the channel and support structures. For reasons of clarity, not all machine elements of the combustion engine are shown. For better understanding only the crankshaft (CSS_{shaft}), the main bearing (CSS_{bearing}) and

the engine block (CSS_{housing}) are shown. The interfaces are represented by the working surface pairs. These are the working surface pairs between the crankshaft and the main bearing ($WSP_{\text{shaft/bearing}}$) and between the bearing and the motor block ($WSP_{\text{bearing/housing}}$). The connectors $C_{\text{engine mount}}$ and C_{flywheel} remain identical in comparison the macroscale level 1. Since only the combustion engine is shown in more detail, there are no changes regarding the connectors.

Since the influence of the surface roughness on friction and wear is investigated in this work, the contact between shaft and bearing is of interest. In order to investigate the surface roughness, the microscopic scale must be taken into account. In Figure 4-2, this point of view corresponds to the microscopic level 3 by examining the contact between the shaft and the bearing ($WSP_{\text{shaft/bearing}}$) in more detail by taking the two surfaces in isolation. Between both surfaces, fluid (CSS_{fluid}) is present. Since the friction regime to be investigated is mixed lubrication, including solid contact, wear particles and dirt, these phenomena are all summarized in the channel and support structure CSS_{solid} . Due to the changed design space, the connectors also change on the microscopic level. For this modelling the input variables are now defined by the crankshaft and the output variables by the bearing. The boundary conditions must therefore be determined for this size scale. A detailed description of the microscopic scale is given in section 4.3. For a better representation, a higher degree of detail has been omitted in this illustration.

4.2 Classification in the product development process

If a developer or a team of developers gets the task of developing a journal bearing with improved friction and wear characteristics, a product development process is launched. In general, this means according to section 2.1.1 that a system of objectives is transferred to a specific system of objects by using an operation system. The system of objectives contains all goals and targets of a development process, including their dependences and boundary conditions within a defined area of interest (Albers, Behrendt et al., 2017). Using the example of a journal bearing, the surface topography to be optimized is part of the system of objectives. The system of objects contains the solutions for the system of objectives and is constantly expanding with the results during the process. Consequently, the system of objects also contains the actual product, in this case the optimized journal bearing with the adapted topography. The vital conversion from objectives to objects is made within the operation system, which is composed of structured activities, methods and processes for the realization (Albers, Behrendt et al., 2017).

As already mentioned in section 2.1.1, these relationships are described in the iPeM - integrated Product engineering Model by Albers. A central activity of the operation system in the product engineering process is the validation, which controls and monitors the continuous adjustment between the achieved actual state and the defined target state. In addition, product related features must also be validated, e.g. by virtual or physical simulations (Albers, Behrendt et al., 2016). Through validation activities, knowledge is generated within the product development process and the product generation process is controlled. For a successful product development, it is therefore essential that the validation is carried out over the entire development time of product generations and from the very beginning (Albers, 2010). It is therefore essential to understand validation as an ongoing activity during the product development process. This procedure corresponds to the pull principle by Albers, Matros, Behrendt and Jetzinger (2015) and describes the definition and development of validation activities, including models and validation environments based on specific validation activities (Albers, Behrendt et al., 2017). Knowledge acquired through validation activities may require an intervention or adaptation of the product development process. The sooner negative or new validation results become known, the lower are the costs that arise during the intervention in product development or in the adaptation of it (Albers, Behrendt et al., 2016).

For the optimization of the topography of journal bearings, this means that appropriate validation environments must be available throughout the product development process. Since the tribological properties can be quantified in respect to friction and wear under mixed lubricated conditions only after the manufacturing of the complete machine element, an early specific design of the inner surface is all the more important. However, the isolated evaluation of the surface roughness has not been possible yet in experimental investigations. Due to different manufacturing and finishing processes of the samples to create various surface structures, the boundary layer and the waviness of the bearing or shaft are changed as well. Since there is no physical approach available, this work presents a virtual approach of a validation environment for the investigation of the influence of surface roughness of tribological systems. This virtual approach first needs to be verified. Verification in this context of numerical models is to check if the model is basically plausible and correct and whether the requirements are met, set out at the beginning. A statement whether the created model describes a real system adequately and thus also meets unspecified requirements, provides the validation (Verein Deutscher Ingenieure, 2004). The development of the virtual validation environment is carried out in a target-orientated way with the iPeM - integrated Product engineering Model in context of PGE. This adapted iPeM offers different layers with an exactly identical structure both for the single product generations and the validation system.

As introduced in section 2.1.3, the modular integrated Product engineering Model in the context of PGE offers the possibility to handle the development of validation systems based on reference systems in addition to the product itself. Since the objective of the present work is to develop a validation system, but the overriding long-term goal is to optimize the topography of a journal bearing earlier in the product development process, the product remains the journal bearing and not the validation system itself. For clarification, the product and the validation system are displayed in the context of the extended iPeM in Figure 4-3.

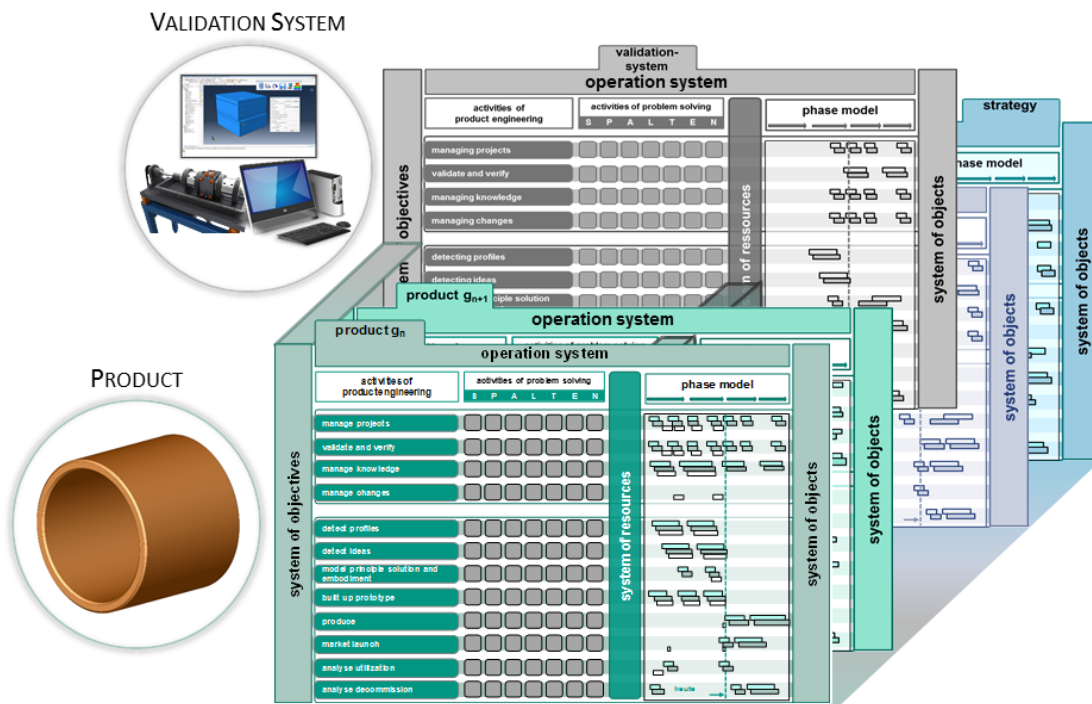


Figure 4-3: Extended iPeM including the product and the validation system (Albers, Reiss, Bursac & Richter, 2016)

The initial journal bearing corresponds in this case to the product generation G_{n-1} in which the topography should be adapted to reduce friction and wear and consequently to design resource efficient machine elements. The journal bearing with the optimized topography corresponds to the product generation G_n . So, the first layer “product” describes the development of the journal bearing itself. As there could be further developments of individual product generations, it is possible to add one layer for each of these generations to interrelate the different generations.

The validation system contains all components which enable the validation of the developed product. These components are the hardware to carry out numerical investigation, the numerical methods to handle investigations on the influence of surface roughness on friction and wear, the different software needed and also the test benches for the validation of the methods. The initial validation system is considered

as validation system generation G_{n-1} . If one component of the validation system is significantly further developed, in the present work the numerical investigation method, the entire validation system will be transferred to the next validation system generation G_n . The development of individual components of the validation system can also be based on reference components. As mentioned in section 2.1.3 it is important that the validation system should not be distinguished from the basic activity 'validation and verification' but provides the essential resources as a result.

Since the investigation of the influence of surface roughness on friction and wear cannot be carried out with physical experimental devices in a sufficient way (see section 4.2), a virtual investigation method is derived in the present work. The present numerical approach is based on the mixed-lubrication model by Albers and Lorentz (2010) (cf. section 2.9.2), taking into account real measured surface roughness. Based on the finite element method, contact interactions in tribological sliding systems were investigated in a mixed lubricated regime. In this model, some assumptions were made, which are to be considered in more detail in the present work. The main assumptions of the previous model are listed below:

- wear phenomena are not taken into account
- boundary layers' physical and chemical properties are not considered (same material properties for the boundary layer as for the macroscopic material properties)
- no direct thermal interactions occur between fluid and solid
- no cavitation effect is taken into account (two phasic model is too complex in this preliminary study)

In this work, the mixed-lubrication model is enhanced through the implementation of existing wear models to describe previously neglected wear phenomena in more detail. This extension cannot be done in a single step and software. A standard software for such complex investigations does not exist yet. The further development of the existing model is consequently done step by step. The individual development steps involved are of varying degrees of complexity, which is why the extent, to which the individual models are verified, differed. The degree of maturity of the various stages of development can also be increased to varying complexity. At the same time, model assumptions can be reduced to varying degrees. In case of coupling different simulation models, the increase in maturity and the reduction of model assumptions is significant. The coupling of different methods to enhance the mixed-lubrication model is described in detail in section 4.4. Some selected development steps based on the reference model, like a force controlled loading, the implementation of wear and residual stresses or the creation of a graphical user interface to support the product developer are shown in Figure 4-4.

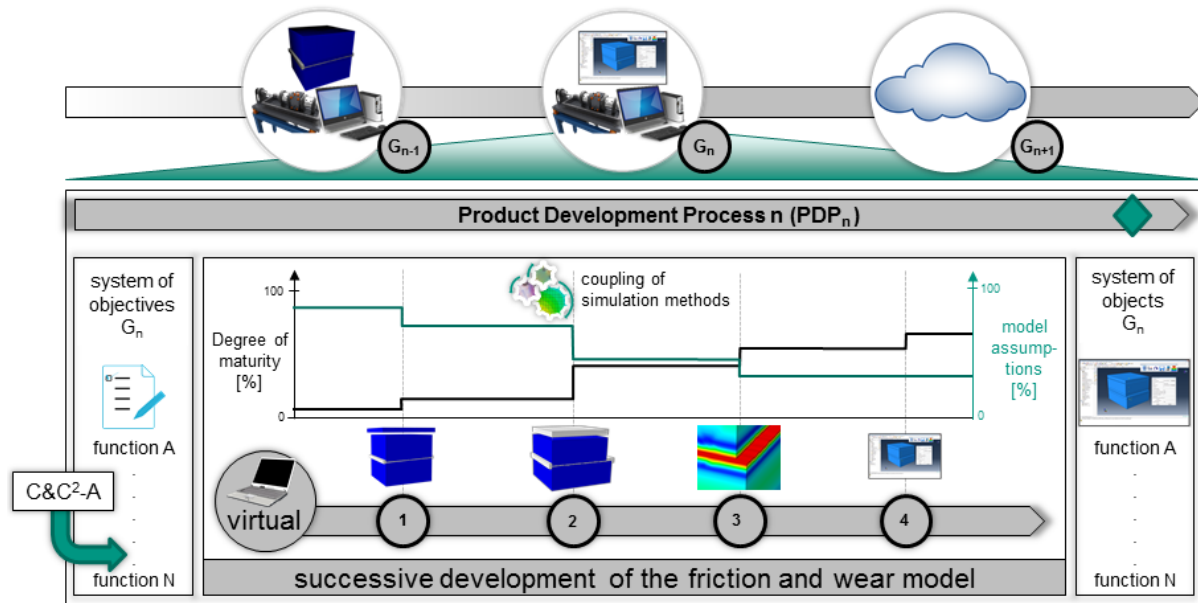


Figure 4-4 Different development steps of the numerical friction and wear model based on the reference model

It is clear to see the significant change in the degree of maturity and the model assumptions, achieved by coupling different simulation methods.

In this work, the Contact and Channel Approach (C&C²-A) (cf. section 2.1.2) was used first to analyze the numerical model of the validation system generation G_{n-1} (system of objects) and second, to derive the system of objectives of the numerical model of the validation system generation G_n , which contains the desired results of the simulation (Albers et al., 2011). In the next section, the analysis of the object system of the numerical model of the validation system generation G_{n-1} and the creation of the system of objectives of the numerical model of validation system generation G_n is described in detail.

4.3 System analysis with the Contact, Channel and Connector Approach (C&C²-A)

In this section, the tribological contact between a rotating shaft and a bearing is analyzed in detail. In order to derive all relevant interactions and boundary conditions, a detailed model of the contact must first be developed. This analysis is carried out with the Contact, Channel and Connector Approach (C&C²-A) from section 2.1.2. In Figure 4-5, two operating conditions of a journal bearing are shown. In a mixed lubricated regime (on the left) as well as in a hydrodynamic regime (on the right), surface roughness need to be taken into account for a precise description of the occurring phenomena.

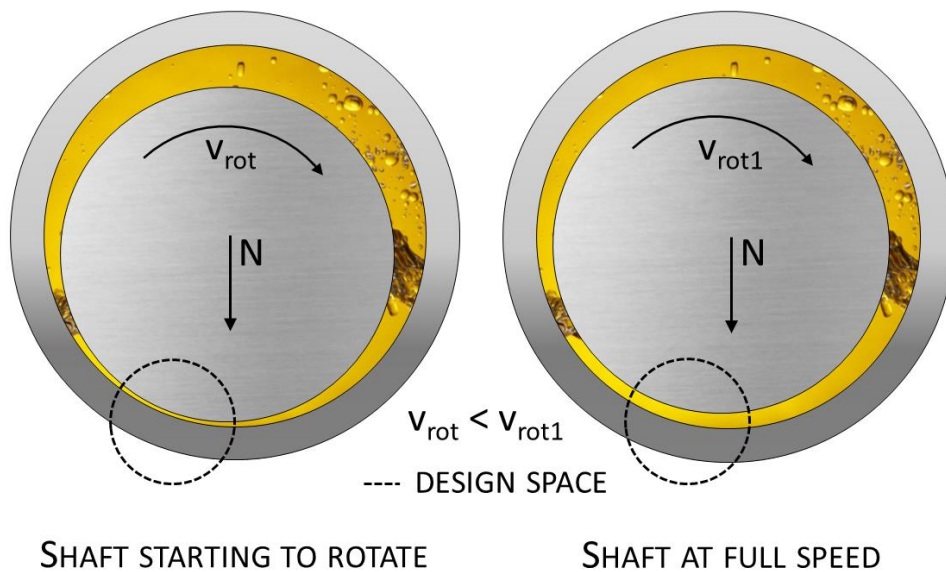


Figure 4-5: Operating conditions of a journal bearing: left: mixed-friction if the shaft is starting to rotate, right: hydrodynamic

In comparison with a hydrodynamic regime, for mixed-lubricated conditions on the microscale level, modeling has to be extended to the contact between solid interactions resulting from the smaller lubrication gap. Figure 4-6 shows the result of the analysis of the previous mixed-lubrication model (reference model) by Albers and Lorentz (2010) with C&C²-A is shown. The surfaces asperities are shown greatly enlarged for the sake of clarity. Inside the design space, various working surface pairs (WSP) and channel and support structures (CSS) are marked. Friction occurs in each WSP and inside the CSS_{fluid}. Friction results from the relative movement of surface asperities and from shearing of the fluid. For the model presentation, an isolated point in time is shown. As presented by Lorentz (2013b), WSP_{solid/solid} includes also the third body (see section 2.4.3), which represents the mixture between corrosion, dirt and lubricant when the film thickness is less than 0.025 μm . At the solid/fluid interactions, there is no slip at the walls of the solids, which is resulting in a friction force due to the mentioned shearing of the fluid. A further problem consists in having cavitation effects. This effect is caused by the rough surfaces provoking low pressure fields and pressure loss. In a hydrodynamic regime, solid/solid interactions disappear and WSP_{solid/solid} does not have to be considered further.

The sum of all channel and support structures is called support structure and contains all the relevant material properties.

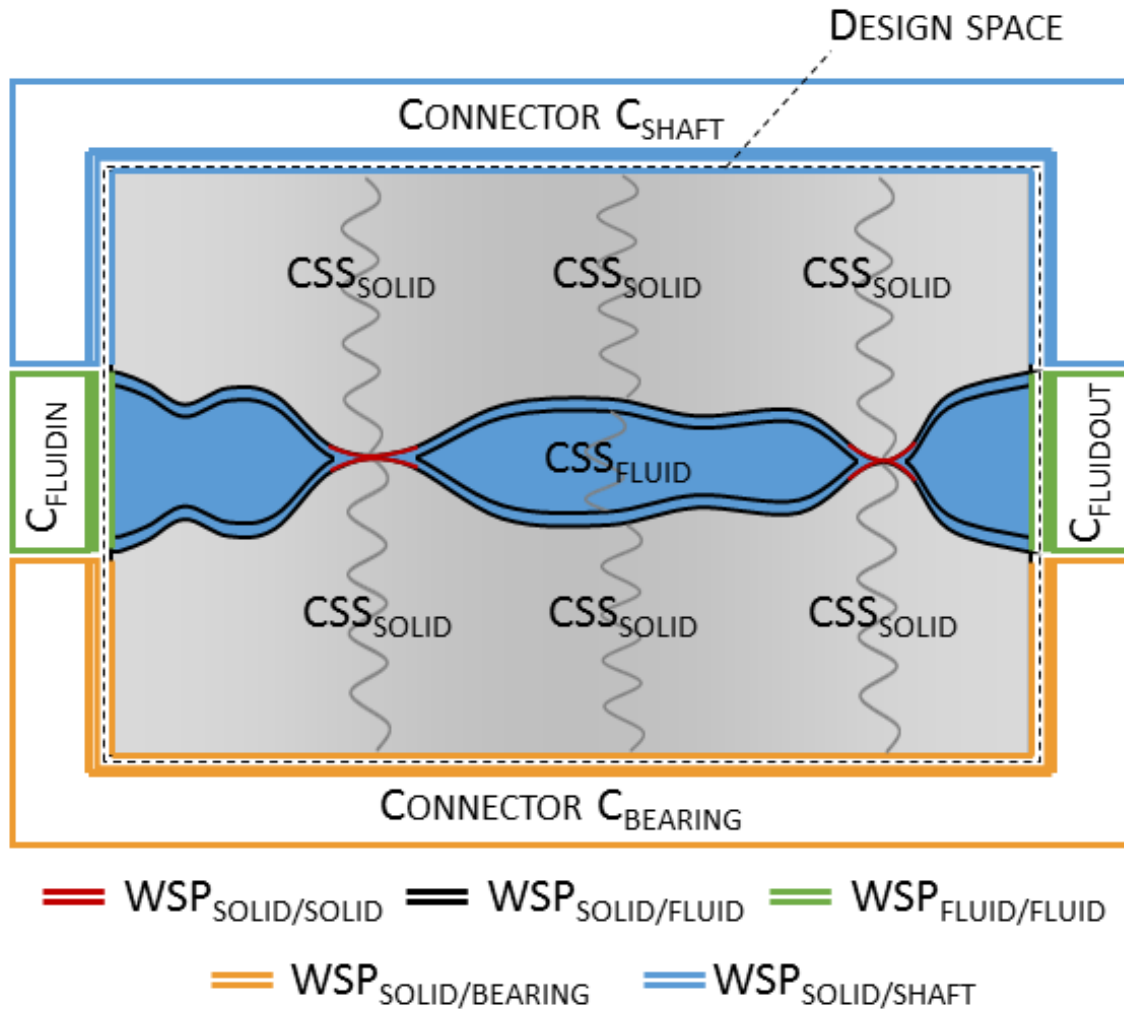


Figure 4-6: Analysis of a mixed-lubricated contact with C&C²-A

By defining the design space as seen in Figure 4-6, this is resulting in four connectors for a journal bearing. The design space is defined in such a way that the microscopic contact interactions can be modelled with sufficient accuracy. The connectors integrate the relevant interrelations in each WSP at the border of the design space that are outside the viewing scope in the system view. The relevant interrelations of the connectors are:

- C_{shaft} : Course of contact pressure, sliding velocity resulting from the rotational speed of the shaft
- $C_{bearing}$: Boundary conditions of the bearing (spatially fixed)
- $C_{fluidin}$: Inlet fluid pressure resulting from macroscopic bearing calculations
- $C_{fluidout}$: Outlet fluid pressure resulting from macroscopic bearing calculations

The relevant parameters inside the design space are defined in the channel and support structures of the involved structures. The parameters of the structures are:

- **CSS_{solid}**: Material properties of the solids (e.g. density, elastic modulus, yield strength, critical shear stress, etc.)
- **CSS_{fluid}**: Material properties (e.g. density, viscosity, etc.)

Through the early analysis with C&C²-A it can be ensured that all relevant working surface pairs and channel and support structures are taken into account in the following numerical models. Due to working surface pairs and channel and support structures, the possibility exists between the connectors in Figure 4-6 to exchange energy, substance and information.

To implement wear due to solid interactions into the mixed lubrication model, $WSP_{solid/solid}$ has to be adapted. At the solid interactions ($WSP_{solid/solid}$), present wear phenomena can be adhesion, abrasion, fatigue or corrosion. The special issue of these adapted working surface pairs is the non-constant contact area. The working surface pair is therefore time dependent and variable. If wear occurs in the $WSP_{solid/solid}$, the real contact area in this micro contact is increasing. Due to the local change of the contact surface, the local pressure also changes. The local pressure is decreasing when the contact surface is increasing under the assumption of a constant contact force. An increased contact surface also influences the friction and wear behavior. Therefore, the local surface pressure, the coefficient of friction and the wear depth are used as meaningful parameters to quantify the influence of the surface roughness.

Due to the consideration of wear on the solid interactions, the channel and support structures of shaft and bearing (CSS_{solid}) have to be extended by the variables which allow a description of the occurring wear phenomena. In detail, such variables are suitable wear laws and material related parameters to describe the amount of material loss due to solid contact. The structures of the solid bodies are containing now the following parameters:

- **CSS_{solid}**: Material properties of the solids (e.g. density, elastic modulus, yield strength, critical shear stress, etc.), suitable wear law to describe the occurring wear phenomena and material related wear parameters like introduced in section 2.4.2

Since only the channel and support structures of the solids (CSS_{solid}) are extended, the actual C&C²-A model shown in Figure 4-6 does not change. As mentioned above, wear on the $WSP_{solid/fluid}$ due to cavitation effects or abrasive particles in the fluid are neglected.

4.4 Benefit by coupling of various simulation methods

As described in section 4.2 and displayed in Figure 4-4, the coupling of various simulation methods or tools allows a significant increase in maturity and reduction of model assumptions. This is due to the fact that new, more complex problems can be addressed by the coupling of various disciplines, as it is not possible with a single standard program. The advantages of well-known and widespread numerical methods can be combined to gain new insights. At the IPEK – Institute of Product Engineering is therefore an approach pursued based on the core concept of linking existing and established commercial methods and tools in order to make complex problems manageable by the product developer and to improve the quality of new products to be developed. One of the main tasks here is to run automatically these coupled methods and to provide suitable user interfaces for the product developer. This approach enables the development of user-friendly tools that are widely accepted in development practice.

The coupling of computer-aided simulation tools offers the possibility to support the product developer during system analysis and synthesis. The possibility of investigating the influence of real technical surfaces on friction and wear by coupling the finite element method (FEM) with wear models based on PYTHON scripts enables the topography of tribological systems to be specially designed at an early stage. According to Albers, Reichert, Serf, Thorén and Bursac (2017), the provision of “Graphic User Interfaces” (GUI) allows the high modelling effort of complex problems to be mastered in a user-friendly manner. The development of this required GUI is described in section 5.5. This step is of enormous importance, since often several programs are necessary to handle a single problem within a numerical framework.

An approach for the visualization of coupling different simulation methods suitable for mathematical, numerical and analytical methods is shown in Figure 4-7.

Within the approach for coupling different simulation methods is distinguished between environment and virtual system. The environment provides the boundary conditions that are linked to the virtual system via interfaces. Such boundary conditions can be, for example, estimated parameters or data sets such as material properties or measurements on a real system. The level of detail is determined by the product developer according to the maturity of the virtual system. In order to illustrate the virtual system, various methods, which can be understood as individual models of the system, are linked together by means of couplings. These individual models are displayed as three-level blocks and contain information about the method used in the upper field, in the middle about the used tool and at the bottom about the model-specific name. Some

predefined methods like finite element method (FEM), finite volume method (FVM) or computer aided design (CAD) are assigned special colors to facilitate recognition of the methods. When these elements interact with each other, a distinction is made between manual coupling (dotted arrow) and automatic coupling (solid arrow), which both can be unidirectional or bidirectional. By means of these couplings, parameter sets (P_x) are transferred between the different models.

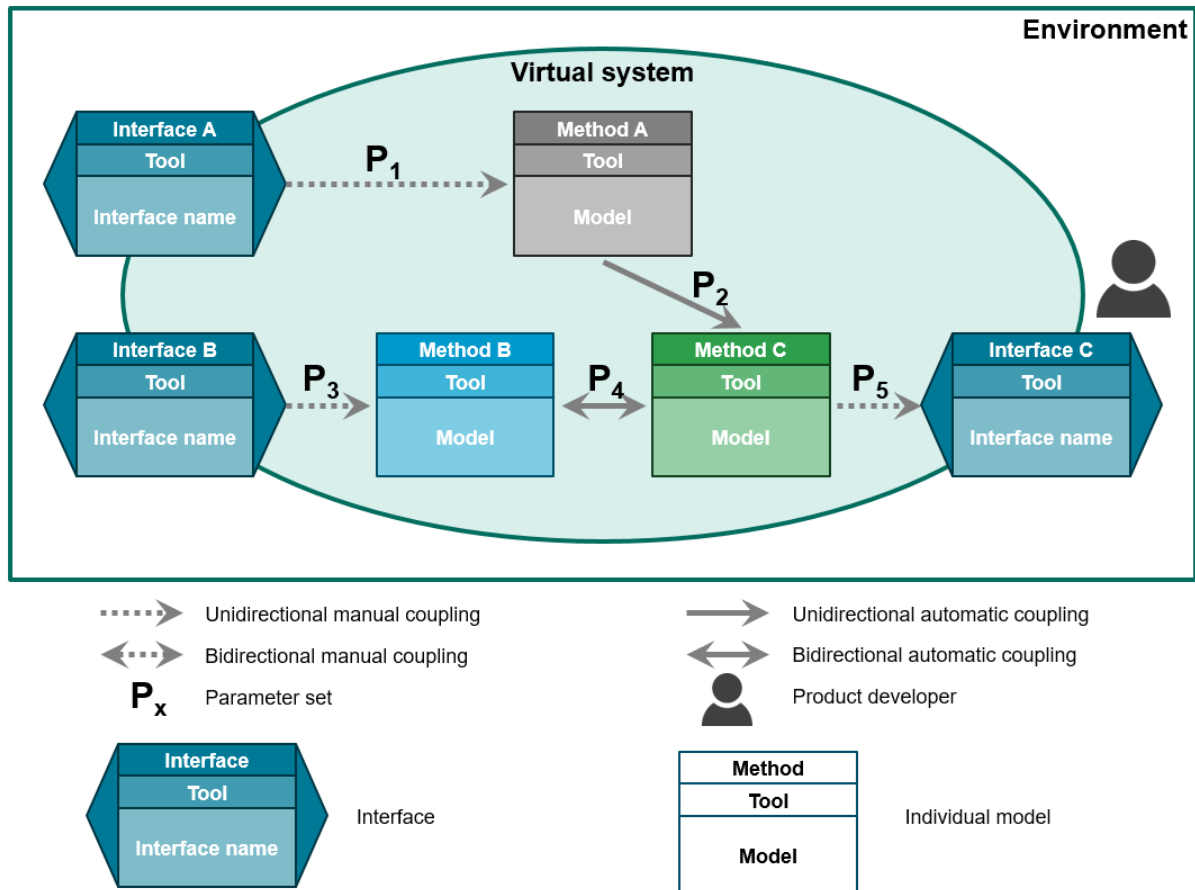


Figure 4-7: Approach for coupling of simulation methods (Albers, Reichert, Serf et al., 2017)

Figure 4-7 shows an automatic, bidirectional coupling of methods B and C, which corresponds to a data transfer of the parameter set P_4 with automatic response. In contrast to the sequencing of individual linearly executed programs, this methodology can also be used to map parallel circuits of subsystems, optimization loops or other coupled loops, for example, in order to be able to map parts of the virtual system that are traversed in parallel or cyclically. As a user of the methodology, the product developer is at the center of product engineering and forms the interface between the virtual system and the environment, in order to transfer the knowledge gained with the help of the overall methodology into a new product generation.

4.5 Establishment of the initial target system

From the research objectives from chapter 3 and the explanations in this chapter, the main objective can be deduced to develop a numerical method, which allows the investigation of the influence of surface roughness on friction and wear in the running in phase under mixed lubricated conditions. This method is part of a validation system that allows the product developer to design new optimized surfaces for tribological systems earlier than previously possible. Due to the lack of appropriate experimental investigation methods, the numerical approach should help to characterize the influence of surface topography on the microscale level. This has to be done for lubricated and non-lubricated contacts, since both types of contact can occur in journal bearings. The influence of surface roughness will be quantified by the effects on:

- Coefficient of friction
- Contact pressure
- Wear depth
- Changes in surface topography (statistical roughness parameter and Abbott-Firestone-Curves)

As mentioned above, changes in surface topography can be characterized with this parameter reliably. In addition to the influence of surface roughness, the effects of specific parameters on friction and wear will be also investigated. These are listed below:

- Material properties of the solid materials (yield strength and E-modulus), since the elastic and plastic material behavior has a great influence on friction and wear.
- Fluid viscosity, since the viscosity can vary by a factor of 100 due to pressure dependence.
- Ratio of fluid pressure and normal load for adjusting the narrowest lubrication gap of the tribological system.
- Influence of the running-in procedure what means in which time sequence the final load level is applied. This is intended to provide information if a severe or a mild running-in procedure helps to minimize wear.
- Surface machining and direction to investigate the influence of different manufacturing processes of the friction partners on friction and wear.
- Residual stresses due to manufacturing processes.

Due to the presence of different disciplines from mechanics, fluid dynamics and fluid-structure-interactions in the development task, a user interface must be created which

allows the product developer to use the developed numerical approach in a goal oriented-way.

There are several steps required to develop a numerical method that allows valid information about the surface properties in tribological systems under sliding conditions and mixed-lubrication. These several steps are:

- Model design of the micro model for mixed lubrication presented in section 5.2 and 5.3.
- User interface to support the product developer described in detail in section 5.5
- Model verification and validation (see chapter 6).
- Results on the influence of the above listed parameters on friction and wear presented in chapter 7 and discussed in chapter 8.

5 Numerical model at the microscopic scale

In this chapter the method to develop the modelling approach based on the finite element method, taking into account technical topography of a tribological system, is presented. First, the operating conditions of journal bearings, resulting from real applications are established and applied to a macroscopic approach. From this approach, the resulting output values are applied to the numerical model on the microscale level as input values. Next to the setting of this numerical model, the importation of real measured surfaces and the implementation of a method to apply wear is introduced. To support the product developer in designing new surfaces and in using the present approach for validation, a graphical user interface (GUI) is developed.

5.1 Establishment of operating conditions in journal bearings

For the calculation of the boundary conditions for the mixed-lubrication model on the microscale level, operating conditions of journal bearings have to be established. The operating conditions of journal bearings are derived from the experimental environment of a journal bearing test bench. The applied working conditions are defined for the operation in mixed friction and shown in Table 5-1.

Table 5-1: Operating conditions of journal bearings in mixed friction

Parameter	Journal bearing
Inner diameter [mm]	20
Outer diameter [mm]	23
Width [mm]	20
Rotational speed [1/min]	100 – 1000
Load [N]	800 - 1500

With the macroscopic approach, based on existing analytical models, the fluid pressure distribution needs to be calculated. To use the Reynolds equation (cf. section 2.5.1) to link fluid pressure and lubricant film thickness, the lubrication regime is considered as

fully hydrodynamic. The results are used to define the assumptions for the fluid pressure on the microscopic scale of the lubricant.

The lubricant is a reference oil FVA 1, defined by the German research association of powertrain technology – FVA (Forschungsvereinigung Antriebstechnik). This oil is available for years with identical quality and with defined additives provided. The aim of this reference oil is to improve the reproducibility and comparability of test results in industry and universities. The properties of the lubricant are shown in Table 5-2.

Table 5-2: FVA 1 lubricant properties

Parameter	FVA 1
Density, 15°C [kg/m ³]	861
Kinematic viscosity, 20°C [mm ² /s]	34
Kinematic viscosity, 40°C [mm ² /s]	15
Kinematic viscosity, 100°C [mm ² /s]	3,36
Density-viscosity constant [-]	0.818

To calculate the fluid pressure distribution, the following equation, derived from the Reynolds equation, is used:

$$p(\theta) = \frac{3 \cdot v \cdot \eta}{h^3 \cdot R} \cdot \frac{dh}{d\theta} \left(y^2 - \frac{L^2}{4} \right) \quad (5-1)$$

with the sliding velocity v , the dynamic viscosity η , the width coordinate y , the bearing radius R , the bearing width L and the film thickness h , which is defined as follows:

$$h = c \cdot (1 + \varepsilon \cdot \cos \theta) = c + e \cdot \cos \theta \quad \text{with } \varepsilon = \frac{e}{c} \quad (5-2)$$

with the bearing clearance c and the eccentricity ratio ε , the ratio of eccentricity e to clearance c . This equation is valid for short bearings where the axial length is less than the shaft diameter. In this case, the pressure gradient along the y -axis is much larger than the pressure gradient along the circumferential direction. The equation gives accurate results for $L/D < 1/3$.

As mentioned above, the lubrication regime is considered as fully hydrodynamic. Since mixed friction appears in journal bearings with smaller sliding velocities, the calculations are carried out under such a small sliding velocity to get the assumption

for the fluid pressure in the friction regime of mixed lubrication. A survey about the mentioned geometrical dimensions of the journal bearing is given in Figure 5-1.

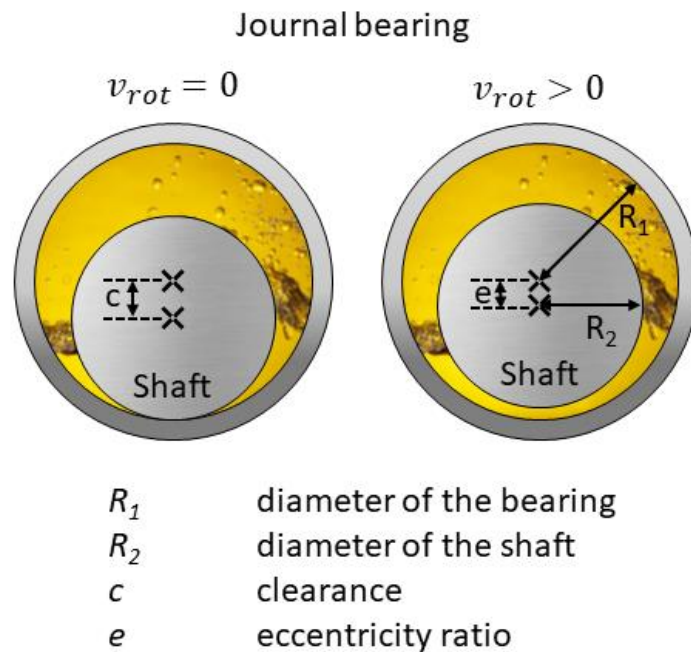


Figure 5-1: Geometric dimensions of a journal bearing

To calculate the pressure curve of the journal bearing, the geometric quantities and operating conditions were derived from the experimental setup, as already mentioned above. The clearance c results from measurements of bearings and shafts. For this purpose, ten journal bearings and ten shafts were measured to determine the inner (bearing) and outer diameter (shaft). The mean measured diameter of the bearing is 20.060 mm and the diameter of the shaft is 20.000 mm. The difference between the diameter of bearing and shaft is consequently 60 μm .

For the fluid pressure boundary condition, the resulting pressure curve is obtained with the parameters from Table 5-3.

Table 5-3: Geometric quantities and operating conditions of the journal bearing

Parameter	FVA 1
Clearance [μm]	30
Eccentricity [μm]	29.5
Rotation velocity range [RPM]	950
Diameter [mm]	20
Length [mm]	20
Fluid	FVA 1

For the microscale level, the pressure in the narrowest gap is used. For the selected boundary conditions, this is approximately 70 MPa, as it can be seen in Figure 5-2. This calculation result is based on Reynolds equation (5-2). Cavitation was neglected when determining the fluid pressure.

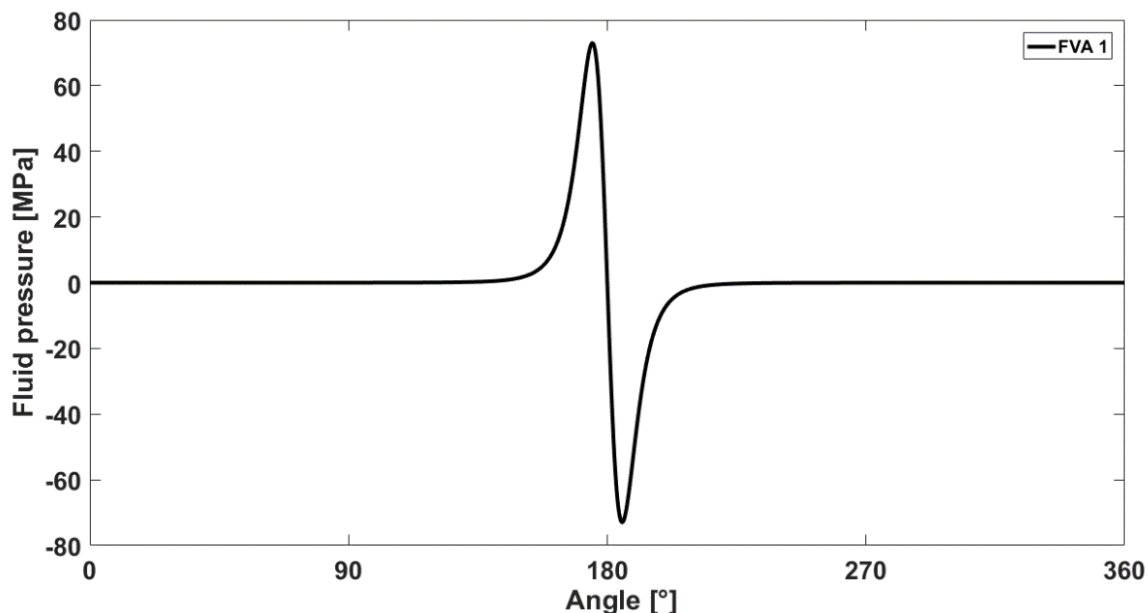


Figure 5-2: Fluid pressure distribution calculated for journal bearing. Cavitation was neglected when determining the fluid pressure distribution.

Since the boundary conditions can vary to a certain degree, the fluid pressure is varied (see section 7.3) to cover a wide spread range in the following investigations.

5.2 Numerical model for mixed-lubrication

To enable the calculation of local wear depths for real rough surfaces, a mixed lubricated model was extended by a wear routine. In this section, the model setup of the mixed lubrication model is described in detail, beginning with the import and preparation of the technical surface profiles, followed by the boundary conditions of the basic body, counter body and the fluid, the used material models for the solid and fluid materials and the contact definitions for solid and solid/fluid interactions. All calculations are carried out with the finite element software ABAQUS on the microscale level.

5.2.1 Discretization of technical surfaces and importation into FEM

The real technical surfaces are measured non-destructively with a white-light interferometer, described in detail in section 2.2.3. A measured surface profile (raw data) of a exemplarily turned specimen is shown in Figure 5-3. The shaft is measured with a discretization of 2.0 μm in x and y direction. The dimension of the measured

surface is $1000 \times 1000 \mu\text{m}$. Due to the high calculation time of the contact simulation, a surface of this size would be too large. For the modelling approach, any section with smaller dimensions can be extracted from the measured data and used for the calculation.

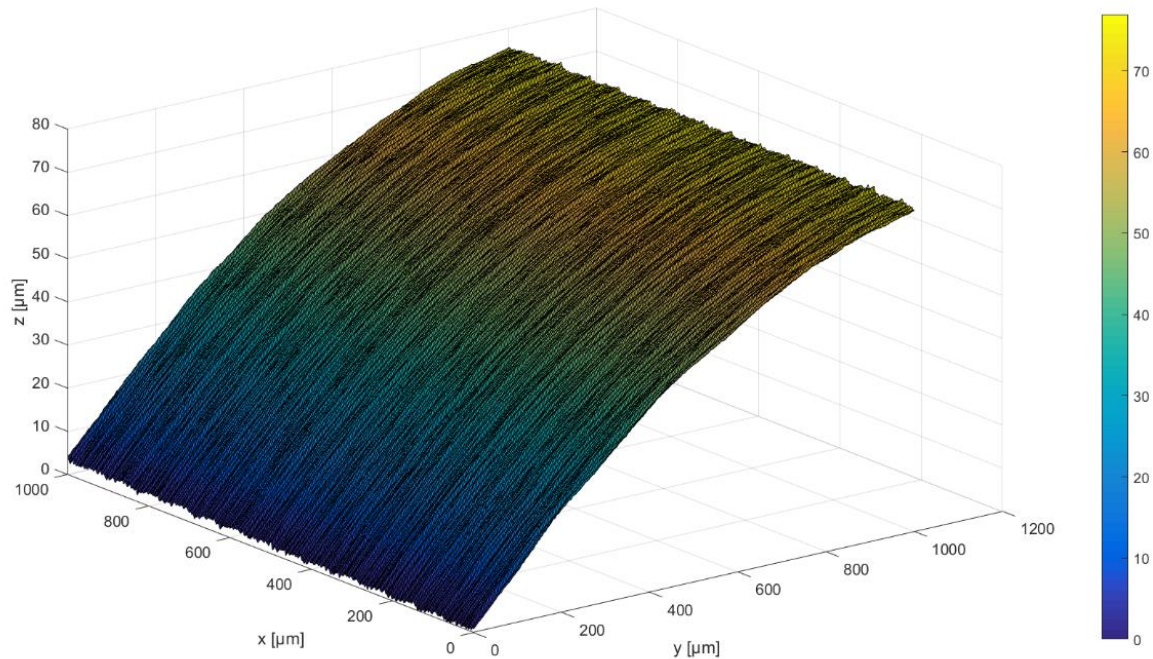


Figure 5-3: Measured surface profile of a specimen with a turned surface

For the investigation of the influence of surface topography on friction and wear, only the extracted roughness profile of the measured data is used. The elimination of the waviness is necessary to avoid too many degrees of freedom to be modelled. To extract the roughness profile, the topography signals are filtered to separate the roughness from the waviness and from the form profile (cf. section 2.2.1).

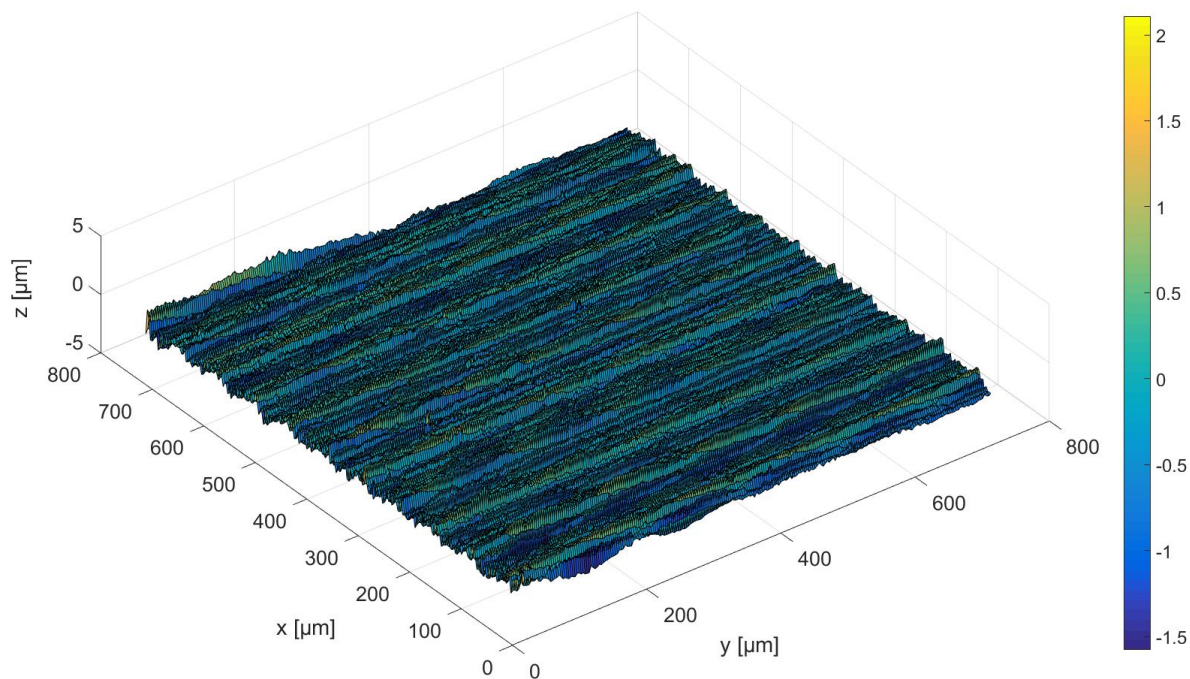


Figure 5-4: Extracted surface roughness of a turned specimen

In Figure 5-4, the filtered roughness profile of the turned specimen is displayed. Due to a high pass filter, the high frequencies are filtered to separate the roughness from the measured profile. In comparison to Figure 5-3, it is clear to see that the form and waviness profile could be eliminated.

In this work, three different tribological pairings are investigated. A pairing with two turned surfaces with a small surface roughness and a pairing with two turned surfaces with a high roughness. The third pairing is a combination of a ground and a honed surface. To handle the measured surface data in a finite element model, the data have to be imported into this simulation framework of the finite element software ABAQUS.

To transfer the measured surface data into the finite element model, the data is exported from the measurement software as a ASCII file, containing the coordinates of each measured discretization point (cf. section 2.2.4). With a MATLAB code, a solid body is build using the 3D B-spline theory. The result is a solid body in the neutral file format IGES. The main advantages of this file format are that it can be imported into arbitrary simulation environments and the flexibility of mesh refinements by using solid bodies to make the simulation model more efficient. The above mentioned solid bodies are shown in Figure 5-5.

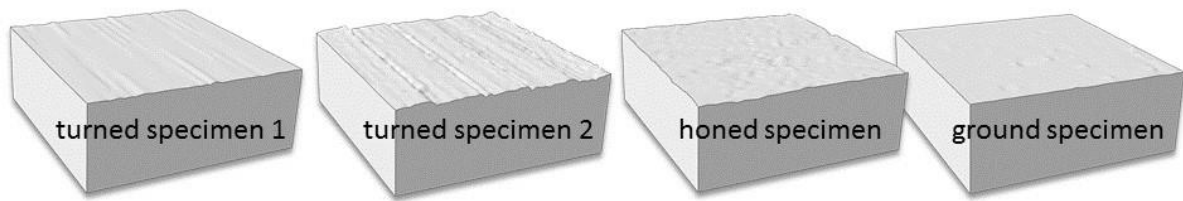


Figure 5-5: Solid bodies of measured surface data in neutral file format IGES

The corresponding main statistical roughness parameters of the surfaces of the three pairings are shown in the following Table 5-4. Both the surface structure and the statistical roughness parameters clearly show the greater roughness of the turned specimen 2 in comparison to the turned specimen 1.

Table 5-4: Statistical roughness parameters of the investigated specimen

Roughness parameter	turned specimen 1	turned specimen 2	honed specimen	ground specimen
sR_a [μm]	0.343	1.171	0.407	0.160
sR_q [μm]	0.437	1.461	0.565	0.247
sR_z [μm]	2.880	9.173	3.260	1.653
sR_{pk} [μm]	0.073	0.759	0.098	0.078
sR_{vk} [μm]	0.416	1.303	0.969	0.294

With this method to create solid bodies, dimensions of 2 x 2 mm with a measurement discretization of 2 μm is possible. Measurements with a smaller discretization have shown no significant changes in topography. In case of larger dimensions, there are so many measurement points that the generation of such surfaces will take a very long time.

5.2.2 Applied boundary conditions

The final setup of the mixed-lubrication model is shown in Figure 5-6. The created rough bodies from section 5.2.1 are arranged vertically and the fluid is between the contacting surfaces. The dimensions of the upper body are 225 x 225 x 80 μm . A height of 80 μm is sufficient to model the elastic-plastic material behavior as Lorentz (2013a) has shown in his work. The lower body is spatially fixed on the bottom and the lateral surface. In a first calculation step, the upper body is loaded force-controlled against the lower body to achieve a constant pressure. In a second calculation step,

the upper body is displaced in tangential direction with a constant velocity. The lower body is extended by 10 μm to a final length of 235 μm , to guarantee a constant average contact pressure during the defined displacing of 10 μm of the upper body. The solid bodies are meshed with linear hexahedron elements with an edge length of 3.0 μm near the contact area. To save calculation time, more distant areas are roughly meshed. The fluid part is also meshed with linear hexahedron elements with an edge length of 2.5 μm . A detailed description of the fluid structure interaction is following in the next section. The influence of the mesh properties is verified in section 6.2.1 for the solid mesh and in section 6.2.2 for the fluid mesh.

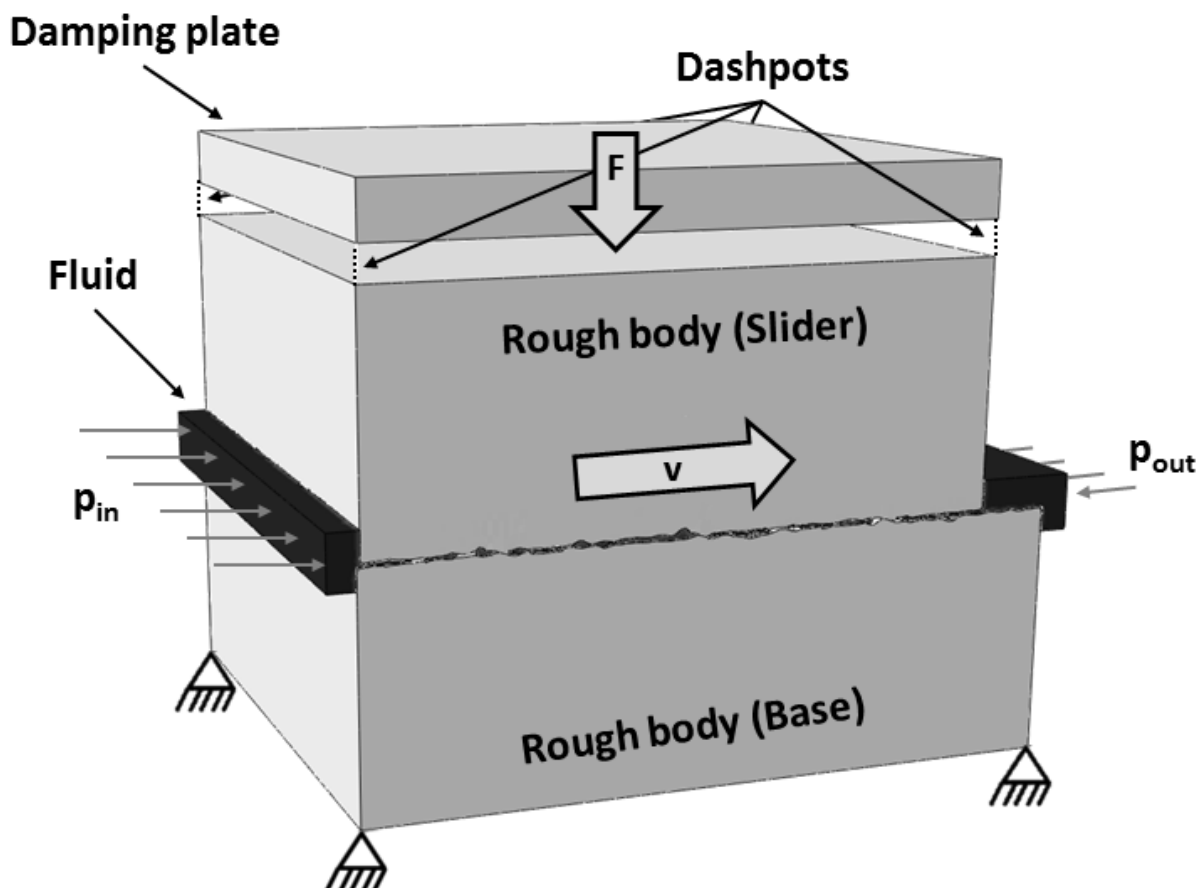


Figure 5-6: Setting of the mixed-lubrication model (Albers & Reichert, 2017)

The upper body is connected via dashpot elements at the four corners with a damping plate, defined as a rigid body with an unlimited stiffness, to avoid vibrations in case of asperity contact of the two bodies. The damping plate is displaced by the same way in tangential direction as the upper body. In normal direction, the damping plate is fixed. The dashpot elements are vertically aligned all the time and therefore only act in normal direction. For comparison, the applied normal force of 10 N for a damped and undamped loading is shown in Figure 5-7. In the reference model of Lorentz (2013a), the load is applied distance-controlled by a normal displacement. Therefore, the investigation of the damping behavior has not the subject of the feasibility study. Since

roughness peaks are removed during the wear process, constant infeed during the sliding process is no longer permissible to avoid varying lubrication gaps.

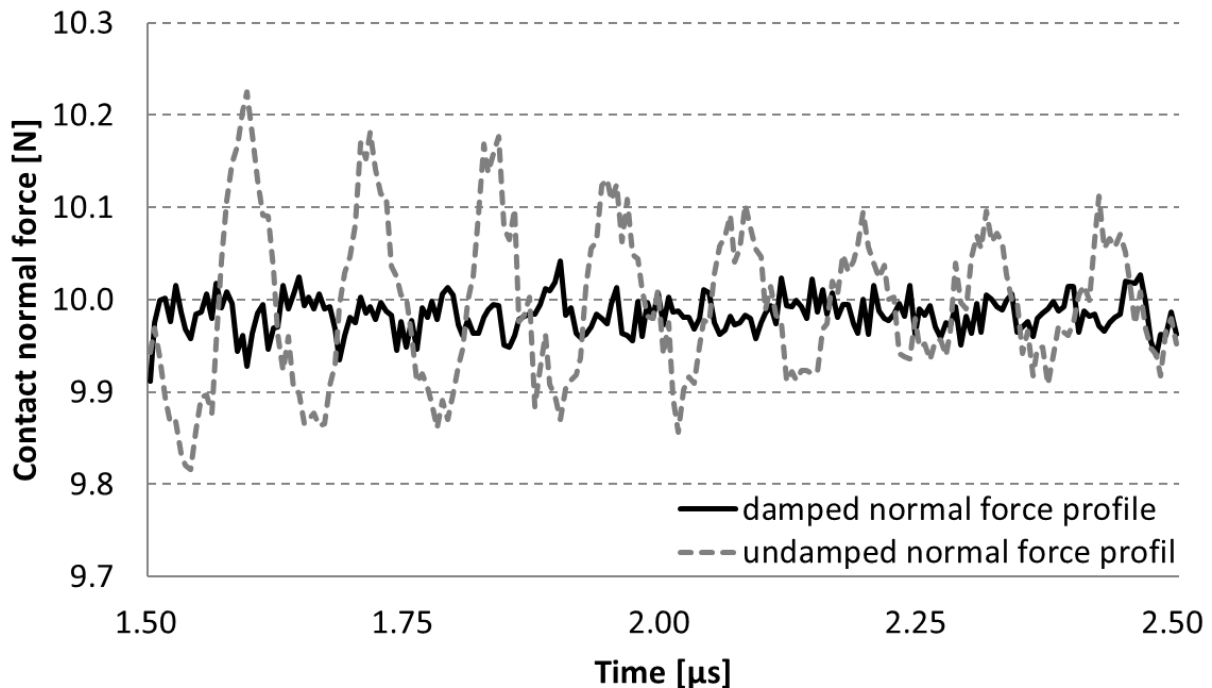


Figure 5-7: Curves of applied normal load for a damped and undamped loading (Reichert, Lorentz & Albers, 2016)

For the fluid, an inlet and outlet pressure are defined. The pressures result from the fluid pressure calculation shown in Figure 5-2. There is a small variation between the inlet and outlet pressure to specify the direction of the flow of the lubricant. By the ratio of the adjusted normal load and the fluid pressure, the mean lubrication gap can be defined. Under a constant normal load, the mean lubrication gap can be increased, if the fluid pressure is increased. Under a constant fluid pressure, the normal load can be increased, to decrease the mean lubrication gap. By adapting the fluid pressure or the normal load, the contact ratio due to solid contact and due to the fluid also change.

5.2.3 Fluid structure interaction and contact definitions

The interaction of the fluid and the solid parts are modelled with the Coupled Eulerian Lagrangian method (CEL). This fluid structure interaction (FSI) is a monolithic coupling system as described in section 2.7.2. The method requires the definition of a control space (fluid domain), where the fluid is allowed to move and an initial fluid part, where the lubricant is located at the beginning of the calculation. In Figure 5-8, these two parts are shown.

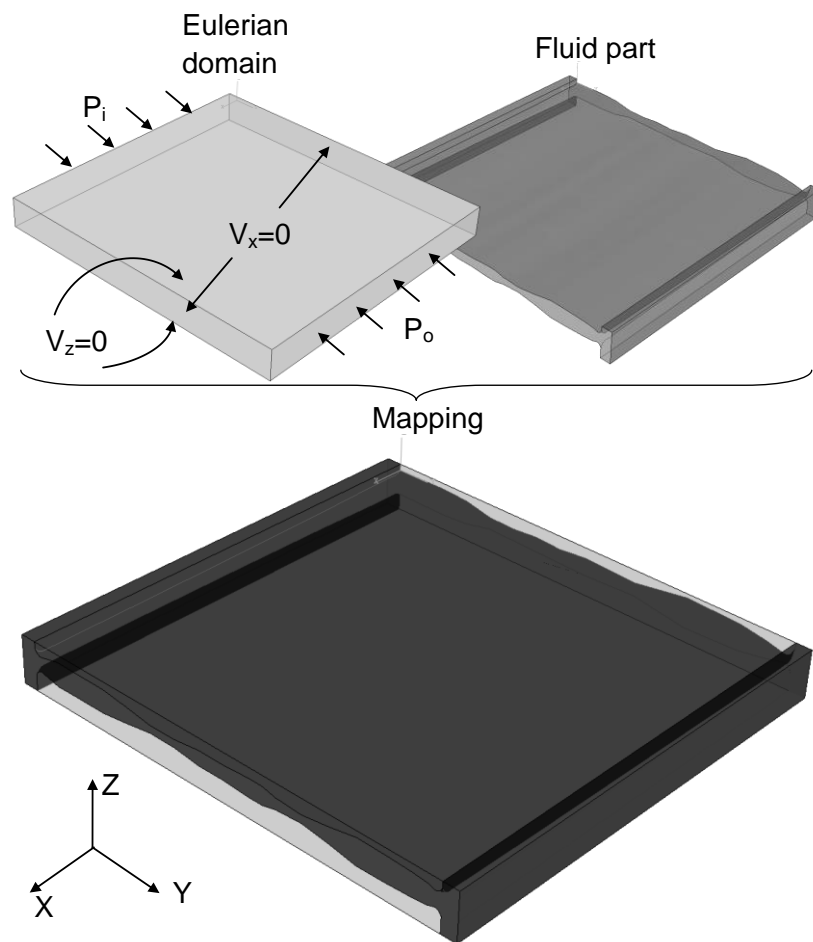


Figure 5-8: Setting of the CEL method for the fluid domain (Lorentz & Albers, 2013)

The initial fluid part is created by intersecting the eulerian domain and the two rough bodies. The figure shows the initial fluid part for an example topography. After this step, the initial part needs to be mapped on the eulerian domain to define the initial fluid location. This step is mandatory in the CEL method. The applied boundary conditions on the fluid part are also shown in Figure 5-8. To control leakage of the fluid, the flow rate at the boundaries of the eulerian domain in x-direction is zero. In z-direction, leakage is inhibited by the contact definitions. The inlet pressure (P_i) and outlet pressure (P_o) boundary conditions are applied to the ending faces in tangential direction (y-direction). The verification of the CEL method is done in section 6.4 by means of a comparable CFD model. With the CFD approach, the reproducibility of pressure fields in a hydrodynamic regime is investigated.

As seen in the system analysis of a mixed-lubricated contact in section 4.3, two types of contact are present. The contact between the fluid and the solid parts and the contact between the solids itself. To handle the transient contact between the fluid and the solid parts, ABAQUS provides the general contact, which automatically detects contact areas and assigns the corresponding conditions to the relevant surface nodes. In normal direction, a hard contact is defined (cf. section 2.6.3), to avoid the penetration

of the fluid into the solid parts. In tangential direction, a no slip boundary is applied to avoid a relative movement between the fluid and the boundaries of the solid parts. This type of flow is also known as Poiseuille flow.

The normal component of the solid contact is also modelled with the hard contact formulation. In this case, normal load is only transmitted between the surfaces, if the distance between two interacting nodes is zero. To initiate sliding between the rough bodies, the friction model by Bowden and Tabor, introduced in section 2.3.3, is used. Within this model, a critical shear stress τ_{crit} is implemented at the contact area for the solid-solid contact, which is defined as a function of the yield strength σ_{crit} (cf. formula (2-20)) of the softer material. The implementation of the critical shear stress is temperature dependent. After the calculation of the nodal temperature in the contact area, the local shear stress is adjusted. The principle of the critical shear stress is displayed in Figure 5-9.

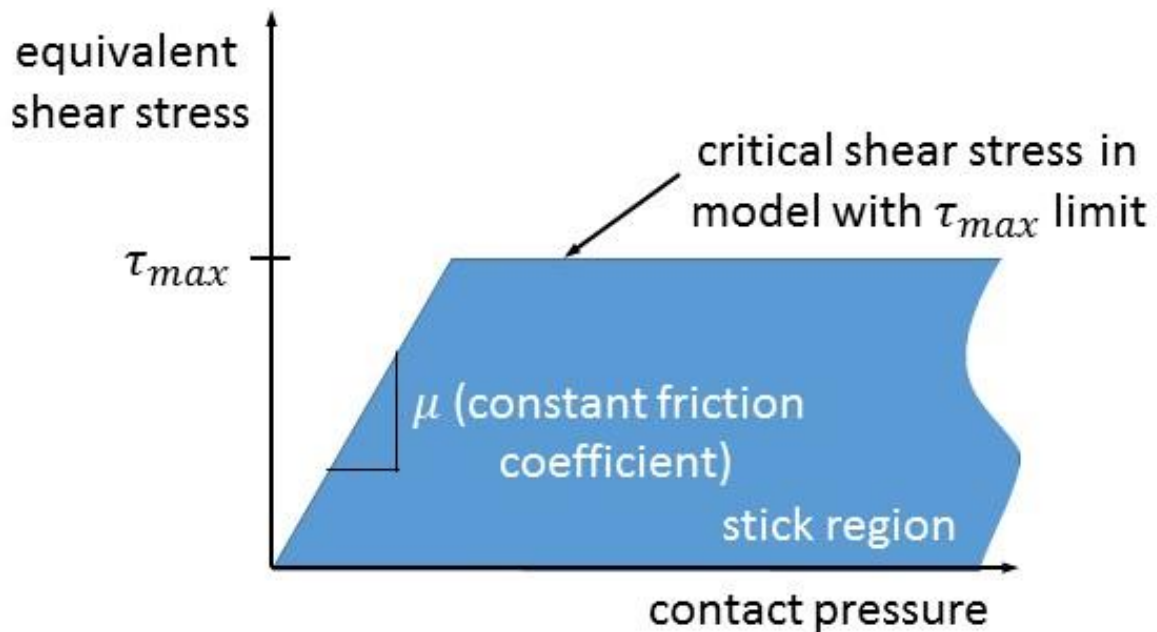


Figure 5-9: Stick region for the Bowden Tabor model with a limit on the critical shear stress ("Abaqus Analysis User's Guide 2016," 2015)

Since the critical shear stress is dependent on the contact pressure, the main advantage is that also the normal contact force, regardless of its magnitude, is taken into account in the calculation of the coefficient of friction.

5.2.4 Material model for solid and fluid parts

To investigate the friction and wear behavior, both the solid and the fluid parts need material assignments. The solid bodies are modelled with an elastic plastic material behavior. In Figure 5-10, the stress-strain curve for the used material AISI 1045

(Russell, 1975) is displayed. In this material model, also the strain-rate hardening effects were taken into account.

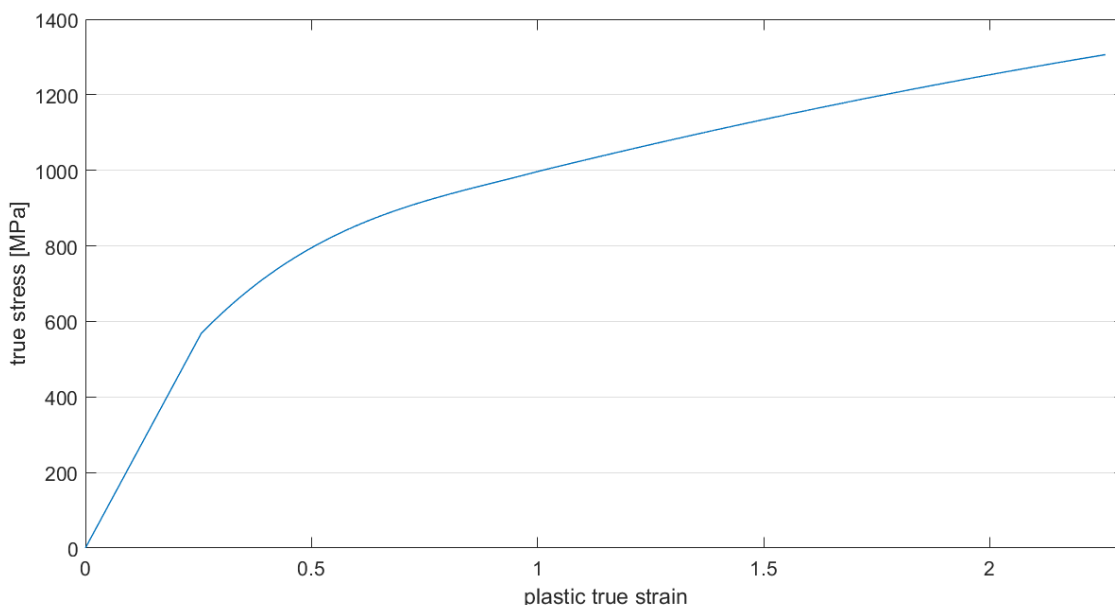


Figure 5-10: Stress-strain curve of AISI 1045

Although in journal bearing systems the shaft is often made of AISI 1045 and the bearing material is a milder one, also the bearing is modelled with AISI 1045. This material has a well-known behavior and is therefore used for both frictional partners in the mixed-lubrication model. The further corresponding material properties for modelling are shown in Table 5-5.

Table 5-5: Solid material properties of AISI 1045

Quantity	Value
Density [kg/m ³]	7860
Elastic Modulus [Pa]	221 x 10 ⁹
Poisson ratio [-]	0.285
Yield strength [Pa]	568 x 10 ⁶

As lubricant, mineral oil FVA 1 is used in the present work. The main properties are already shown in Table 5-3. The lubricant is assumed to be incompressible. Further, the fluid is assumed strictly Newtonian, and the flow is laminar and no turbulences are taken into account. To simplify the modelling of the fluid, cavitation effects, occurring at the surface asperities are neglected.

5.2.5 Implementation of residual stresses

In order to take into account residual stresses caused by manufacturing processes in the friction and wear simulation, which can occur during machining of the work piece, they can be implemented into the modelling approach with an own PYTHON code as initial state. For this purpose, the residual stress curves, which for example result from machining simulations, are mapped onto the mesh of the FE model. The coordinates of each individual node read out and the corresponding value from the depth progressions of the residual stress is then assigned to this node. Residual stresses can be implemented for all spatial directions. An exemplarily distribution of implemented residual stresses in the FE model is shown in Figure 5-11.

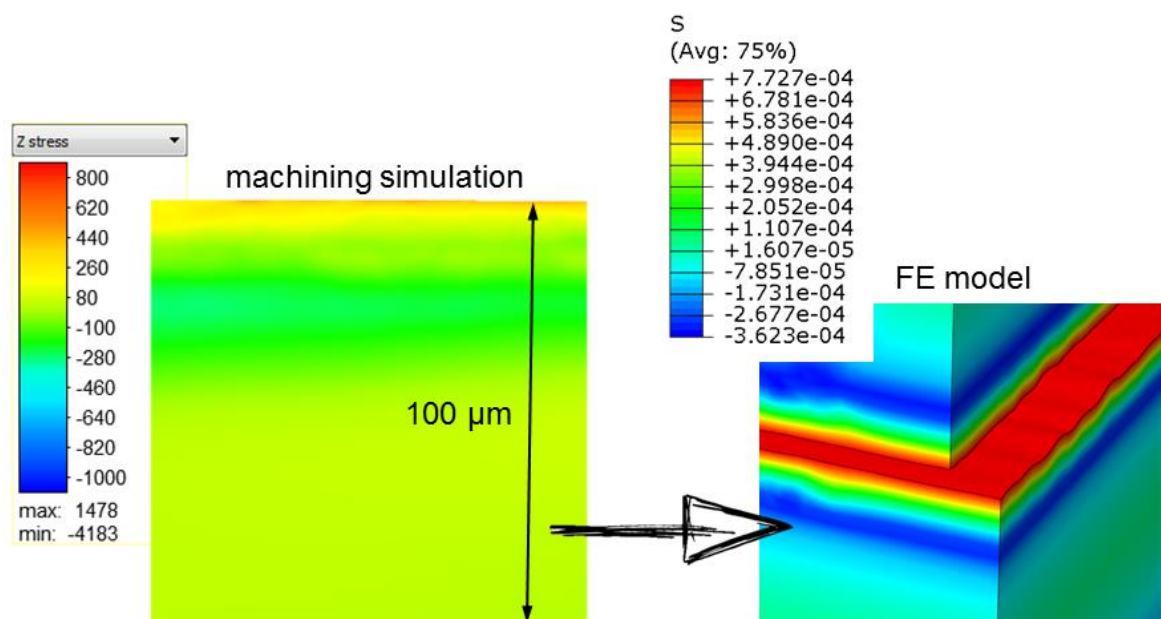


Figure 5-11: left: exemplarily depth progression of residual stresses from machining simulation¹, right: implemented residual stresses in mixed-lubrication model

In this figure, the residual stresses in tangential sliding direction are shown. This method is adaptable to various depth progressions of residual stresses from simulations or measurements.

5.3 Implementation of wear

For modelling the wear behavior of real technical surfaces on the microscopic scale using the finite element method, an approach for the calculation of very small local wear depths of a few nanometer is necessary, which results from a single rotation of a

¹ Machining simulation carried out by wbk – Institute of Production Science, Kaiserstraße 12, 76131 Karlsruhe

journal bearing, for example. Since the mixed-lubrication model is limited to the calculation of short periods of only a few microseconds, the new wear approach must be extended to include the possibility of scaling the wear depths. This is necessary to model the entire running-in phase of a tribological system.

The approach for modelling wear is based on the empirical wear law of Archard, introduced in detail in section 2.4.2. This wear law is usually used to model adhesive wear. Wear particles resulting from abrasive wear cannot be taken into account in this preliminary model due to the resulting high computing time. There is a first approach for modelling abrasive wear under sliding conditions (Reichert, Lorentz, Heldmaier et al., 2016) by means of a damage law. In this approach, wear particles occur due to abrasive wear, but do not interact with the solids.

Archard describes the resulting wear volume V_V as a function of the normal load F_N , the sliding distance s , the wear coefficient K and the hardness H of the softer material. For a better understanding of the following explanations, formula (2-29) is listed here again:

$$V_V = K \cdot \frac{F_N \cdot s}{H} \quad (5-3)$$

In order to use this wear law in the finite element model, Archard's global approach must be adapted to an incremental local wear calculation. It is assumed that the contact surface can be discretized into small several contact surfaces corresponding to a single element size for which Archard's wear law is applied. Implementing a wear volume loss in FE-model would result in having a discontinuous contact surface topography, so that models would have high singularities and thus deliver a poor result quality. To override this limitation, wear volume can be reduced to a surface height loss $h_{v,i}$, that can be formulated for each element i of the contact. In this case, formula (5-3) is changing to:

$$h_{v,i} = K \cdot \frac{p_i \cdot s_i}{H} \quad (5-4)$$

Assuming that the wear coefficient K is time independent in the running-in phase, the time derivative delivers the following incremental local wear law:

$$h_{v,i+1,n} = h_{v,i,n} + k \cdot p_{i,n} \cdot \Delta s_{i,n} \quad (5-5)$$

Within this local formulation $h_{v,i+1,n}$ is the summed wear depth of a single surface node, $h_{v,i,n}$ is the summed wear depth of the previous time increment, $p_{i,n}$ is the local contact

pressure of a single surface node, $\Delta s_{i,n}$ is the incremental sliding distance of a single node and k is the wear coefficient. This wear coefficient is related to the global formulation K/H . The local wear depths are calculated for each surface node on the contact surfaces (for both friction partners) and for each time increment.

Figure 2-18, the wear spectrum of Czichos, shows that the wear coefficient for a dry running contact (a lubrication gap of zero) is approximately $10^{-5} \text{ mm}^3/(N \cdot m)$. As the lubrication gap increases, the wear coefficient decreases, which correlates with the decreasing solid contact. For this reason a wear coefficient of $10^{-5} \text{ mm}^3/(N \cdot m)$ is also used in the mixed-lubrication model on the microscopic scale to model the solid interactions. This is accompanied by the assumption that the same probability of wear is given for each solid contact. The wear coefficient by Archard depends on the entire tribological system and is determined from experimental test or by simulation as mentioned in section 2.4.2.

A scheme of the simulation method is shown in Figure 5-12. First the normal load is applied to the upper body and then the upper body is displaced in tangential direction against the lower body. This is in accordance to the calculation step i_0 . At the end of the displacement, the wear depth of each node is calculated following the wear law by Archard and afterwards the surface nodes are adjusted. In the next calculation step i_1 ($i_1 > i_0$), the initial tangential position of the upper body corresponds to the final tangential ending position of the previous calculation step. Thus the upper body is continuously displaced in tangential direction.

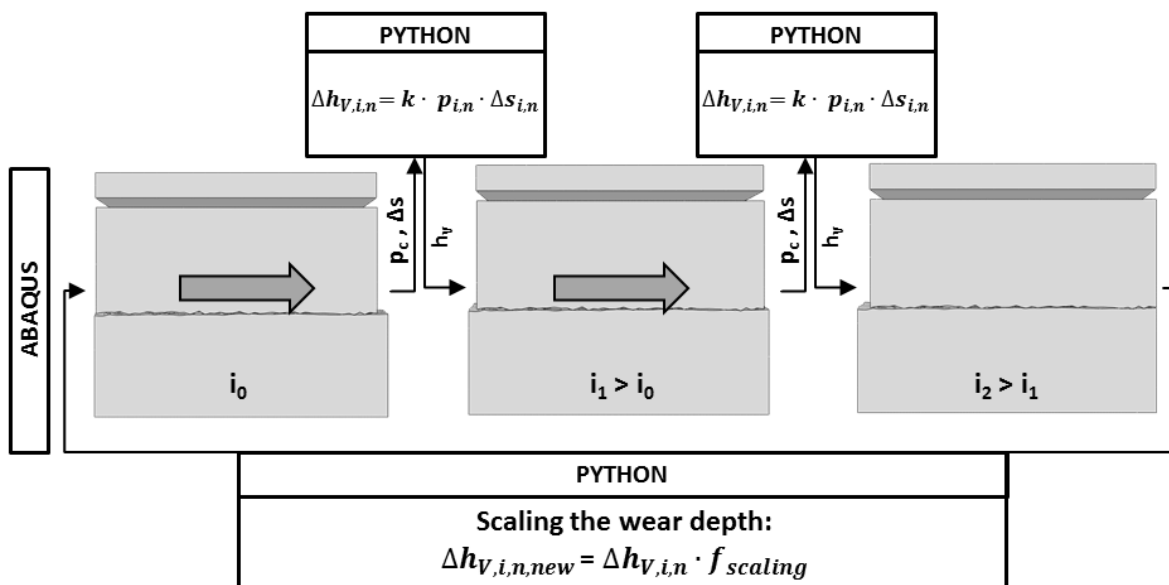


Figure 5-12: Workflow of the simulation method following the wear law by Archard (Albers & Reichert, 2017)

At the beginning of the new calculation step, the normal position of the upper body is reset to initial state. In order to obtain the new contact pressure distribution, the normal load is applied again. The total displacement in tangential direction of the upper body, which results from the sum of the single displacements of the various calculation steps i_0 , i_1 and i_2 can be divided into various detailed calculation steps. If the calculation steps are very small, the worn surface can be updated with any degree of accuracy. The first cycle of the calculation is finished if the upper body reaches the maximum defined displacement. This corresponds to the calculation step i_2 in Figure 5-12. Also the maximum displacement can be adjusted, according to the desired sliding distance. In relation to the cycle, the cumulative incremental wear depths of each surface node are scaled with the factor $f_{scaling}$. With this method, longer operating times can be calculated. After the scaling of the local wear depths, the upper body is reset to its initial position and the new wear depths are calculated for the next cycle.

In order to reduce mesh distortion caused by the displacement of the surface nodes, also the nodes below the surface are adjusted by a percentage of the calculated wear depths. Due to this method, the simulation time can be extended and the whole running-in phase can be investigated.

Since in a single calculation step there are no wear-related node displacements, no problem in matching the residual contact forces calculated by the explicit solver of ABAQUS occurs. The surface nodes are adjusted in an unloaded state before the next calculation step begins. Consequently, no problems in reaching convergence are created. This described method is valid both for dry and mixed-lubricated conditions.

5.4 Numerical model of dry friction

Due to the removal of the lubricant, the dry running contact model is considerably less complex than the mixed-lubrication model. The boundary conditions and loading steps are identical. The setup of the dry running model is shown in Figure 5-13.

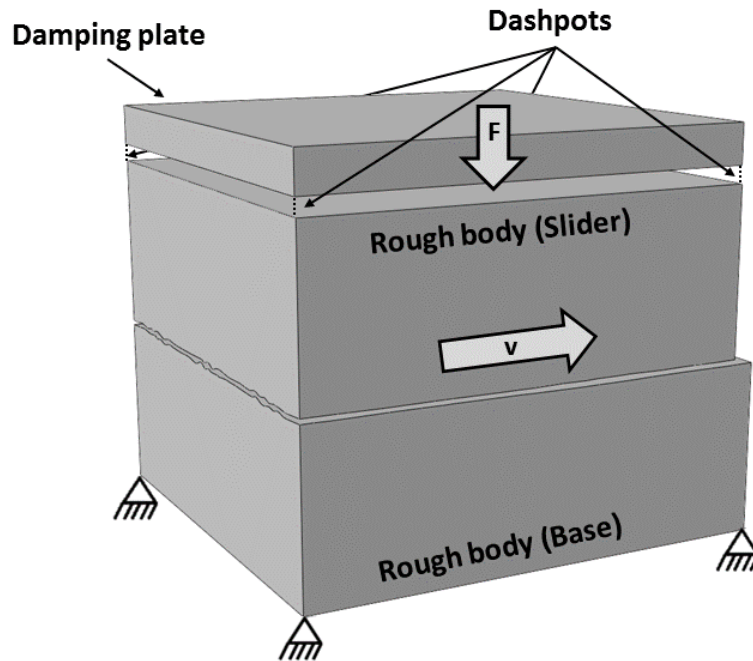


Figure 5-13: Setting of the dry running model

The lower body (base) is spatially fixed. Also in a first step, the upper body (slider) is pressed force-controlled against the lower one to achieve a constant pressure. In a second step, the upper body is displaced in tangential direction velocity-controlled. In a same way like the mixed-lubrication model, the dry running model is meshed with linear hexahedron elements with an edge length of $3.0\ \mu\text{m}$ in the contact zone. Due to the omission of the lubricant and consequently the missing fluid structure interaction, the computational time is decreasing and therefore, the dimensions of the solid bodies can be extended to a size of $500 \times 500 \times 80\ \mu\text{m}$. The lower body is also extended in tangential direction by a few micrometers, to achieve a constant pressure while displacing the upper body.

Since the dimensions have been enlarged, it is also possible to take into account the real measured topography without extracting the roughness. This is necessary for the validation with a real technical system in order to realistically represent the contact conditions occurring in experiment.

5.5 User interface to couple the various simulation methods

As described above, there are different simulation techniques necessary, to handle the problem of simulating wear of real rough surfaces under mixed-lubricated conditions. The main couplings are the implementation of the real rough bodies into the finite element model and the creation of the model itself including the material definitions, boundary conditions, meshing and solving. In order to get an overview of this complex

calculation problem, all necessary calculation methods, measurement techniques and tools are displayed in Figure 5-14 in the framework of coupling various simulation methods introduced in section 4.4. Due to the different programs, the imperative necessity of a coupling framework becomes clear.

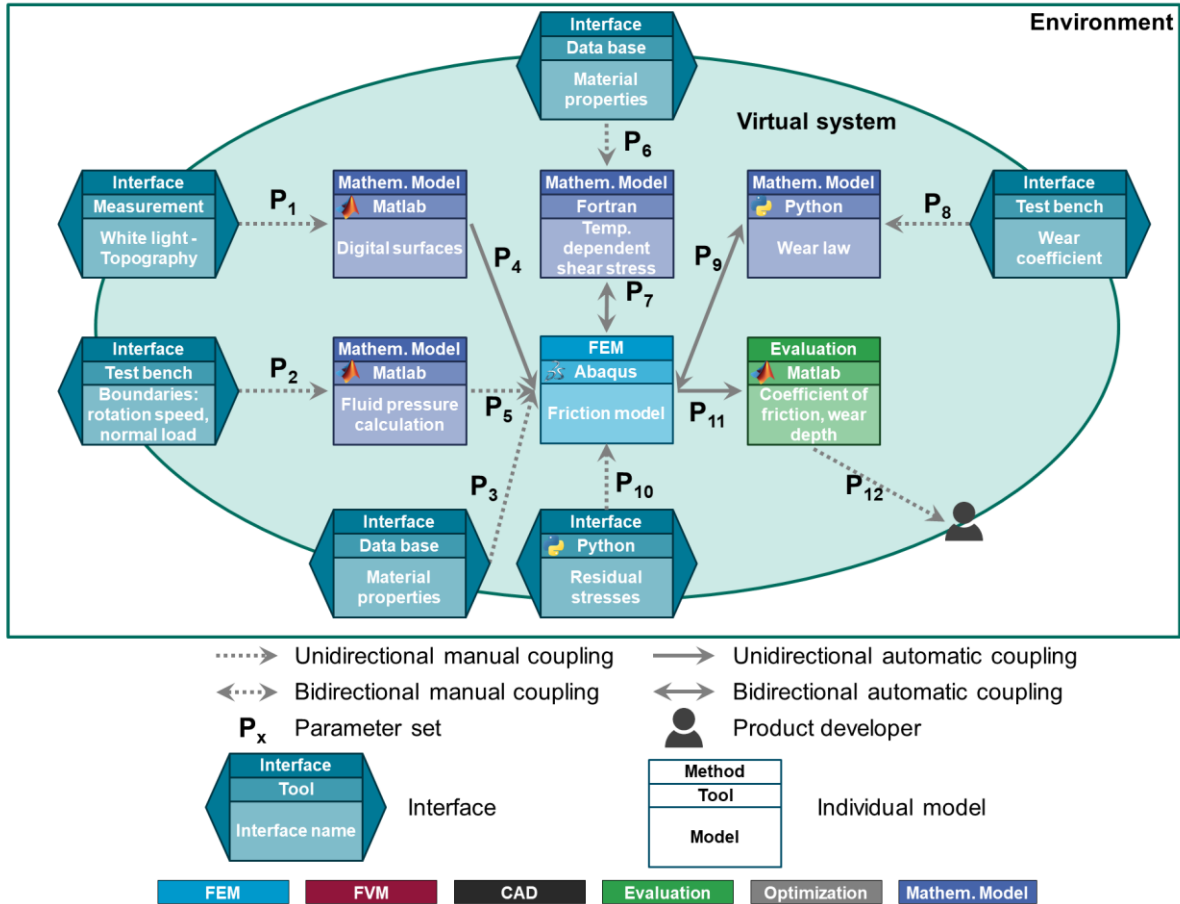


Figure 5-14: Comprehensive method for the numerical mapping of wear on real surfaces (Albers, Reichert, Serf et al., 2017)

The knowledge for the individual areas can be provided by an experienced product engineer. However, the transfer of the specific data formats and the interaction of the various programs not. For this reason, a suitable calculation environment must be created, that supports the product developer in applying the simulation tool correctly and without operating errors.

This support was realized within a GUI, implemented into the commercial finite element software ABAQUS. This GUI is displayed in Figure 5-15.

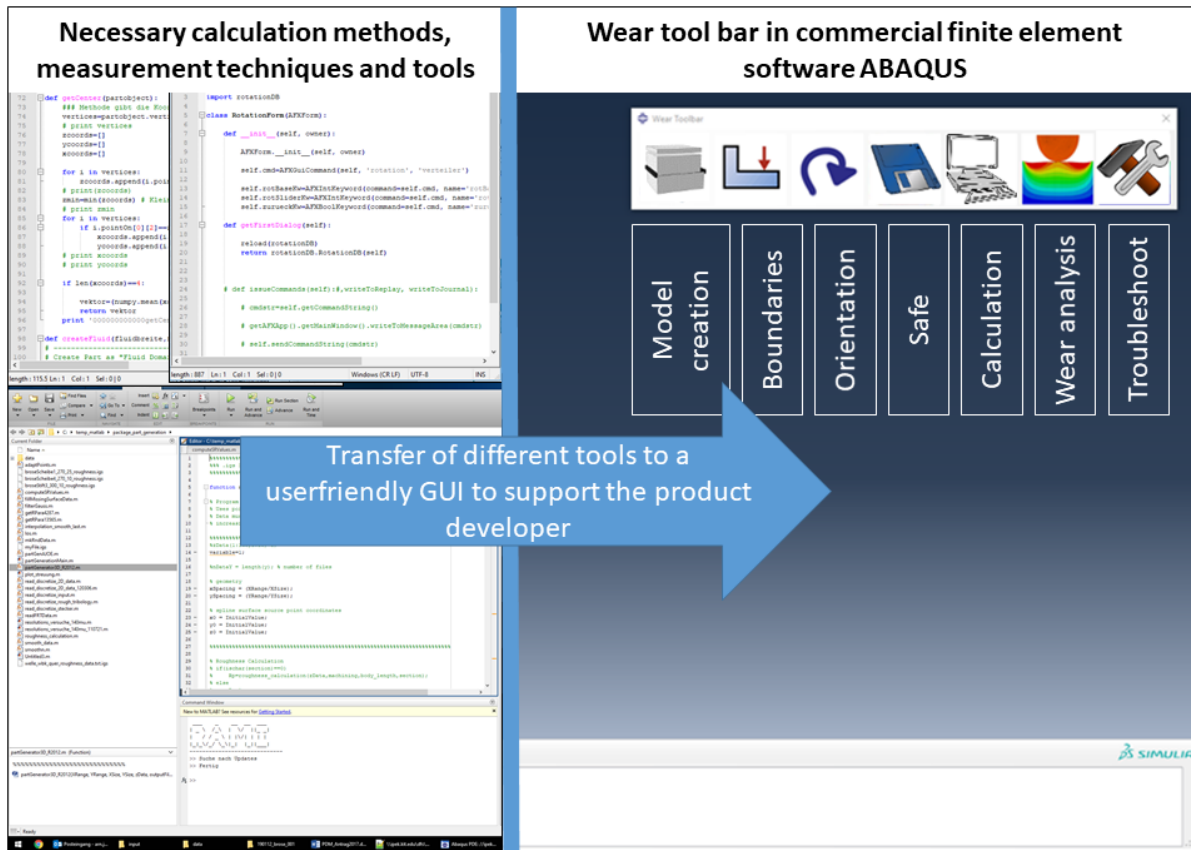


Figure 5-15: Graphical user interface in the finite element software ABAQUS to support the product developer in applying the complex simulation tool correctly without operating errors

The GUI is integrated into the software in form of a toolbar. This toolbar consists of seven icons, which support the product developer intuitively in carrying out the wear simulation. The various icons are explained in more detail in the following Table 5-6.

Table 5-6: Explanation of the single icons in the wear toolbar implemented into the finite element software ABAQUS

Model creation



- Implementation of solid bodies into the finite element software
- Defining of the dimensions of the solid bodies
- Defining of material properties (also with material cards)
- Including/excluding the lubricant

Boundary conditions



- Defining normal load
- Defining sliding velocity
- Defining inlet and outlet pressure

**Orientation**

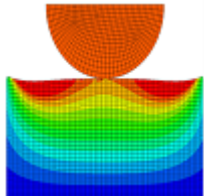
- Rotating the lower and upper body to change the orientation of the surface topography

**Save**

- Saving of the adapted final model

**Start calculation**

- Starting a single calculation for model evaluation without using the wear tool

**Wear analysis**

- Defining number of calculation steps
- Defining wear coefficients for both friction partners
- Defining scaling factor
- Defining the number of CPUs

**Troubleshoot**

- Continuation of the calculation in case of errors like license problems or distorted elements

For the realization of the trouble shooting function, a data file is created after each successful calculation step, containing all relevant information needed for the continuation of the following calculation step. From the point of view of very long computing times, this function is absolutely necessary.

6 Verification and validation of the microscale model

This chapter provides a numerical verification of the mixed lubrication and wear model and an experimental validation of the dry running model. Verification means in this context to check, if the model is basically plausible and correct and whether it meets the requirements set out in section 4.5. Due to huge calculation time, the validation of the mixed lubricated wear model is not possible yet. Therefore, the dry running model was used for the validation while comparing the calculated results with experimental friction test on a nanoindenter. Validation in this context means, whether the created model describes a real system adequately and thus also meets unspecified requirements like temperature dependency or changes in material properties.

The first step of the micro model verification is to check the convergence of the solid and fluid mesh regarding friction and wear. On basis of the convergence study, the final mesh setup can be derived for the relevant parameter studies carried out in chapter 7. Further the fluid structure interaction (CEL from section 2.7.2) is compared to a CFD simulation under hydrodynamic conditions, which is an established calculation method for fluid mechanics. The time scaling mentioned in section 5.3 to calculate the whole running-in phase is investigated in detail, to guarantee an efficient calculation method for long durations.

Finally, the friction and wear model is validated under dry friction. The experimental tests were carried out on a nanoindenter, where a small tip is sliding on a plate. Due to the small dimensions of the experimental device, the whole setup could be handled within the finite element model.

6.1 Validation of rough surface generation

If the measured surface data is transferred into a digital solid body, deviations in surface topography can occur due to the discretization of the measurement, the spline generation in MATLAB and the meshing in ABAQUS as described in section 5.2.1. On the example of the honed specimen and turned specimen 1, (cf. Figure 5-5) the creation process is validated. To compare the measured surface data and the discretized solid bodies, the statistical roughness parameters R_a and R_z (cf. section 2.2.2) and the Abbott-Firestone-Curves are taken into account. Both the bearing and the shaft are measured at three different areas. The results of the comparison are

shown in Figure 6-1 for R_a on the left and for R_z on the right. In this figure, the honed specimen corresponds to the bearing and the turned specimen 1 to the shaft.

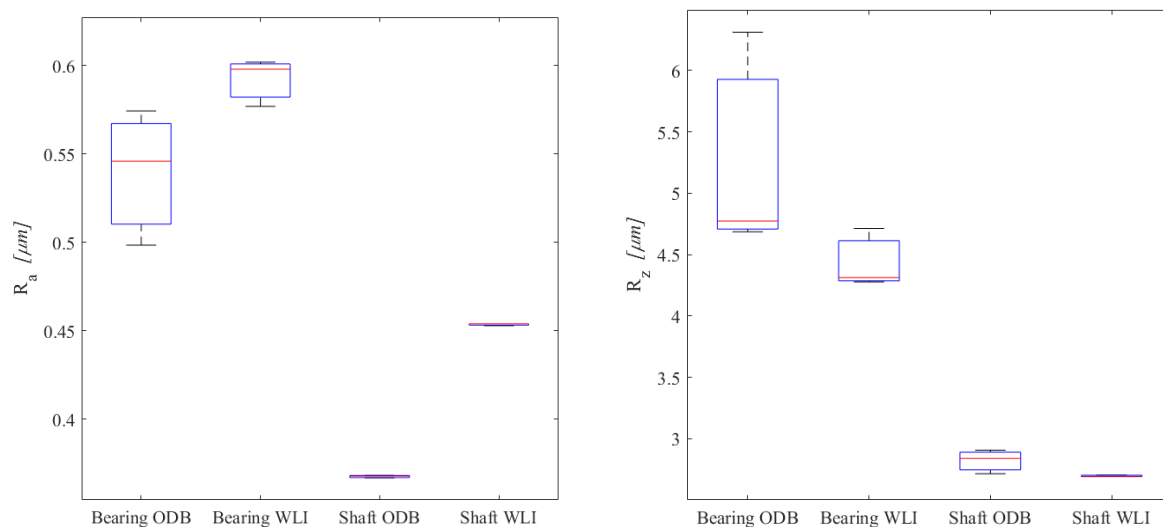


Figure 6-1: Computed (ODB) and measured (WLI) roughness parameter, left: R_a , right: R_z (Albers, Reichert & Joerger, 2017)

As it can be seen in Figure 6-1, the effects of splining and meshing, necessary for the calculation, leads to a deviation of the two investigated roughness parameters in comparison to the measured surface data. Both for the bearing and the shaft, the arithmetical mean deviation of the assessed profiles R_a has decreased by 9 % (bearing) and 18 % (shaft) for the created solid bodies. As a consequence, the process of surface generation leads to smaller R_a values, which can be seen as the result of spline generation over the measured points. Further clear to see in Figure 6-1 on the right, the slightly increasing mean roughness depth R_z . This parameter differs less from the measured surface data because the points of peaks and valleys do not strongly influence spline generation. The deviation of the calculated parameter R_z from the measured parameter is 6 % for the bearing and 1 % for the shaft.

Since the lack of meaning of single roughness parameters in isolation, the Abbott-Firestone-Curve is a proper way to evaluate the differences which arise during the transfer process, as described in section 2.2.2. As it can be seen in Figure 6-2 on the left for the bearing and on the right for the shaft, there are only very few deviations between the computed curves from the finite element mesh and the measured surface data.

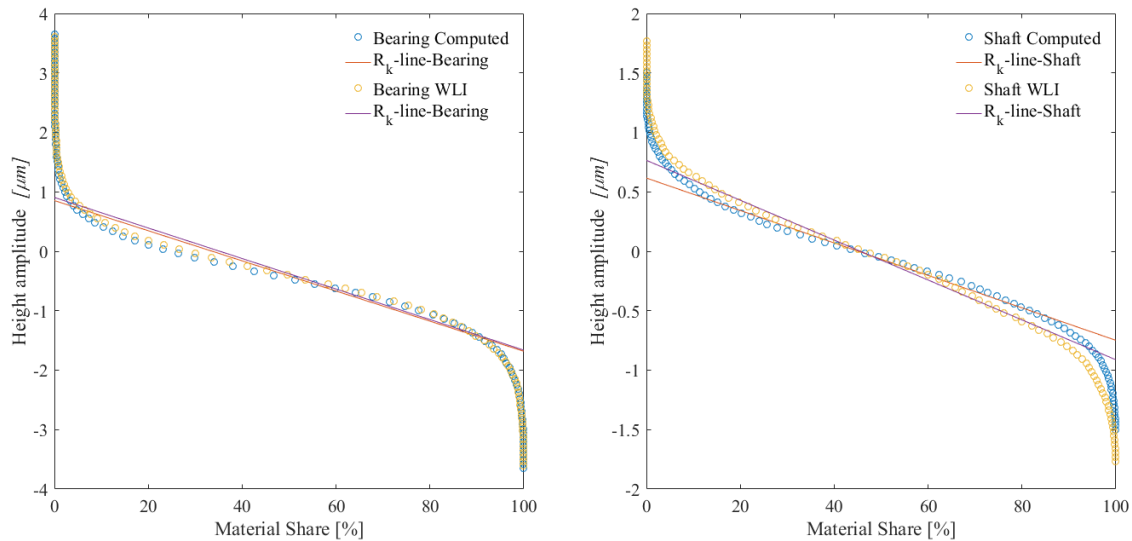


Figure 6-2: Computed and measured (WLI) Abbott-Firestone-Curves, left: for the bearing, right: for the shaft (Albers, Reichert & Joerger, 2017)

The evaluation of the statistical surface parameters has shown, that the real measured surfaces can be implemented in a numerical model with only small deviations. Particularly noteworthy are the small deviations of the R_z values (in maximum about 6 %). The maxima of the surface profile are significantly involved in the solid contact and with these minor deviations, a good approximation of the real contact area can be assumed. Since, in addition to the statistical surface parameters, the Abbott-Firestone-Curves also show minimal differences, the generated surfaces (solid bodies) can consequently be considered valid.

6.2 Convergence of the mixed lubrication model

After the surface generation process has been successfully validated, the next step is to check the convergence of the wear model. Since the target values contact pressure and sliding distance for calculating wear are obtained from the mixed lubrication model, the influence of the element size is first examined in this model. Subsequently, the influence of the element size on the wear depth is investigated in the wear model. This investigation is carried out on the dry-running wear model, as in this case, wear is considerably higher. As this model contains two different meshes, the solid and the fluid mesh, for both the convergence is checked.

6.2.1 Convergence of the solid mesh

The used elements of the solid mesh are linear hexahedron elements. The edge lengths to be examined vary from a coarse mesh with an edge length of $3.0 \mu\text{m}$ to a

fine mesh with an edge length of $1.5\ \mu\text{m}$. To reduce the calculation time, the mesh is only refined near the contact zone. In Figure 6-3, the solid body of a turned specimen with the refined mesh near the contact zone is shown.

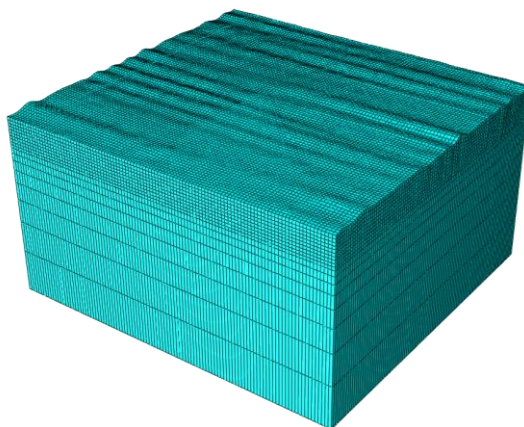


Figure 6-3: Solid mesh with the refined elements near the contact zone

To check convergence of the mixed lubrication model, the influence of the element size on normal and tangential forces is investigated. The time range from 1.0 to $2.0\ \mu\text{s}$ is displayed for both the evaluation of the normal and the tangential force. This range corresponds to the sliding phase of the model in which the target values are evaluated. The result of the influence of the edge length of the fine mesh near the contact zone on normal load is shown in Figure 6-4.

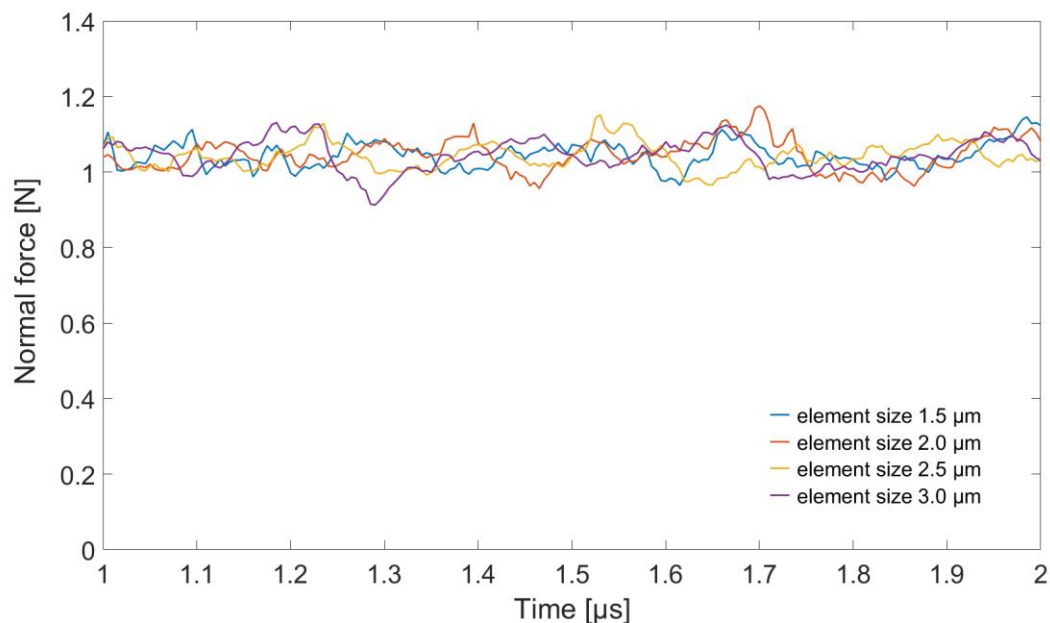


Figure 6-4: Influence of the edge length of the solid mesh on normal force

As can be seen, the edge length has a negligibly small influence on the normal force. The defined normal force of $1.0\ \text{N}$ can be reproduced with sufficient accuracy for all edge lengths examined.

The results of the influence of the edge length of the solid mesh on tangential force is shown in Figure 6-5.

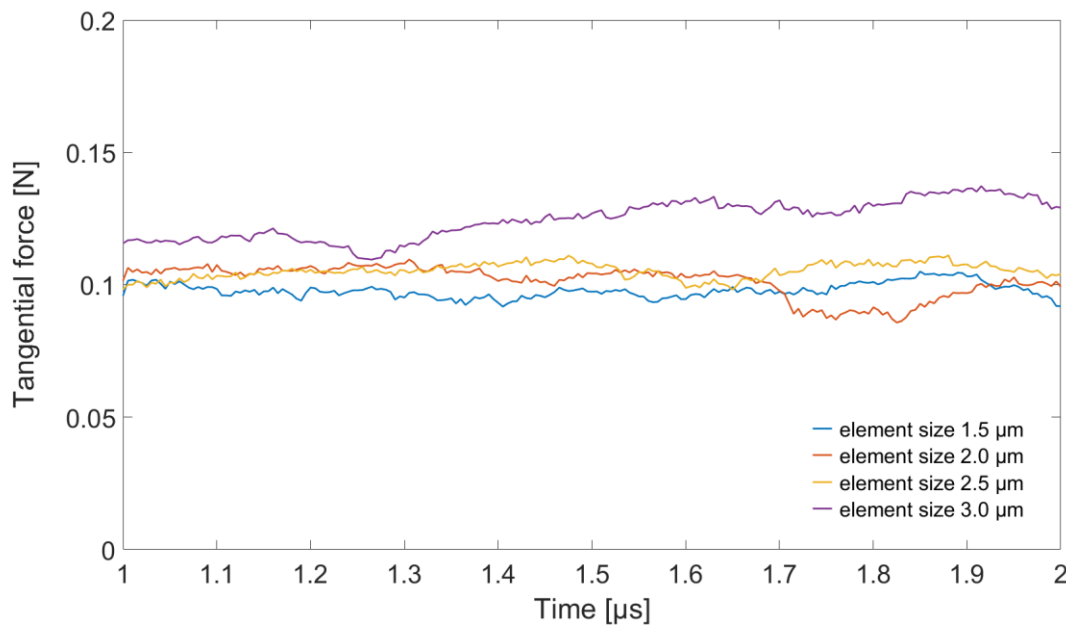


Figure 6-5: Influence of the edge length of the solid mesh on tangential force

The influence of the element size on tangential force is much more significant than on normal force. For the edge lengths of 1.5, 2.0 and 2.5 μm, there are only small deviations occurring. For an edge length of 3.0 μm, the maximum deviation from the next smaller element size is approximately 25 %. The increase in tangential force at the largest edge length can be explained by the increase in real contact area with coarse mesh. With an edge length of 3.0 μm, the real contact area is also approximately 25 % higher than with an edge length of 2.5 μm. With smaller element sizes, the change in real contact area is not so significant. Following equation (2-17), the tangential force is dependent on critical shear stress τ_{crit} and the real contact area A_r . Under the given assumption of a constant defined critical shear stress (c.f. section 2.3.3), the increase in tangential force can be explained with the increasing real contact area with a coarse mesh.

Due to the accuracy of the results, an edge length of 2.5 μm is recommended. From the point of view of the very large number of single calculations for the investigation of the whole running-in phase, a solid mesh of 3.0 μm is used for the further investigations. Since the deviations are known, the higher tangential force can be compensated by adjusting the critical shear stress. As a result, the calculation time saving per calculation is approximately 60 %.

6.2.2 Convergence of the fluid mesh

Like the solid bodies, the eulerian fluid part (c.f. section 5.2.3) is also meshed with linear hexahedron elements. The range of investigated element sizes reaches from 2.5 μm to a refinement of 1.5 μm . The influence of the edge length of the fluid mesh on normal force is shown in Figure 6-6.

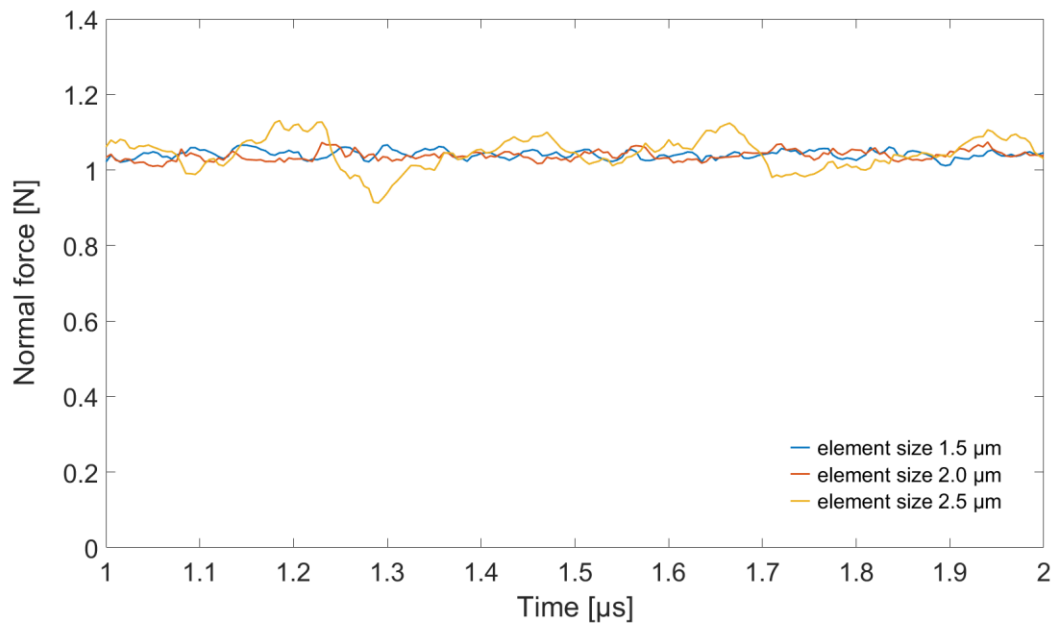


Figure 6-6: Influence of the edge length of the fluid mesh on normal force

The influence of the edge length of the fluid mesh is also very low. Only minimal deviations from the set normal force of 1 N is observed for all three different element sizes. Influences of the edge length on the application of the normal load are not further investigated here. The considerations take place again within the sliding phase.

In Figure 6-7, the influence of the element size on the tangential friction force is shown. This illustration shows, that compared to the solid mesh, the influence of the edge length of the fluid mesh is significantly less. This result shows, that due to the low friction component of the fluid, the influence of the edge length on friction force is significantly lower. As soon as solid contact, most of the tangential force is generated. For this reason, an element edge length of the fluid mesh of 2.5 μm is chosen. An even increased edge length has proved to be unsuitable with regard to the modelling of the fluid-structure-interaction.

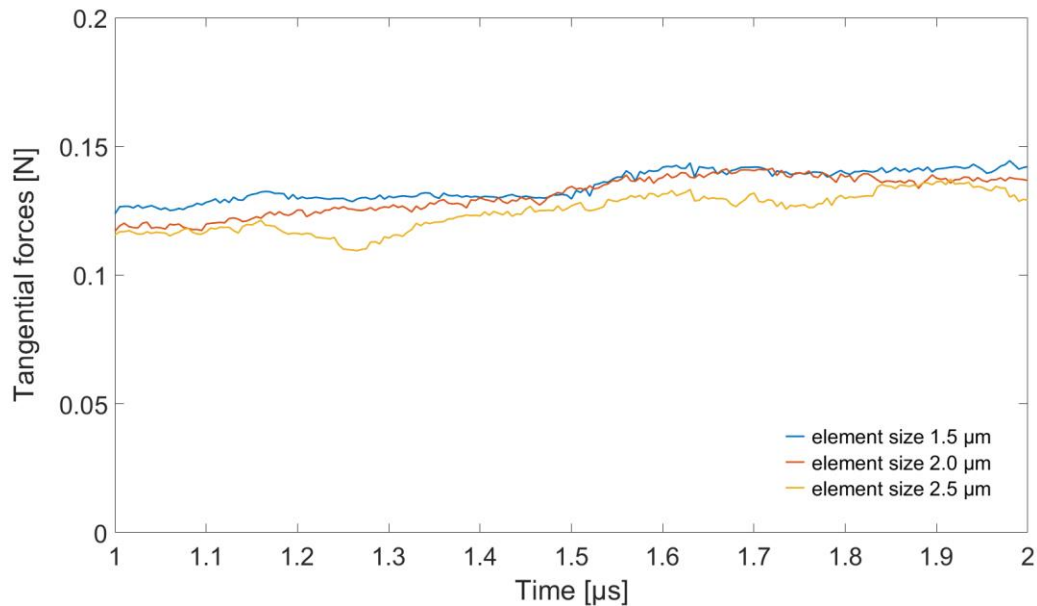


Figure 6-7: Influence of the edge length of the fluid mesh on tangential force

Finally, the convergence studies of the mixed lubrication model have shown that the combination of a solid mesh with an edge length of $3.0\ \mu\text{m}$ and a fluid mesh with an edge length of $2.5\ \mu\text{m}$ is a suitable compromise in terms of result quality and calculation time.

6.3 Convergence of the wear model

As noted in the previous section, the fluid contributes only a small amount to friction in a mixed-lubricated regime. Since increased wear is still expected under dry-running conditions and the computing time is less, the convergence analysis is carried out for a dry-running model. Consequently, only the element size of the solid mesh is varied.

The element sizes taken into account are 2.5 , 3.0 and $3.5\ \mu\text{m}$ to investigate the influence of a coarser mesh. The results, regarding the wear depth, are shown in Figure 6-8. In this context, the wear depth is the distance of the centre lines of the surface profiles under a constant loading. For a better understanding, two arbitrary roughness profiles with the distance of the centre lines are shown in Figure 6-9. The deviation of the influence of the investigated edge lengths of 2.5 , 3.0 and $3.5\ \mu\text{m}$ is nearly 4 %. This shows that a finer mesh doesn't influence the wear depth significantly.

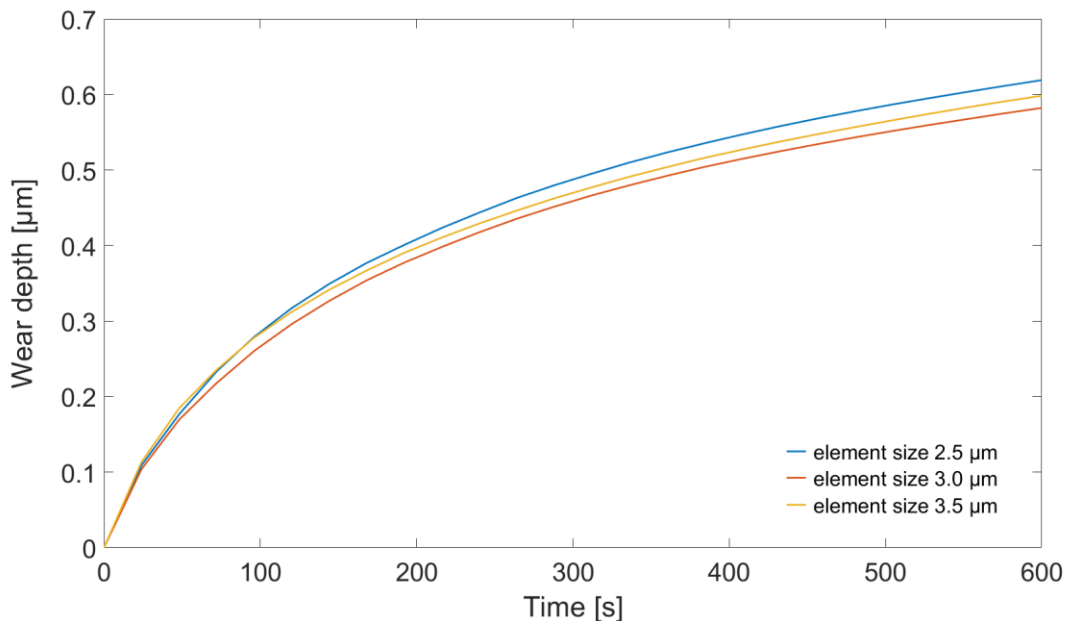


Figure 6-8: Convergence study on the influence of the edge length of the fluid mesh on the wear depth.

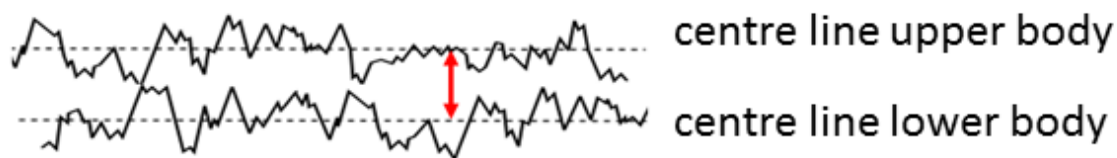


Figure 6-9: Measurement of the distance of the centre lines of the roughness profiles.

Based on the results of the convergence study of the wear model, the mesh can be defined even more roughly. Since the identified edge lengths from the mixed lubrication model have already proven to be suitable, these mesh settings are used for all further calculations.

6.4 Comparison between the CEL- and CFD method in a hydrodynamic regime

In this section, the Coupled-Eulerian-Lagrangian (CEL) method is compared with the computational fluid dynamics (CFD) method, which is a widely used and recognized method for the investigation of hydrodynamic problems. In comparison to the CEL method, which is based on the finite element method (FEM), the CFD method is based on the finite volume method (FVM). Both methods are described in detail in section 2.6.1 and 2.7. The CFD model is built with the simulation software ANSYS

WORKBENCH. This CFD model was derived within the supervised bachelor thesis of Haefele².

For this investigation, the lubrication gap of the mixed-lubricated model, described in section 5.2, is increased, to avoid solid interactions and to achieve hydrodynamic conditions. As mentioned, the lubrication gap can be adjusted by the ratio of normal load and fluid pressure. In order to ensure identical boundary conditions in both models, the loading of the mixed lubrication model was changed from a force-controlled loading to a way-controlled loading. This step allows the adjustment of identical lubrication gap heights in both models. The adjusted model and the corresponding CFD model are shown in Figure 6-10.

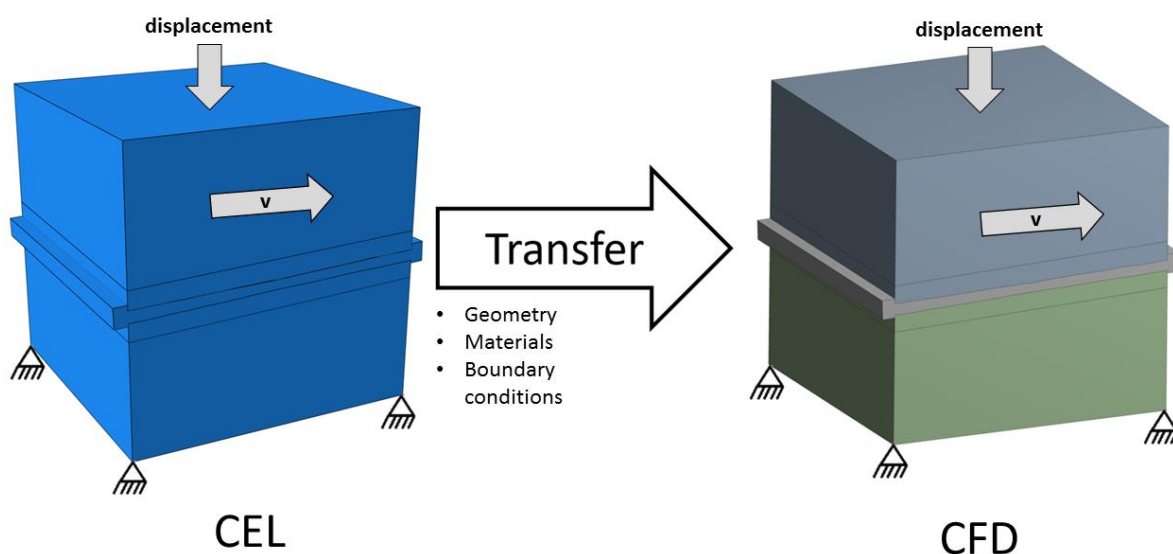


Figure 6-10: model setting for the comparison of the CEL and CFD method, left: setting of the CEL model, right: setting for the CFD model²

Both models have the same geometry, material definitions and boundary conditions. The materials of the solid parts are of AISI 1045 (material properties are defined in Table 5-5) and the fluid is the reference oil FVA 1 with the corresponding material properties from Table 5-2. The inlet pressure is 100 MPa and the outlet pressure is 99 MPa. For the verification of the CEL method, the fluid pressure at five different points within the fluid part is considered as a function of time. These five points can be seen in the sectional view of the fluid in Figure 6-11.

² Haefele 2017 - supervised bachelor thesis

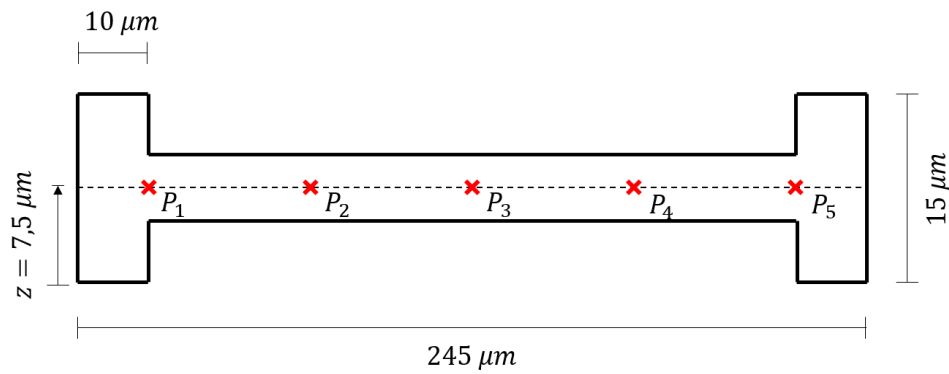


Figure 6-11: Position of the selected points in the fluid part³

In Figure 6-12 the calculated fluid pressure of the CEL method and in Figure 6-13 the fluid pressure of the CDF model are shown. At the points P_{1-5} the pressure is determined over the whole simulation time $\Delta t = 2.25 \mu\text{s}$ in a time increment of $\Delta t_{inc} = 0.1 \mu\text{s}$. The pressure values between the increments are interpolated in the diagrams. On the abscissa time t is plotted in μs and the pressure $p(t)$ is noted on the ordinate in MPa .

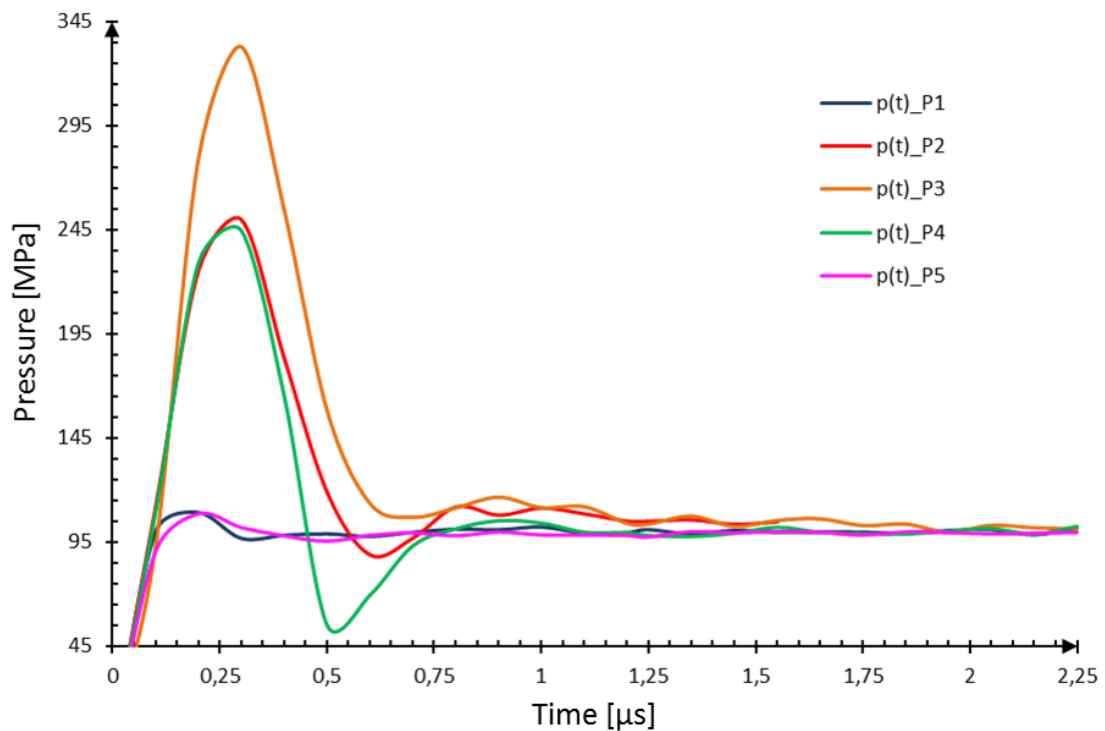


Figure 6-12: Fluid pressure as a function of time of the CEL method³

³ Haefele 2017 - supervised bachelor thesis

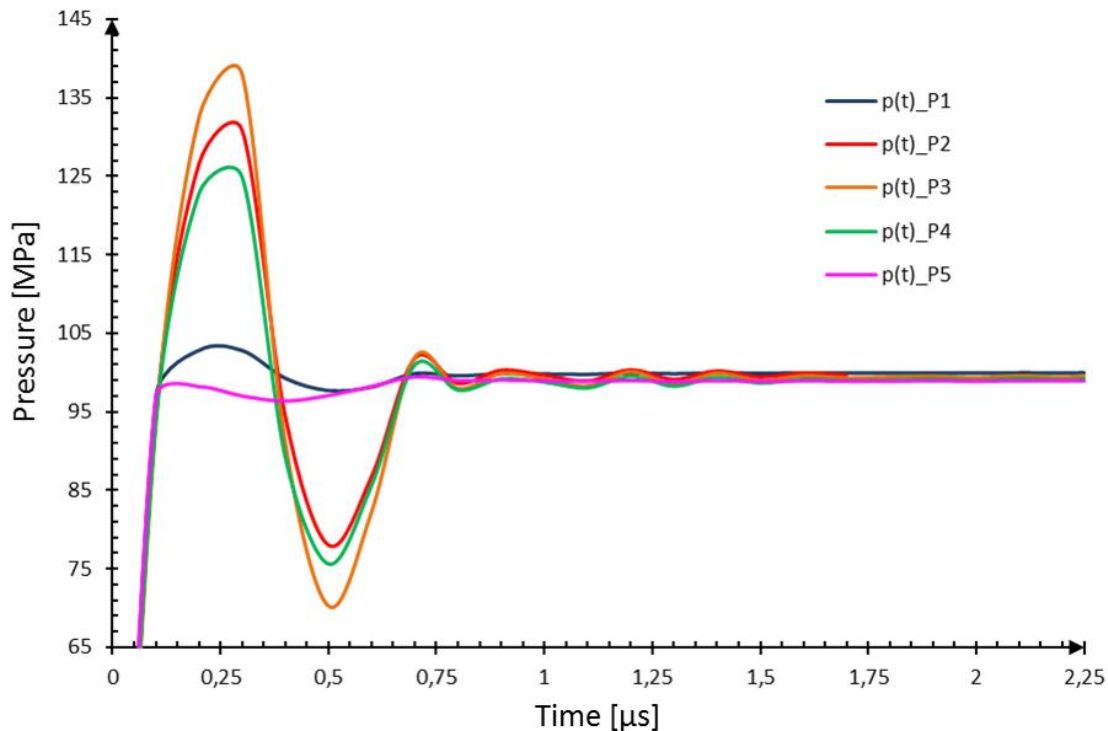


Figure 6-13: Fluid pressure as a function of time of the CFD method⁴

Both models show a qualitative similar behavior regarding the fluid pressure as a function of time. While applying the normal load in the first $0.75 \mu\text{s}$, a strong increase in fluid pressure at the points P_{2-4} can be observed. At the points P_1 and P_5 , there is a constant fluid pressure over the whole simulation time corresponding to the pressure of 100 MPa. Both the ABAQUS and ANSYS model have the highest pressure at about $0.25 \mu\text{s}$. This is to be expected, as the vertical displacement of the upper body has the highest feed speed here. When evaluating the maximum pressure, the CEL model shows a 60 % higher pressure than the CFD model ($p_{CEL,max} = 333 \text{ MPa}$, $p_{CFD,max} = 138 \text{ MPa}$). In the CEL model, a drop to the constant level of 100 MPa can be observed after the pressure maximum. In the CFD model, the pressure drops even below the constant level of 100 MPa after the pressure peak before a constant fluid pressure is reached.

Since after initial differences in load application, both models reach a constant pressure level during sliding, this comparison proves, that the CEL method is capable of reproducing flow simulations with sufficient accuracy in a quasistatic analysis. Valid values can be assumed on the basis of the good agreement between the two calculation methods, since in the used wear approach the target values contact pressure and sliding distance are evaluated at the end of the sliding phase.

⁴ Haefele 2017 - supervised bachelor thesis

These results correlate with the investigations of Donatellis et al. (2009) from section 2.7.2. regarding a laminar flow-through pipe. Here it was also found that with the CEL method, the flow is fully developed after a certain period of time.

6.5 Investigation of permitted scaling factors for wear simulation

As already described in section 5.3, the wear approach must offer the possibility of scaling the calculated wear depths in order to be able to take a holistic view of the running-in phase. The few microseconds that can be calculated in the mixed-lubrication model would not be sufficient for this. The calculated wear depths are multiplied by the scaling factor and thus scaled over a longer period of time. This method is already explained in detail in section 5.3 and the corresponding Figure 5-12.

In the same way like the studies on convergence of the wear model from section 6.3, this study is carried out with a dry-running model. Under non-lubricated conditions, the expected local wear depths are higher than in a lubricated contact and therefore they react much more sensitively to higher scaling factors. For the turned specimen 1 from Figure 5-5, the global wear depths are evaluated. The influence of the scaling factor on the global wear depth is shown in Figure 6-14.

Scaling factors from 50,000 to 2,400,000 are investigated. For example, with a scaling factor of 1,000,000, the calculated time of 1 μ s is interpolated to 1 s. Each point on a curve corresponds to a scaled overrun. For every scaling factor, 26 overrun cycles are calculated. It can be clearly seen that all curves with a lower scaling factor match the wear depth curve with a scaling factor of 2,400,000 very well, which is why the highest scaling factor can be assumed to be permissible. Higher scaling factors are not investigated because the highest factor allows the calculation of the entire running-in phase in an adequate time. In summary it can be concluded that the highest investigated scaling factor examined of 2,400,000 is permissible for scaling the wear depth distribution on the contacting surfaces. No deviations could be found with different scales for the global wear depths. The scaling factor of 2,400,000 is consequently applied in all subsequent calculations.

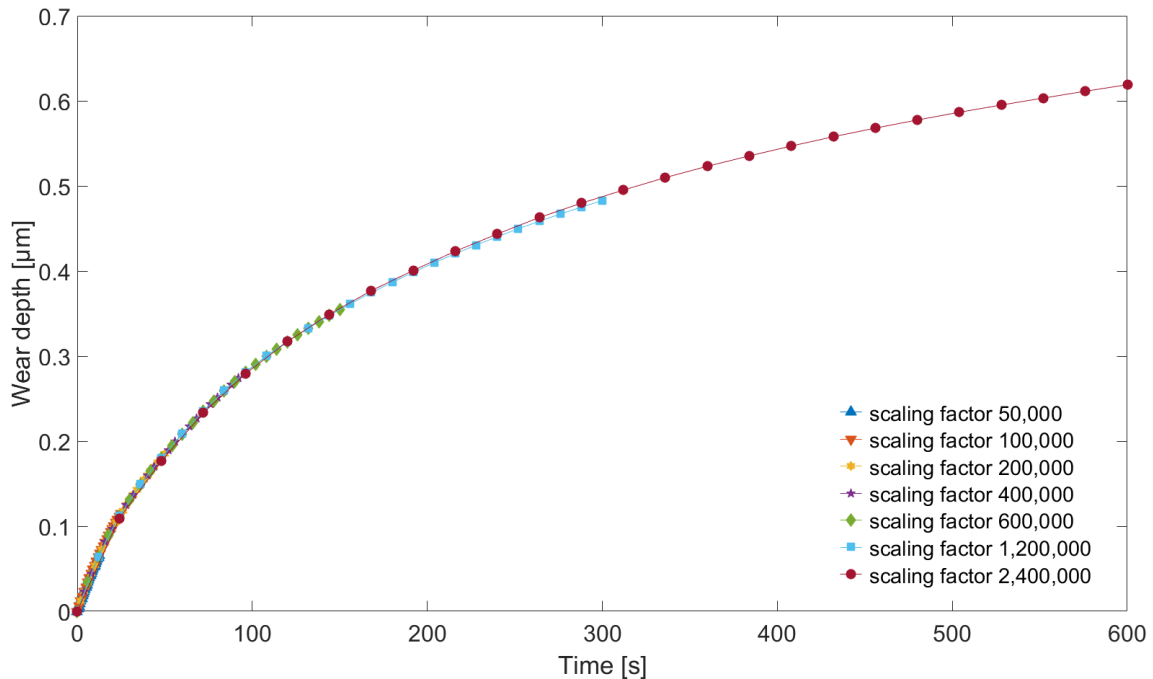


Figure 6-14: Development of the global wear depth depending on the investigated scaling factors

6.6 Validation of the dry running wear model with nanoindenter device

For the validation of the present wear approach under dry running conditions, a nanoindenter device is used. This experimental setup allows the investigation of very small geometrical dimensions of the specimen, which in turn leads to acceptable computing times for the simulation. First, the experimental and numerical setup is described. In a second step, the frictional forces and the surface topographies of the experimental test and the simulation are validated.

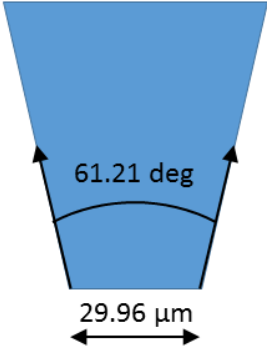
6.6.1 Demonstrator of dry running model

The experimental tests are carried out on a Hysitron standalone nanomechanical test instrument TI 950 Triboindenter in combination with a 3D Omniprobe, which is a bandwidth transducer which can operate in closed loop feedback in either force or displacement control. This experimental setup offers the possibility to quantify friction coefficients with simultaneous normal and lateral forces and displacement monitoring. The experimental tests are carried out by the Institute of Advanced Materials – Computational Materials Science at the Karlsruhe Institute of Technology⁵. The pairing

⁵ Experimental tests carried out by IAM-CMS – Institute of Advanced Materials – Computational Materials Science, Straße am Forum 7, 76131 Karlsruhe

is composed of a diamond flat tip and a ground plate of AISI 1045. The nominal flat diameter of the indenter is about 30 μm . Material properties and geometric dimensions of the indenter are shown in Table 6-1.

Table 6-1: Material properties and geometric dimensions of indenter tip

	Quantity	Value
	Nominal flat diameter [μm]	29.96
	Nominal cone angle [deg]	61.21
	Young's modulus [GPa]	1140
	Poisson's ratio [-]	0.07

For AISI 1045, the material properties are determined separately for the boundary layer, as these are clearly different from the lower macroscopic material areas. The production related differences in material properties of the boundary layer are already shown in Figure 2-23.

For this reason, micro columns and bending beams are manufactured in the boundary layer of the specimen and loaded with a nanoindenter. A material model according to Ludwik (1909) could be determined by adjusting the force-displacement curves of the FE-model with the curves determined experimentally. The determined yield strength of $2750 \times 10^6 \text{ Pa}$ clearly exceeds the yield strength of the macroscopic material model shown in Table 5-5. Density, young modulus and poisson's ratio remain unchanged.

The experimental setup up is shown in Figure 6-15. The indenter tip is oscillating five times with different amplitudes. The normal load is constant at 0.1 N. The sliding velocity of 0.0019 mm/s is chosen very low in order to neglect the influence of temperature. The lateral displacement and the normal load as a function of time are shown in Figure 6-16.

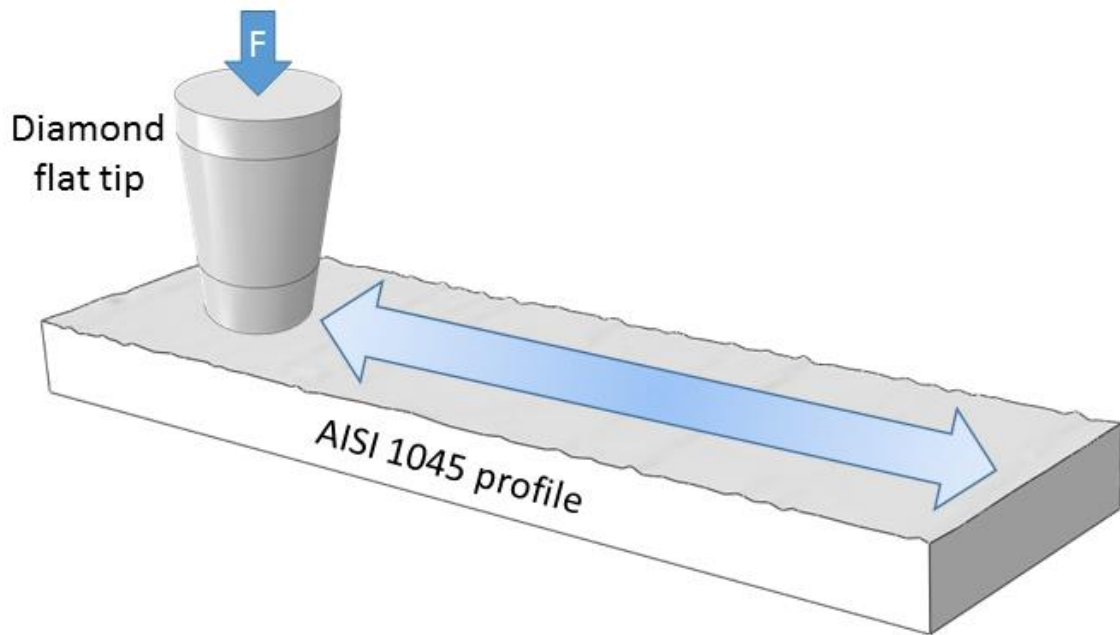


Figure 6-15: Experimental setup of the non-lubricated model

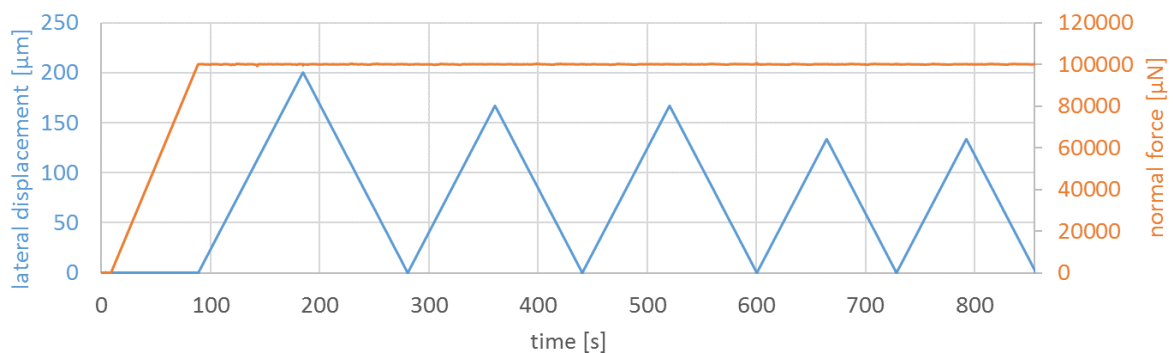


Figure 6-16: Lateral displacement and applied normal load of the experimental setup

The corresponding numerical setup of the dry running model is shown in Figure 6-17. The ground plate was measured with the white-light interferometer and transferred into a solid body as described in detail in section 5.2.1. The indenter is modelled according to the material properties and geometric dimensions from Table 6-1.

Both the indenter and the plate are meshed with linear hexahedron elements of type C3D8R. Due to the shorter computing time of the dry running model, the element edge length determined in the convergence study in section 6.2.1 and 6.3 can be reduced from 3.0 to 2.5 μm. The numerical model was loaded with the identical boundary conditions as the experimental setup in order to obtain comparable results. Initially, the misalignment of the indenter tip caused by the experimental setup was determined by an insertion test. By measuring the impression, the indenter could be aligned identically

in the numerical model. The sliding direction in relation to the manufacturing direction of the surface was also chosen identical.

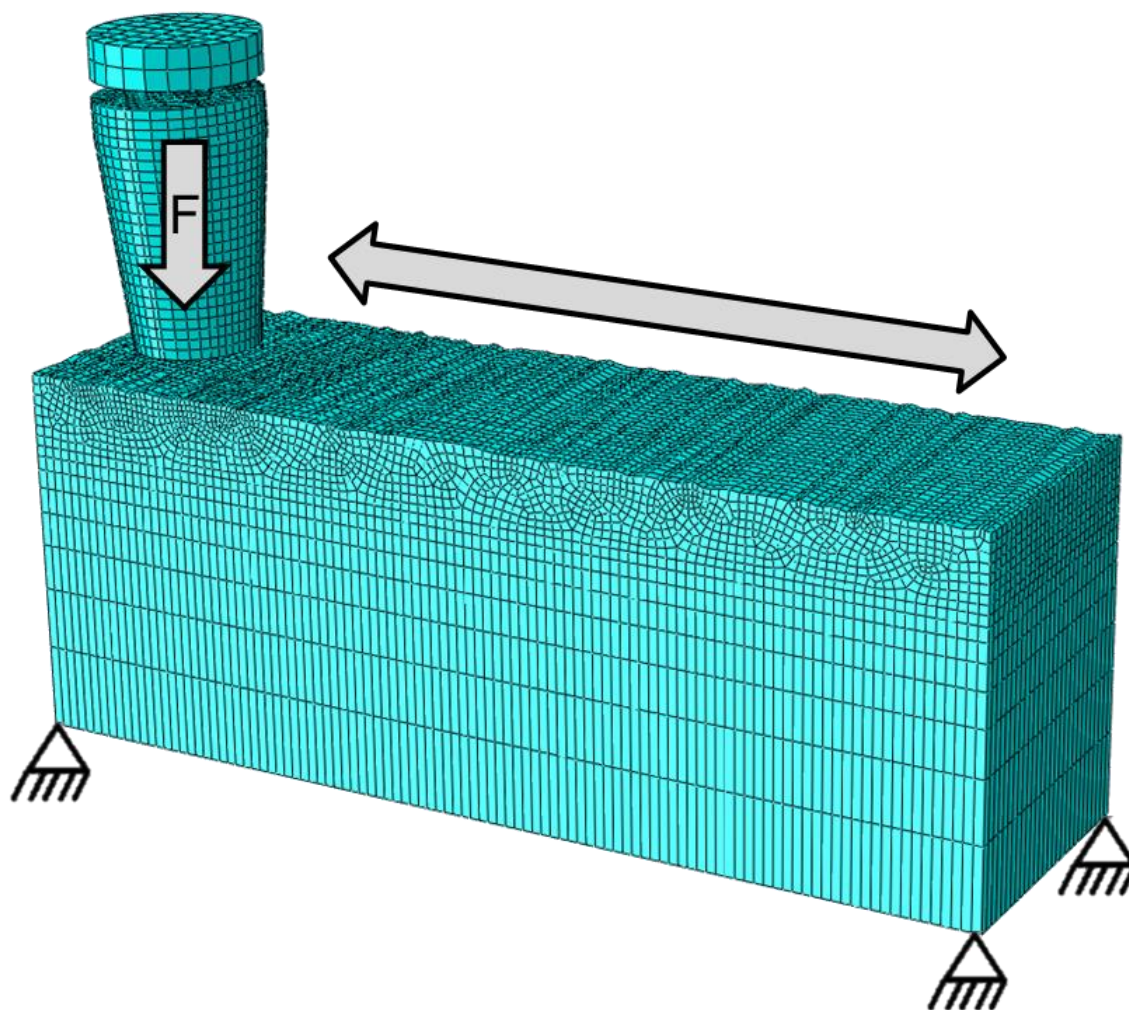


Figure 6-17: Numerical setup of the non-lubricated model

For the validation of the numerical model, the resulting friction force and the changes in surface topography are evaluated.

6.6.2 Comparison between experimental and numerical results

The resulting wear mark from the relative displacement of the indenter tip is shown in Figure 6-18. As can be seen in this figure, this is not a continuous trace of wear. Only the asperities are partially removed.

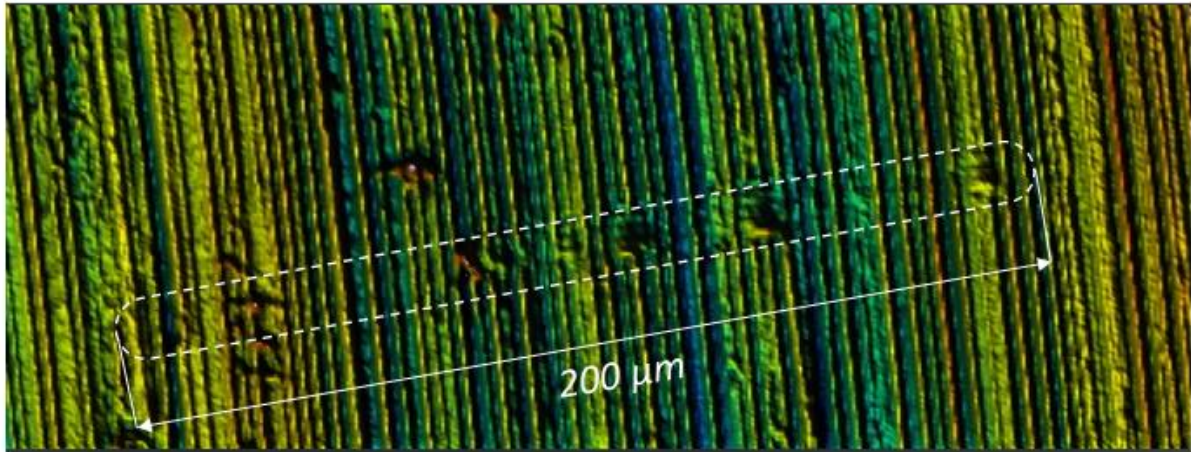


Figure 6-18: Wear trace of the plate resulting from the test procedure of the nanoindenter device

In order to compare the change in topography before and after testing, the surface was measured with the white light interferometer in new and worn condition and evaluated in the middle of the wear mark. The corresponding result is shown in Figure 6-19.

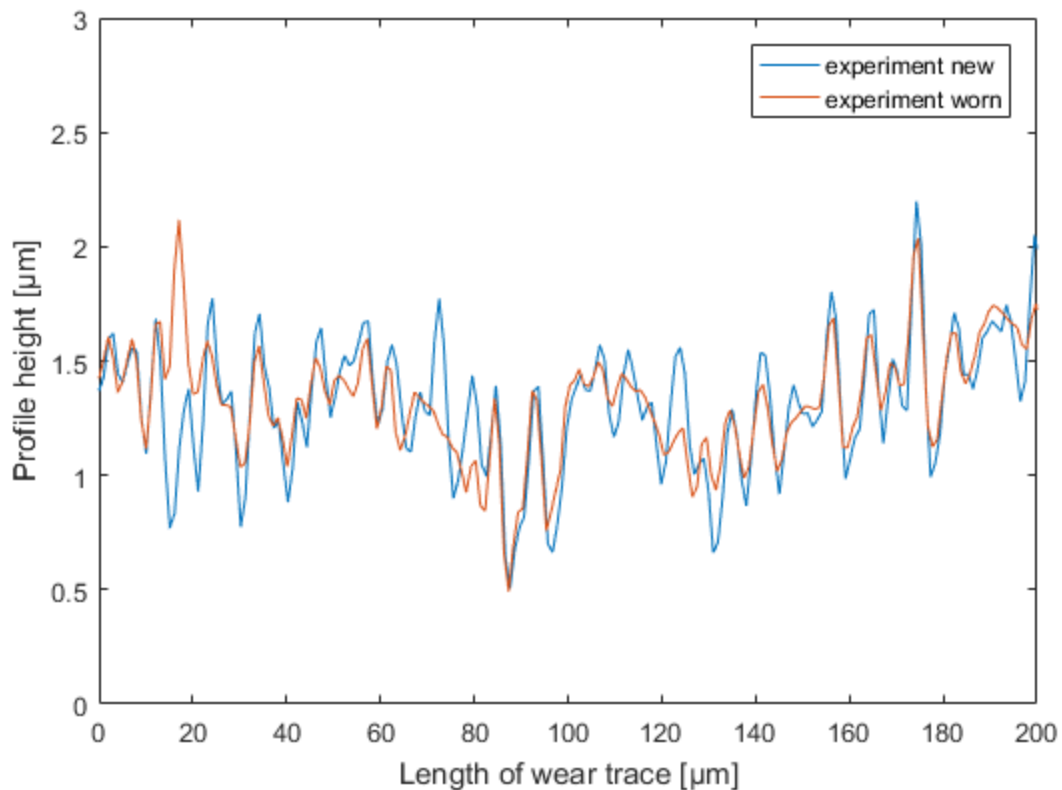


Figure 6-19: Comparison of the measured surface profiles in the middle of the wear mark before (blue profile) and after (red profile) testing

The optical impression from Figure 6-18 is confirmed in the comparison of the new and worn surface profile. It can be clearly seen that the roughness peaks of the surface

asperities have been removed. The roughness peak at the beginning of the measured profiles after testing results from plastic deformation of the material during the continuous return of the indenter tip to its initial position. Further, wear particles that lead to this profile peak deposited in this area.

In order to check whether the initial profile from experiment and simulation are comparable, the surface profiles in new condition were superimposed. As already shown in section 6.1, the real topography and the generated topography are very similar. There are almost no deviations between the two profiles. The two surface profiles from experiment and simulation in new condition are shown in Figure 6-20.

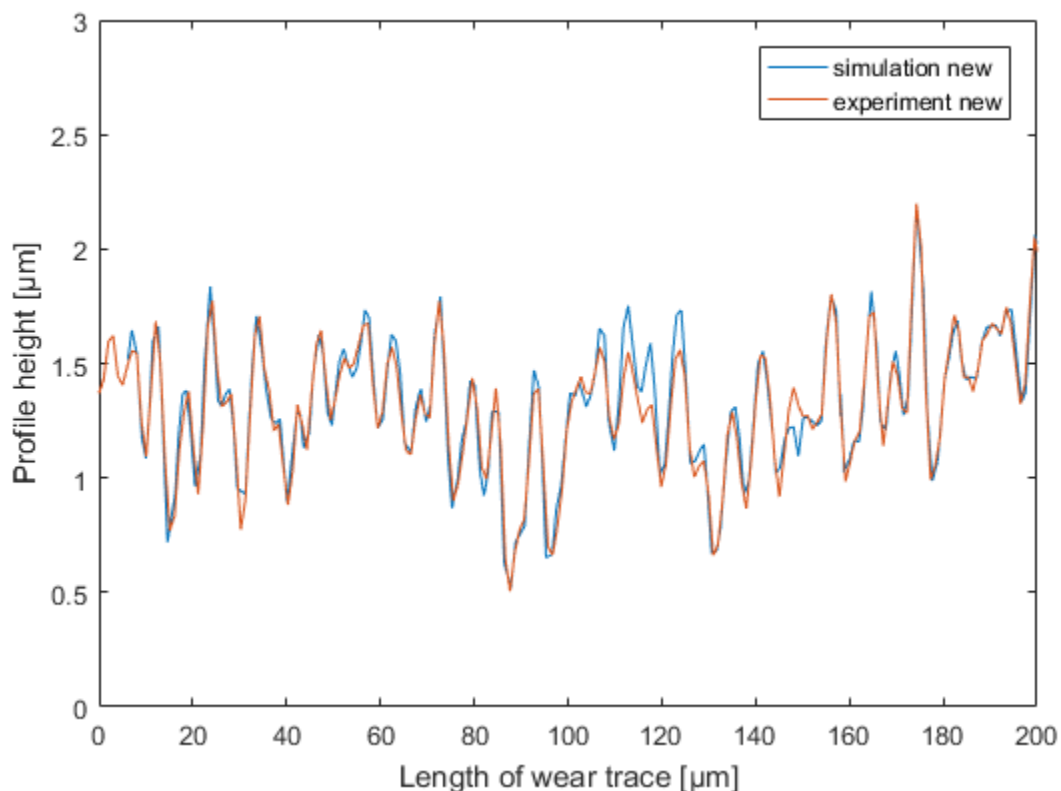


Figure 6-20: Comparison of the new surface profiles in the middle of the wear mark for the generated surface (blue profile) and the real topography (red profile)

The wear coefficient for the calculation is determined according to equation (5-3) from the wear volume of the plate and the boundary conditions of the experiment. The resulting wear volume V_V is determined by the comparison of the new and the worn surface from experiment and is approximately $600 \mu\text{m}^3$. With a normal load F_N of 0.1 N and a total sliding distance s of 1560 μm , the wear coefficient is determined to $3.846 \mu\text{m}^3/\text{N}\cdot\mu\text{m}$. The wear coefficient of the pin is assumed to be 0, as there is no wear detected at the diamond tip while the experimental investigation.

With the identical boundary conditions in the numerical model, comparable local wear depths are calculated. The worn surface profile from simulation and the worn surface profile from experiment are compared in Figure 6-21.

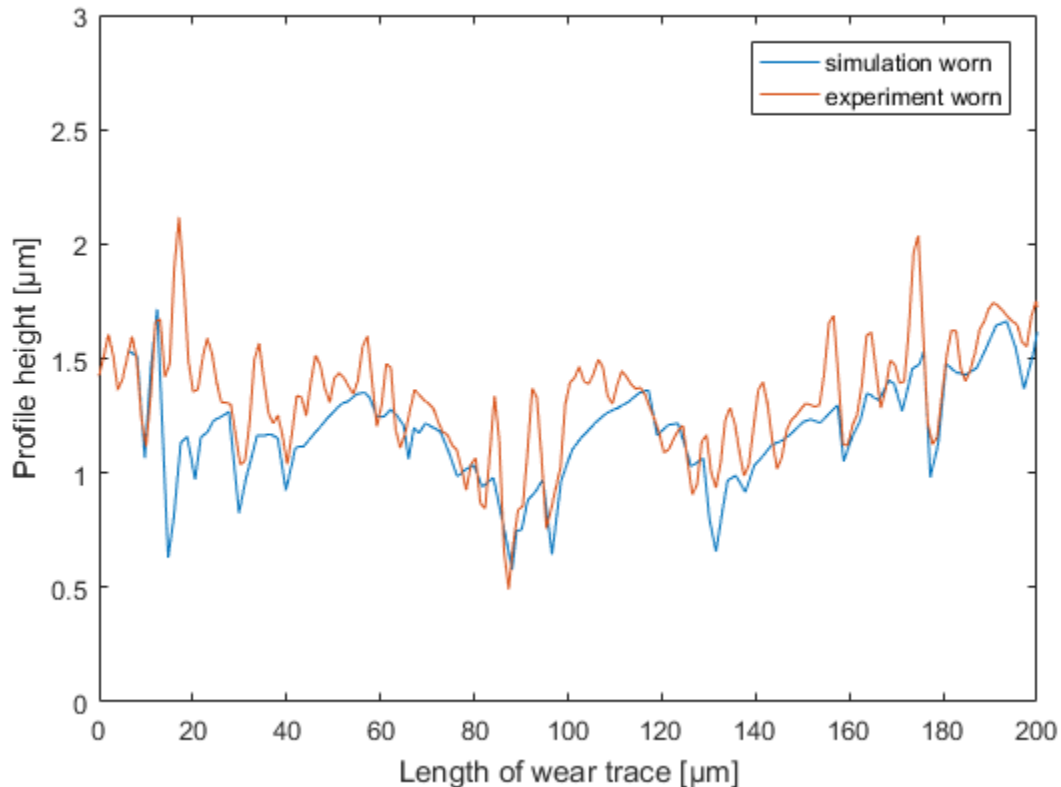


Figure 6-21: Comparison of the worn surface profiles in the middle of the wear mark for the generated surface (blue profile) and the real topography (red profile)

As it can be seen in Figure 6-21, the surface asperities are more reduced in the numerical model than in the experimental test. This phenomenon is due to the averaged wear coefficient. However, the form profile of the surfaces is identical. Despite the slight deviation of the worn surfaces from simulation and experiment, the comparison can be considered as very well consistent. Even better matches can be achieved by slightly adjusting the wear coefficient.

After investigating the changes in surface topography the calculated frictional force from simulation is compared to the measured frictional force from experiment. The result is shown in Figure 6-22. The abscissa shows the accumulated sliding distance and the ordinate shows the calculated (blue curve) and the measured (red curve) frictional force.

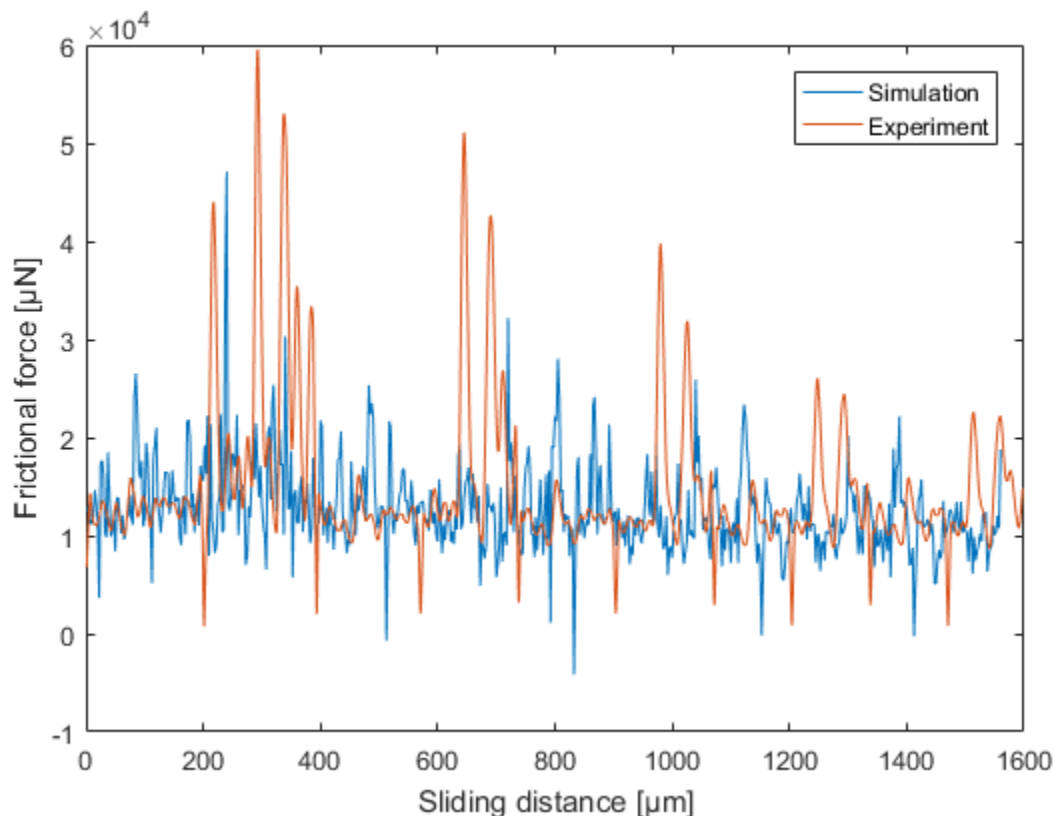


Figure 6-22: Comparison between calculated frictional force from finite element model (blue curve) and measured frictional force from experiment (red curve)

The decrease in the peaks of the measured frictional force from experiment (red curve) is clearly visible. This decrease correlates with the reduction in deformation due to the lower heights of the asperities. This phenomenon can also be observed in the numerical approach. Here, too, the peaks resulting from a high amount of deformation in the frictional force are becoming smaller and smaller. The fact that the peaks in the simulation model are less pronounced is due to the slightly higher wear compared to the experiment. As shown in Figure 6-21, the surface in simulation is slightly more worn out, which leads to a lower deformation rate and thus the peaks are less pronounced.

The mean value of the calculated and measured frictional force is almost identical. The deviation is about 5 %. Due to the good agreement of the results, the present method can be considered valid. To validate the mixed-lubricated model, this must be further reduced to deduce the needed computing time.

6.7 Summary

In this chapter could be shown that real measured surfaces can be converted into digital solid bodies without major deviations. Convergence studies on friction and wear have shown that the model is very robust to changes in element edge length. Changes have therefore no significant influence on normal load, frictional force and wear depth.

Comparison of the modelling with the CEL method in the present approach and the established CFD flow simulation has also shown that comparable results can be achieved after a certain time of load initiation. This could already be proven in the fundamentals in section 2.7.2 in other works. The final comparison of the dry-running model with experimental investigations showed a very good agreement. With the parameters identified here, the following calculations are carried out in this work.

7 Results on friction and wear under mixed-lubricated conditions

In this section, different parameters are varied to investigate their influence on friction and wear under mixed lubricated conditions. Beginning with the material properties of the fluid and solid bodies, second parameters are the boundary conditions regarding fluid pressure and normal load to adjust the lubrication gap and consequently the friction regime. After the investigation of the influence of surface topography on friction and wear, different residual stresses resulting from various manufacturing processes are examined. Finally, the development of roughness parameters as a function of time is investigated to locate the areas where wear is likely to occur.

7.1 Influence of the fluid viscosity on friction and wear

As Lorentz (2013b) has shown in the previous work, the viscosity of the lubricant can vary by a factor of 100 due to high fluid pressures. It could be shown that viscosity has a huge influence on the coefficient of friction in a hydrodynamic regime.

In the present work, the fluid viscosity is varied by a factor of 1000 for a mixed-lubricated regime and the influence on friction and wear is investigated. The influence of dynamic fluid viscosity, varying from 0.262255 to 262.255 mPas, on the wear depth under otherwise constant boundary conditions (normal load 1 N, fluid pressure 30 MPa) is shown in Figure 7-1. Both, the surfaces of the basic and the counter body are the turned surfaces from pairing 1 shown in Figure 5-5. Since the contact ratio of the fluid in a mixed-lubricated regime is only a small proportion, the influence of the viscosity on the wear depth is, as expected, significantly lower than under a hydrodynamic regime. Consequently, no trend can be observed under mixed-lubricated conditions, which means that the pressure dependence of the fluid is subordinate and does not need to be taken into account under the chosen boundary conditions.

However, the calculated wear curves show the typical running-in behavior (compared to Figure 2-19). During the first 150 s the significantly high wear rate is clearly visible.

After an almost constant ratio of normal load due to solid contact and real contact area has been established ($t \geq 150$ s), the wear rate decreases and a constant lower level of wear is achieved. Furthermore, it can be seen that with increasing viscosity the wear depth trends become smoother. This is because the damping behavior is easier to control with increasing viscosity and the normal force can be applied almost constantly. At lower viscosities, the application of a constant normal force is subjected to slight deviations.

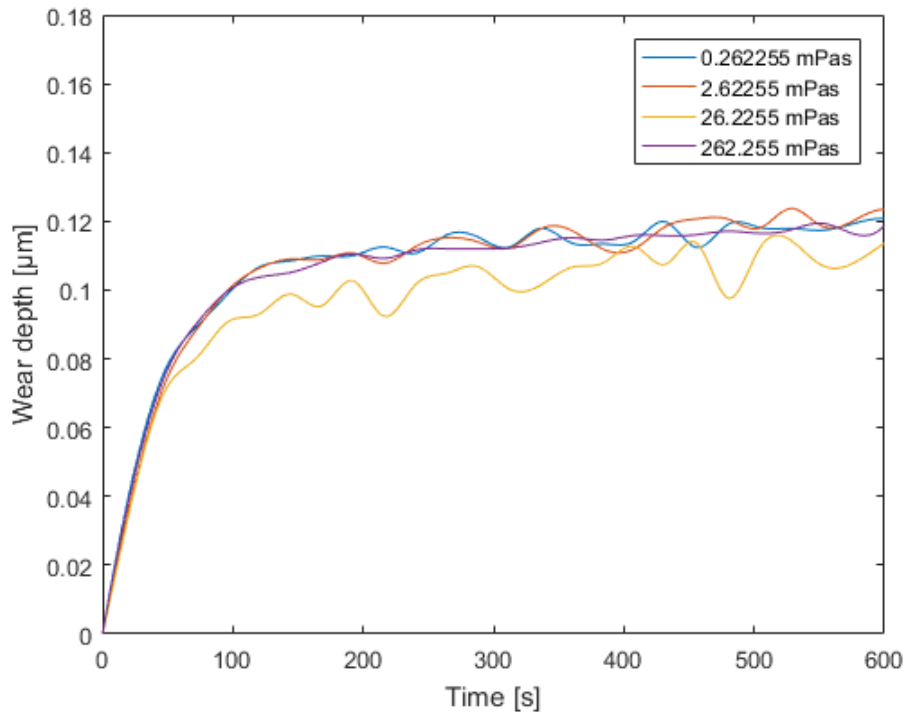


Figure 7-1: Influence of various viscosities on wear depth

With regard to the friction behavior, there is also no clear influence of fluid viscosity on the coefficient of friction as shown in Figure 7-2. Here, too, under mixed-lubricated conditions, the ratio of frictional force transmitted by the fluid is very low and shows almost no influence. However, it can be clearly seen that all calculated curves show the typical running-in behavior as described in section 2.4 in Figure 2-19. After 150 s, the coefficient of friction has decreased to a steady state level. This correlates also with the decreasing wear rate after 150 s. In this case it seems that after this time, the tribological system has passed the running-in phase.

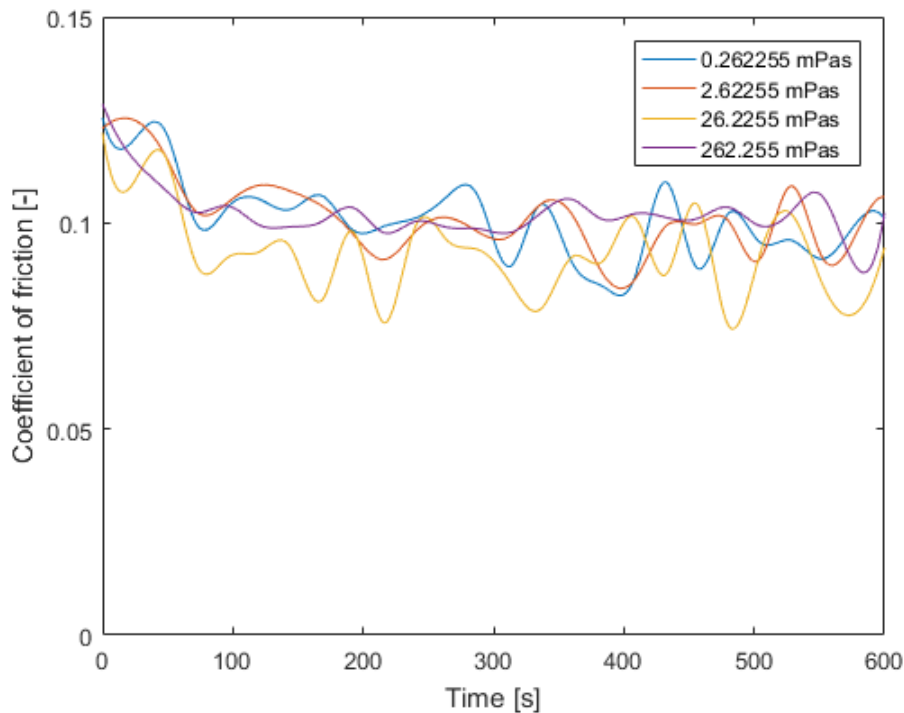


Figure 7-2: Influence of fluid viscosity on coefficient of friction

After the investigation of the material properties of the fluid, the influence of the solid properties on friction and wear is taken into account.

7.2 Impact of solid properties on friction and wear

In addition to the reference material AISI 1045, further materials are investigated in order to determine their influence on the friction and wear behavior. The main solid properties of these materials regarding elasticity and plasticity are shown in Table 7-1.

Table 7-1: Solid properties of the investigated materials

Quantity	Value		
	AISI 1045	Ti6Al4V	42CrMo4
Density [kg/m ³]	7860	4430	7805
Elastic modulus [Pa]	221 x 10 ⁹	112 x 10 ⁹	212 x 10 ⁹
Poisson ratio [-]	0.285	0.404	0.288
Yield strength [Pa]	568 x 10 ⁶	965 x 10 ⁶	1447 x 10 ⁶

In order to investigate the influence of yield strength and elastic modulus, the critical shear stress was not adjusted to the yield strength as described in formula (2-20), but kept constant. Both the surface topography (turned sample 1 from Figure 5-5) and the boundary conditions (normal load 1 N, fluid pressure 30 MPa) and the wear coefficient were identical in all calculations. The influence of the solid properties on the wear depth is shown in Figure 7-3. In the calculations, both the material of the basic body and the counter body were changed.

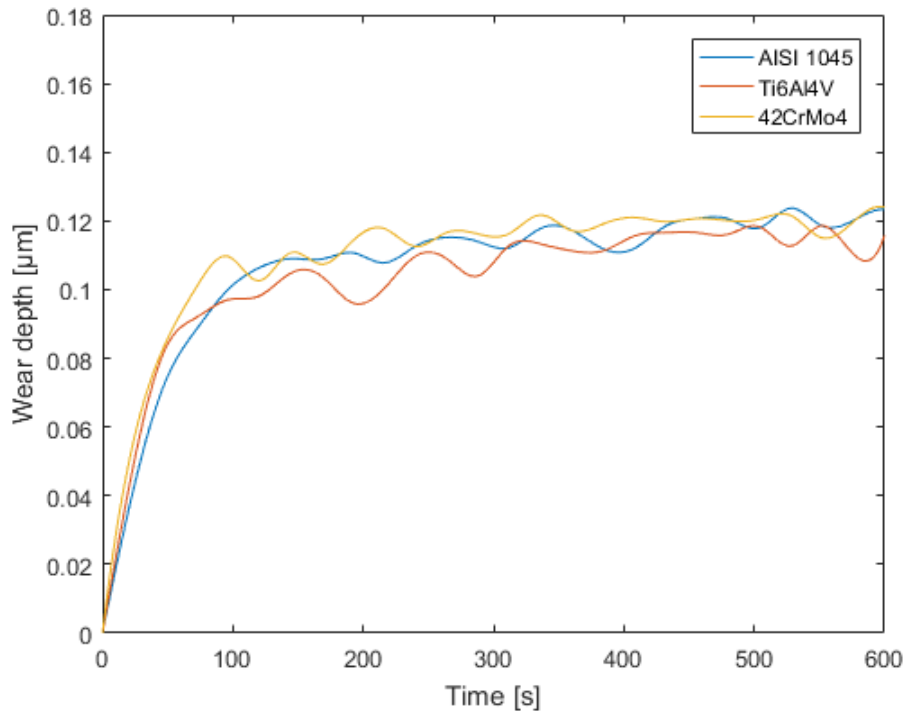


Figure 7-3: Influence of solid properties on wear depth

Due to the identical surface pressure, the same surface topography and wear coefficient, the influence of the solid materials on the wear depth is low. There are no significant changes in wear depth if the material properties of the solids change. Also in this case, the typical running-in behavior is clear to see. Since the same boundary conditions are used as in section 7.1, the running-in phase is passed also after 150 s.

However, the influence of the material properties on the friction behavior is clearly visible. The dependence of the coefficient of friction on the solid properties is shown in Figure 7-4. Here, too, it can be clearly seen that all calculated friction curves show the typical running behavior. Also after 150 s, the coefficients of friction have decreased to a steady state level in comparison to the higher coefficient of friction at the beginning of the calculation.

Furthermore, the lowest coefficient of friction for the pairing of 42CrMo4 is clearly visible. Comparing the mechanical properties of 42CrMo4 and AISI 1045, it is noticeable that these materials differ mainly in terms of yield strength. The young

modulus of both materials are nearly identical. Due to the higher yield strength, the pairing of 42CrMo4 has less plastic deformation at the surface asperities and the real contact area is smaller. The lower real contact area leads to the lowest coefficient of friction. These results are supported by the observations of the real contact area in Figure 7-5. Both at the beginning and at the end of the calculation, the pairing of 42CrMo4 has the smallest real contact area. This explains both the initial lowest and the lowest coefficient of friction at the end of the calculation.

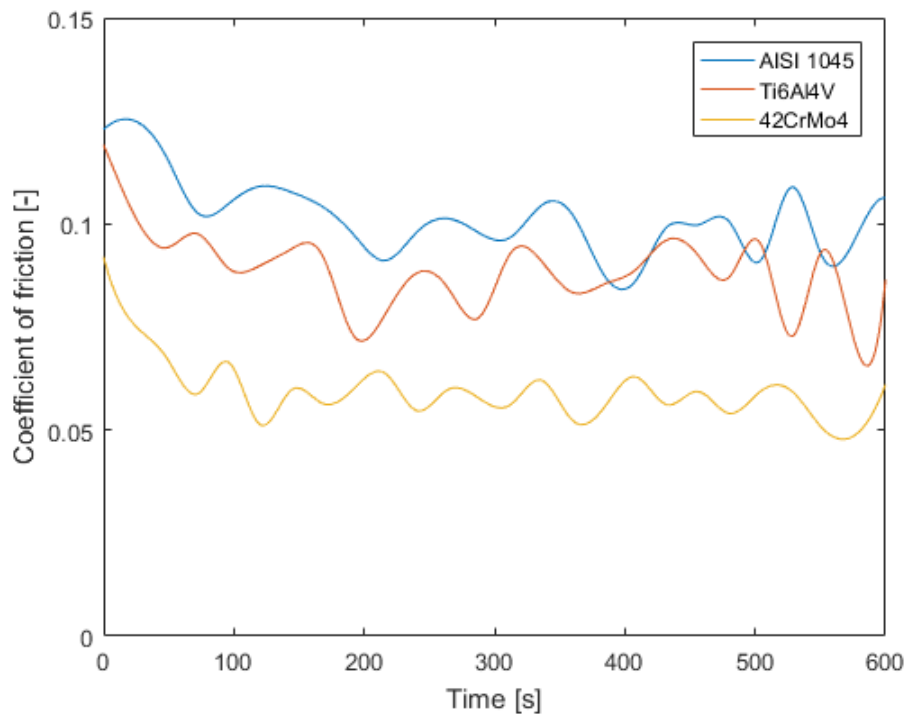


Figure 7-4: Influence of solid properties on coefficient of friction

A comparison of the material properties of Ti6Al4V and AISI 1045 reveals that the material properties differ considerably in terms of both elasticity and plasticity. Due to the higher young modulus of AISI 1045, the resistance to elastic deformation is higher. With Ti6Al4V, less plastic deformation is to be expected due to the higher yield strength. It must be therefore assumed that elastic and plastic effects overlap. If the real contact areas for both materials from Figure 7-5 are compared, it becomes clear that they are very similar. For this reason, the two coefficients of friction are very close together. At the end of the calculation, the pairing of Ti6Al4V has a minimal smaller real contact area, which also leads to minimal reduction in coefficient of friction. The initial real contact area for the pairing of 42CrMo4 is smaller, therefore a smaller initial coefficient of friction is present.

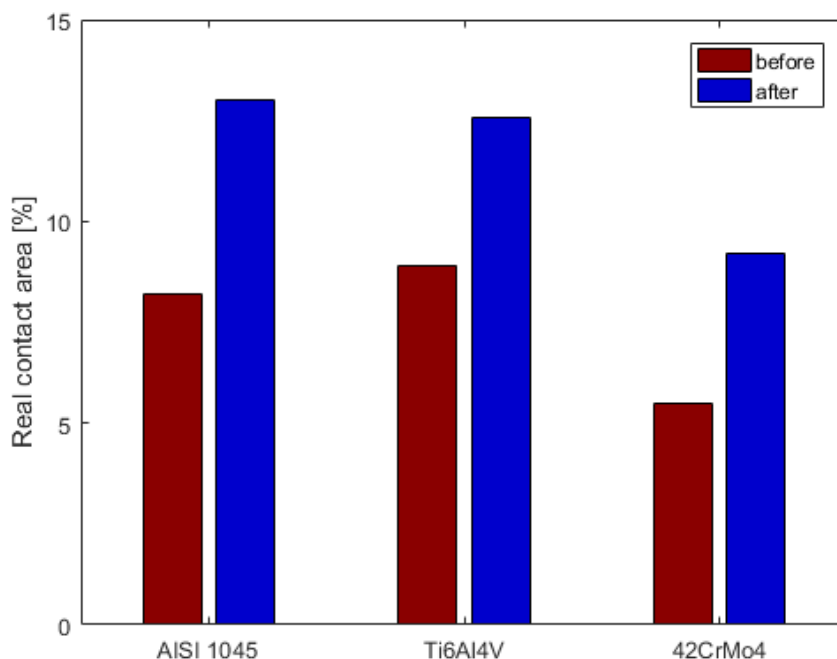


Figure 7-5: Changes in real contact area before and after running-in for different materials

The investigation has shown that the method can be used to determine the suitability of different solid materials. It became clear that it is imperative to consider not only elastic material behavior but also plastic material behavior. With identical boundary conditions, a small contact surface is better to achieve low friction. As identical wear coefficients were used for better comparability, it is not possible to make a statement about the wear depth of the different material pairs.

In the next two sections, the fluid pressure and the normal load are varied, to investigate the influence of different friction regimes in mixed-lubrication (height of the lubrication gap) on friction and wear.

7.3 Influence of fluid pressure on friction and wear

To adjust the mean height of the lubrication gap in a mixed-lubricated regime, the ratio of fluid pressure and normal load can be varied. In this section, the influence of various fluid pressures under constant normal load of 1.0 N is investigated. The fluid pressure is varied in a range from 10 MPa to 40 MPa. Also in this investigation, the surfaces of basic and counter body are the turned surfaces from Figure 5-5. With an increasing fluid pressure under a constant normal load, the mean lubrication gap is increasing and the tribological system trends from a mixed-lubricated regime to hydrodynamic. A hydrodynamic regime is reached, if the fluid pressure has the same size as the mean surface pressure. This tribological behavior that the wear depth is decreasing if the

tribological system trends to hydrodynamic, can be seen in Figure 7-6. It is important to mention, that in all calculations are carried out under mixed-lubricated conditions. Consequently, solid interactions are still present with increasing the fluid pressure to 40 MPa.

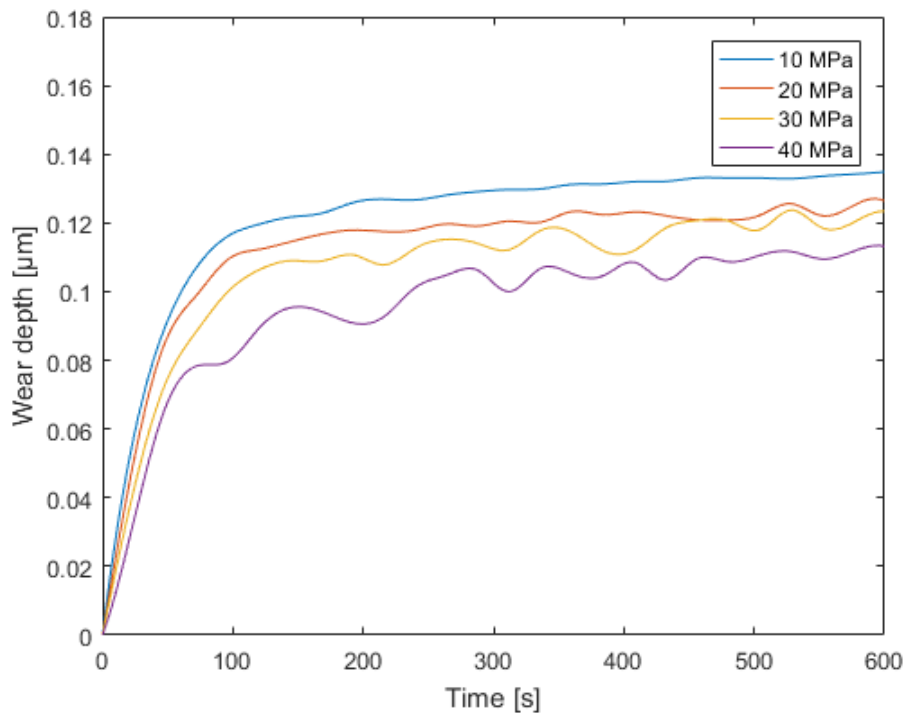


Figure 7-6: Influence of applied fluid pressure on wear depth

Decreasing fluid pressure causes the proportion of normal forces transmitted by solid contact to increase. If no more fluid is present, the complete normal load is transmitted by solid contact. At the same time, the proportion of the normal load transmitted by the fluid continues to decrease. This behavior is visualized in Figure 7-7 for the normal force component due to solid contact and in Figure 7-8 for the normal force component transmitted by the fluid.

As mentioned above, a decreasing fluid pressure leads to a higher normal load transmitted due to solid contact and with a constant contact area at the beginning, there is a higher surface pressure and wear depth increases while the running-in phase in the first 150 s. The wear rates after the running-in phase are nearly constant due to the constant ratio of normal load due to solid contact and the real contact area. Also to see is the increasing vibration behavior of the wear curves with increasing fluid pressure. This is caused by the difficult control of the damping behavior, if the tribological systems trends to a hydrodynamic regime. Increasing vibrations in the wear depth trends are related to small vibrations in the applied normal load. However, these deviations are very small and therefore do not have much influence. The mean value of the normal load is still nearly constant.

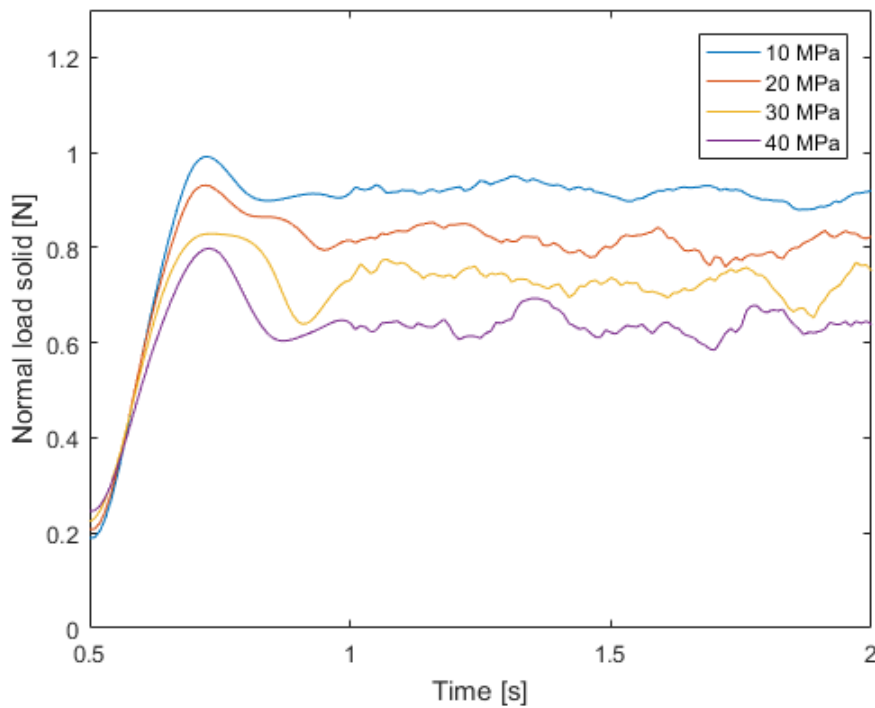


Figure 7-7: Influence of applied fluid pressure on normal load, transmitted due to solid interaction

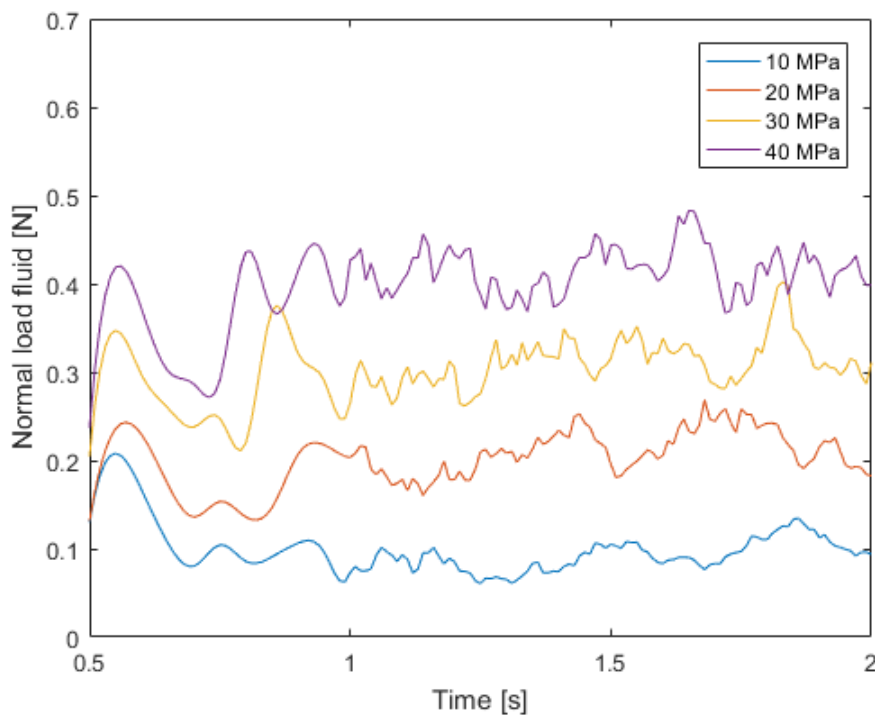


Figure 7-8: Influence of applied fluid pressure on normal load, transmitted due to solid/fluid interaction

Next to the wear depth, the coefficient of friction is investigated. In Figure 7-9 can be seen, that with increasing fluid pressure, the coefficient of friction is decreasing. In case of higher fluid pressure, normal load transmitted by solid contact is decreased and

consequently also the real contact area is decreased. This leads to a decreasing coefficient of friction due to the decreasing solid interactions. Further, for higher fluid pressures, the same vibration behavior in coefficient of friction can be observed like for the wear depth curves. This is also due to the damping behavior in a regime with less mixed-lubrication.

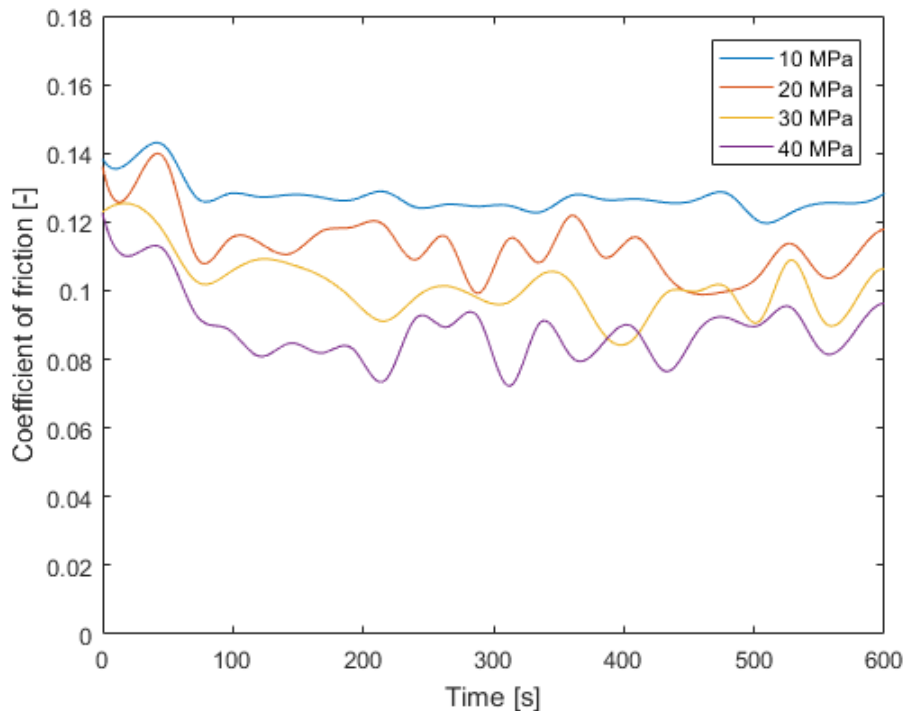


Figure 7-9: Influence of applied fluid pressure on coefficient of friction

In this section could be shown, that the fluid pressure has a huge influence on friction and wear in the running-in phase. The higher the fluid pressure is under constant normal load, the smaller is the wear depth and the coefficient of friction.

In the next section, the height of the mean lubrication gap is adapted by varying the normal load. The fluid pressure is kept constant during these investigations.

7.4 Influence of normal load on friction and wear

As already mentioned in section 5.2.2, the height of the mean lubrication gap can also be adjusted by varying the normal load. To investigate the influence of the normal load on friction and wear, a pairing of two identical turned surfaces (turned surface 1 from Figure 5-5) is loaded with normal loads of 0.5, 0.75 and 1.0 N. These normal loads are chosen to vary the height of the lubrication gap within the mixed-lubricated regime. The fluid pressure is kept constant at 30 MPa. First of all, the influence of increasing normal loads on the proportion of normal load due to solid contact and due to the fluid is

investigated. The results are shown in Figure 7-10 for the normal force component due to solid contact and in Figure 7-11 for the normal force component due to the fluid.

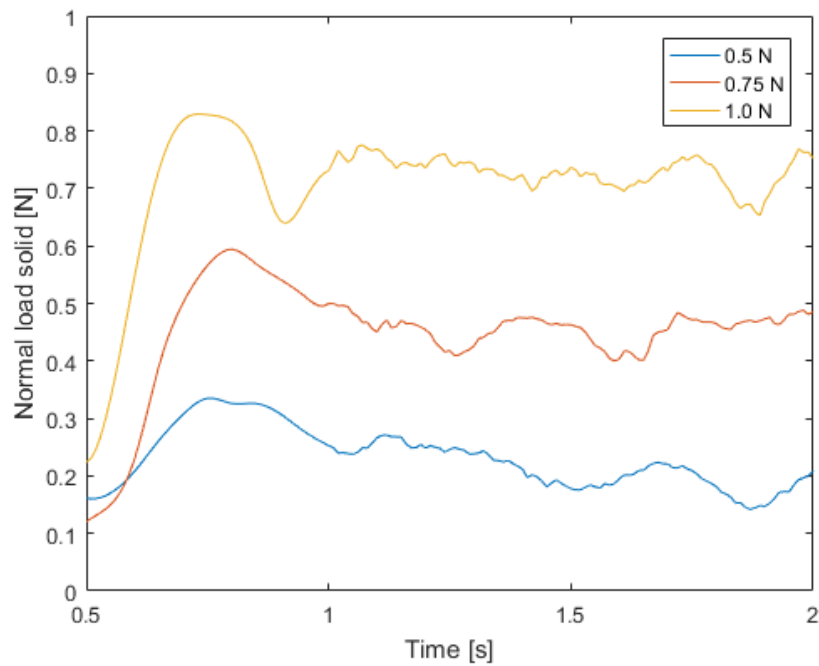


Figure 7-10: Influence of applied normal load on normal load, transmitted due to solid interaction

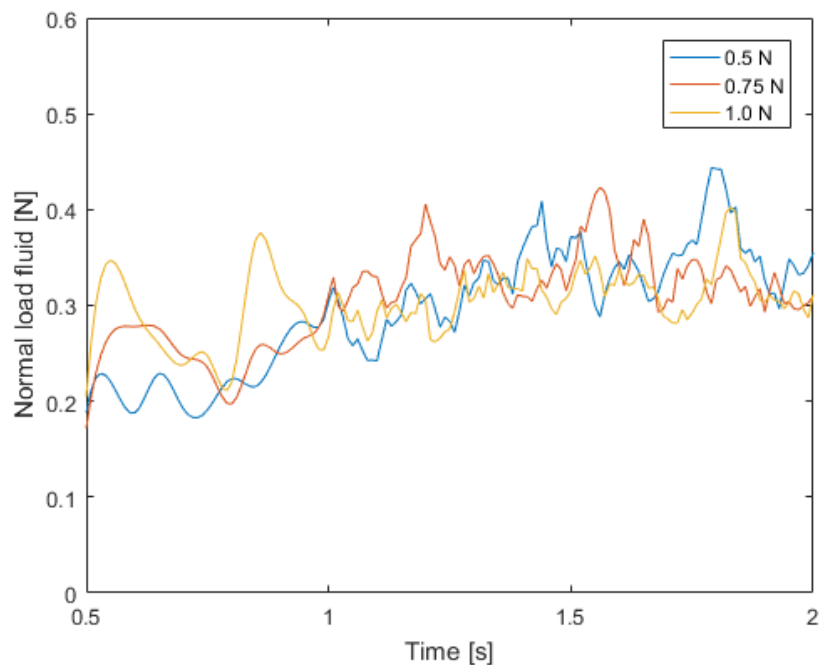


Figure 7-11: Influence of applied normal load on normal load, transmitted due to solid/fluid interaction

Under constant fluid pressure of 30 MPa, the normal force component due to solid interactions is increasing with increasing applied normal load. At the same time, the

ratio of normal load transmitted by the fluid pressure does not change. Consequently, with increasing normal load, the mean height of the lubrication gap is reduced and the tribological system trends to boundary friction (compared to Figure 2-10).

The influence of increasing normal load on the wear depth can be seen in Figure 7-12. With increasing normal load, the wear depth is also increasing. As mentioned above, increasing the normal load leads to an increase of the normal load due to solid contact. Under a higher normal load due to solid contact and a constant surface topography, there is an increased surface pressure, which leads to an increasing wear depth while the running-in phase. Increasing the applied normal load correlates consequently with a decreasing fluid pressure. After the running-in phase ($t \geq 150$ s), the ratio of normal load due to solid contact and the real contact area is nearly constant and the same wear rates for different applied normal loads are observed. The vibrations in the wear depth curve of the smallest normal load are once again visible. This is the same case like for a high fluid pressure, where the tribological system trends to a hydrodynamic regime.

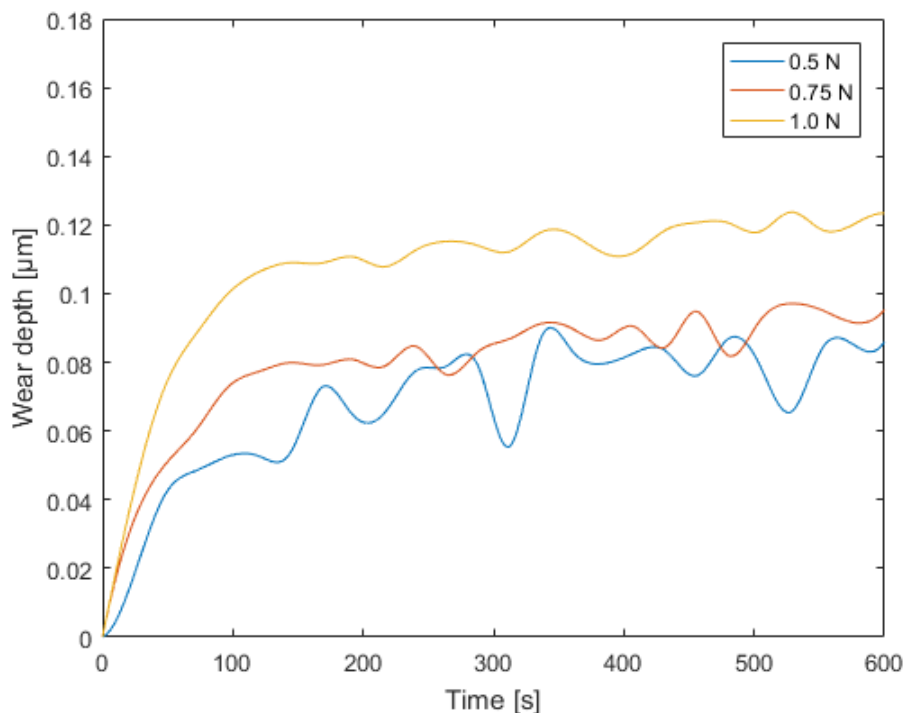


Figure 7-12: Influence of applied normal load on wear depth

In Figure 7-13, the influence of the applied normal load on the coefficient of friction is shown. With increasing normal load, also the coefficient of friction is increasing. The increasing normal load due to solid contact leads to an increased real contact area and consequently the coefficient of friction is increasing. Further clear to see is the decreasing slope of all coefficients of frictions after 150 s, what correlates with the changing wear rate after this time. After the running-in phase ($t \geq 150$ s) the coefficient

of friction has reached a steady state level. In this case it can be assumed that the tribological system has passed the running-in phase.

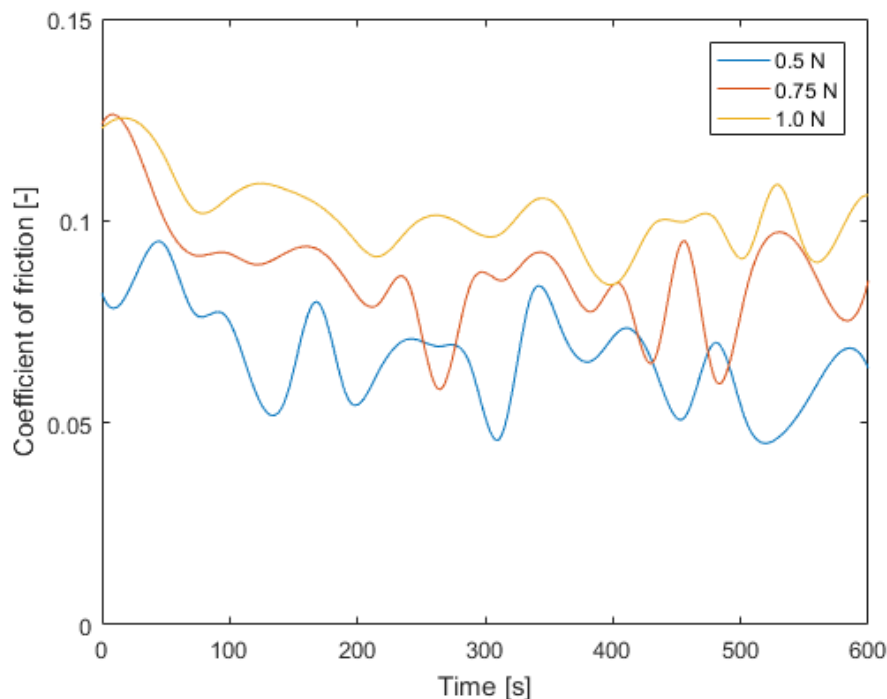


Figure 7-13: Influence of applied normal load on coefficient of friction

It can be summarized that an increasing normal load increases both wear and friction. This phenomenon corresponds to same mechanisms that occur when the fluid pressure is decreased. In conclusion, it can be said that a higher lubrication gap also leads to less friction and wear.

7.5 Influence of running in procedure on friction and wear

In order to investigate the influence of the running-in procedure on friction and wear, the tribological system is loaded with two different load functions. The two load functions are shown in Figure 7-14. In addition to a time constant normal load of 1.0 N (red curve), a second load function has been defined, whereby the load is increased from 0.5 N to 1.0 N in three stages. The fluid pressure is constantly 30 MPa as within the ratio of the normal loads and this pressure, different regimes in mixed-lubrication can be investigated. The surfaces are, as in previous investigations, the turned surfaces 1 from Figure 5-5. It is to be investigated whether a higher load at the beginning or the continuous increase of the normal load leads to a better running-in behavior with less wear.

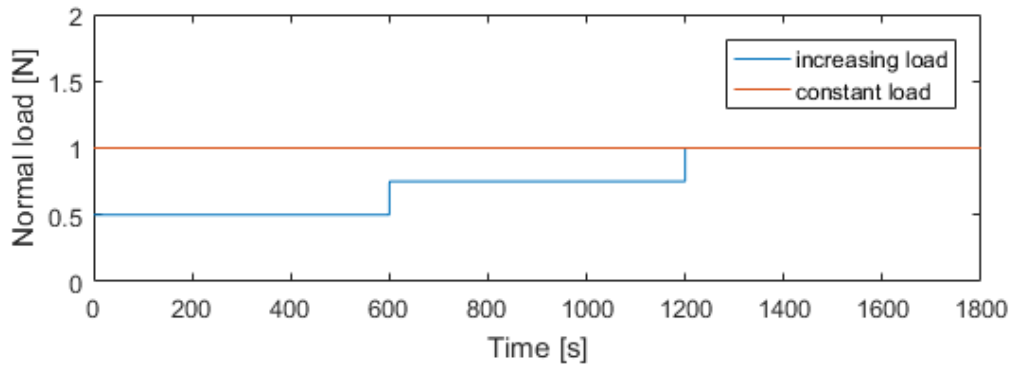


Figure 7-14: Load functions to investigate the influence of the running-in procedure on friction and wear: increasing normal load (blue curve) and constant normal load of 1.0 N (red curve)

The influence of the running-in procedure on the wear depth is shown in Figure 7-15. Although the identical normal load is applied from a time of 1200 seconds, the wear depth is considerably higher with an increased normal load in comparison to a constant normal load. It follows that a heavy running-in procedure, which corresponds to the application of a high load at the beginning, has a positive effect on the final wear depth.

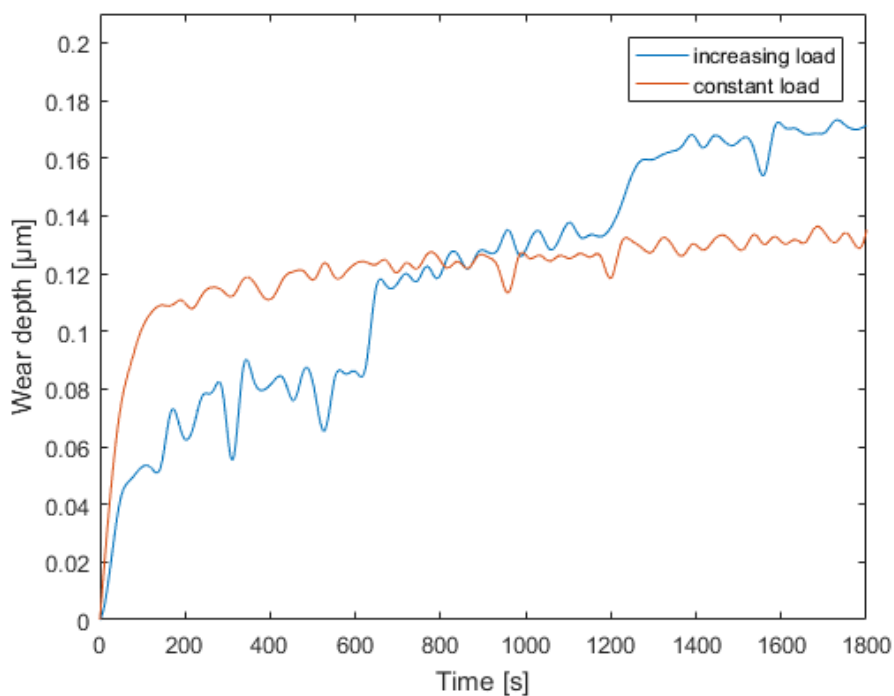


Figure 7-15: Influence of the running-in procedure on wear depth: increasing normal load (blue curve), which leads to a higher wear depth and constant normal load (red curve), which leads to less wear of the tribological system

It is also conspicuous that only one running-in is visible when a constant normal load is applied. If the load is applied in steps a running-in can be detected with every load change. It has already been shown in Figure 7-12 that the wear depth of the initial running-in at a load of 1.0 N is higher than at a load of 0.5 N. In order to investigate the phenomenon of multiple running-in phases for the increasing load, the mean surface

pressure is examined in detail. The contact pressure curves for the two load functions are shown in Figure 7-16.

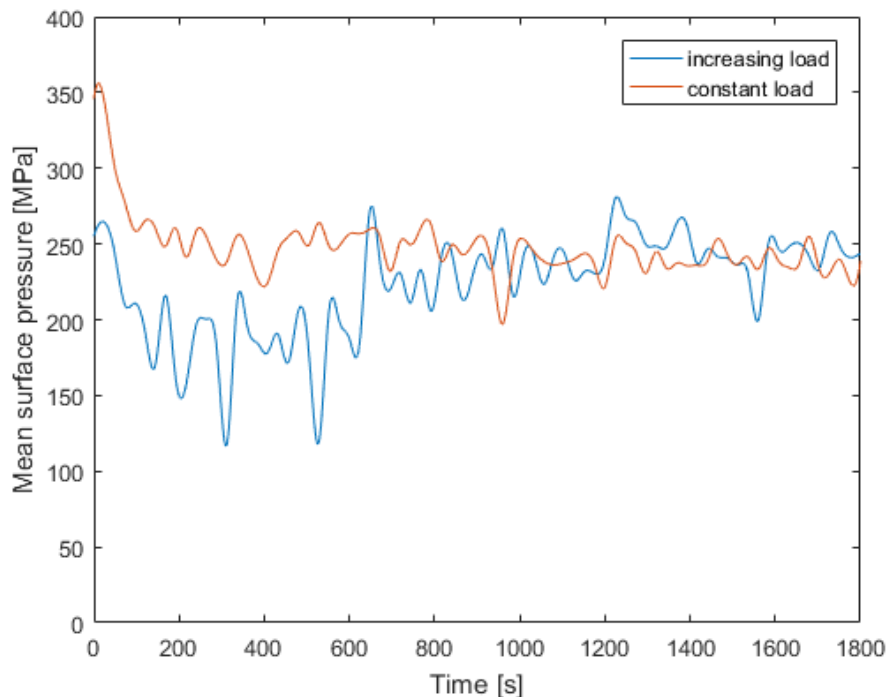


Figure 7-16: Mean surface pressure for the two investigated load functions: increasing normal load (blue curve) and constant normal load (red curve)

It can be seen that a higher surface pressure occurs at the beginning for the higher normal load. Since the wear depth is linearly dependent on the contact pressure (compared to formula (5-4)), the initial wear depth is also significantly higher than with a lower load of 0.5 N. For the constant load of 1.0 N, an almost constant surface pressure of approximately 240 MPa arises after the running-in phase. This constant surface pressure correlates with the constant wear depth curve. A significant change in wear depth is not visible after the running-in.

In the case of an increasing load, the increased surface pressure during load changes at 600 seconds and 1200 seconds is clearly visible. After each running-in process, the decrease of the contact pressure to a constant level is visible. With each load increase, an excessive surface pressure therefore acts for a short period of time, which leads to a significant increase in wear depth. At the end of the calculation after 1800 seconds, a surface pressure of 240 MPa has been set for both load functions. This makes it clear that the running-in phases have a decisive influence on the evolution of the wear depth. After passing through the running-in phase, constant wear rates are achieved. This shows that the normal load in the steady state phase has a minor influence on the final wear depth.

Finally, the influence of the running-in procedure on friction behavior is investigated. The result is shown in Figure 7-17. At the beginning, the same trend as in Figure 7-13 is visible. For an initial smaller load, also the coefficient of friction is smaller. For the constant load of 1.0 N, a constant coefficient of friction of approximately 0.09 is achieved after the running-in phase. If the normal load is increased from 0.5 N to 0.75 N, a slightly lower coefficient of friction ($\mu \approx 0.08$) is achieved as with the constant load of 1.0 N. If the normal load is further increased to 1.0 N, the same level of the coefficient of friction is achieved as with the constant normal load of 1.0 N. The single running-in process after raising the normal load is also visible in the trend of the coefficient of friction. After a short increase in the coefficient of friction at the beginning of each running-in process, a constant level is reached. This correlates with the wear behavior, if the normal load is increased.

Due to the same coefficient of friction at the end of the calculation under identical normal loads of 1.0 N, it can be stated that the running-in procedure therefore has no influence on the friction behavior as much as on the wear behavior.

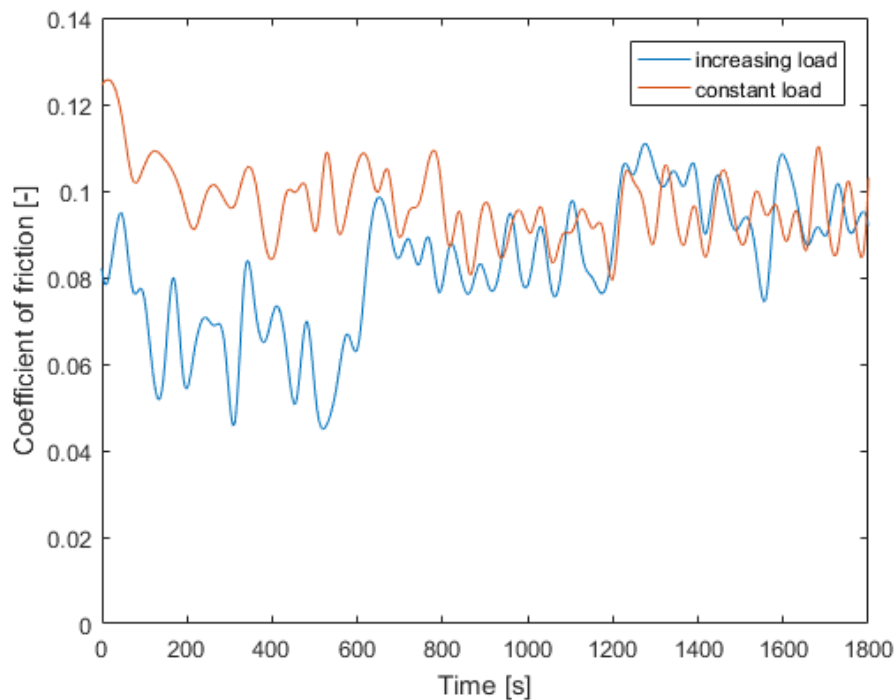


Figure 7-17: Influence of the running-in procedure on the coefficient of friction: for an increasing load (blue curve) and for a constant load (red curve)

In this section could be shown that the running-in procedure has a clear influence on the wear behavior. If a final force is applied abruptly, wear is lower than if the normal load is gradually increased. For this reason, it can be concluded that a heavy running-in is significantly better for the tribological system such as a mild running-in. Such experimental results on the running-in procedure could also be shown by Scherge,

Shakhvorostov and Pöhlmann (2003). on the example of a pin on disc device. No significant influence on the friction behavior could be determined.

7.6 Influence of the surface machining on friction and wear

In order to investigate the influence of different real measured surface topographies on friction and wear, two pairings consisting of two turned surfaces and one pairing consisting of a honed and ground surface are taken into account. For a turned pairing, the orientation is then varied to determine its influence. In the following investigations, the basic and the counter body are made of AISI 1045.

7.6.1 Impact of the machining type

If the two turned surfaces from Figure 5-5 are compared with each other, the markedly greater roughness of turned surface 2 is immediately noticeable. This is also clearly evident from the corresponding roughness parameters in Table 5-4. This topography with an extremely high roughness was specifically selected in the present work in order to clearly show the influence of surface roughness. Regarding the pairing of the honed and ground surface, the ground surface has the smallest roughness. The roughness parameters of the honed surface indicate, that the roughness is slightly greater than that of the turned surface 1. To achieve comparable results, the boundary conditions kept constant. The normal load is 1.0 N and the fluid pressure is 30 MPa.

The result on the influence of different surface topographies on the wear depth is shown in Figure 7-18. The running-in behavior can be observed for the two turned pairings. A running-in can also be seen for the pairing of a honed and ground surface, although not as pronounced as for the two turned pairings. What can be clearly seen, however, is that the topography not only influences the final wear depth after the running-in, but also has a strong influence on the duration of the running-in phase and the wear rate in the steady state phase. Comparing the two turned pairings, it can be observed that a higher surface roughness leads to higher wear in the running-in and the steady state phase and that the duration of the running-in phase is increasing with increasing surface roughness. The pairing of the honed and ground surface has an initial significantly larger real contact area due to the surface properties. As no pronounced roughness peaks are removed here, as in the turned pairings, it becomes clear why the running-in phase is less significant. It can be assumed that the topography before and after the running-in phase is not as different as for the turned pairings.

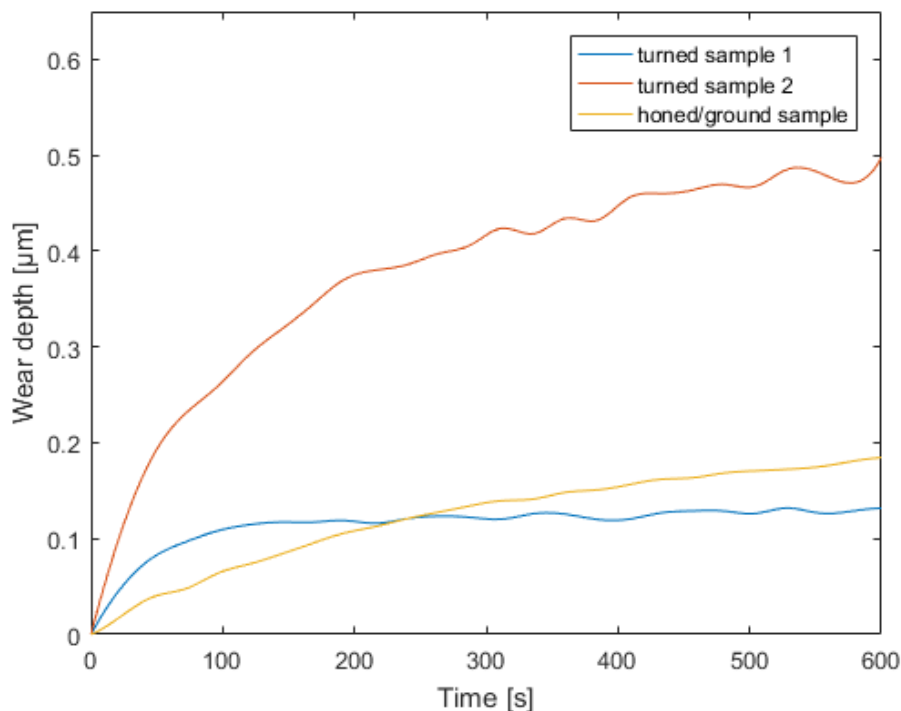


Figure 7-18: Influence of different surface topographies on the wear depth

In order to investigate the described effects more precisely, the contact pressure of the three pairings is taken into account. The mean surface pressures for the three pairings are shown in Figure 7-19.

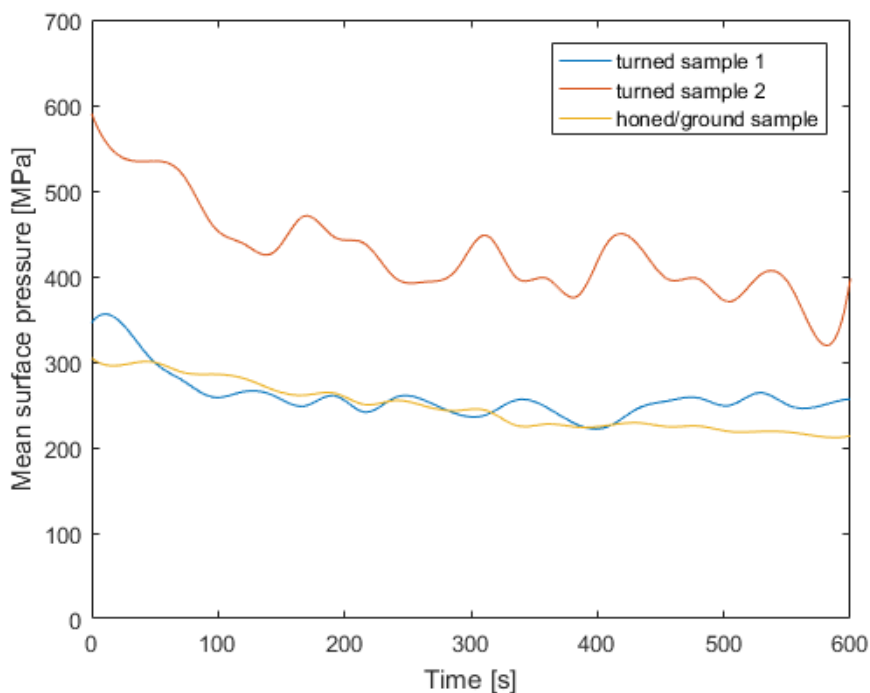


Figure 7-19: Mean surface pressure for the three investigated pairings

As already observed at the wear depth, the running behavior for the two turned pairings can be clearly seen in contact pressure. The higher initial contact pressure for the

turned pairing with the high surface roughness results in a significant higher wear depth during the running-in phase. The significantly longer duration of the running-in period can also be seen in the contact pressure. It takes longer to reach a constant level of contact pressure. The higher contact pressure level after the running-in is responsible for the fact that the wear rate in the steady state phase is also higher than in the rotated pairing with the lower roughness. The statement that the differences in the topography before and after the running-in are less pronounced for the pairing of the honed and ground surface is confirmed by the course of the contact pressure. The change in contact pressure is significantly lower than with the other two turned pairings. A closer look at the wear depth and contact pressure for this pairing reveals that a constant level has not yet been reached. It is therefore assumed that the running-in phase of this pairing is not yet finalized. Finally, the friction behavior of the three different pairings is investigated. The friction coefficient curves are shown in Figure 7-20.

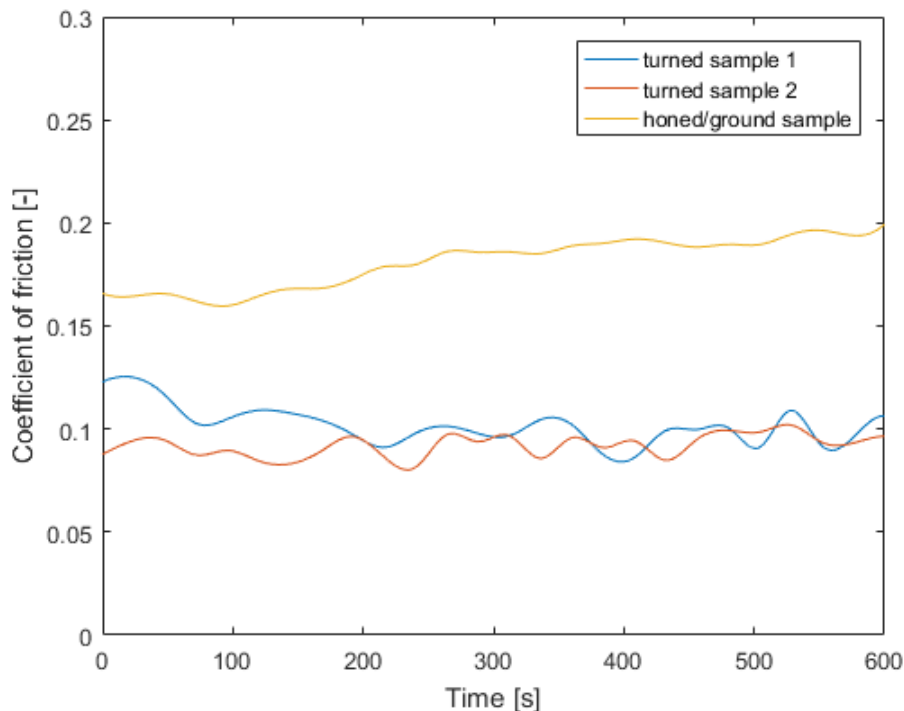


Figure 7-20: Influence of surface topography on coefficient of friction for the three investigated pairings

How it can be seen, high wear does not mean high friction at the same time for the turned pairing with the high surface roughness. Despite maximum wear (compared to Figure 7-18), this pairing has the lowest coefficient of friction. This low coefficient of friction results from the small contact area. In contrast, the pairing of honed and ground surfaces has the highest coefficient of friction, although wear is low. Also here, the real contact area is decisive, which, as described above, is considerably larger for this pairing. It is also noticeable that the coefficient of friction increases. This phenomenon also results from the increasing real contact area.

Finally, it can be summarized that friction and wear do not have to correlate. Low wear does not mean a low coefficient of friction at the same time. A large contact surface is advantageous for low wear. For low friction a small contact surface is advantageous. It is therefore crucial to find a suitable compromise regarding friction and wear. However, it is important to mention that these statements apply only under the model's underlying assumptions and boundary conditions. Further, the transferability to the macroscale has to be investigated in the following work.

7.6.2 Impact of the machining direction

For the turned pairing with less surface roughness, two different orientations are examined regarding friction and wear in the following. The two orientations of the surfaces to each other are shown in Figure 7-21. Both calculations are carried out under constant normal load of 1.0 N and a constant fluid pressure of 30 MPa.

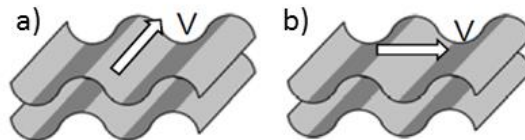


Figure 7-21: Investigated orientations of the two surfaces: **a)** 0° configuration, **b)** 180° configuration

The influence of the surface orientation on the wear depth is shown in Figure 7-22.

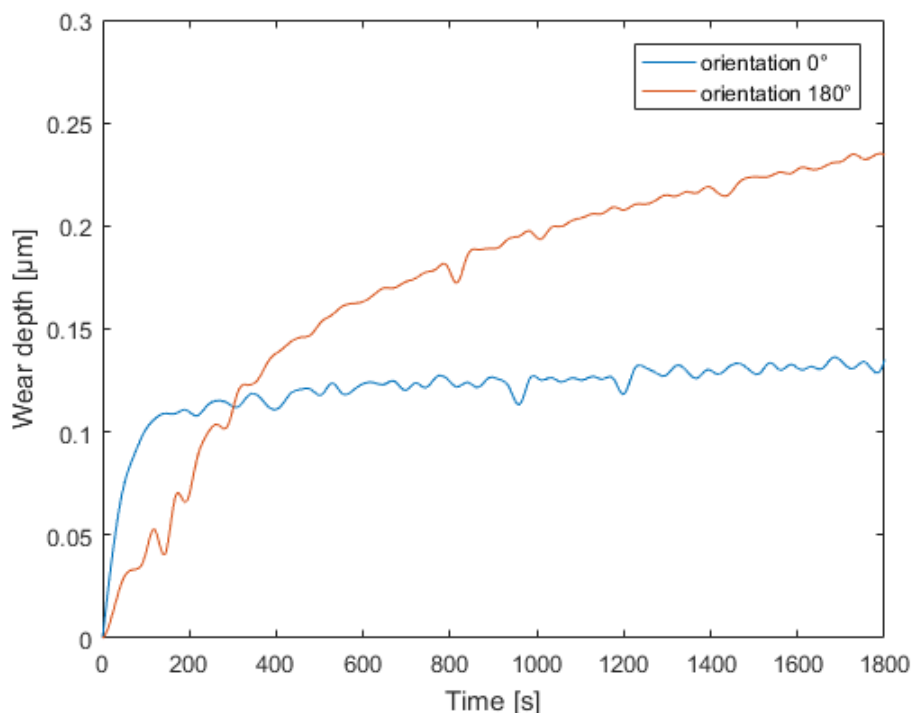


Figure 7-22: Influence of surface orientation on wear depth: 0° orientation (blue curve), 180° orientation (red curve)

It can be seen that the wear depth of the 180° orientation is considerably higher than that of the 0° orientation. In addition to the wear depth after the running-in phase, the running-in period and the wear rate during the steady state phase are also higher. Since there was no clear running-in behavior observed after 600 s, the time was extended to 1800 s. In order to understand these phenomena, the next step is to investigate the mean surface pressure. The two contact pressure curves for the two orientations are shown in Figure 7-23.

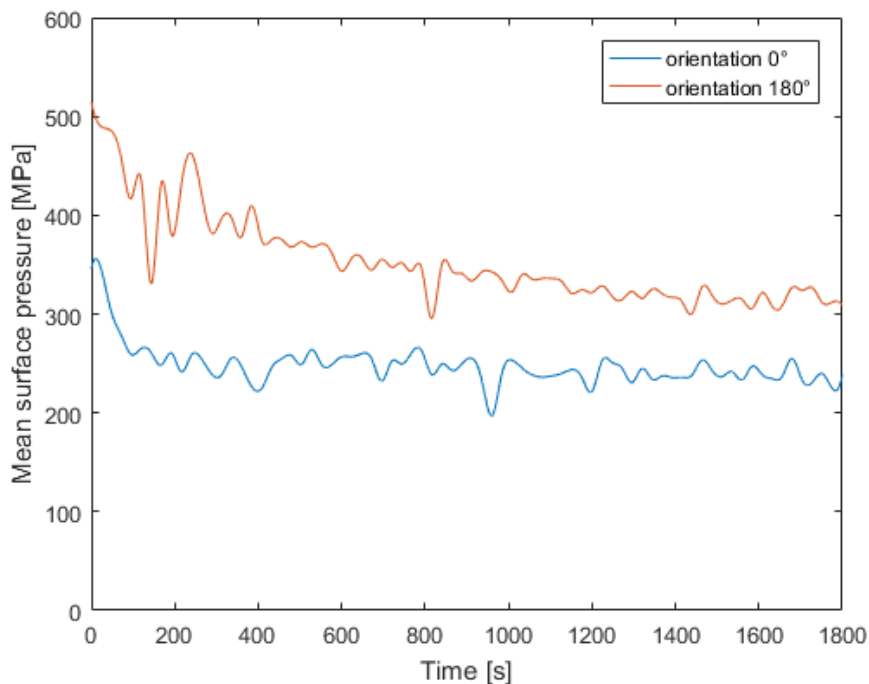


Figure 7-23: Mean surface pressure for the two investigated orientations: 0° orientation (blue curve) and 180° orientation (red curve)

The running-in behavior is visible in both curves of mean contact pressure. For the 180° orientation, the running-in time is visibly longer than for the 0° orientation. This observation corresponds to the result of the wear depth. The higher contact pressure level for the 180° orientation is also clearly visible. This high contact pressure can be attributed to the smaller contact area in comparison to the 0° orientation. This higher contact pressure consequently leads to a higher wear depth.

Figure 7-24 shows the two curves of the coefficient of friction. The friction behavior and the real contact area can be correlated again. For the 180° orientation there is a much lower coefficient of friction. For this orientation, the contact area is also smaller. For the 0° orientation the coefficient of friction is correspondingly higher, which results from the larger real contact surface.

The running-in behavior can also be seen for both curves. As already observed for the wear depth and the mean contact pressure, the running-in time is also longer for the 180° orientation.

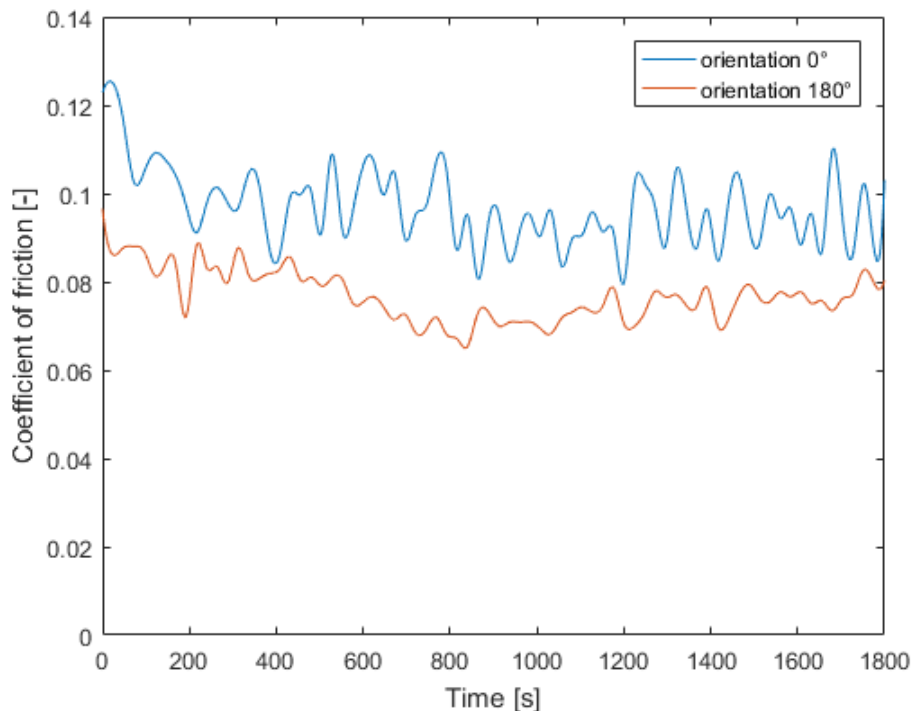


Figure 7-24: Coefficient of friction for the two investigated orientations: 0° orientation (blue curve) and 180° orientation (red curve)

Also in this section it could be shown that high wear does not have to mean a high coefficient of friction at the same time. As shown in section 7.6.1, friction and wear are also counter-rotating when examining the orientation of the basic body and the counter body.

7.7 Influence of residual stresses from metal cutting on friction and wear

As described in section 5.2.5, the friction and wear approach is extended to include residual stresses, which arise during the machining process, for example. By taking residual stresses into account, the microstructural properties of the boundary zones of the basic and counter body can be examined more closely. Three residual stress depth curves are investigated, which were calculated in cutting simulations by wbk – Institute of Production Science (see section 5.2.5). The three curves are shown in Figure 7-25. The residual stresses were determined in sliding direction. The three curves were varied in such way that tensile residual stresses (blue curve), neutral residual stresses (grey curve) and residual compressive stresses (grey curve) are present on the surface.

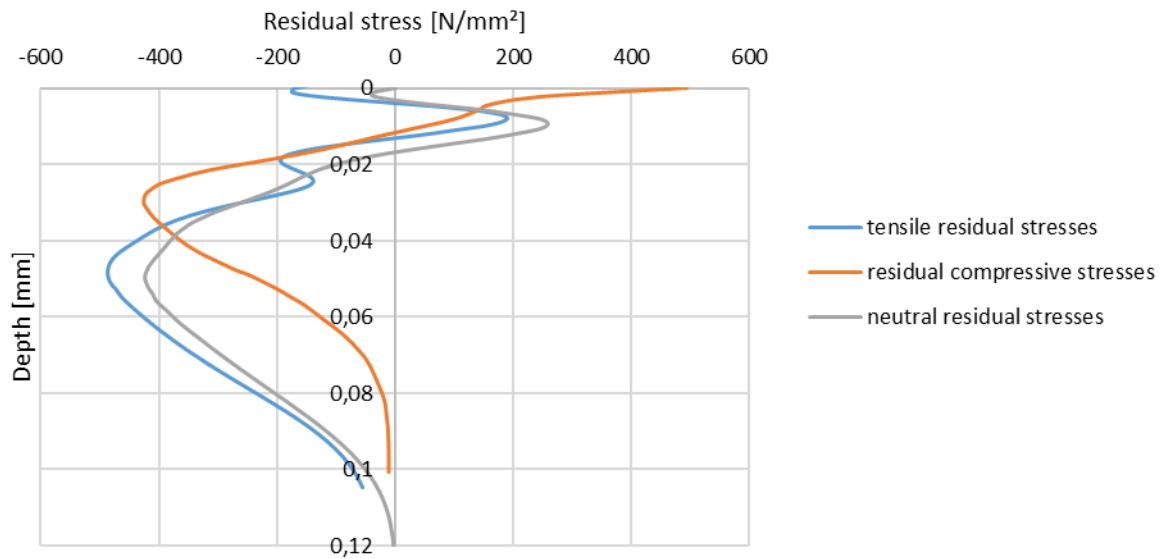


Figure 7-25: Residual stresses from cutting simulation in sliding direction: tensile residual stresses (blue curve), residual compressive stresses (orange curve) and neutral residual stresses (grey curve)

The result of the wear depth calculation for the different residual stress curves is shown in Figure 7-26. As can be seen, there is no clear tendency to identify the influence of residual stresses on the wear behavior. Since residual stresses only affect the solid contact in the present model, it is assumed that the influence in a mixed-lubricated regime is not so significant that a clear trend on wear depth can be observed.

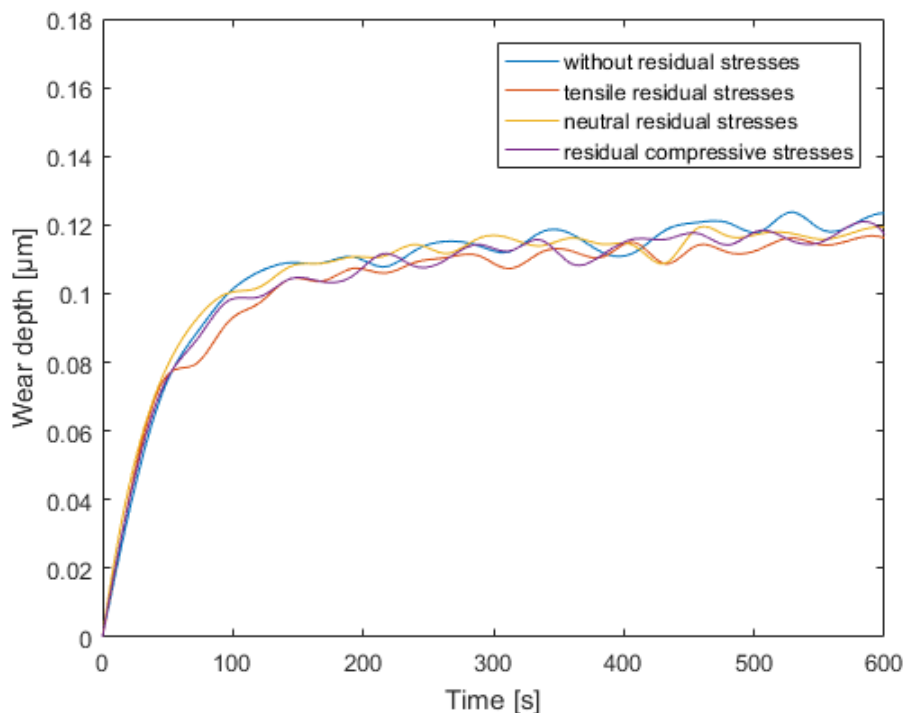


Figure 7-26: Influence of residual stresses on wear depth: without residual stresses (blue curve), tensile residual stresses (red curve), neutral residual stresses (yellow curve) and residual compressive stresses (purple curve)

7.8 Evolution of roughness parameter

For the two turned pairings and the pairing of the honed and ground surface from section 7.6.1, the development of the surface topography is examined in more detail in this section. In addition to the temporal development of statistical roughness parameters (section 2.2.2), the changes in the Abbott-Firestone-Curves (also see section 2.2.2) are investigated. The results on changes in surface topography are intended to provide information about the locations of existing wear. The changes in statistical roughness parameters for the three pairings are shown in Table 7-2. The values of the initial new condition correspond to the beginning of the calculation. The values at the end of the calculations are reported after a time of 600 seconds, when the running-in phase is passed.

Table 7-2: Development of the statistical roughness parameters for the three investigated pairings

Quantity [μm]	turned pairing 1		turned pairing 2		honed/ground pairing	
	initial	worn	initial	worn	initial	worn
R_a	0,2932	0,2815	0,9252	0,9094	0,2715	0,2449
R_q	0,3715	0,3546	1,1598	1,1174	0,3828	0,3402
R_z	2,0178	1,8669	5,0214	4,8392	3,2459	2,5056
R_p	1,5289	1,5280	4,1943	4,2152	2,0683	1,4790
R_v	0,9789	0,9657	2,6948	2,6739	2,4768	2,4367
R_k	0,9287	0,9091	3,0968	3,1163	0,7479	0,7024
R_{pk}	0,0764	0,0263	0,7860	0,7804	0,1176	0,0172
R_{vk}	0,3142	0,324	0,4343	0,4299	0,6299	0,6231

Comparing the statistical roughness parameters R_a , R_q , R_z , R_p , and R_v at the beginning and at the end of the calculation, it can be seen that the values are mainly decreasing. Although individual parameters are not meaningful, in combination with the other parameters a flattening of the surfaces due to sliding wear can be observed. The roughness parameters were determined for the basic body. For the turned pairing 2, the flattening of the surface profile after testing is less pronounced in comparison the other ones.

In order to check whether there is actually a flattening of the surface profile, the Abbott-Firestone-Curves for the three pairings are compared at the beginning and at the end

of the calculation. Figure 7-27 shows the curves for the turned pairing 1. The R_k -lines show, whether the core roughness of the profile has changed. For the turned pairing 2, the result is shown in Figure 7-28 and for the pairing of the honed and ground surface, the change in Abbott-Firestone-Curves is shown in Figure 7-29.

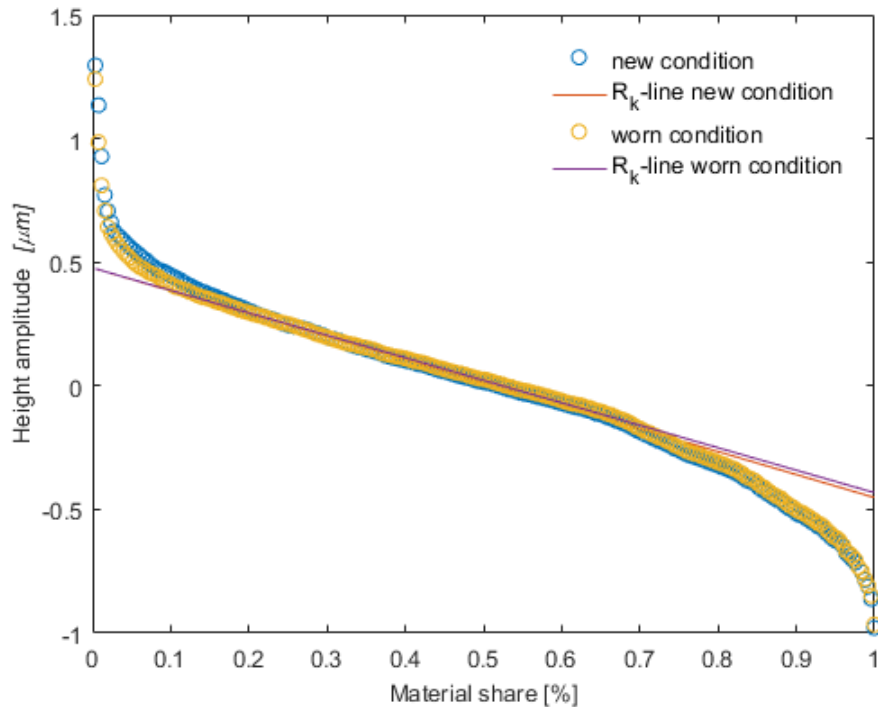


Figure 7-27: Abbott-Firestone-Curves for the turned pairing 1: new condition (blue markers) and worn condition (yellow markers)

Figure 7-27 clearly shows that a change in surface topography occurs only at the roughness asperities in the first 25 % of the material share. For a total amount of 75 % of the material share, the surface profile remains constant. Since the Abbott-Firestone-Curves are identical in this area, this is an indication, that there is no wear in the valleys of the roughness profile. The change in the roughness peaks is also not very pronounced, which is why the R_k value is almost the same. For the turned pairing 2 (see Figure 7-28) a similar behavior could be determined. The changes in roughness profile at the asperities is much more pronounced here. This result correlates with the maximum wear depth for this pairing, shown in Figure 7-18.

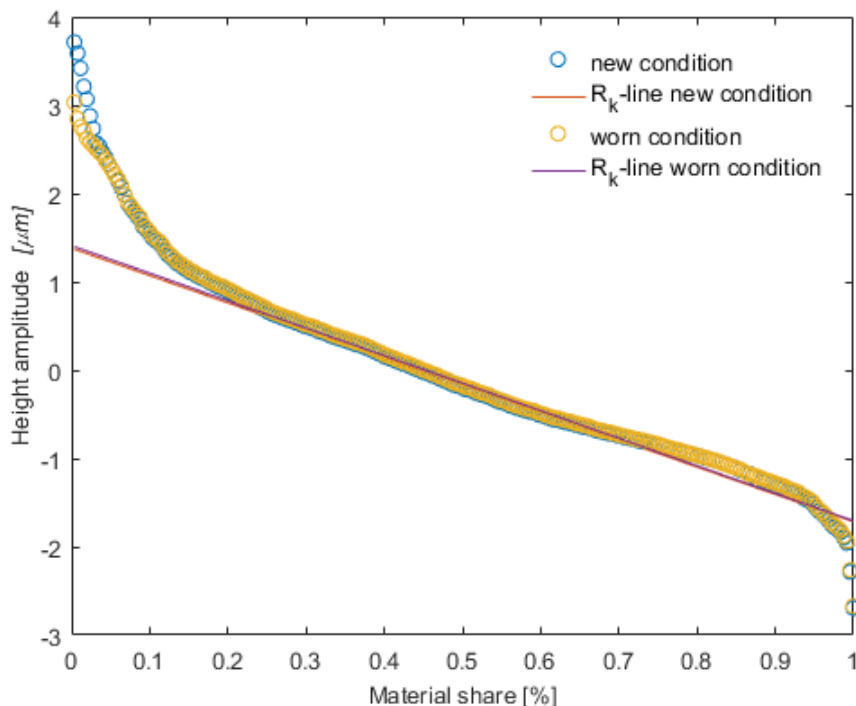


Figure 7-28: Abbott-Firestone-Curves for the turned pairing 2: new condition (blue markers) and worn condition (yellow markers)

However, the proportion of the material share in which a change is present is lower. The larger gradient of the R_k -line (corresponding with the clearly larger R_k value of this pairing in comparison with the other two pairings) indicates a profile with significantly higher roughness peaks. Since only the tips of the roughness asperities are removed, the small amount of material share in which changes are present, seems to be reasonable. The R_{pk} values from Table 7-2 are so similar, since for the calculation method of these parameter, the highest peaks (typically 5 %) are removed. They cannot absorb contact forces during the loading (c.f. section 2.2.2).

In Figure 7-29, the Abbott-Firestone-Curves for the pairing of the honed and ground surface are shown. Here it is also clear that wear occurs only at the roughness peaks. The change in R_k value is also very small, as there is almost no change in core roughness and in the roughness valleys. For the honed surface (corresponding to the basic body of the pairing) the smallest R_k value can be determined. If the R_k value is relatively small compared to the R_z value, a plateau-like character of the surface can be assumed. The smaller the R_k value in this comparison, the more resilient the surface is. The plateau-like character of the honed surface is already evident when examining the coefficient of friction. In Figure 7-20, the highest coefficient of friction for the pairing of the honed and ground surface can be observed. This effect is attributed to the large real contact surface.

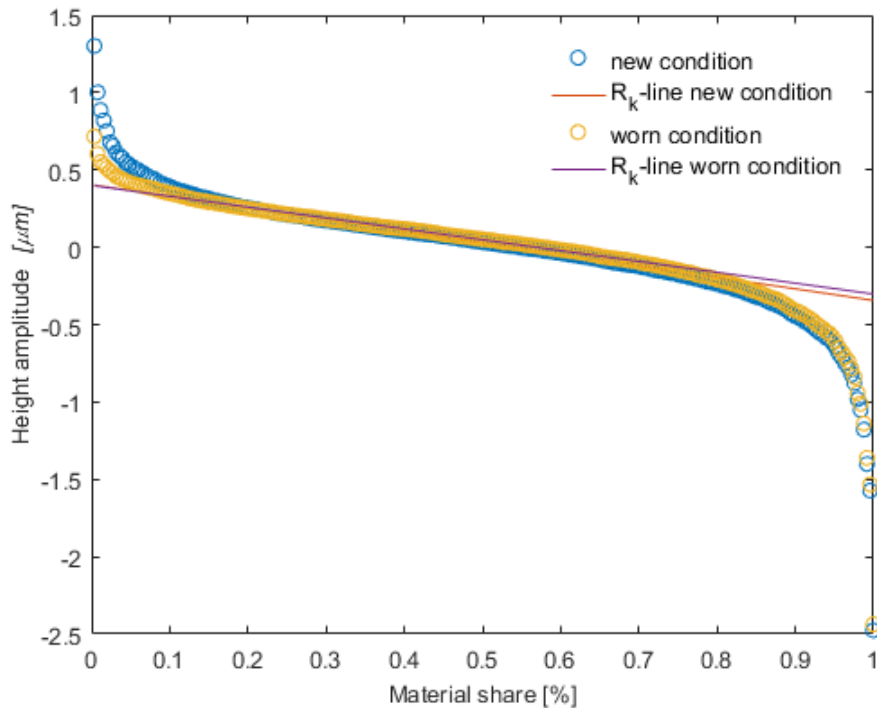


Figure 7-29: Abbott-Firestone-Curves for the pairing of a honed and ground surface: new condition (blue markers) and worn condition (yellow markers)

Experimental results on a journal bearing test bench have also revealed a flattening of the bearing surface. There are five test runs of bearings with a bronze layer (CuPb10Sn10) and a shaft made of 42CrMo4. The normal loading of the experimental setup was 650N, the rotational speed was 400 rpm and the duration was 3 hours. The results of the surface roughness of the plain bearings before and after the test are shown in Figure 7-30.

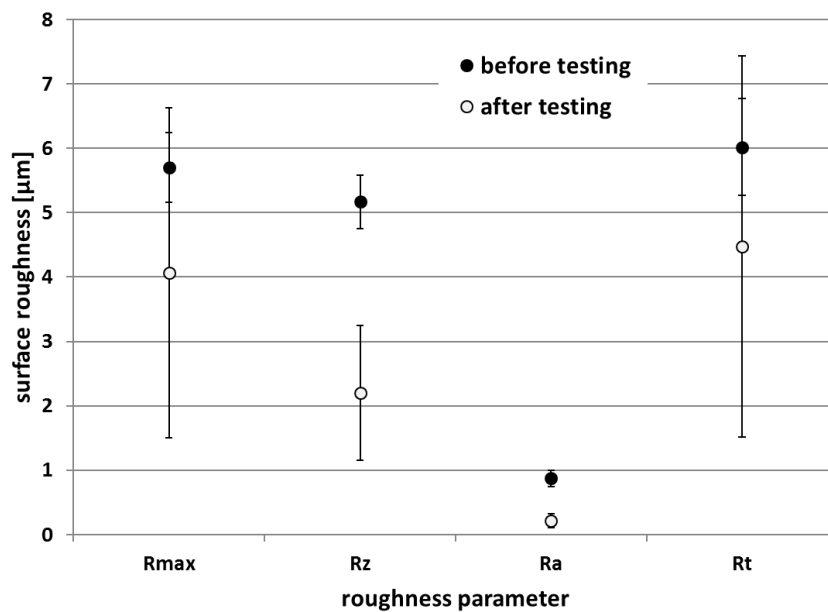


Figure 7-30: Changes in selected roughness parameter for a journal bearing in an experimental setup after a duration of 3 h (Albers & Reichert, 2017)

It can be seen that the surface is also flattened. These results show the same tendency of the numerical results, which have also shown a decrease in roughness parameters by reducing the surface asperities of the bearing due to sliding wear in a mixed-lubricated regime.

8 Conclusion and outlook

Proposed developed method to investigate the influence of surface roughness on friction and wear enables an early validation of surface quality in tribological systems. With this method, a profound understanding of the influence of topography on the friction and wear behavior, especially in the running-in phase, can be created. The product developer can use the existing method and the acquired knowledge to be supported by the specific design of technical surfaces of tribological systems in order to design resource-efficient machine elements with a long lifetime. The great advantage of the numerical model developed here over investigations on physical test benches is that the influence of surface roughness can be investigated without interfering into the contact in contrary to experimental analyses. Although this numerical approach offers this decisive advantage, other tribological phenomena such as the structure and chemistry of the boundary layer are not taken into account.

In order to operationalize the objectives, two research questions were raised and answered in this thesis. The first research question is aimed at the finding out that the finite element method is a suitable tool for the modelling of friction and wear under consideration of real rough surfaces. Based on the finite element method and the preliminary work of Albers and Lorentz (Lorentz, 2013b; Lorentz & Albers, 2013), a friction model was developed which was coupled with the wear law by Archard (see section 5.3). This wear law has been converted into a locally valid approach, whereby the local wear depths can be calculated. The resulting wear is achieved by displacing surface nodes, which enables the modelling of extremely small wear depths of a few nanometers. Furthermore, the approach of node displacement offers the possibility to extrapolate the calculated wear depths and thus to calculate longer periods of time. This scaling is also required to calculate the entire running-in phase. Convergence studies and the validation of the model have shown that the developed approach is suitable for calculating friction and wear under mixed lubricated conditions (see section 6). For this purpose, an experimental test on a nanoindenter (pin on disc) was compared with a simulation with identical surfaces and boundary conditions. The resulting topographies showed a good agreement and the deviations in friction force were less than 5 %. This has shown that the finite element method is a suitable method for modelling friction and wear on real technical surfaces. Due to the good agreement for the dry running model and the relative calculated friction coefficients under mixed-lubricated conditions, it can be assumed that this model is also suitable for mixed friction.

That the derived numerical approach consists of many complex simulation techniques, was shown in Figure 5-14. In order to clearly illustrate the interactions, the different techniques have been integrated into the coupling framework. The second research question therefore aims to find out how the product developer can be supported in using the developed approach. Knowledge of tribology and numerical methods can be assumed, but not knowledge of every single component of the method. Within the scope of this work, a graphical user interface was therefore developed in ABAQUS that supports the product developer in calculating friction and wear. Intuitively, the required input parameters are required in an input mask and the model is created automatically, including the surfaces, material properties and boundary conditions. The wear calculation is also automated. The product developer must then critically check the results for plausibility. The application of the method has thus been made considerably easier.

Based on the developed method, calculations were carried out to identify the most important influencing parameters on friction and wear. The following results could be achieved:

- Under mixed lubricated conditions, fluid viscosity has a low influence on friction and wear, which is why the pressure dependence of the fluid viscosity can be neglected.
- When examining different solid materials, it could be shown that it is very important to consider next to the elastic material behavior the plastic behavior as well. A high young modulus and a high yield strength result in a small real contact area and thus in a low coefficient of friction. The material model for the solids is therefore of highest importance. The more accurate a material model is, the more accurate the results of the simulation can be.
- Increasing fluid pressure or a lower normal load leads to a lower coefficient of friction and less wear. The individual load-bearing components due to solid and fluid contact could be used as an explanation for this.
- It could be shown that the running-in procedure has a huge influence on the wear behavior. If a final load is applied abruptly, the resulting wear depth is much lower than with a gradual increase of the normal load to the same level. For this reason, it can be concluded that a severe running-in procedure is better for a tribological system under the underlying assumptions of the model, such as a mild running-in.
- Investigations of differently manufactured surfaces have shown that surfaces with greater roughness cause higher wear, but due to smaller real contact area, smaller coefficient of frictions are achieved.

- In addition to the different surfaces, also the orientation was examined. It could be shown that the alignment of the surfaces has a great influence on wear. For the investigated pairing, the wear depth varied by a factor of 2.5.
- Changes in topography over time have shown that wear occurs mainly at the roughness peaks. The roughness valleys remain almost unchanged. This phenomenon could be shown both by statistical roughness parameter and by Abbott-Firestone-Curves and further in experimental investigations on a journal bearing test bench.

The research topic discussed here offers further potential what should be investigated in future work. The wear coefficient, which is included into the wear calculation, has so to be determined experimentally. In order to decouple the calculation method from complex experiments, methods must be derived that allow the numerical calculation of these wear coefficients. Preliminary investigations of Reichert, Lorentz, Heldmaier et al. (2016) have therefore to be continued.

Another point to be investigated is the consideration of thermal behavior. Temperature has already been implemented in the mixed lubrication model (Albers, Reichert, Lorentz, Knoll & Lang, 2015; Lorentz, 2013b), but since target values like the local wear depth are scaled in the wear model, there is no suitable scaling approach for the temperature available. This should be developed in future work, as the temperature has a huge influence on the mechanical properties and thus on friction and wear.

Previous investigations are limited to metallic materials, as there is sufficient material data available. With regard to the transferability of the method to clutches and brakes, the development of material models for inhomogeneous organic materials is recommended.

9 References

- Abaqus Analysis User's Guide 2016. (2015). Retrieved from <http://50.16.225.63/v2016/books/usb/default.htm>
- Albers, A., Behrendt, M., & Ott, S. (2006). Systemtribometer zur Untersuchung hochbelasteter nasslaufender Friktionskontakte unter mehrachsigen Gleitbewegungen. *Reibung, Schmierung Und Verschleiß. Forschung Und Praktische Anwendungen, 47. Tribologie-Fachtagung, 25. Bis 27. September 2006 in Göttingen.*
- Albers, A., Blust, M., Lorentz, B., & Burger, W. (2014). A New Tribological Test Bench for Lightweight Hydraulic Components. *Proceedings TAE – 19th International Colloquium Tribology – Industrial and Automotive Lubrication.*
- Albers, A., Dickerhof, M., & Burger, W. (2008). Condition-Monitoring Based on Structure-borne Ultrasound Analysis. *Proceedings of the ASME International Design Engineering Technical Conferences and Computers and Information in Engineering Conference - 32nd Annual Mechanisms and Robotics Conference (MR), 2008.*
- Albers, A., & Lorentz, B. (2010). An Approach to Investigate Mixed lubricated Systems in the Micro Scale by Means of the Coupled-Eulerian-Lagrangian Method. *ASME 2010 International Mechanical Engineering Congress and Exposition. (9), 553–561.*
- Albers, A., & Lorentz, B. (2012a). A Numerical Method for Investigating Mixed Lubrication Phenomena. *Tools and Methods of Competitive Engineering: Proceedings of the Ninth International Symposium on Tools and Methods of Competitive Engineering (TMCE 2012), 357–368.*
- Albers, A., Matros, K., Behrendt, M., & Jetzinger, H. (2015). Das Pull-Prinzip der Validierung - Ein Referenzmodell zur effizienten Integration von Validierungsaktivitäten in den Produktentstehungsprozess. *Konstruktion, 67(6), 74–81.*
- Albers, A., & Meboldt, M. (2007). IPEMM - Integrated product development process management model, based on systems engineering and systematic problem solving. *Proceedings of ICED 2007, the 16th International Conference on Engineering Design. (42), 611–612.*
- Albers, A., Nguyen, H. T., & Burger, W. (2012). Energy-efficient hydrodynamic journal bearings by means of condition monitoring and lubrication flow control. *International Journal of Condition Monitoring, 2(1), 18–21.*
<https://doi.org/10.1784/204764212800028860>

- Albers, A., Nowicki, L., & Enkler, H.-G. (2006). Development of a method for the analysis of mixed friction problems. *International Journal of Applied Mechanics and Engineering*, 11(3), 479–490.
- Albers, A., Rapp, S., Spadinger, M., Richter, T., Birk, C., Marthaler, M., Heimike, J., Kurtz, V., Wessels, H. (2019) Das Referenzsystem im Modell der PGE – Produktgenerationsentwicklung: Vorschlag einer generalisierten Beschreibung von Referenzprodukten und ihrer Wechselbeziehungen. *KIT Scientific Working Papers* 96.
- Albers, A., & Reichert, S. (2017). On the influence of surface roughness on the wear behavior in the running-in phase in mixed-lubricated contacts with the finite element method. *Wear*, 376-377, 1185–1193.
<https://doi.org/10.1016/j.wear.2017.01.035>
- Albers, A., Reichert, S., & Joerger, A. (2017). Investigation of roughness parameters of real rough surfaces due to sliding wear under mixed-lubricated conditions with the finite-element-method. *World Tribology Congress 2017*.
- Albers, A., Reichert, S., Lorentz, B., Knoll, G., & Lang, J. (2015). Untersuchung des Reibungsverhaltens von geschmierten Kontakten unter Berücksichtigung verschiedener Gleitbedingungen mit Hilfe der Finiten-Elemente-Methode. *GFT Tribologie-Fachtagung*, 7/1-7/11.
- Albers, A., Reichert, S., Serf, M., Thorén, S., & Bursac, N. (2017). Kopplung von CAE-Methoden zur Unterstützung des Produktentwicklers. *Konstruktion*, 69(9), 76–82.
- Albers, A., Savio, D., & Lorentz, B. (2010). A model to investigate the influence of surface roughness on the tribological behavior of dry friction systems. *GFT Tribologie-Fachtagung*.
- Albers, A. (2010). Five Hypotheses about Engineering Processes and their Consequences. *Proceedings of the TMCE 2010*.
- Albers, A., Behrendt, M., Klingler, S., & Matros, K. (2016). Verifikation und Validierung im Produktentstehungsprozess. In U. Lindemann (Ed.), *Handbuch Produktentwicklung* (pp. 541–569). München: Hanser.
- Albers, A., Behrendt, M., Klingler, S., Reiß, N., & Bursac, N. (2017). Agile product engineering through continuous validation in PGE – Product Generation Engineering. *Design Science*, 3, 16. <https://doi.org/10.1017/dsj.2017.5>
- Albers, A., Bernhardt, J., & Ott, S. (2010). Development and Validation of Lubricated Multi-Disk Clutch Systems with Advanced Ceramics. In D. Singh, J. A. Salem, S. Mathur, & T. Ohji (Eds.), *Ceramic Engineering and Science Proceedings: v. 31, issue 2. Mechanical properties and performance of engineering ceramics and composites V: A collection of papers presented at the 34th International Conference on Advanced Ceramics and Composites, January 24-29, 2010, Dayton Beach, Florida* (pp. 309–315). Hoboken, N.J, Chichester: Wiley.
<https://doi.org/10.1002/9780470944127.ch29>

- Albers, A., & Braun, A. (2011a). Der Prozess der Produktentstehung. In F. Henning & E. Moeller (Eds.), *Handbuch Leichtbau: Methoden, Werkstoffe, Fertigung* (pp. 3–30). München: Hanser.
- Albers, A., & Braun, A. (2011b). A generalised framework to compass and to support complex product engineering processes. *International Journal of Product Development*, 15(1/2/3), 6. <https://doi.org/10.1504/IJPD.2011.043659>
- Albers, A., Bursac, N., & Rapp, S. (2017). PGE – Produktgenerationsentwicklung am Beispiel des Zweimassenschwungrads. *Forschung Im Ingenieurwesen*, 81(1), 13–31. <https://doi.org/10.1007/s10010-016-0210-0>
- Albers, A., Bursac, N., Urbanec, J., & Rachenkova, G. (2014). Knowledge management in product generation development - An empirical study. In D. Krause (Ed.), *Design for X: Beiträge zum 25. DfX-Symposium, Oktober 2014* (pp. 13–24). Hamburg: TuTech-Verl.
- Albers, A., Bursac, N., & Wintergerst, E. (2015). Product Generation Development - Importance and Challenges from a Design Research Perspective. In N. E. Mastorakis, S. To, & Cho W. (Eds.), *Recent advances in mechanical engineering series: Vol. 13. New developments in mechanics and mechanical engineering: Proceedings of the International Conference on Mechanical Engineering (ME 2015), Proceedings of the International Conference on Theoretical Mechanics and Applied Mechanics (TMAM 2015) Vienna, Austria, March, 15-17, 2015* (pp. 16–21).
- Albers, A., Enkler, H. G., & Ottnad, J. (2011). Managing complex simulation processes: The generalised contact and channel model. *International Journal of Product Development*, 13(3), 204. <https://doi.org/10.1504/IJPD.2011.040267>
- Albers, A., Gladysz, B., Kniel, J., Aschoff, M., & Meyer, A. (2016). Integration von Versuchsergebnissen in C&C²-Modellen zur Wiederverwendung in der Produktgenerationsentwicklung am Beispiel eines trockenlaufenden Kupplungssystems. In K. Brökel, J. Feldhusen, K.-H. Grote, F. Rieg, R. Stelzer, P. Köhler, . . . G. Scharr (Eds.), *Berichte aus der Konstruktionstechnik. 14. Gemeinsames Kolloquium Konstruktionstechnik 2016: Traditio et Innovatio - Entwicklung und Konstruktion, am 6. und 7. Oktober 2016 in Rostock ; Klaus Brökel, Jörg Feldhusen, Karl-Heinrich Grote, Frank Rieg, Ralph Stelzer, Peter Köhler, Norbert Müller, Gerhard Scharr (Hrsg.) ; Vorwort Klaus Brökel* (pp. 10–20). Aachen: Shaker Verlag.
- Albers, A., & Lorentz, B. (2012b). A numerical way for investigating the impact of surface roughness on mixed lubrication friction.
- Albers, A., Matthiesen, S., Bursac, N., Moeser, G., & Luedcke, R. (2015). Abstraktionsgrade der Systemmodellierung-von der Sprache zur Anwendung. In M. Maurer, S.-O. Schulze, & J. Abulawi (Eds.), *Tag des Systems Engineering: Bremen, 12. - 14. November 2014; [TdSE]* (pp. 183–192). München: Hanser.

- Albers, A., Reiss, N., Bursac, N., & Breitschuh, J. (2016). 15 Years of SPALTEN Problem Solving Methodology in Product Development. In C. Boks (Ed.), *Proceedings of NordDesign 2016: August 10-12, 2016, Trondheim, Norway* (pp. 411–420). Bristol, United Kingdom: The Design Society.
- Albers, A., Reiss, N., Bursac, N., & Richter, T. (2016). iPeM – Integrated Product Engineering Model in Context of Product Generation Engineering. *Procedia CIRP*, 50, 100–105. <https://doi.org/10.1016/j.procir.2016.04.168>
- Albers, A., & Wintergerst, E. (2014). The Contact and Channel Approach (C&C²-A) – relating a system’s physical structure to its functionality. In A. Chakrabarti (Ed.), *An anthology of theories and models of design: Philosophy, approaches and empirical explorations* (pp. 151–172). London u.a.: Springer.
- Ali, M. (2013). Computational and Theoretical Contact Computational and theoretical contact modelling of hip implant devices with the application of wear simulations. *PhD thesis, University of Warwick*.
- Almqvist, A., Fabricius, J., Spencer, A., & Wall, P. (2011). Similarities and Differences Between the Flow Factor Method by Patir and Cheng and Homogenization. *Journal of Tribology*, 133(3), 31702. <https://doi.org/10.1115/1.4004078>
- Andersson, S., Söderberg, A., & Björklund, S. (2007). Friction models for sliding dry, boundary and mixed lubricated contacts. *Tribology International*, 40(4), 580–587. <https://doi.org/10.1016/j.triboint.2005.11.014>
- Andreasen, M. M. (1994). Modelling—The Language of the Designer. *Journal of Engineering Design*, 5(2), 103–115. <https://doi.org/10.1080/09544829408907876>
- Ansys, I. (2016). *System Coupling User’s Guide - Release 17.2*.
- Archard, J. F. (1953). Contact and Rubbing of Flat Surfaces. *Journal of Applied Physics*, 24(8), 981–988. <https://doi.org/10.1063/1.1721448>
- Argatov, I. I., & Fadin, Y. A. (2011). A Macro-scale Approximation for the Running-in Period. *Tribology Letters*, 42(3), 311–317. <https://doi.org/10.1007/s11249-011-9775-9>
- Bakar, A. R. A., Li, L., James, S., & Ouyang, H. *Wear Simulation and Its Effect on Contact Pressure Distribution and Squeal of a Disc Brake*.
- Bakolas, V. (2003). Numerical generation of arbitrarily oriented non-Gaussian three-dimensional rough surfaces. *Wear*, 254(5-6), 546–554. [https://doi.org/10.1016/S0043-1648\(03\)00133-9](https://doi.org/10.1016/S0043-1648(03)00133-9)
- Barrio, R., Rodríguez, M., Abad, A., & Blesa, F. (2011). Breaking the limits: The Taylor series method. *Applied Mathematics and Computation*, 217(20), 7940–7954. <https://doi.org/10.1016/j.amc.2011.02.080>
- Bartel, D., Bobach, L., Illner, T., & Deters, L. (2011). Simulation des Langzeitverhaltens von mischreibungsbeanspruchten Radialgleitlagern. *GFT Tribologie Tagung Göttingen*.

- Bartel, D. (2010). *Simulation von Tribosystemen: Grundlagen und Anwendungen*. Wiesbaden: Vieweg+Teubner Verlag / GWV Fachverlage GmbH Wiesbaden. Retrieved from <http://dx.doi.org/10.1007/978-3-8348-9656-8>
- Bernhardt, J., Albers, A., & Ott, S. (2013). Advanced ceramics as friction material in lubricated clutch systems. *Tribology International*, 59, 267–272. <https://doi.org/10.1016/j.triboint.2012.08.002>
- Bhattacharya, S. (2011). *Predictive Finite Element Modeling of Artificial Cervical Discs in a Ligamentous Functional Spinal Unit*. Dissertation. Ohio.
- Bhushan, B. (2002). *Introduction to tribology*. New York, NY: Wiley.
- Bielsa, J. M., Canales, M., Martínez, F. J., & Jiménez, M. A. (2010). Application of finite element simulations for data reduction of experimental friction tests on rubber–metal contacts. *Tribology International*, 43(4), 785–795. <https://doi.org/10.1016/j.triboint.2009.11.005>
- Bowden, F. P., & Tabor, D. (2001). *The friction and lubrication of solids* (1st ed.): Oxford University Press.
- Braun, A. (2013). „Modellbasierte Unterstützung der Produktentwicklung - Potentiale der Modellierung von Produktentstehungsprozessen am Beispiel des integrierten Produktentstehungsmodells (iPeM)“. In *IPEK – Forschungsberichte published by A. Albers vol. 72. Dissertation*. Karlsruhe Institute of Technology (KIT): IPEK – Institute of Product Engineering. ISSN: 1615-8113
- Browning, T. R., Fricke, E., & Negele, H. (2006). Key concepts in modeling product development processes. *Systems Engineering*, 9(2), 104–128. <https://doi.org/10.1002/sys.20047>
- Bucher, F., Dmitriev, A. I., Ertz, M., Knothe, K., Popov, V. L., Psakhie, S. G., & Shilko, E. V. (2006). Multiscale simulation of dry friction in wheel/rail contact. *Wear*, 261(7-8), 874–884. <https://doi.org/10.1016/j.wear.2006.01.046>
- Bursac, N. (2016). „Model Based Systems Engineering zur Unterstützung der Baukastenentwicklung im Kontext der Frühen Phase der Produktgenerationsentwicklung“. In *IPEK – Forschungsberichte published by A. Albers vol. 93. Dissertation*. Karlsruhe Institute of Technology (KIT): IPEK – Institute of Product Engineering. ISSN: 1615-8113
- Chang, L. (1995). Deterministic modeling and numerical simulation of lubrication between rough surfaces—a review of recent developments. *Wear*, 184(2), 155–160. [https://doi.org/10.1016/0043-1648\(94\)06570-5](https://doi.org/10.1016/0043-1648(94)06570-5)
- Chmiel, A. (2008). *Finite Element Simulation Methods for Dry Sliding Wear. Master Thesis at Air Force Institute of Technology. Wright-Patterson Air Force Base, Ohio*
- Cooper, R. G. (1994). Third-Generation New Product Processes. *Journal of Product Innovation Management*, 11(1), 3–14. <https://doi.org/10.1111/1540-5885.1110003>
- Czichos, H. (1971). Festkörperreibung - Teilgebiet der Tribologie. *Umschau in Wissenschaft Und Technik*, 71(4), 116–120.

- Czichos, H., & Habig, K.-H. (Eds.). (2015). *Tribologie-Handbuch: Tribometrie, Tribomaterialien, Tribotechnik* (4., vollst. überarb. u. erw. Aufl. 2015). Wiesbaden: Springer Fachmedien Wiesbaden. Retrieved from <http://dx.doi.org/10.1007/978-3-8348-2236-9>
- Deters, L., Fischer, A., Santer, E., & Stolz, U. (2002). GfT Arbeitsblatt 7 - Tribologie: Verschleiß, Reibung - Definitionen, Begriffe, Prüfung, 1–50.
- Dickerhof, M. (2011). „*Potentiale der Schallemissionsanalyse zur Überwachung und Diagnose tribologischer Systeme*“. In *IPEK – Forschungsberichte published by A. Albers vol. 49. Dissertation*. Karlsruhe Institute of Technology (KIT): IPEK – Institute of Product Engineering. ISSN: 1615-8113
- DIN Deutsches Institut für Normung e. V., DIN German Institute for Standardization (1977). *Reibung in Lagerungen; Begriffe, Arten, Zustände, physikalische Größen*. (DIN, 50281). Berlin: Beuth Verlag GmbH.
- Dmitriev, A. I., Österle, W., & Kloß, H. (2008). Numerical simulation of typical contact situations of brake friction materials. *Tribology International*, 41(1), 1–8. <https://doi.org/10.1016/j.triboint.2007.04.001>
- DoITPoMS - TLP Library The Stiffness of Rubber - Lennard-Jones potential. Retrieved from <https://www.doitpoms.ac.uk/tlplib/stiffness-of-rubber/lennard-jones.php>. [06.04.2019].
- Donatellis, M., Gelosa, E., Sangalli, R., Spinelli, M., & Vitali, R. (2009). *Virtual Treaded Tire Simulation as a Design Predictive Tool: Application to Tire Hydroplaning*. Retrieved from http://www.simulia.com/forms/world/pdf2009/Donatellis_SCC2009.pdf
- Donea, J., & Huerta, A. (2003). *Finite Element Methods for Flow Problems*. Chichester, UK: John Wiley & Sons, Ltd.
- Dowson, D., & Taylor, C. M. (1979). Cavitation in Bearings. *Annual Review of Fluid Mechanics*, 11(1), 35–65. <https://doi.org/10.1146/annurev.fl.11.010179.000343>
- Drescher, H. (1959). Die Mechanik der Reibung zwischen festen Körpern. *VDI-Z.* (101), 697–707.
- Durrant, D. R. (1991). The Third-Order Adams-Bashforth Method: An Attractive Alternative to Leapfrog Time Differencing. *Monthly Weather Review*, 119(3), 702–720. [https://doi.org/10.1175/1520-0493\(1991\)119<0702:TTOABM>2.0.CO;2](https://doi.org/10.1175/1520-0493(1991)119<0702:TTOABM>2.0.CO;2)
- Effendi, J. (1987). Die numerische Lösung der elasto-hydrodynamischen Kontaktprobleme unter Berücksichtigung der Oberflächenrauheiten: Lehrstuhl und Institut für Maschinenelemente und Maschinengestaltung. *PhD Thesis RWTH Aachen University*.
- Europäisches Komitee für Normung (1996a). *DIN EN ISO 12085 - Geometrische Produktspezifikationen (GPS) Oberflächenbeschaffenheit: Tastschnittverfahren Motifkenngrößen*. (DIN EN ISO, 12085). Berlin: Beuth Verlag GmbH.

- Europäisches Komitee für Normung (1996b). *DIN EN ISO 3274 - Oberflächenbeschaffenheit: Tastschnittverfahren Nenneigenschaften von Tastschnittgeräten*. (DIN EN ISO, 3274). Berlin: Beuth Verlag GmbH.
- Europäisches Komitee für Normung (1998, January 26). *DIN EN ISO 4287 - Geometrische Produktspezifikation (GPS) — Oberflächenbeschaffenheit: Tastschnittverfahren — Benennungen, Definitionen und Kenngrößen der Oberflächenbeschaffenheit*. (DIN EN ISO, 4287). Berlin: Beuth Verlag GmbH.
- Ferziger, J. H., & Perić, M. (2008). *Numerische Strömungsmechanik*. Berlin, Heidelberg: Springer.
- Gao, H., Barber, G. C., & Shillor, M. (2002). Numerical Simulation of Engagement of a Wet Clutch with Skewed Surface Roughness. *Journal of Tribology*, 124, 305–312.
- García de Jalón, J., & Bayo, E. (1994). *Kinematic and Dynamic Simulation of Multibody Systems: The Real-Time Challenge. Mechanical Engineering Series*. New York, NY: Springer. Retrieved from <http://dx.doi.org/10.1007/978-1-4612-2600-0>
- Gausemeier, J., Hahn, A., Kespohl, H.-D., & Seifert, L. (2006). *Vernetzte Produktentwicklung: Der erfolgreiche Weg zum Global Engineering Networking*. München, Wien: Hanser.
- Green, A. P. (1954). The plastic yielding of metal junctions due to combined shear and pressure. *Journal of the Mechanics and Physics of Solids*, 2(3), 197–211. [https://doi.org/10.1016/0022-5096\(54\)90025-3](https://doi.org/10.1016/0022-5096(54)90025-3)
- Greenwood, J. A., Minshall, H., & Tabor, D. (1961). Hysteresis Losses in Rolling and Sliding Friction. *Proceedings of the Royal Society a: Mathematical, Physical and Engineering Sciences*, 259(1299), 480–507. <https://doi.org/10.1098/rspa.1961.0004>
- Greenwood, J. A., & Williamson, J. B. P. (1966). Contact of nominally flat surfaces. *GREENWOOD, J. a.; WILLIAMSON, J. B. P. Contact of Nominally Flat Surfaces. in: Proceedings of the Royal Society of London a: Mathematical, Physical and Engineering Sciences*, 300–319.
- Hegadekatte, V., Kurzenhäuser, S., Huber, N., & Kraft, O. (2008). A predictive modeling scheme for wear in tribometers. *Tribology International*, 41(11), 1020–1031. <https://doi.org/10.1016/j.triboint.2008.02.020>
- Heilmann, P., & Rigney, D. A. (1981). An energy-based model of friction and its application to coated systems. *Wear*, 72(2), 195–217. [https://doi.org/10.1016/0043-1648\(81\)90367-7](https://doi.org/10.1016/0043-1648(81)90367-7)
- Hu, Y.-Z., & zhu, D. (2000). A Full Numerical Solution to the Mixed Lubrication in Point Contacts. *Journal of Tribology*. (1221), 1.

- Ismail, R., Tauviqirrahman, M., Saputra, E., Jamari, J., & Schipper, D. J. (2013). Modeling of Repeated Rolling Contact of Rigid Ball on Rough Surface: Residual Stress and Plastic Strain Analysis. *Procedia Engineering*, 68, 593–599. <https://doi.org/10.1016/j.proeng.2013.12.226>
- Jackson, R. L., & Green, I. (2008). The Thermoelastic Behavior of Thrust Washer Bearings Considering Mixed Lubrication, Asperity Contact, and Thermoviscous Effects. *Tribology Transactions*, 51(1), 19–32. <https://doi.org/10.1080/10402000701739271>
- Jackson, R. L., & Streater, J. L. (2006). A multi-scale model for contact between rough surfaces. *Wear*, 261(11-12), 1337–1347. <https://doi.org/10.1016/j.wear.2006.03.015>
- Johnson, G. R., & Cook, W. H. (1985). Fracture characteristics of three metals subjected to various strains, strain rates, temperatures and pressures. *Engineering Fracture Mechanics*, 21(1), 31–48. [https://doi.org/10.1016/0013-7944\(85\)90052-9](https://doi.org/10.1016/0013-7944(85)90052-9)
- Khader, I., Kürten, D., & Kailer, A. (2012). A study on the wear of silicon nitride in rolling–sliding contact. *Wear*, 296(1-2), 630–637. <https://doi.org/10.1016/j.wear.2012.08.010>
- Knoll, G., Boucke, A., Winijst, A., Stapelmann, A., & Auerbach, P. (2016). Reduction of Friction Losses in Journal Bearings of Valve Train Shaft by Application of Running-in Profile. *Tribologie und Schmierungstechnik Heft 4*, 17–21.
- Knoll, G., Schlerege, F., Brandt, S., Busche, E., & Longo, C. (2007). Kolbenringreibung (Simulationstechniken zur Berechnung der Reibungsverluste von Kolbenringen bei Mischreibung und hydrodynamischer Schmierfilmbildung). *GFT Tribologie-Fachtagung Göttingen*.
- Kogut, L., & Etsion, I. (2004). A static friction model for elastic-plastic contacting rough surfaces. *Journal of Tribology*, 126.1, 34–40.
- Krupka, I., Sperka, P., & Hartl, M. (2016). Effect of surface roughness on lubricant film breakdown and transition from EHL to mixed lubrication. *Tribology International*, 100, 116–125. <https://doi.org/10.1016/j.triboint.2015.12.008>
- Kubiak, K. J., & Mathia, T. G. (2009). Influence of roughness on contact interface in fretting under dry and boundary lubricated sliding regimes. *Wear*, 267(1-4), 315–321. <https://doi.org/10.1016/j.wear.2009.02.011>
- Larsson, R. (2009). Modelling the effect of surface roughness on lubrication in all regimes. *Tribology International*, 42(4), 512–516. <https://doi.org/10.1016/j.triboint.2008.07.007>
- Laurien, E., & Oertel, H. (2013). *Numerische Strömungsmechanik: Grundgleichungen und Modelle - Lösungsmethoden - Qualität und Genauigkeit; mit über 530 Wiederholungs- und Verständnisfragen* (5., überarb. und erw. Aufl.). *Lehrbuch*. Wiesbaden: Springer Vieweg.

- Le, H. R., Sutcliffe, M. P. F., & Williams, J. A. (2005). Friction and material transfer in micro-scale sliding contact between aluminium alloy and steel. *Tribology Letters*, 18(1), 99–104. <https://doi.org/10.1007/s11249-004-1762-y>
- Lecheler, S. (2009). *Numerische Strömungsberechnung: Schneller Einstieg durch ausführliche praxisrelevante Beispiele* (1. Aufl.). Studium. Wiesbaden: Vieweg + Teubner.
- Leu, D.-K. (2009). A simple dry friction model for metal forming process. *Journal of Materials Processing Technology*, 209(5), 2361–2368. <https://doi.org/10.1016/j.jmatprotec.2008.05.027>
- Linsler, D., Schlarb, T., Weingärtner, T., & Scherge, M. (2015). Influence of subsurface microstructure on the running-in of an AISi alloy. *20th International Conference on Wear of Materials*, 332–333, 926–931. <https://doi.org/10.1016/j.wear.2015.02.044>
- Linsler, D., Schröckert, F., & Scherge, M. (2016). Influence of subsurface plastic deformation on the running-in behavior of a hypoeutectic AISi alloy. *Tribology International*, 100, 224–230. <https://doi.org/10.1016/j.triboint.2016.01.033>
- Lorentz, B., & Albers, A. (2013). A numerical model for mixed lubrication taking into account surface topography, tangential adhesion effects and plastic deformations. *Tribology International*, 59, 259–266. <https://doi.org/10.1016/j.triboint.2012.08.023>
- Lorentz, B. (2013a). *A numerical model for mixed lubrication taking into account surface topography, tangential adhesion effects and plastic deformations* (Vol. 59): Elsevier.
- Lorentz, B. (2013b). „An approach to investigate surface roughness influence on non-lubricated and lubricated contacts by means of the finite element analysis“. In *IPEK – Forschungsberichte published by A. Albers vol. 63. Dissertation*. Karlsruhe Institute of Technology (KIT): IPEK – Institute of Product Engineering. ISSN: 1615-8113.
- Ludwik, P. (1909). *Elemente der technologischen Mechanik*. Berlin: Springer.
- Mäki, R. (2016+0200). *Wet clutch tribology: Friction characteristics in limited slip differentials*: Luleå tekniska universitet. Retrieved from <http://www.diva-portal.org/smash/get/diva2:999829/FULLTEXT01> [06.04.2019]
- Marklund, P., & Larsson, R. (2008). Wet clutch friction characteristics obtained from simplified pin on disc test. *Tribology International*, 41(9-10), 824–830. <https://doi.org/10.1016/j.triboint.2007.11.014>
- Martínez-Ortiz, F., Molina, A., & Laborda, E. (2011). Electrochemical digital simulation with highly expanding grid four point discretization: Can Crank–Nicolson uncouple diffusion and homogeneous chemical reactions? *Electrochimica Acta*, 56(16), 5707–5716. <https://doi.org/10.1016/j.electacta.2011.04.043>
- Masouros, G., Dimarogonas, A., & Lefas, K. (1977). A model for wear and surface roughness transients during the running-in of bearings. *Wear*, 45(3), 375–382. [https://doi.org/10.1016/0043-1648\(77\)90028-X](https://doi.org/10.1016/0043-1648(77)90028-X)

- McColl, I.R., Ding, J., & Leen, S.B. (2004). Finite element simulation and experimental validation of fretting wear. *Wear*, 256(11-12), 1114–1127. <https://doi.org/10.1016/j.wear.2003.07.001>
- Mihailidis, A., Retzepis, J., Salpistis, C., & Panajiotidis, K. (1999). Calculation of friction coefficient and temperature field of line contacts lubricated with a non-Newtonian fluid. *Wear*, 232(2), 213–220. [https://doi.org/10.1016/S0043-1648\(99\)00148-9](https://doi.org/10.1016/S0043-1648(99)00148-9)
- Nowicki, L. (2008). „*Raue Oberflächen in geschmierten Tribokontakten*“. In *IPEK – Forschungsberichte published by A. Albers vol. 30. Dissertation*. Karlsruhe Institute of Technology (KIT): IPEK – Institute of Product Engineering. ISSN: 1615-8113
- Özel, T., Thepsonthi, T., Ulutan, D., & Kaftanoğlu, B. (2011). Experiments and finite element simulations on micro-milling of Ti–6Al–4V alloy with uncoated and cBN coated micro-tools. *CIRP Annals - Manufacturing Technology*, 60(1), 85–88. <https://doi.org/10.1016/j.cirp.2011.03.087>
- Patir, N. (1978). A numerical procedure for random generation of rough surfaces. *Wear*, 47(2), 263–277. [https://doi.org/10.1016/0043-1648\(78\)90157-6](https://doi.org/10.1016/0043-1648(78)90157-6)
- Patir, N., & Cheng, H. S. (1978). An Average Flow Model for Determining Effects of Three-Dimensional Roughness on Partial Hydrodynamic Lubrication. *Journal of Lubrication Technology*, 100(1), 12. <https://doi.org/10.1115/1.3453103>
- Patir, N., & Cheng, H. S. (1979). Application of Average Flow Model to Lubrication Between Rough Sliding Surfaces. *Journal of Lubrication Technology*, 101(2), 220. <https://doi.org/10.1115/1.3453329>
- Pödra, P., & Andersson, S. (1999). Simulating sliding wear with finite element method. *Tribology International*, 32(2), 71–81. [https://doi.org/10.1016/S0301-679X\(99\)00012-2](https://doi.org/10.1016/S0301-679X(99)00012-2)
- Rabinowicz, E. (1995). *Friction and wear of materials* (2. ed.). A Wiley-Interscience publication. New York, NY: Wiley. Retrieved from <http://www.loc.gov/catdir/bios/wiley047/94032860.html>
- Redlich, C. (2002). *Simulation von Punktkontakten unter Mischreibungsbedingungen*. Dissertation. *Fortschritte der Maschinenkonstruktion: 3/2002*. Aachen: Shaker.
- Reichert, S., Lorentz, B., & Albers, A. (2016). Influence of flattening of rough surface profiles on the friction behaviour of mixed lubricated contacts. *Tribology International*, 93, 614–619. <https://doi.org/10.1016/j.triboint.2015.01.003>
- Reichert, S., Lorentz, B., Heldmaier, S., & Albers, A. (2016). Wear simulation in non-lubricated and mixed lubricated contacts taking into account the microscale roughness. *Tribology International*, 100, 272–279. <https://doi.org/10.1016/j.triboint.2016.02.009>

- Reynolds, O. (1886). On the Theory of Lubrication and Its Application to Mr. Beauchamp Tower's Experiments, Including an Experimental Determination of the Viscosity of Olive Oil. *Proceedings of the Royal Society of London*, 40(242-245), 191–203. <https://doi.org/10.1098/rspl.1886.0021>
- Ropohl, G. (2009). *Allgemeine Technologie: Eine Systemtheorie der Technik*: KIT Scientific Publishing.
- Russell, J. V. (1975). Steels for Cold Forming: Sourcebook on Cold Forming. *American Society of Metals*. Page 106
- Sander, D. E., Allmaier, H., & Pribsch, H.-H. (2016). Friction and Wear in Automotive Journal Bearings Operating in Today's Severe Conditions. In P. H. Darji (Ed.), *Advances in Tribology*. InTech. <https://doi.org/10.5772/64247>
- Sander, D. E., Allmaier, H., Witt, M., & Skiadas, A. (2017). Journal Bearing Friction and Wear in Start/Stop Operation. *MTZ Worldwide*, 78(02/2017), 46–51.
- Sarkar, A. D. (1980). *Friction and wear*. London: Acad. Pr.
- Savio, D. (2010). Numerische Untersuchung der Einflüsse der Oberflächenrauheit auf das Reibverhalten bei trockener Reibung (Diplomarbeit). Karlsruher Institut für Technologie (KIT), Karlsruhe.
- Schäfer, M. (2008). *Numerical Simulation of Coupled Fluid-Structure Systems*. Université Lille. FSI Summer School,
- Schäfer, M. (2006). *Computational engineering: Introduction to numerical methods*. Berlin, New York: Springer.
- Scherge, M., Pöhlmann, K., & Gervé, A. (2003). Wear measurement using radionuclide-technique (RNT). *Wear*, 254(9), 801–817. [https://doi.org/10.1016/S0043-1648\(03\)00230-8](https://doi.org/10.1016/S0043-1648(03)00230-8)
- Scherge, M., Shakhvorostov, D., & Pöhlmann, K. (2003). Fundamental wear mechanism of metals. *Wear*, 255(1-6), 395–400. [https://doi.org/10.1016/S0043-1648\(03\)00273-4](https://doi.org/10.1016/S0043-1648(03)00273-4)
- Sedlaček, M., Podgornik, B., & Vižintin, J. (2012). Correlation between standard roughness parameters skewness and kurtosis and tribological behaviour of contact surfaces. *Tribology International*, 48, 102–112. <https://doi.org/10.1016/j.triboint.2011.11.008>
- Sin, H., Saka, N., & Suh, N. P. (1979). Abrasive wear mechanisms and the grit size effect. *Wear*, 55(1), 163–190. [https://doi.org/10.1016/0043-1648\(79\)90188-1](https://doi.org/10.1016/0043-1648(79)90188-1)
- Sommer, K., Heinz, R., & Schöfer, J. (2014). *Verschleiß metallischer Werkstoffe: Erscheinungsformen sicher beurteilen* (2., korr. u. erg. Aufl. 2014). Wiesbaden: Springer Fachmedien Wiesbaden. Retrieved from <http://dx.doi.org/10.1007/978-3-8348-2464-6>
- Stachowiak, G. W., & Batchelor, A. W. (2005). *Engineering tribology* (3. ed.). Amsterdam u.a.: Elsevier.

- Szeri, A. Z. (2011). *Fluid film lubrication* (Second edition). Retrieved from <http://lib.myilibrary.com/Open.aspx?id=305543>
- Telliskivi, T. (2004). Simulation of wear in a rolling–sliding contact by a semi-Winkler model and the Archard's wear law. *Wear*, 256(7-8), 817–831. [https://doi.org/10.1016/S0043-1648\(03\)00524-6](https://doi.org/10.1016/S0043-1648(03)00524-6)
- Tzeng, S. T., & Saibel, E. (1967). Surface Roughness Effect on Slider Bearing Lubrication. *A S L E Transactions*, 10(3), 334–348. <https://doi.org/10.1080/05698196708972191>
- Van Zuijlen, A. H. (2006). Fluid-structure interaction simulations: Efficient higher order time integration of partitioned systems. *Faculty of Aerospace Engineering. TU Delft*.
- Verein Deutscher Ingenieure (May 1993). *VDI-Richtlinie 2221 - Methodik zum Entwickeln und Konstruieren technischer Systeme und Produkte*. (VDI-Richtlinie, 2221).
- Verein Deutscher Ingenieure (June 2004). *VDI-Richtlinie 2206 - Entwicklungsmethodik für mechatronische Systeme*. (VDI-Richtlinie, 2206).
- Volk, R. (2013). *Rauheitsmessung: Theorie und Praxis* (2., überarb. Aufl.). *Beuth Praxis: Messwesen*. Berlin: Beuth.
- Wiersch, P. (2004). *Berechnung thermo-elastohydrodynamischer Kontakte bei Mischreibung*. Dissertation. *Fortschrittsberichte des Instituts für Tribologie und Energieumwandlungsmaschinen: Vol. 3*. Aachen: Shaker.
- Wisniewski, M. (2000). *Elastohydrodynamische Schmierung: Grundlagen und Anwendungen mit 12 Tabellen*. *Handbuch der Tribologie und Schmierungstechnik: Vol. 9*. Renningen-Malmsheim: expert-Verl.
- Wolf, C. (2014). *Verschleißberechnung auf Basis der energetischen Verschleißtheorie*. IST mbH. First User Meeting,
- Wriggers, P. (1996). Finite element methods for contact problems with friction. *Tribology International*, 29(8), 651–658.
- Wu, J.-J. (2000). Simulation of rough surfaces with FFT. *Tribology International*, 33(1), 47–58. [https://doi.org/10.1016/S0301-679X\(00\)00016-5](https://doi.org/10.1016/S0301-679X(00)00016-5)
- Yastrebov, V. A., Durand, J., Proudhon, H., & Cailletaud, G. (2011). Rough surface contact analysis by means of the Finite Element Method and of a new reduced model. *Comptes Rendus Mécanique*, 339(7-8), 473–490. <https://doi.org/10.1016/j.crme.2011.05.006>
- Yue, T., & Abdel Wahab, M. (2017). Finite element analysis of fretting wear under variable coefficient of friction and different contact regimes. *Tribology International*, 107, 274–282. <https://doi.org/10.1016/j.triboint.2016.11.044>

- Zum Gahr, K.-H. (1981). *Abrasiver Verschleiß metallischer Werkstoffe*. *Fortschrittberichte der VDI-Zeitschriften Reihe 5, Grund- und Werkstoffe: Vol. 57*. Düsseldorf: VDI-Verl.
- Zum Gahr, K.-H. (1987). *Microstructure and wear of materials*. *Tribology series: Vol. 10*. Amsterdam: Elsevier. Retrieved from <http://www.sciencedirect.com/science/publication?issn=01678922&volume=10>

Supervised Diploma, Bachelor and Master theses

Atlihan 2016

Atlihan, O.: Untersuchung des Verschleißverhaltens in tribologischen Kontakten mit dem Schadensmodell nach Johnson-Cook, in IPEK – Abschlussarbeiten: Bachelor Thesis vol. 3056, Supervisor: Albers, A., Co-Supervisor: Reichert, S., Karlsruhe Institute of Technology (KIT), IPEK – Institute of Product Engineering, 2016

Duong 2016

Duong, M.: Entwicklung von Methoden zur Verringerung der Elementverzerrung bei Anwendung des Verschleißgesetzes nach Archard mit der FEM, in IPEK – Abschlussarbeiten: Bachelor Thesis vol. 3239, Supervisor: Albers, A., Co-Supervisor: Reichert, S., Karlsruhe Institute of Technology (KIT), IPEK – Institute of Product Engineering, 2016

Haefele 2017

Haefele, F.: Numerische Untersuchung hydrodynamischer Schmierkontakte - Vergleich der Coupled Eulerian-Lagrangian und der Computational Fluid Dynamics Methode, in IPEK – Abschlussarbeiten: Bachelor Thesis vol. 3298, Supervisor: Albers, A., Co-Supervisor: Reichert, S., Karlsruhe Institute of Technology (KIT), IPEK – Institute of Product Engineering, 2017

Heldmaier 2014

Heldmaier, S.: FEM Simulation von Gleitverschleiß an zwei trockenlaufenden technischen Oberflächen, in IPEK – Abschlussarbeiten: Master Thesis vol. 2717, Supervisor: Albers, A., Co-Supervisor: Reichert, S., Karlsruhe Institute of Technology (KIT), IPEK – Institute of Product Engineering, 2014

Jung 2015

Jung, P.: FEM Entwicklung einer Methodik zur Bewertung der Flankentragfähigkeit von Evolventenverzahnungen, in IPEK – Abschlussarbeiten: Master Thesis vol. 2795, Supervisor: Albers, A., Co-Supervisor: Reichert, S., Karlsruhe Institute of Technology (KIT), IPEK – Institute of Product Engineering, 2015

Joerger 2015

Joerger, A.: Bestimmung der Johnson-Cook-Parameter zum Abbilden von Verschleiß auf realen Oberflächen mit der Finite-Elemente-Methode, in IPEK – Abschlussarbeiten: Bachelor Thesis vol. 2881, Supervisor: Albers, A., Co-Supervisor: Reichert, S., Karlsruhe Institute of Technology (KIT), IPEK – Institute of Product Engineering, 2015

Kohler 2016

Kohler, F.: Untersuchung des Zahneingriffs in der Freilauffunktion von Fahrrad-Hinterradnaben mit Hilfe der Finite-Elemente-Methode, in IPEK – Abschlussarbeiten: Diploma Thesis vol. 2777, Supervisor: Albers, A., Co-Supervisor: Reichert, S., Karlsruhe Institute of Technology (KIT), IPEK – Institute of Product Engineering, 2016

Koobar 2017

Koobar, W.: Verschleißmodellierung von Gleitlagerungen, in IPEK – Abschlussarbeiten: Master Thesis vol. 3384, Supervisor: Albers, A., Co-Supervisor:

Reichert, S., Karlsruhe Institute of Technology (KIT), IPEK – Institute of Product Engineering, 2017

Murad 2016

Murad, J.: Untersuchung der Modellierbarkeit von realen, technischen Oberflächen, in IPEK – Abschlussarbeiten: Bachelor Thesis vol. 3171, Supervisor: Albers, A., Co-Supervisor: Reichert, S., Karlsruhe Institute of Technology (KIT), IPEK – Institute of Product Engineering, 2016

Moreira 2017

Moreira, P.: Verifizierung eines trockenlaufenden Reibungs- und Verschleißmodells am Beispiel des Modellversuchs Stift-Scheibe Tribometer, in IPEK – Abschlussarbeiten: Bachelor Thesis vol. 3284, Supervisor: Albers, A., Co-Supervisor: Reichert, S., Karlsruhe Institute of Technology (KIT), IPEK – Institute of Product Engineering, 2017

Pflugfelder 2014

Pflugfelder, H.: Abbildung von Profilabflachungen in geschmierten tribologischen Kontakten mit Hilfe der Finite-Elemente-Methode, in IPEK – Abschlussarbeiten: Bachelor Thesis vol. 2668, Supervisor: Albers, A., Co-Supervisor: Reichert, S., Karlsruhe Institute of Technology (KIT), IPEK – Institute of Product Engineering, 2014

Renz 2017

Renz, R.: Numerische Untersuchung eines Dünnschichtensors für Mischreibungsanwendungen, in IPEK – Abschlussarbeiten: Bachelor Thesis vol. 3350, Supervisor: Albers, A., Co-Supervisor: Reichert, S., Karlsruhe Institute of Technology (KIT), IPEK – Institute of Product Engineering, 2017

Sanner 2018

Sanner, A.: Modellierung des dynamischen Verhaltens von Zylinderrollenlagern inklusive Bordkontakt und EHD-Reibungsmodelle, in IPEK – Abschlussarbeiten: Bachelor Thesis vol. 3492, Supervisor: Albers, A., Co-Supervisor: Reichert, S., Karlsruhe Institute of Technology (KIT), IPEK – Institute of Product Engineering, 2018

Schreyer 2017

Schreyer, L.: Numerische Untersuchung des Einflusses von Verschleißpartikeln auf das Reibungsverhalten, in IPEK – Abschlussarbeiten: Bachelor Thesis vol. 3379, Supervisor: Albers, A., Co-Supervisor: Reichert, S., Karlsruhe Institute of Technology (KIT), IPEK – Institute of Product Engineering, 2017

Sümer 2014a

Sümer, Y.: Abbilden von Verschleißphänomenen in ungeschmierten Kontakten durch die Finite Elemente Methode, in IPEK – Abschlussarbeiten: Bachelor Thesis vol. 2661, Supervisor: Albers, A., Co-Supervisor: Reichert, S., Karlsruhe Institute of Technology (KIT), IPEK – Institute of Product Engineering, 2014

Uhle 2018

Uhle, C.: Modellbildung und Simulation von Verzahnungen in Schneckengetrieben, in IPEK – Abschlussarbeiten: Master Thesis vol. 3541, Supervisor: Albers, A., Co-Supervisor: Reichert, S., Karlsruhe Institute of Technology (KIT), IPEK – Institute of Product Engineering, 2017

Wang 2017

Wang, Z.: Charakterisierung und Modellierung von hydraulischen Scheibenbremsen für E-Bikes, in IPEK – Abschlussarbeiten: Master Thesis vol. 3344, Supervisor: Albers, A., Co-Supervisor: Reichert, S., Karlsruhe Institute of Technology (KIT), IPEK – Institute of Product Engineering, 2017

Welle 2015

Welle, R.: Verschleißuntersuchung nach Archard mit der Finite Elemente Methode, in IPEK – Abschlussarbeiten: Bachelor Thesis vol. 2932, Supervisor: Albers, A., Co-Supervisor: Reichert, S., Karlsruhe Institute of Technology (KIT), IPEK – Institute of Product Engineering, 2015

Wieseler 2015

Wieseler, D.: Untersuchung der Gleitbedingungen bei ungeschmierten Kontakten mit der Finite Elemente Methode, in IPEK – Abschlussarbeiten: Bachelor Thesis vol. 2920, Supervisor: Albers, A., Co-Supervisor: Reichert, S., Karlsruhe Institute of Technology (KIT), IPEK – Institute of Product Engineering, 2015

Xiao 2016

Xiao, K.: Simulation von Laufwerk dichtungen mit einem paramterischen Finite-Elemente-Modell, in IPEK – Abschlussarbeiten: Master Thesis vol. 3164, Supervisor: Albers, A., Co-Supervisor: Reichert, S., Karlsruhe Institute of Technology (KIT), IPEK – Institute of Product Engineering, 2016

Zhong 2016

Zhong, Z.: Verschleißsimulation einer Diesel Einspritzdüse, in IPEK – Abschlussarbeiten: Master Thesis vol. 3149, Supervisor: Albers, A., Co-Supervisor: Reichert, S., Karlsruhe Institute of Technology (KIT), IPEK – Institute of Product Engineering, 2016